Cryogenic Detectors
for low-energy astronomy :
Why, When and How

prof. Paolo de Bernardis
Dipartimento di Fisica
Sapienza Università di Roma

Radiation Detection at Low Temperature
La Londe Les Maures (France)

May 23, 2012

Low-energy astronomy

- Low-energy with respect to …
  …. typical atomic transition energies (eV)
- So medium and far IR, mm waves and $\mu-$waves.
- Let's say (quite arbitrarily) the range
  - E = 0.0001 – 0.1 eV
  - ν = 30 GHz – 25 THz
  - λ = 10 mm – 12 μm
- This range is very important for modern astronomy and cosmology, but very difficult to study.

Very important :
The cold / early universe

- Low-energy photons present in our universe in this range have been produced in three ways:

  - Thermally in low-temperature regions (typically in the interstellar medium, far from stars)

  - Non-thermally in the interstellar medium (synchrotron)

  - Thermally in the early and hot universe, as visible / high energy photons, converted afterwards into low energy photons by the expansion of the universe.

Relevant Physical Processes

- Low Temperature Blackbody
  - Interstellar dust
  - Cosmic Microwave Background (CMB spectrum)
- Molecular lines
  - Rotation
  - Vibration
  - PAH
- Fine and Hyperfine Atomic lines (CII, OI, … 21 cm)
- Synchrotron

- Redshift and the CMB, again, in all its finest details:
  - Anisotropy & cosmological parameters
  - Polarization & inflation
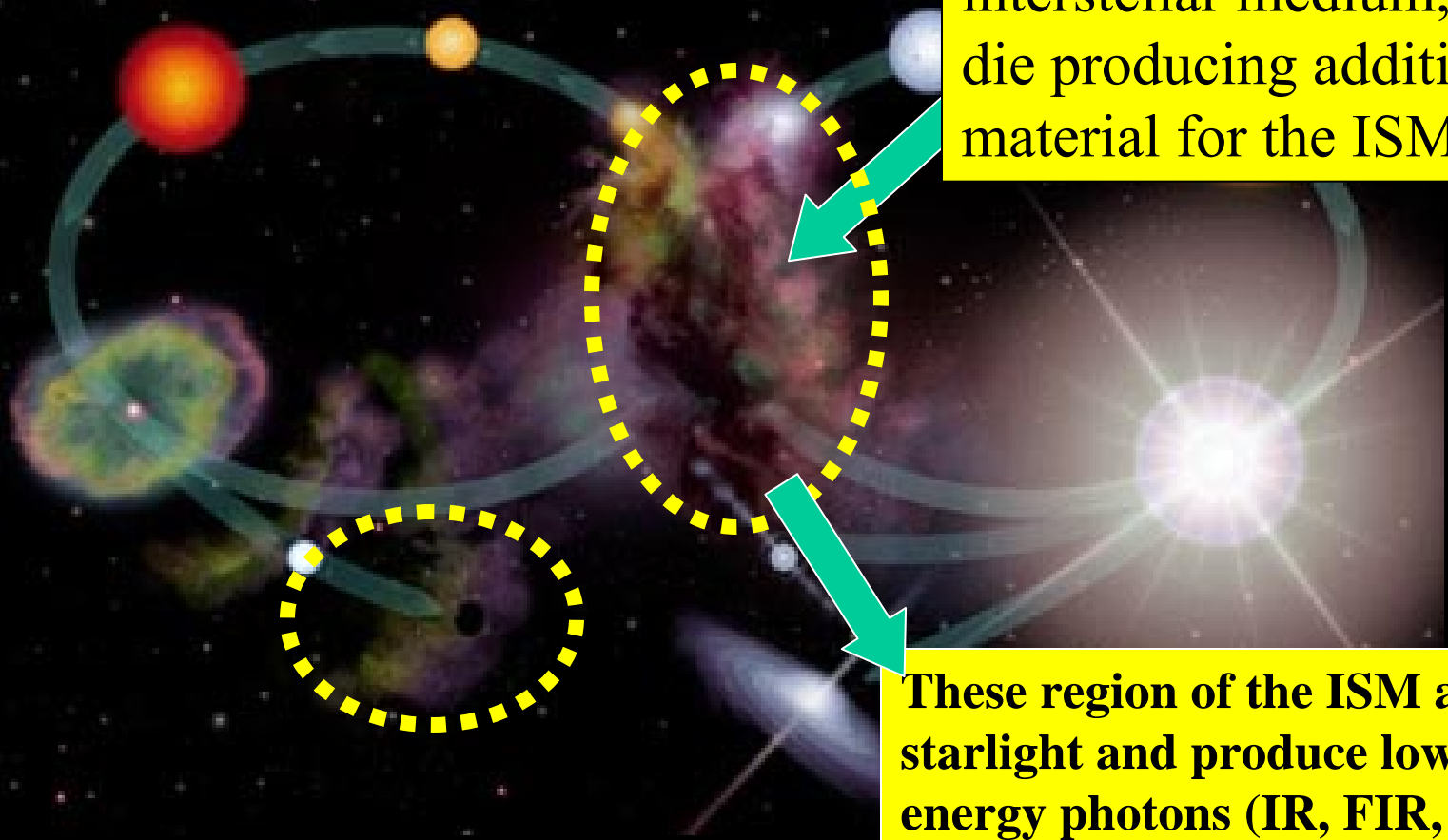 - Sunyaev-Zeldovich effect, clusters & structure formation

- Star life cycle
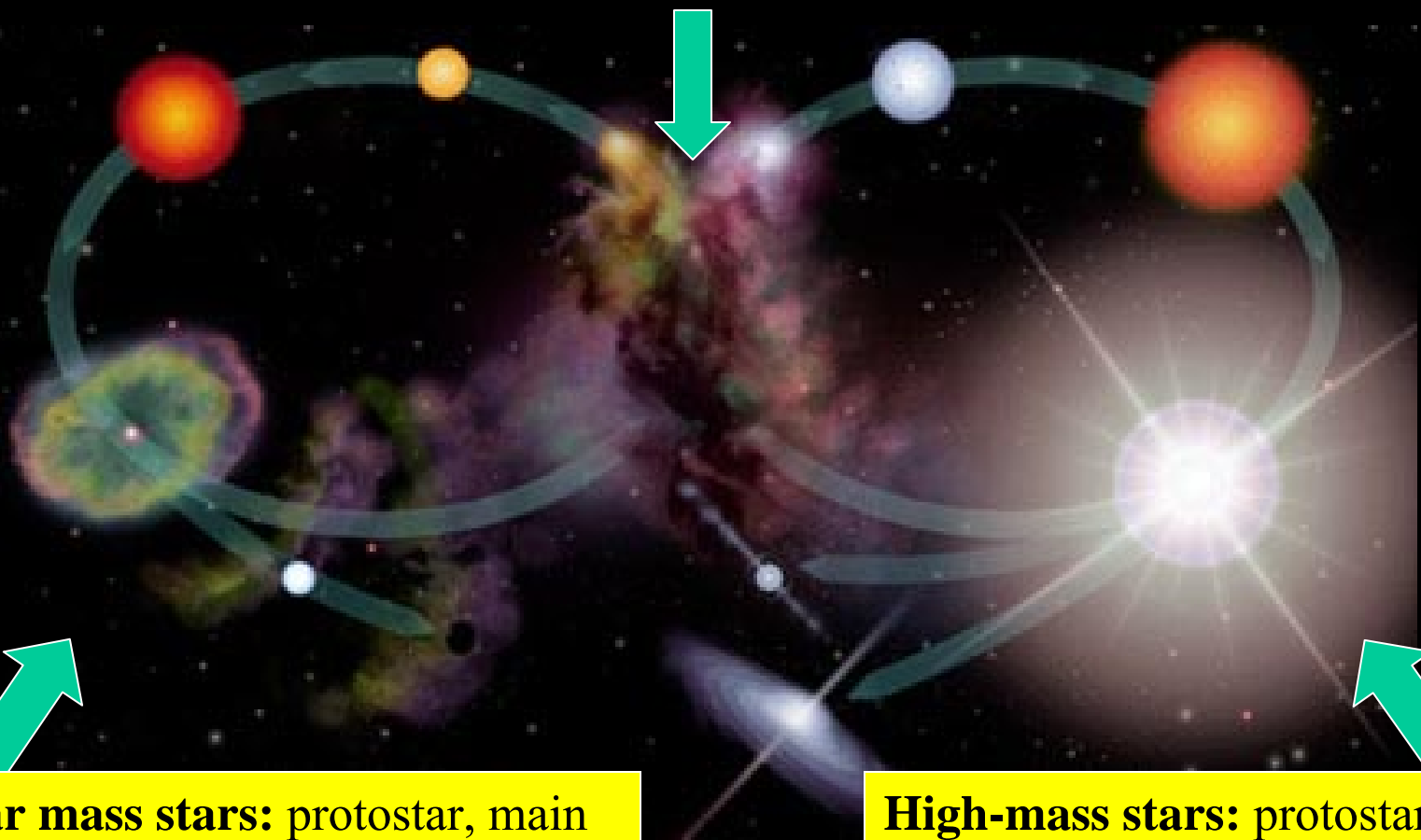
Solar mass stars: protostar, main sequence star, red giant, planetary nebula, white dwarf, brown dwarf (with expelled material)

High-mass stars: protostar, main sequence star, red giant, supernova, compact object (with expelled material)
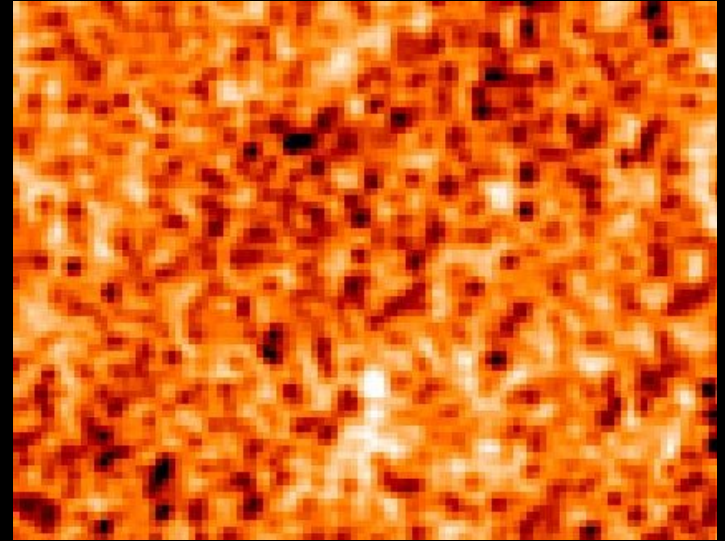
- Star life cycle

Stars are born from high density regions in the interstellar medium, and die producing additional material for the ISM

These region of the ISM absorb starlight and produce low energy photons (IR, FIR, mm)

Image of Solar Granulation

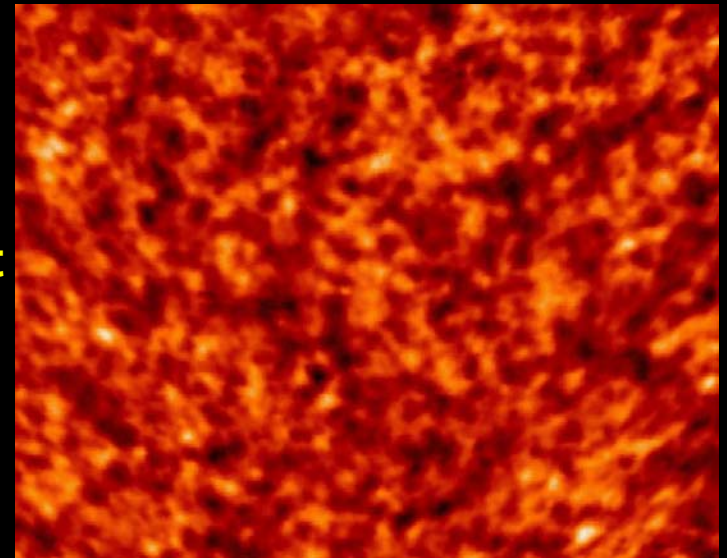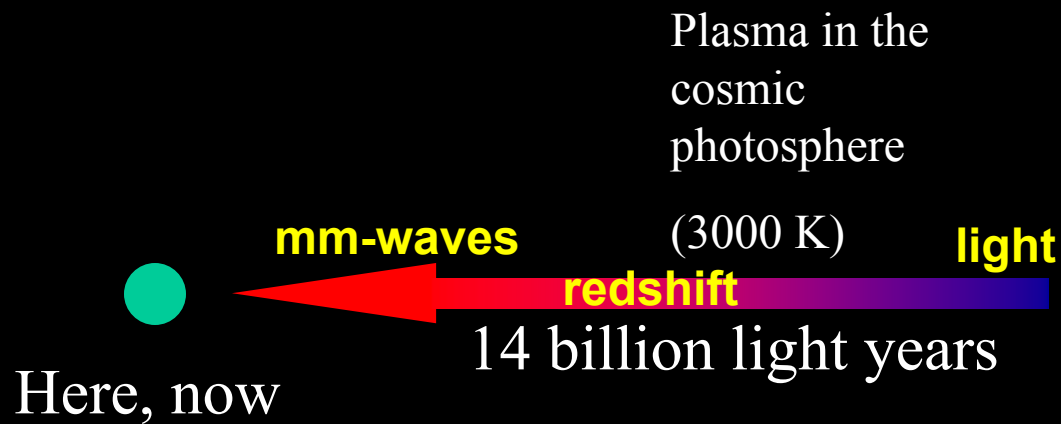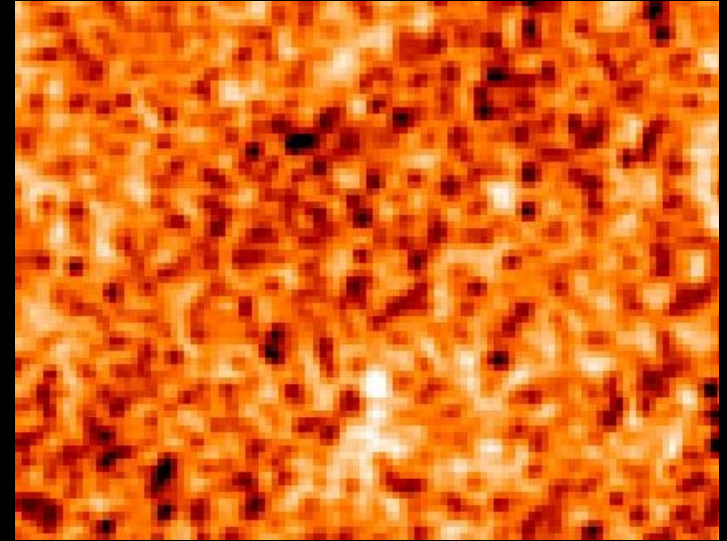Plasma in the solar photosphere

(5800 K)

8 light minutes

Here, now

Image of Solar Granulation

Plasma in the
solar photosphere

(5800 K)

Here, now

8 light minutes

Plasma in the
cosmic
photosphere

(3000 K)

mm-waves

light

redshift

Here, now

14 billion light years

The BOOMERanG map of the CMB

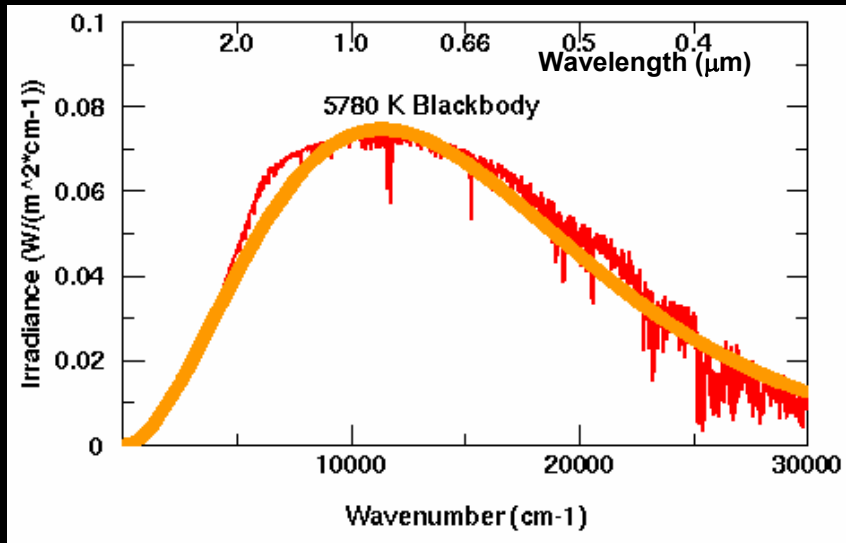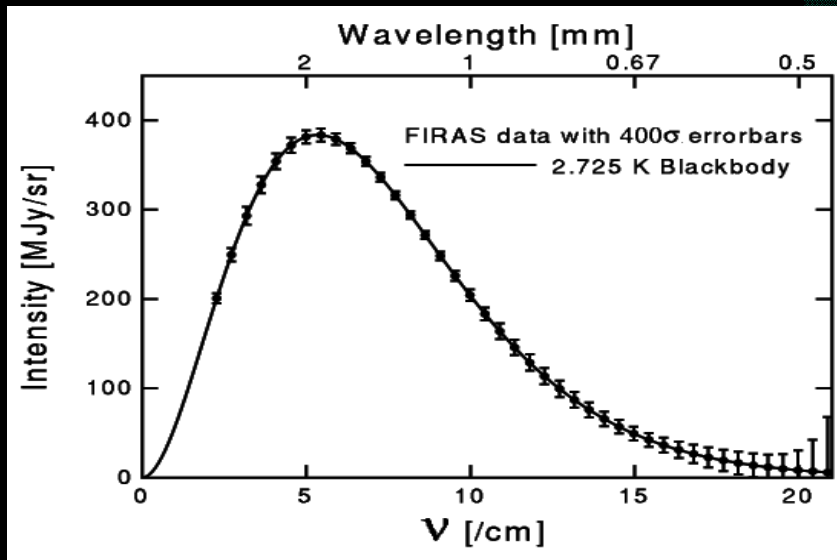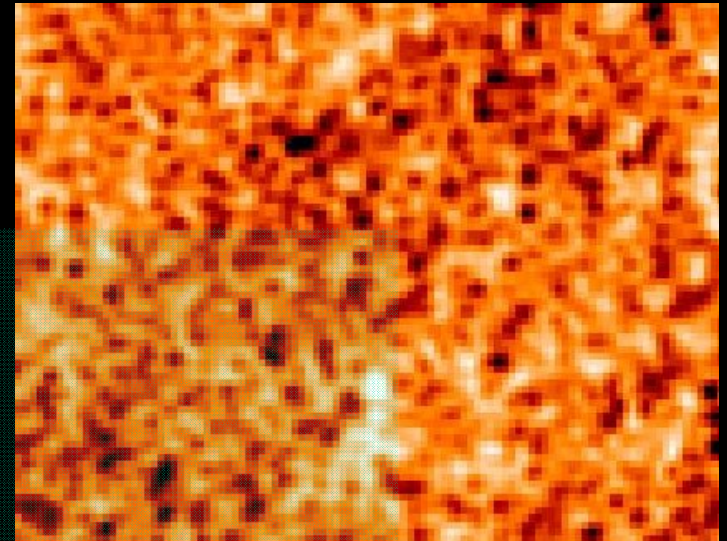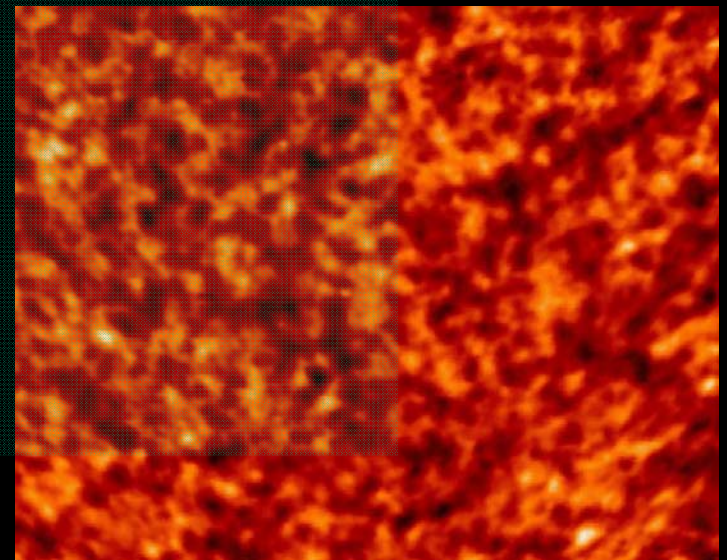Low-resolution spectrum of the sun compared to a blackbody

Image of Solar Granulation

Low-resolution spectrum of the CMB compared to a blackbody

The BOOMERanG map of the CMB

Blackbody brightness

$$B(\nu, T) = \frac{2h\nu^3}{c^2} \frac{1}{e^{\frac{h\nu}{kT}} - 1}$$

$$B(\lambda, T) = \frac{2hc^2}{\lambda^5} \frac{1}{e^{\frac{hc}{kT\lambda}} - 1}$$

- No intersection
- Maximum brightness:

$$\lambda_{max} T = 0.290 \, cm \, K$$

- $\begin{cases} B(\nu, T) \approx \dfrac{2\nu^2}{c^2} kT \\ h\nu \ll kT \end{cases}$
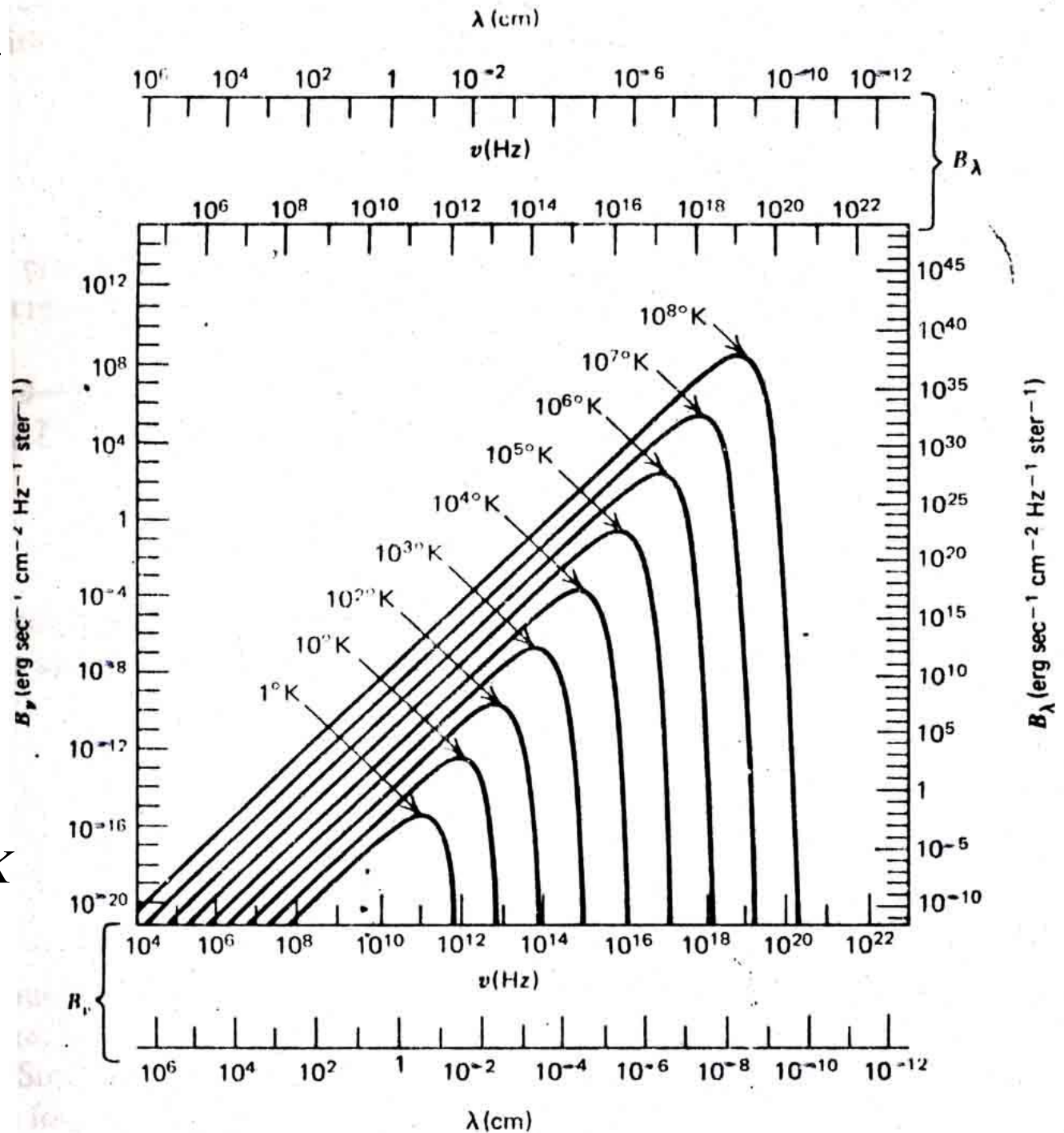
Blackbody brightness
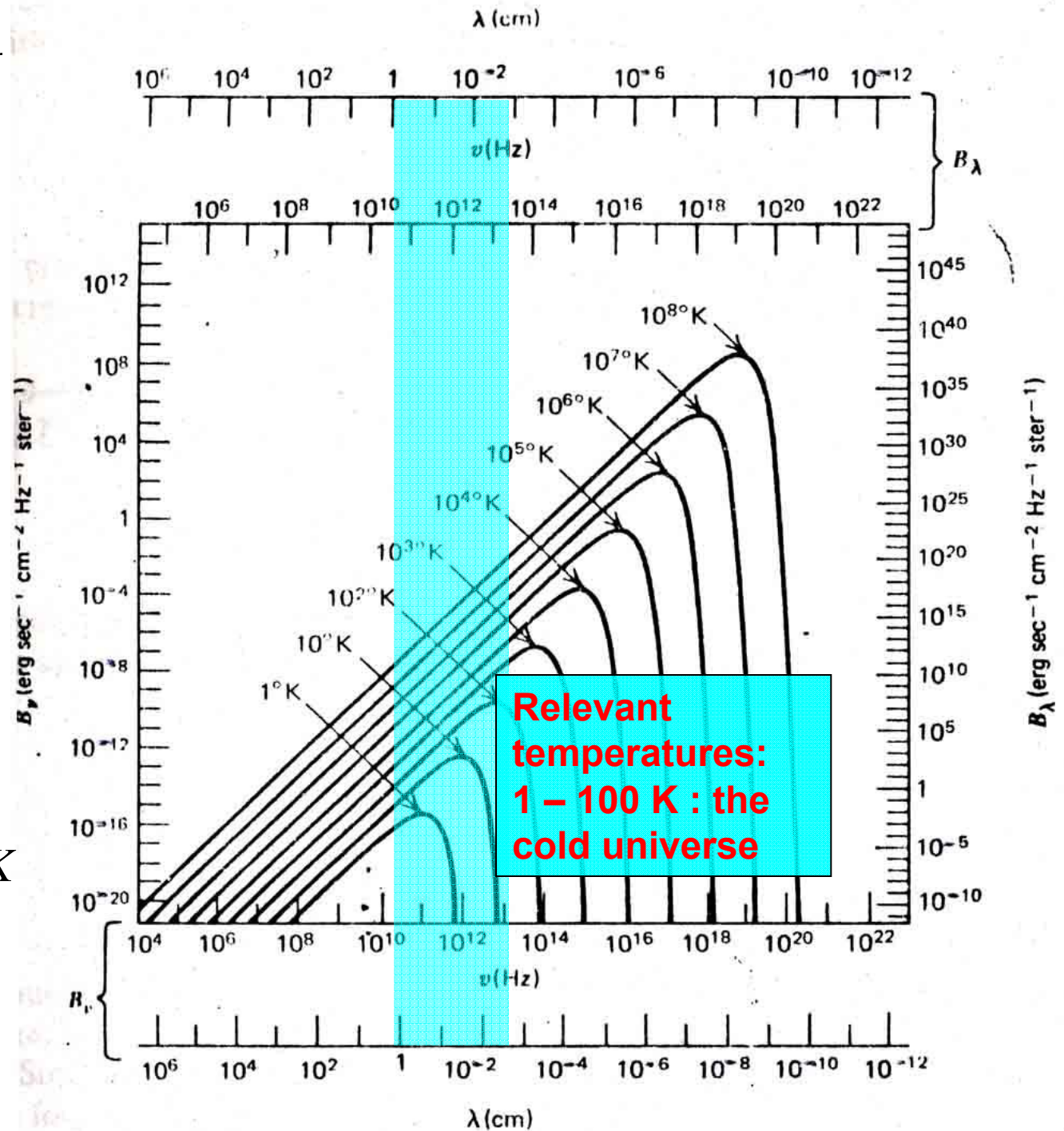
$$B(\nu,T) = \frac{2h\nu^3}{c^2} \frac{1}{e^{\frac{h\nu}{kT}} - 1}$$

$$B(\lambda,T) = \frac{2hc^2}{\lambda^5} \frac{1}{e^{\frac{hc}{kT\lambda}} - 1}$$

- No intersection
- Maximum brightness:

$$\lambda_{max} T = 0.290 \, cm \, K$$

- $$\begin{cases} B(\nu,T) \approx \dfrac{2\nu^2}{c^2} kT \\ h\nu << kT \end{cases}$$

Relevant temperatures: 1 – 100 K : the cold universe

Interstellar Dust (ISD)

- C and Si aggregates produced in the latest phases of stellar evolution and injected in the ISM by stellar explosions. Typical size 0.1 μm. Aggregated in clouds with different densities.

- Thermal Radiation transfer : (neglecting scattering)
$$\frac{dI_\nu}{d\tau_\nu} = -I_\nu + B(\nu,T)$$

- In the limit of small optical depth, the brightness produced by a cloud of material with optical depth τ_ν and temperature T is
$$I_\nu = \tau_\nu B(\nu,T)$$

- While the absorption of radiation propagating through the cloud is described by
$$\Delta I_\nu = \tau_\nu I_\nu$$

Dust (extinction)

- Optical image of our Galaxy: dust extinction of starlight (by absorption and scattering) is evident in the disk.

© 2000, Axel Mellinger

Dust (emission)

- Far IR image of our Galaxy (12, 25, 60, 100 µm) from the IRAS survey: the darkest regions in visible light are the brightest ones in FIR. Stellar radiation is processed by dust grains and degraded to low-energy radiation.
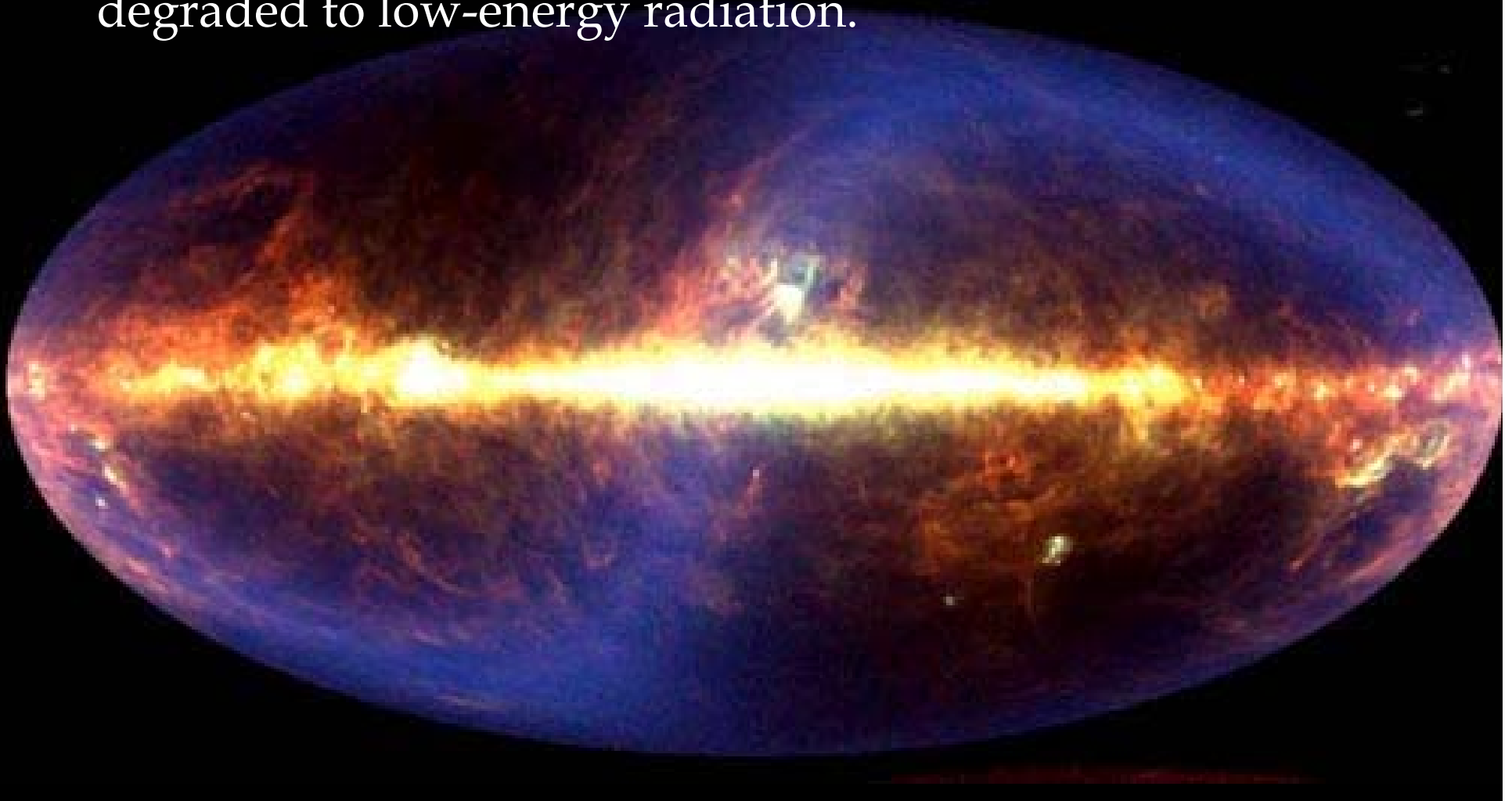
Dust extinction and emission

- The Aquila nebula in visibile light and in the far infrared (ISO)

# Temperature of dust grains

- ## Large (0.1 μm) grains:
  - The equilibrium temperature is determined by the balance between absorbed starlight (UV) and re-emitted IR. Typically 20K; most of the emission around 100-200 μm.

- ## Small (<1 nm) grains
  - They are transiently heated at higher temperatures. Most of the emission around 10 μm.


B. T. Draine 2002.12.24
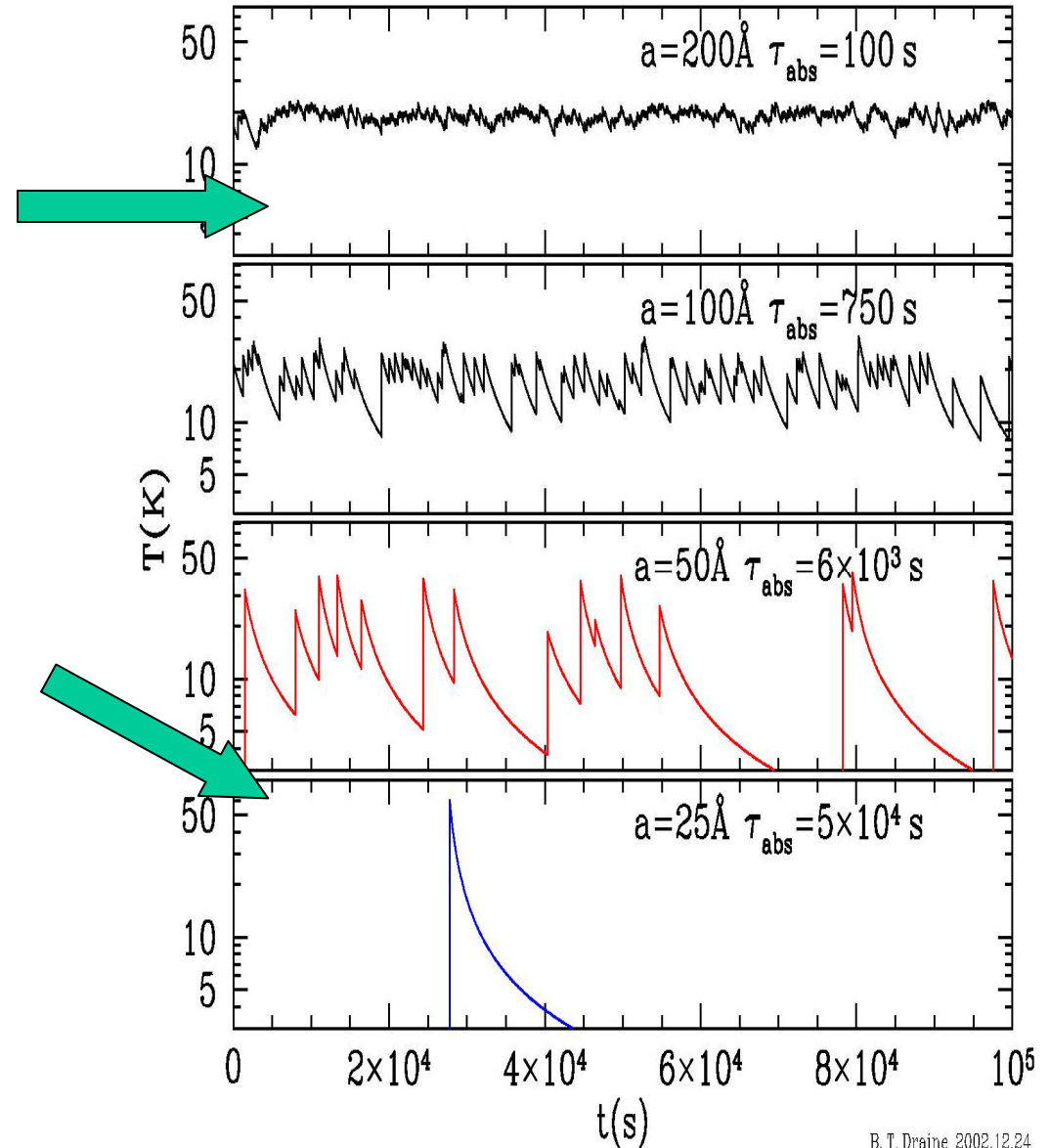
Cirrus dust clouds

- FIR (100 μm) image of the south celestial pole

- Cirrus-like dust clouds in the diffuse medium are evident, and their spectrum is consistent with a 20K physical temperature

- Their emission is a foreground for precision measurements of CMB anisotropy (and polarization, since ISD emission is polarized)

30°

LMC

SCP

30
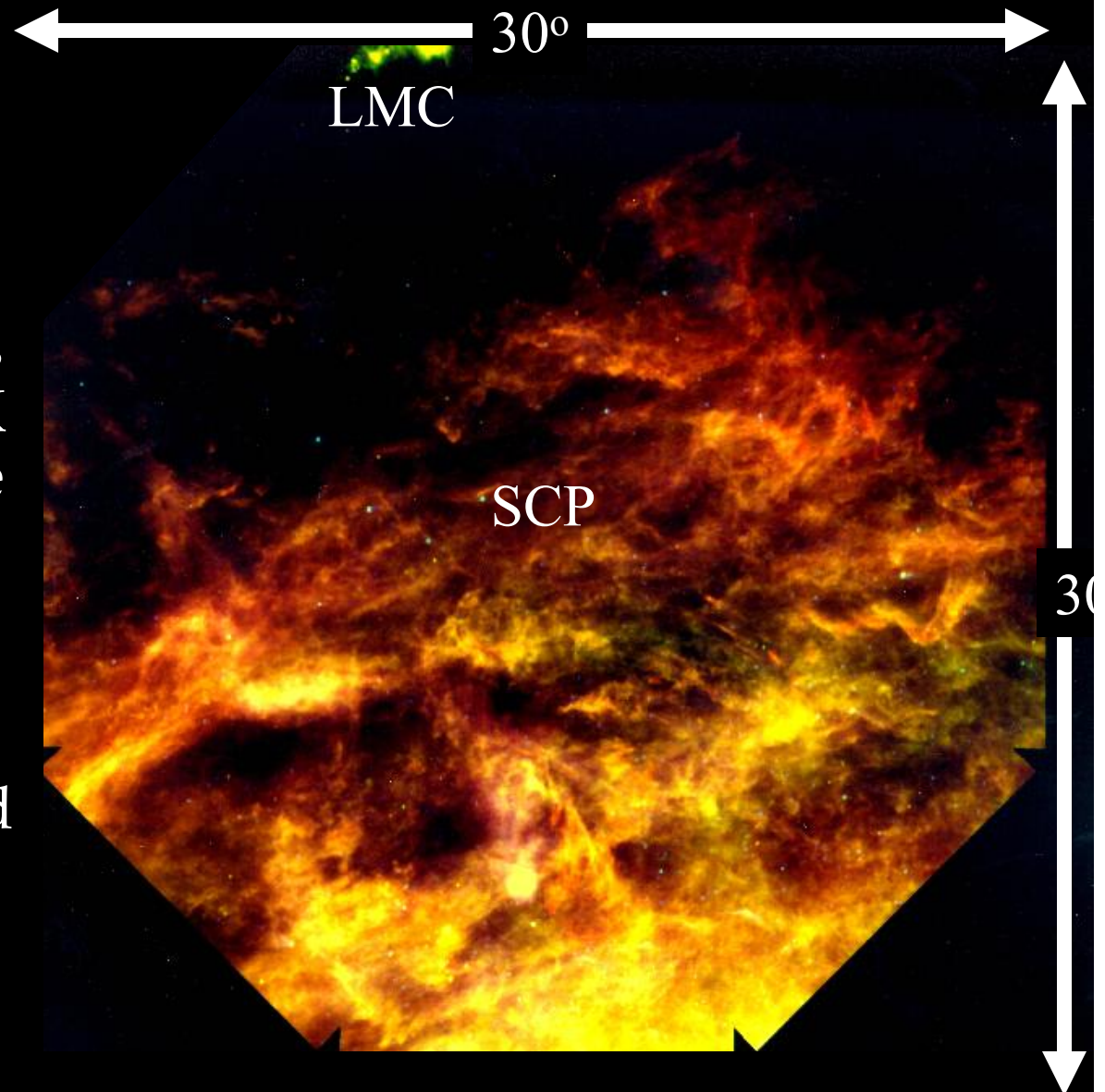
Cirrus dust clouds

- There are "cosmological windows" where ISD emission is fainter and CMB measurements are cleaner, but the issue of foregrounds removal is a very important one

- the Planck mission has been developed focusing on this issue and fighting foregrounds by means of multiwavelength observations (9 bands ranging from 30 to 900 GHz)

$30°$

LMC

SCP

30

From flux to mass

L

D
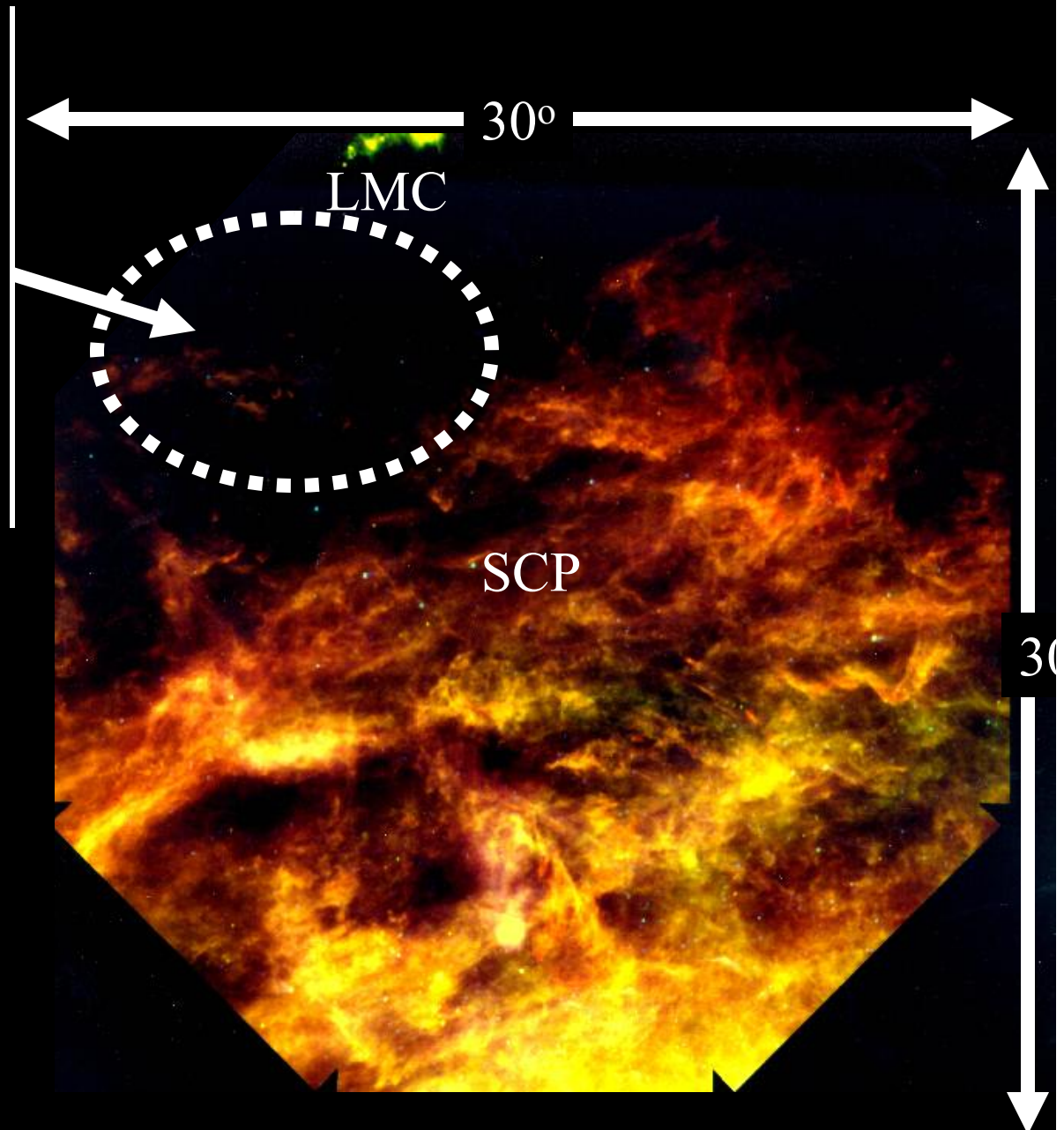
Dust clouds are optically thin at mm wavelengths (size $<< \lambda$). So a mass determination is possible.
Emitted brightness:

$$I_\nu = \tau_\nu B(\nu, T_d)$$

Measured flux :

$$F_\nu = I_\nu \Omega = \tau_\nu B(\nu, T_d) \Omega = \tau_\nu B(\nu, T_d) \frac{A}{D^2}$$
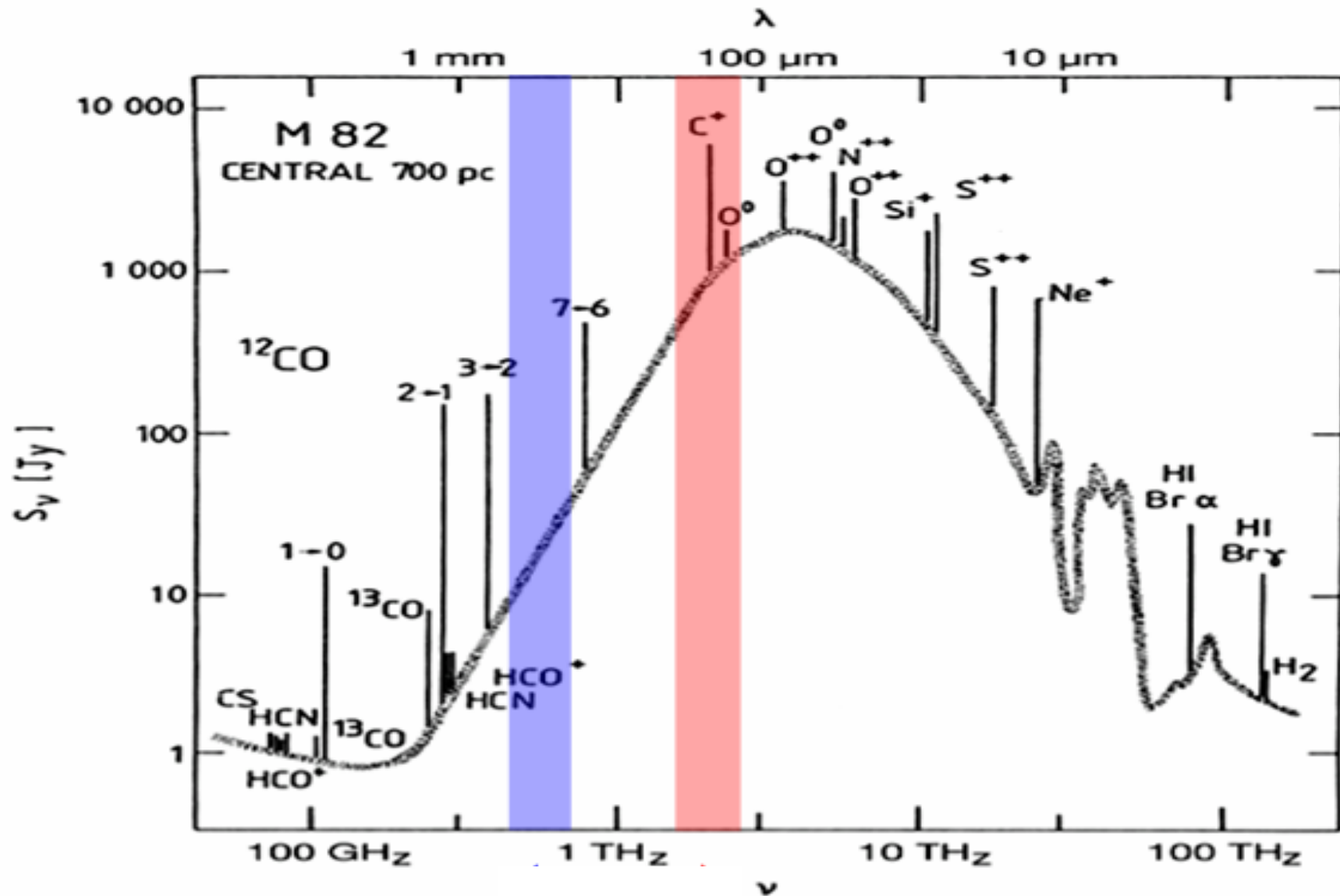
but

$$\tau_\nu = n\sigma_\nu L = \frac{M}{V} \frac{n}{\rho} \sigma_\nu L = \frac{M}{A} \frac{n}{\rho} \sigma_\nu = \frac{M}{A} \kappa_\nu$$

So:

$$F_\nu = \frac{M}{A} \kappa_\nu B(\nu, T_d) \frac{A}{D^2} \rightarrow \boxed{M = \frac{F_\nu D^2}{\kappa_\nu B(\nu, T_d)}}$$

FIR spectrum of M82
a local starburst galaxy

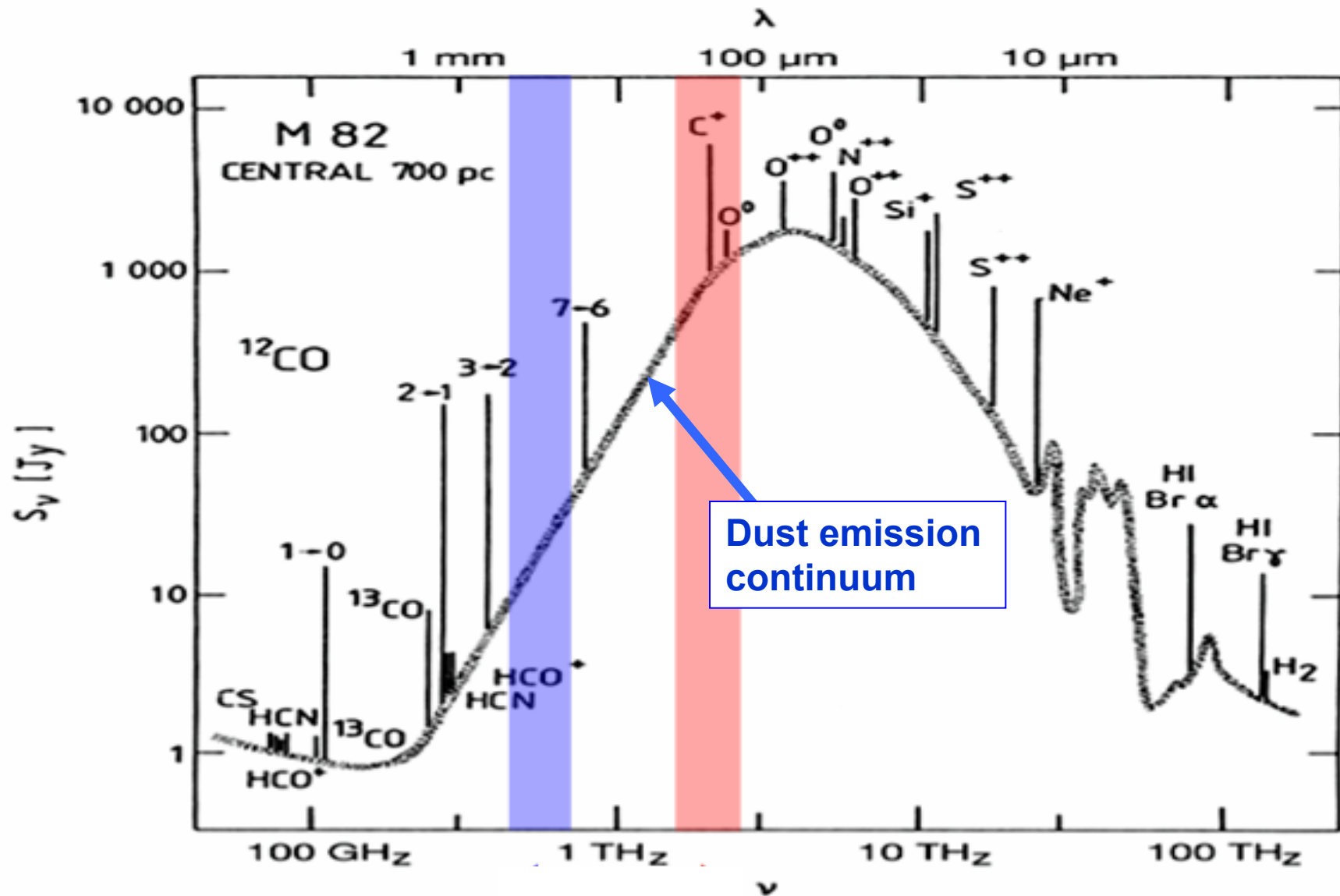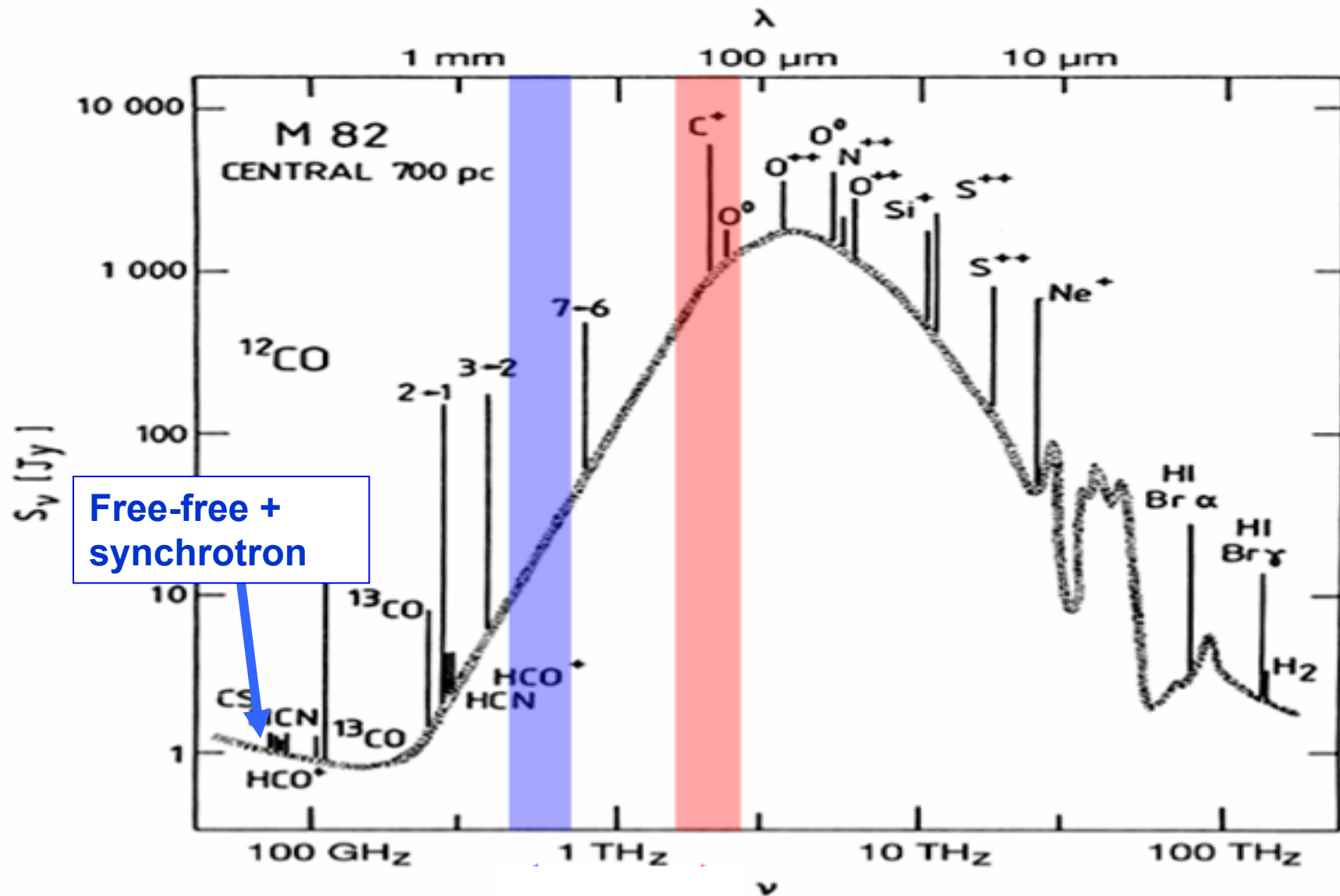# FIR spectrum of M82
a local starburst galaxy

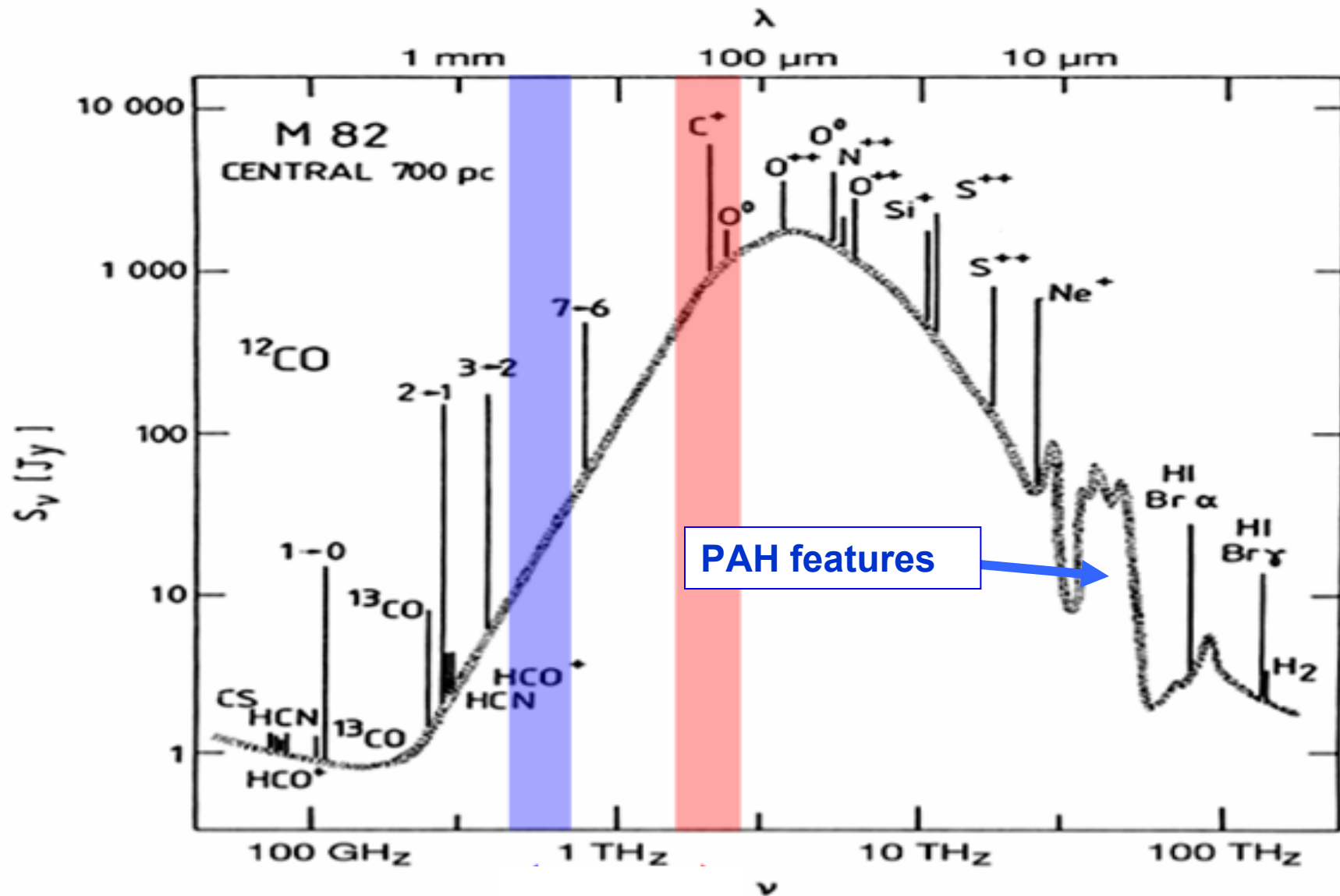# FIR spectrum of M82
a local starburst galaxy

FIR spectrum of M82
a local starburst galaxy

FIR spectrum of M82
a local starburst galaxy

FIR spectrum of M82
a local starburst galaxy
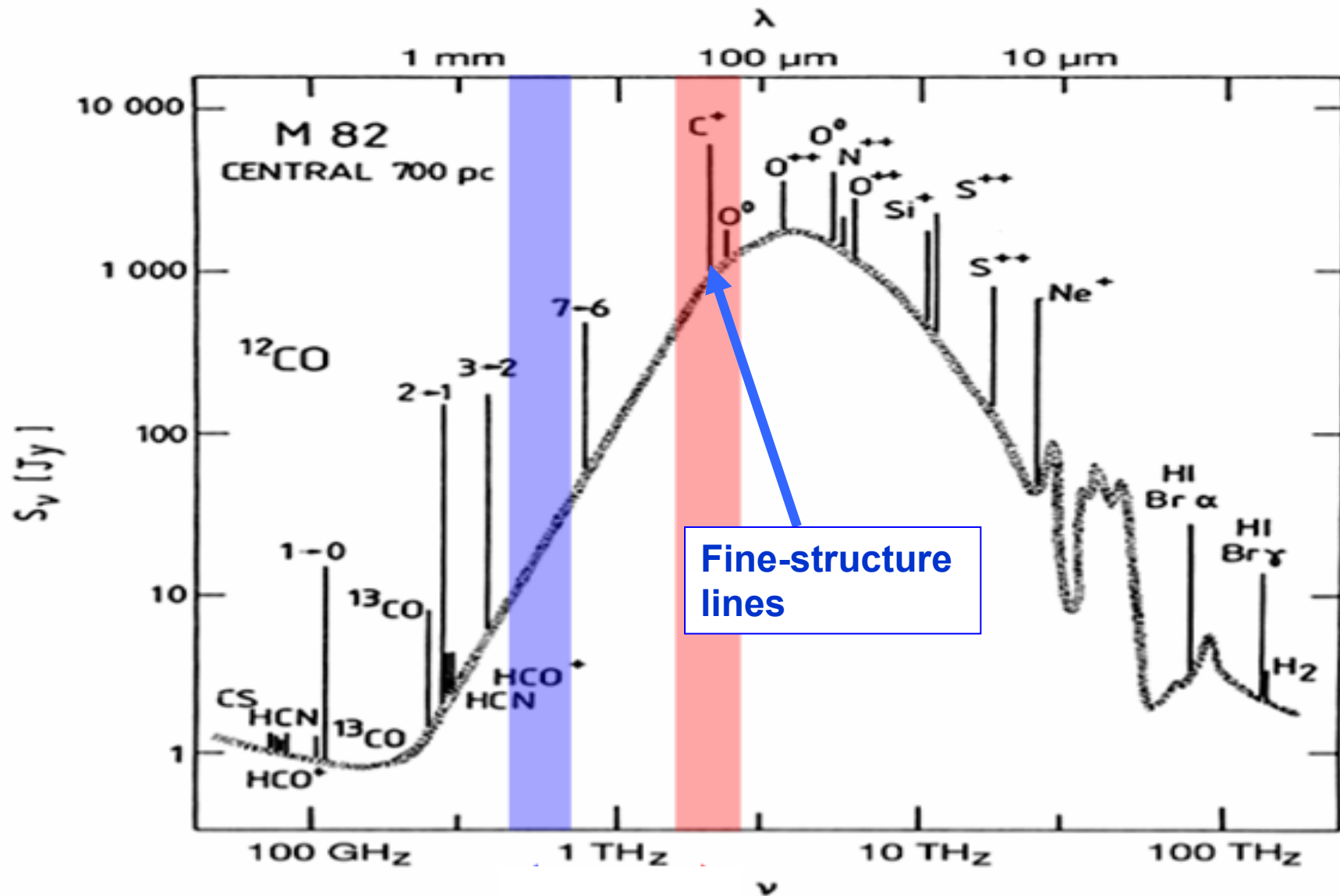
Cooling lines

- abundant atoms having fine structure levels close to the fundamental level:
- In the neutral medium
  - CII 158 μm
  - OI 63 μm
- In the ionized medium (HII regions)
  - OII, OIII, NII, NIII, NeII and NeIII
- These lines are called cooling lines, since the ISM is basically transparent at these wavelengths, and the lines are easily produced due to the small energy required to excite these levels.

The Cosmic Far IR background
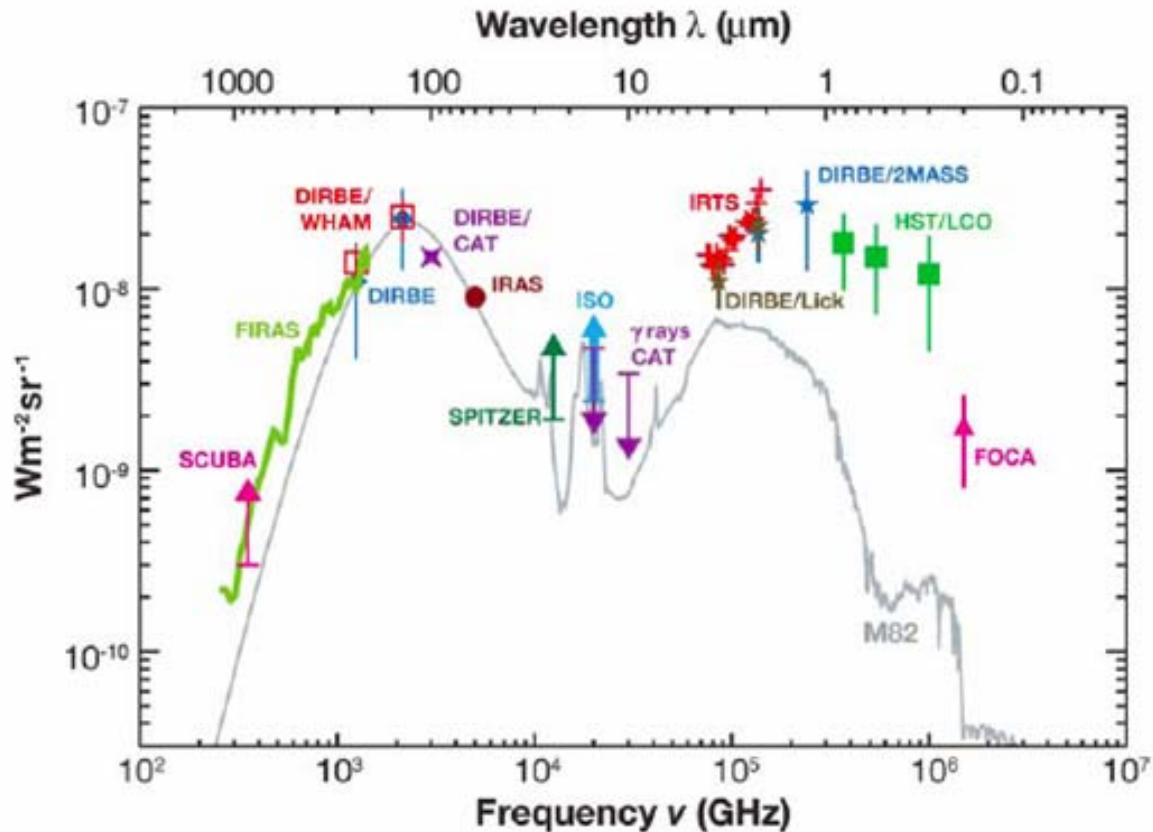
The integrated extragalactic background light in the far-infrared and sub-millimeter region of the spectrum is approximately equal to the integrated background light in the optical and UV part of the spectrum. To develop a complete understanding of galaxy formation, this background light must be resolved into galaxies and their properties must be characterized.

Modern Cosmology

- If
  - we do not occupy a special position in the Universe
  - the Universe at large scales is the same everywhere (homogeneity and isotropy)
  - the correct description of Gravity is General Relativity

- then we get the Friedmann equation describing the evolution of the metric.

$$R(t) = a(t)\chi$$

Physical distance

Comoving distance

Scale factor

$$ds^2 = c^2 dt^2 - a(t)^2 \left[\frac{d\chi^2}{1 - k\chi^2} + \chi^2 \left(d\theta^2 + \sin^2 \theta \, d\varphi^2 \right) \right]$$

FRW: the most general homogenous isotropic metric

Evolution of the scale factor

- *a(t)* is the solution of the Friedmann equation, which can be re-written

$$\left(\frac{\dot{a}}{a}\right)^2 = H_o^2\left\{\Omega_{Ro}\left(\frac{a_o}{a}\right)^4 + \Omega_{Mo}\left(\frac{a_o}{a}\right)^3 + \Omega_{Ko}\left(\frac{a_o}{a}\right)^2 + \Omega_\Lambda\right\}$$

Hubble constant (expansion rate)   Radiation   Matter   Curvature   Cosmological constant

- The result depends on the different kinds of energy densities relevant at the considered epoch
- The result is that the universe is not static: *a=a(t)*.
- From observations we know that the universe expands today, *a(t)* is growing today
- An isotropic expansion of the universe.

Cosmological Redshift

- In an expanding universe the wavelengths of photons expand in the same way as all other lengths ($a(t)$).
- Consider a source at distance $R(t)=a(t) \chi_1$ (comoving coordinate χ_1)
- Photons emitted from the source propagate radially towards us along coordinate χ, occupying sequentially all coordinates between χ_1 and 0.
- From the FRW metric,

$$(ds)^2 = c^2 dt^2 - a(t)^2 \left[\left(\frac{d\chi}{\sqrt{1-k\chi^2}} \right)^2 + (\chi d\theta)^2 + (\chi \sin \theta d\varphi)^2 \right]$$

- Assuming ds=0 for photons,

$$cdt = a(t) \frac{d\chi}{\sqrt{1-k\chi^2}}$$

Cosmological Redshift

- Consider a first crest of the EM wave emitted at time t_1 and received at time t_o; next crest is emitted at $t_1 + \lambda_1/c$ and rreceived at $t_o + \lambda_o/c$. Since χ_1 is constant, we have that

$$\int_0^{\chi_1} \frac{d\chi}{\sqrt{1 - k\chi^2}} = \int_{t1}^{to} \frac{cdt}{a(t)} = \int_{t1+\lambda1/c}^{to+\lambda o/c} \frac{cdt}{a(t)} \Rightarrow \int_{t1}^{t1+\lambda1/c} \frac{cdt}{a(t)} = \int_{to}^{to+\lambda o/c} \frac{cdt}{a(t)}$$

t_1 $t_1 + \lambda_1/c$ t_o $t_o + \lambda_o/c$

t

- However, the times λ_o/c e λ_1/c are both $<< H_o^{-1}$, the typical variation time of $a(t)$. So we can consider $a(t)$ as constant in the integrals. So we get

Redshift of the source

$$\frac{c}{a(t_1)} \frac{\lambda_1}{c} = \frac{c}{a(t_o)} \frac{\lambda_o}{c} \Rightarrow \frac{a(t_o)}{a(t_1)} = \frac{\lambda_o}{\lambda_1} \underset{def}{=} (1 + z_1)$$
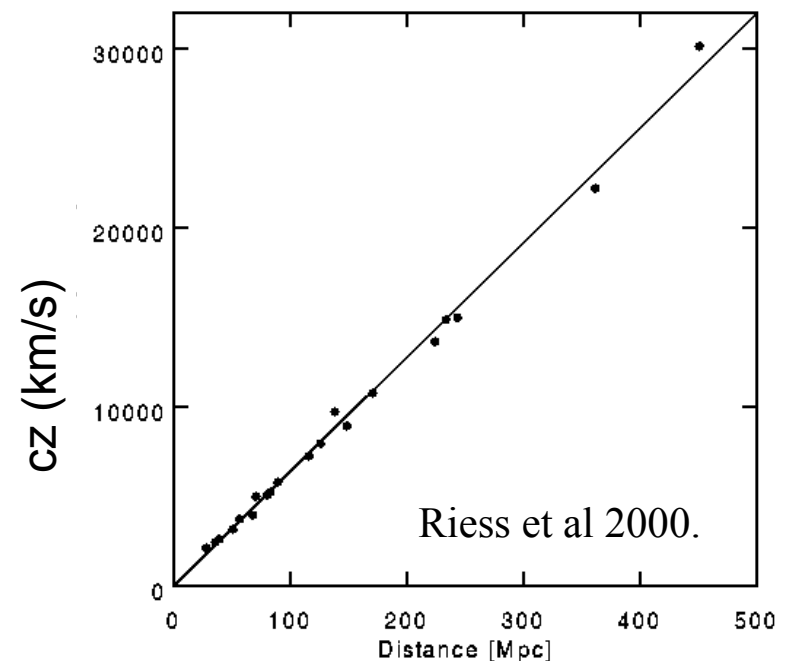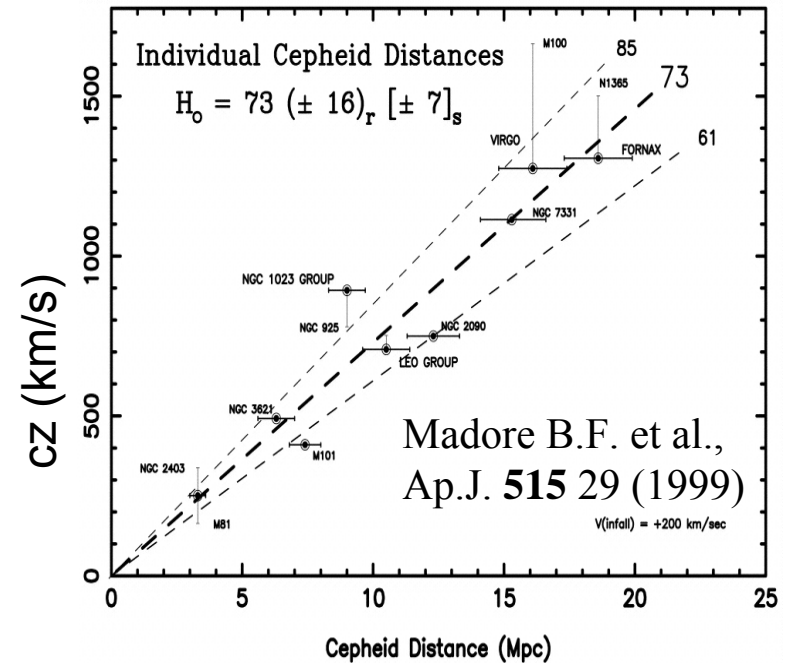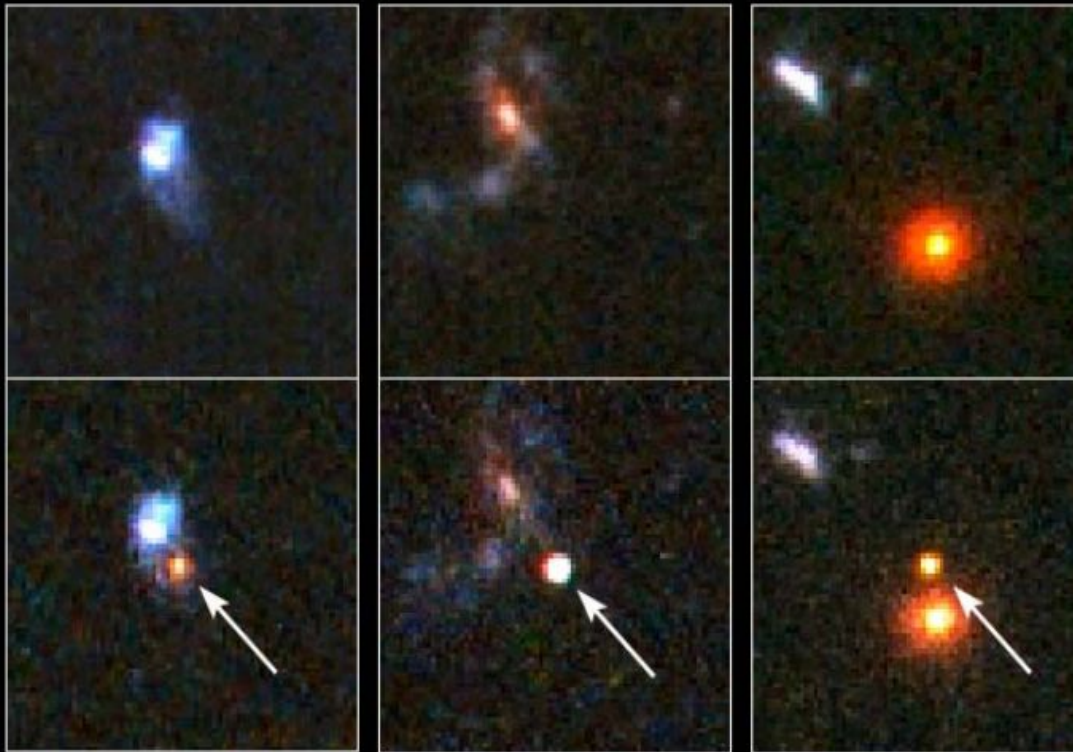
- The wavelengths of photons elongate in the same way as all other cosmological distances, following the same scale factor $a(t)$.

Observations of the recession of Galaxies:

- Measurements using standard candles (Cepheids, SN1a, …)
- $H_o \approx 75$ km s^{-1} Mpc^{-1}

Madore B.F. et al., Ap.J. **515** 29 (1999)
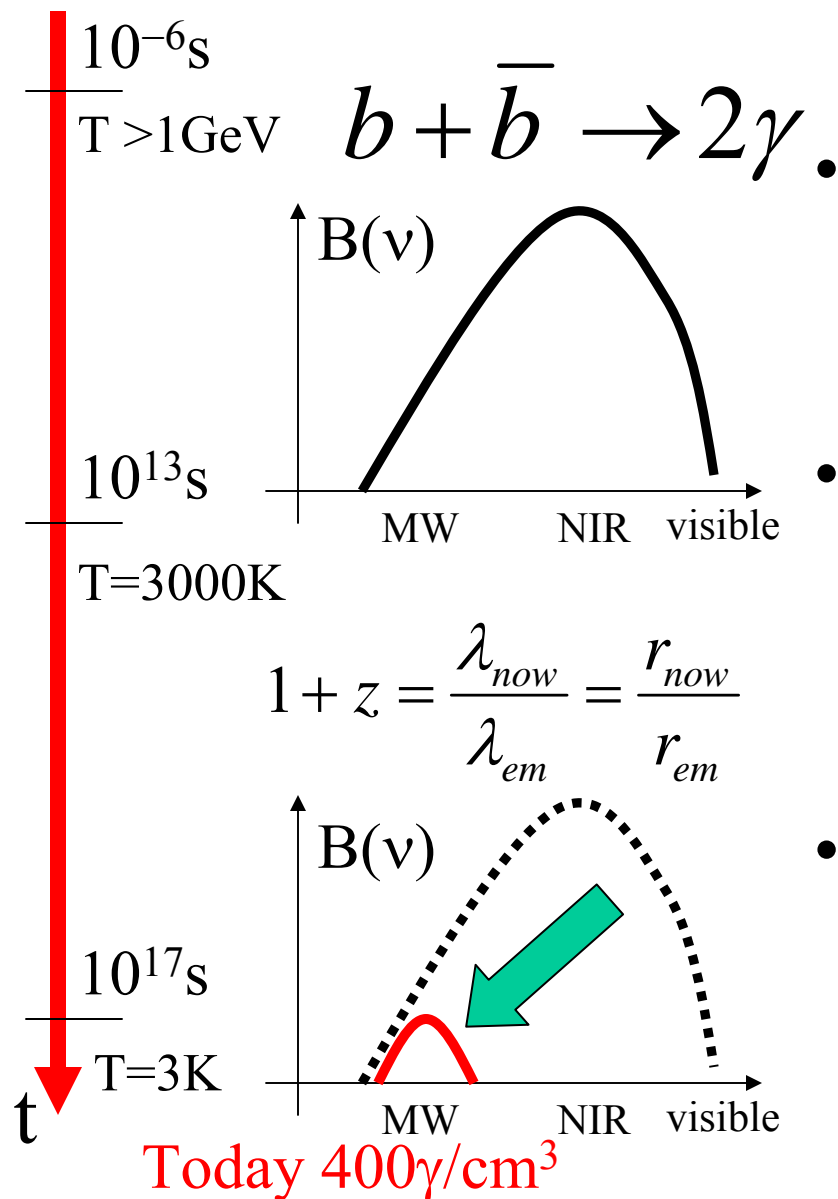

Riess et al 2000.

- **An isotropic expansion of the Universe.**

Primeval Fireball

- If the Universe is expanding, it was denser and hotter in the past .

- In the Early Universe, the temperature was high enough that nuclear reactions produced light elements starting from a plasma of particles (the primeval fireball).

- The observed primordial abundance of light elements can be produced only if an abundant background of photons is present (10^9 γ/baryon).

- This background should be observed today, redshifted in the micorwaves: the Cosmic Microwave Background.

What is the CMB

10^{-6}s

$T > 1\text{GeV}$ $b + \bar{b} \rightarrow 2\gamma$

$B(\nu)$

MW   NIR   visible

10^{13}s

$T = 3000\text{K}$

$$1 + z = \frac{\lambda_{now}}{\lambda_{em}} = \frac{r_{now}}{r_{em}}$$

$B(\nu)$

10^{17}s

$T = 3\text{K}$

t

MW   NIR   visible

Today $400\gamma/\text{cm}^3$

According to modern cosmology:

An abundant background of photons filling the Universe.

- **Generated** in the very early universe, less than 4 μs after the Big Bang ($10^9\gamma$ for each baryon) from a small $b - \bar{b}$ asymmetry

- **Thermalized** in the primeval fireball (in the first 380000 years after the big bang) by repeated scattering against free electrons

- **Redshifted** to microwave frequencies (z_{CMB}=1100) **and diluted** in the subsequent 14 Gyrs of expansion of the Universe (3K BB)

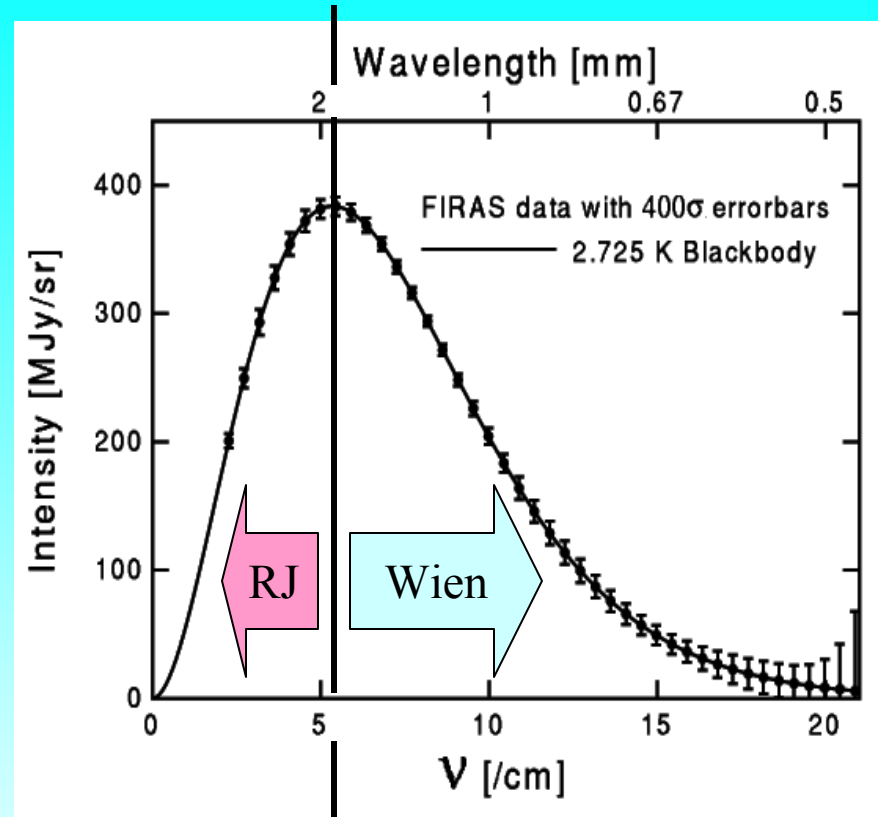## • The spectrum

$$B(v,T) = \frac{2h}{c^2} \frac{v^3}{e^x - 1}$$

$$T_{CMB} = 2.725K$$
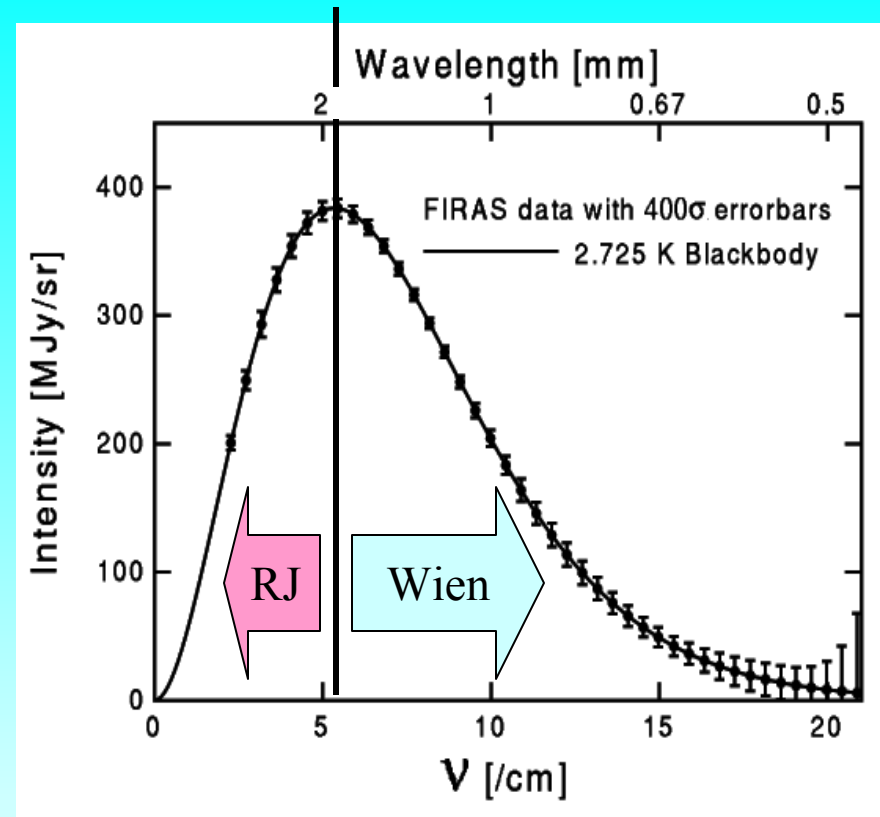
$$x_{CMB} = \frac{hv}{kT_{CMB}} \cong \frac{v}{56\,GHz}$$

Wavelength [mm]

FIRAS data with 400σ errorbars
— 2.725 K Blackbody

RJ   Wien

Intensity [MJy/sr]

v [/cm]

$$1 - e^{-x_{max}} = \frac{x_{max}}{3} \quad \Rightarrow x_{max} = 2.82 \quad \Rightarrow$$

$$v_{max} = 159\,GHz \quad (\sigma_{max} = 5.31\,cm^{-1})$$

$$B(v,T) = \frac{\lambda}{v} B(\lambda,T) \quad \Rightarrow \quad \lambda_{max} = 1.06\,mm$$

- **Techniques ?**

Wavelength [mm]

FIRAS data with 400σ errorbars

2.725 K Blackbody

RJ | Wien

$\nu << \nu_{max} = 160\,GHz \quad \Rightarrow \quad$ coherent detectors

$\nu >> \nu_{max} = 160\,GHz \quad \Rightarrow \quad$ bolometers

$\nu \approx \nu_{max} = 160\,GHz \quad \Rightarrow \quad$???

History: early days

- The infrared range has been *discovered* by astronomers!
  - Friedrich Wilhelm Herschel, using a prism and balckened bulb thermometers, detects the infrared section of the solar spectrum (calorific rays, 1800)

- The final demonstration that IR is also EM waves happens a bit later
  - Macedonio Melloni in 1829 develops the *thermomultiplier*, a sensitive IR detector. With this system he demonstrates that calorific rays have the same nature as light, also demonstrating that they have *polarization properties* exactly like light rays. He names the calorific rays "ultrared radiation".

- The first astronomical observation is carried out soon after:
  - IR radiation from the moon is detected by Charles Piazzi Smyth in Tenerife, using a *thermocouple*. He also shows that IR radiation is better detected at higher altitudes.
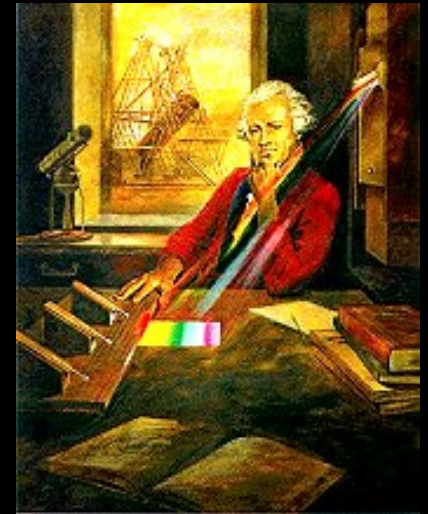
History: early days

- The first bolometers were developed for astronomy, and allowed the first IR spectroscopy of an astronomical source
  - Samuel Pierpoint Langley in 1878 develops the bolometer: a thin blackened platinum strip, sensitive enough to measure *the heat of a cow from a distance of ¼ mile*.
  - The detector works because the resistance of the Pt strip changes when heated by the absorbed radiation.
  - The detector is differential: 4 strips are placed in a Wheatstone bridge but only one is blackened and exposed to incoming radiation. Common-mode effects are rejected by the bridge and tiny variations of bolometer resistance can be measured.
- With his bolometer Langley is able to measure the IR spectrum of the sun, discovering atomic and molecular lines.
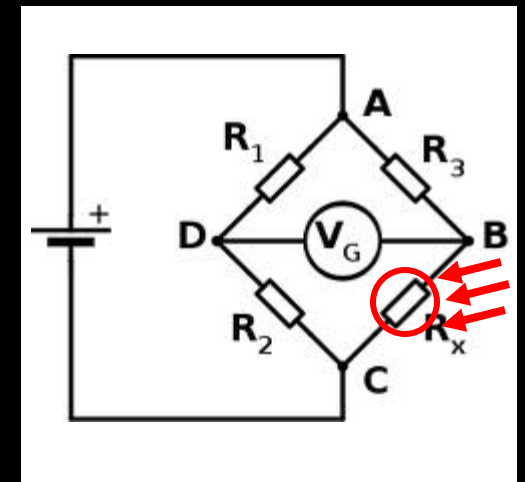
Old times

- ## Further developments:
    - 1915 : William Coblentz uses thermopiles (an improved version of Macedonio Melloni's detector !) to measure the infrared radiation from 110 stars, as well as from planets, such as Jupiter and Saturn, and several nebulae.
    - 1920's : systematic IR observations with vacuum thermopiles (Seth B. Nicholson, Edison Pettit and others): diameters of giant stars
    - 1948: IR observations show that the moon is covered by dust.
    - 1950s: Lead Sulphide photodetectors – Johnson's star photometry
    - First Semiconductor bolometers, slicing carbon resistors to make the thermistor (W. S. Boyle and K. F. Rodgers, J . Opt . Soc . Am . 49 :66 (1959))

One generation ago

- ## The revolution :
  - 1961: Franck J. Low develops the first *cryogenic* Ge bolometer, boosting the sensitivity by orders of magnitude.
  - 1960's and ff. bolometers and semiconductors detectors with their telescopes are carried to space using stratospheric balloons and rockets.

- ## Consequence:
  - First sky surveys @ λ 100 μm
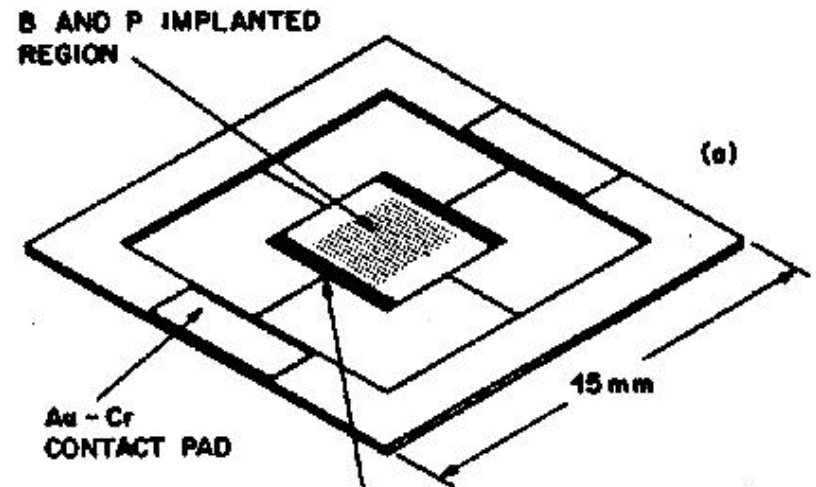 - 1968 First IR ground based large area sky survey (2 μm, from Mt. Wilson)
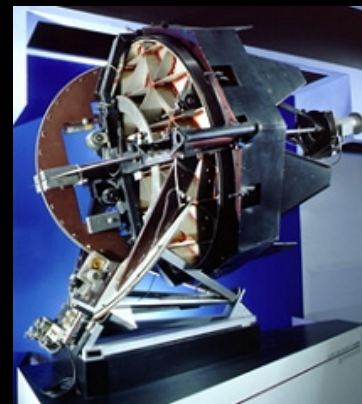
Few decades ago

- mm-wave bolometers
  - cooled at 1.5K or 0.3K
  - operating from space
- become sensitive enough to measure the finest details of the Cosmic Microwave Background.

- Breakthrough:
  - The composite bolometer (absorber and thermistor separated and each optimized independently): N. Coron, P. Richards …

Ga:Ge Thermometer
attached with epoxy

Sapphire
Substrate

Brass Wire

Nylon Threads

Bi Absorber
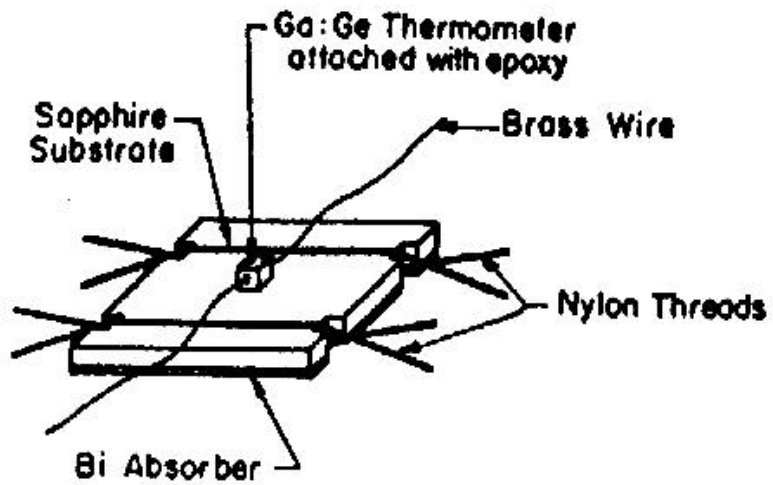
Circa 1970

**Composite
Bolometer
(Coron, Richards …)**

B AND P IMPLANTED
REGION

(a)

15 mm

Au ~ Cr
CONTACT PAD

Circa 1980

**monolitic
bolometer
(Goddard, ..)**

Bi FILM

As IMPLANTED
AREA

(b)

75 μ WIDE
Si THREAD

IMPLANTED
THERMOMETER
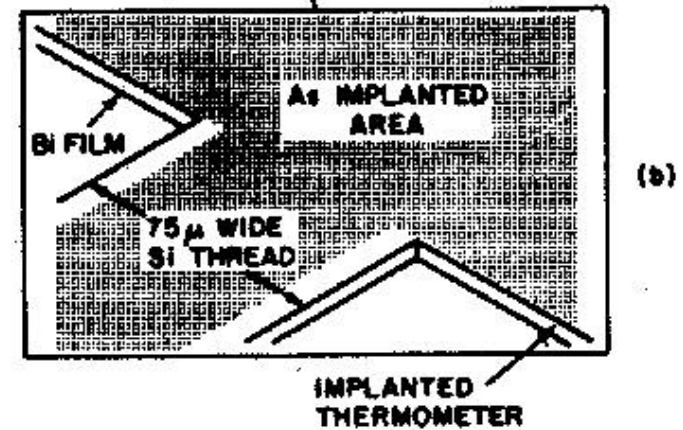
Arno Penzias and Robert Wilson (1965):
We get microwaves isotropically from every direction of the sky. It's the Cosmic Microwave Background.
Nobel Prize in Physics, 1977

© 2004 Pearson Education, publishing as Addison Wesley.

F. Melchiorri (high mountain, 1974), ….
P. Richards et al. (balloon, 1980) … and then John Mather et al. (1992) with the FIRAS on the COBE satellite: these microwaves have **exactly** a blackbody spectrum
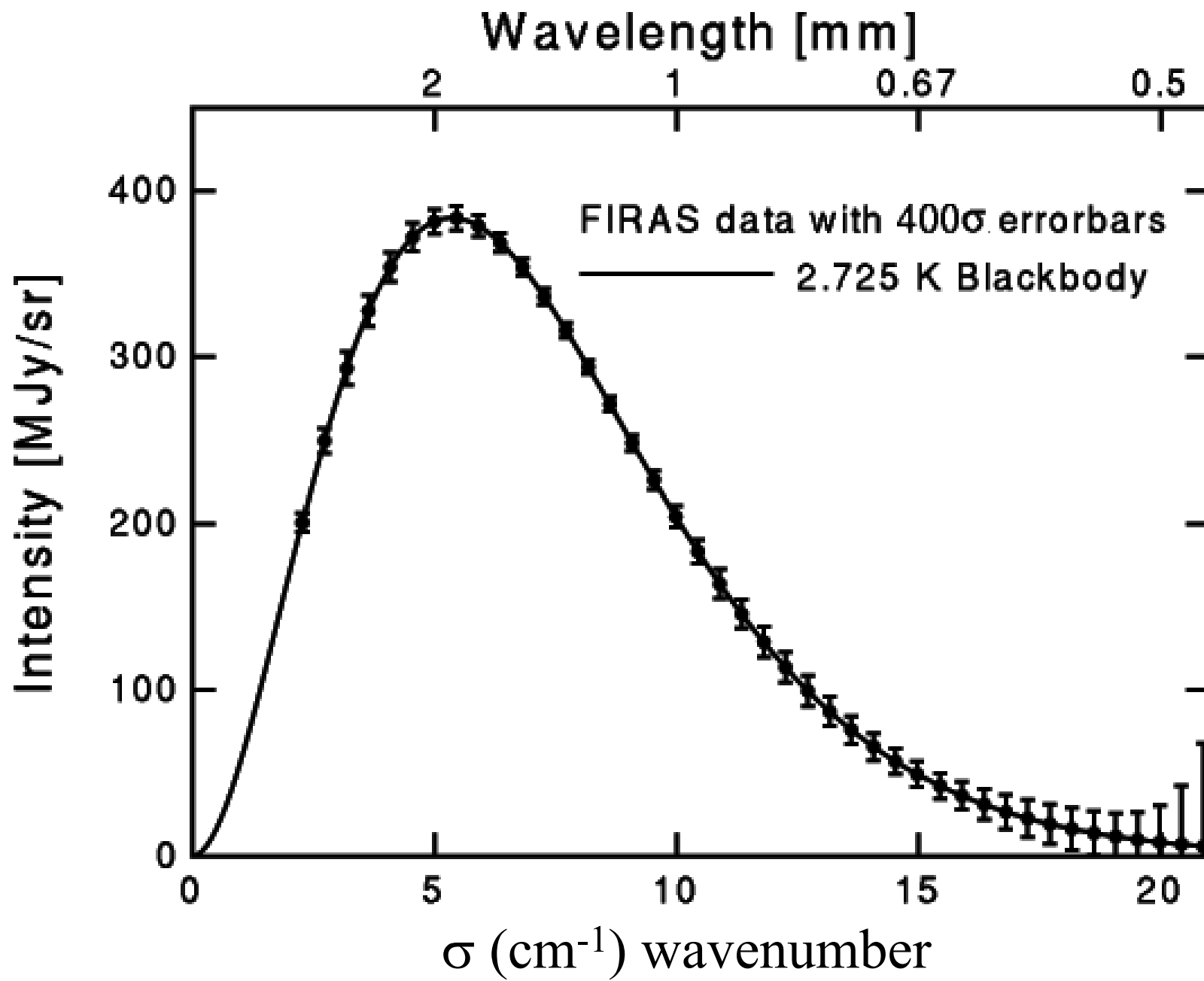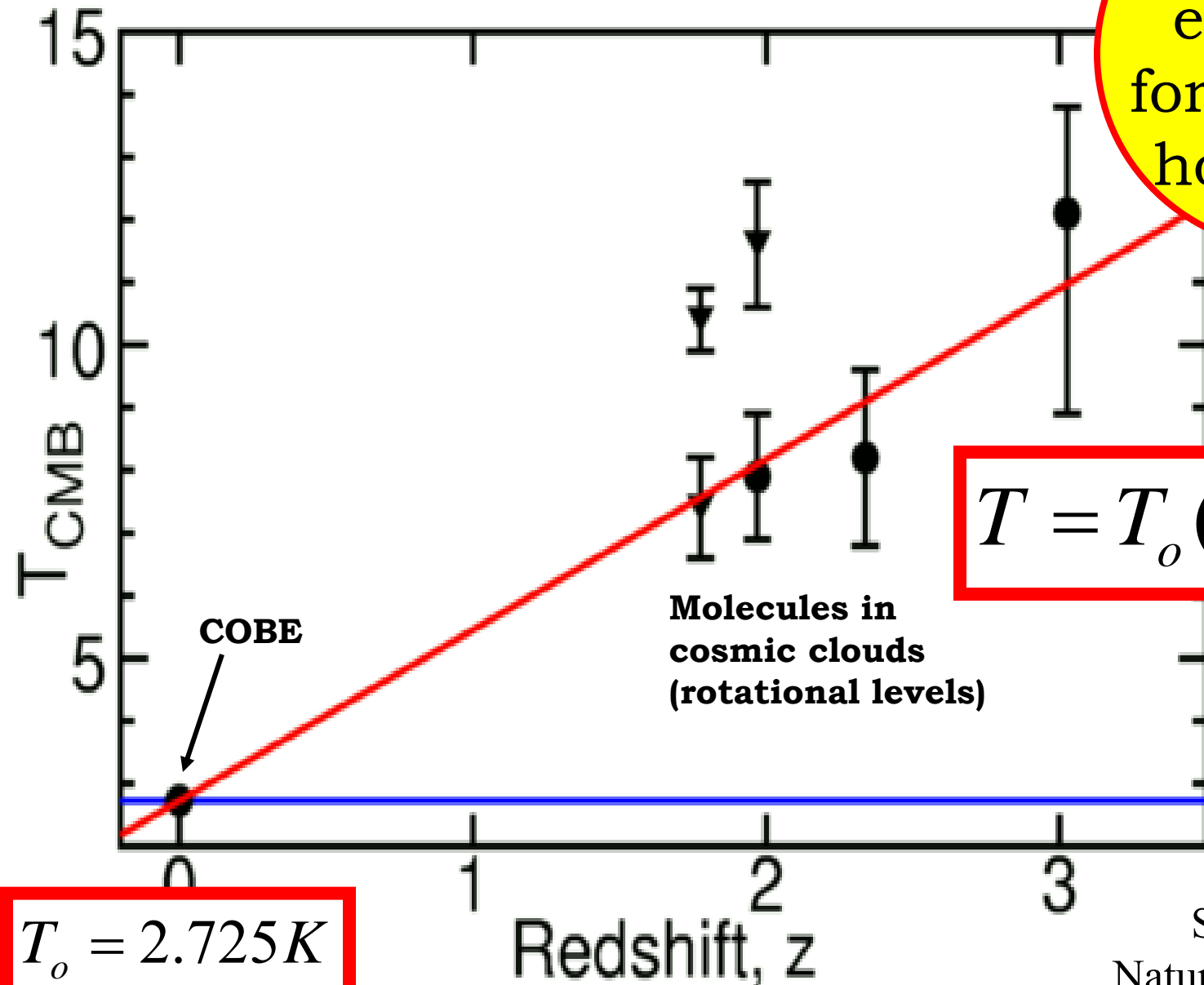
Nobel Prize in Physics, 2006

Wavelength [mm]

FIRAS data with 400σ errorbars
— 2.725 K Blackbody
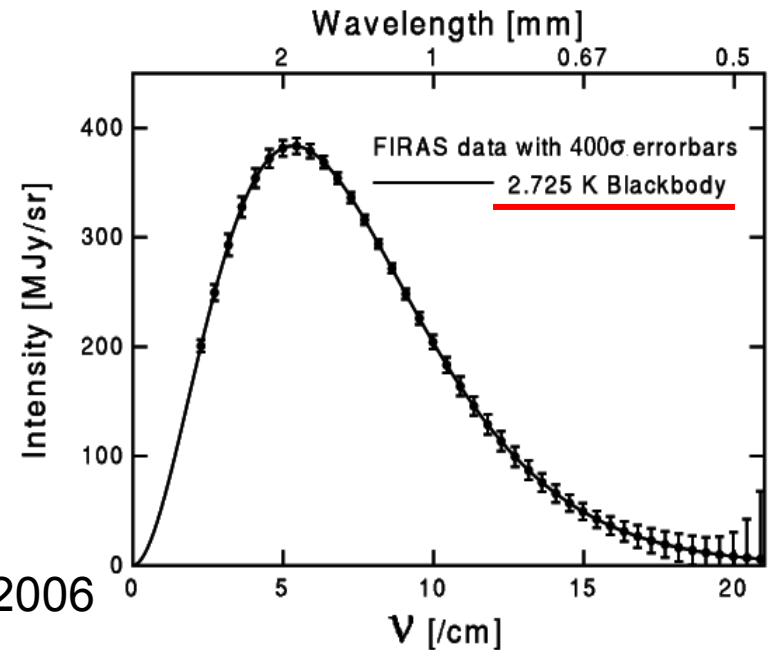
COBE-FIRAS

- COBE-FIRAS was a Martin-Puplett Fourier-Transform Spectrometer with composite bolometers. It was placed in a 400 km orbit.

- A zero instrument comparing the specific sky brightness to the brightness of a cryogenic Blackbody

- The output was nulled (within detector noise) for T_{ref}=2.725 K

- The brightness of empty sky is a blackbody at the same temperature !

- The early universe was in thermal equilibrium at high Temperature.

Det_LL

Det_RL

Det_LH

Sky Horn

DICHROICS

FL

EL

PL

Det_RH

CL

Dihedral L

ER

ML

ICAL

FR

PR

B

Reference Horn

A

Mirror Mechanism

MR

Dihedral R

CR

XCAL

Sky

Movable Black Calibrator

Movable Mirror

To Detectors

Beamsplitter

Reference Input Black Body

Movable Mirror

To Detectors
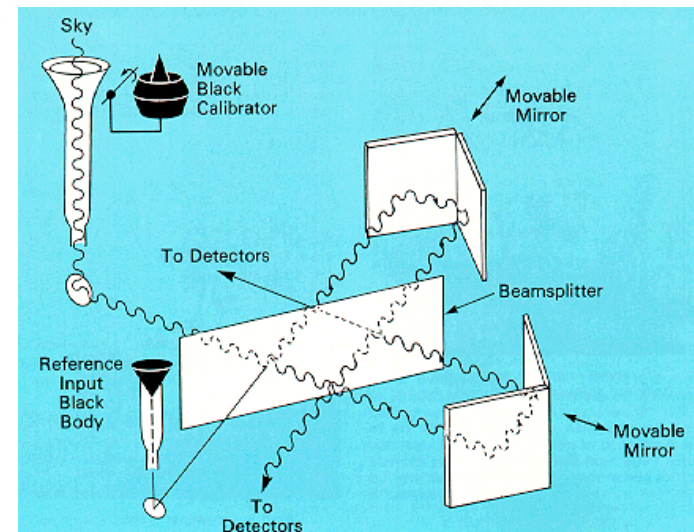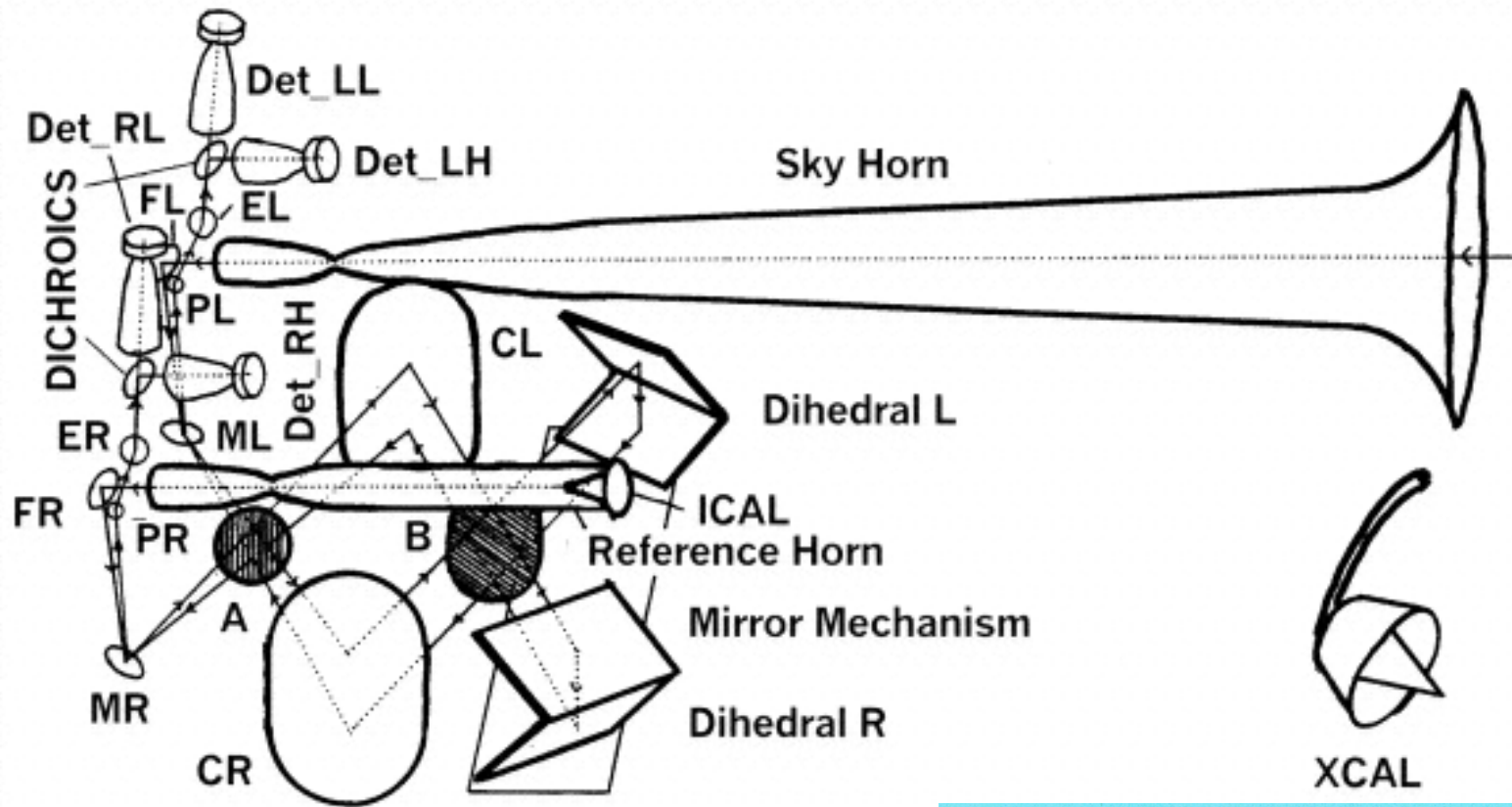
Primeval Fireball

Additional evidence for an early hot phase

$T = T_o(1 + z)$

COBE

Molecules in cosmic clouds (rotational levels)

$T_o = 2.725K$

Srinand et al.
Nature 408 931 (2000)

T_{CMB}

Redshift, z

Two decades ago

- The spider-web absorber is developed
  - It minimizes the heat capacity of the absorber
  - It minimizes the cross-section to cosmic rays, while maintaining high cross-section for mm-waves

Spider-Web Bolometers

- The absorber is micro machined as a web of metallized Si_3N_4 wires, 2 µm thick, with 0.1 mm pitch.

- This is a good absorber for mm-wave photons and features a very low cross section for cosmic rays. Also, the heat capacity is reduced by a large factor with respect to the solid absorber.

- NEP ~ 2×10^{-17} W/Hz$^{0.5}$ is achieved @0.3K

- $150\mu K_{CMB}$ in 1 s

- Mauskopf *et al.* Appl.Opt. **36**, 765-771, (1997)

Built by JPL

Signal wire

Absorber

Thermistor

2 mm
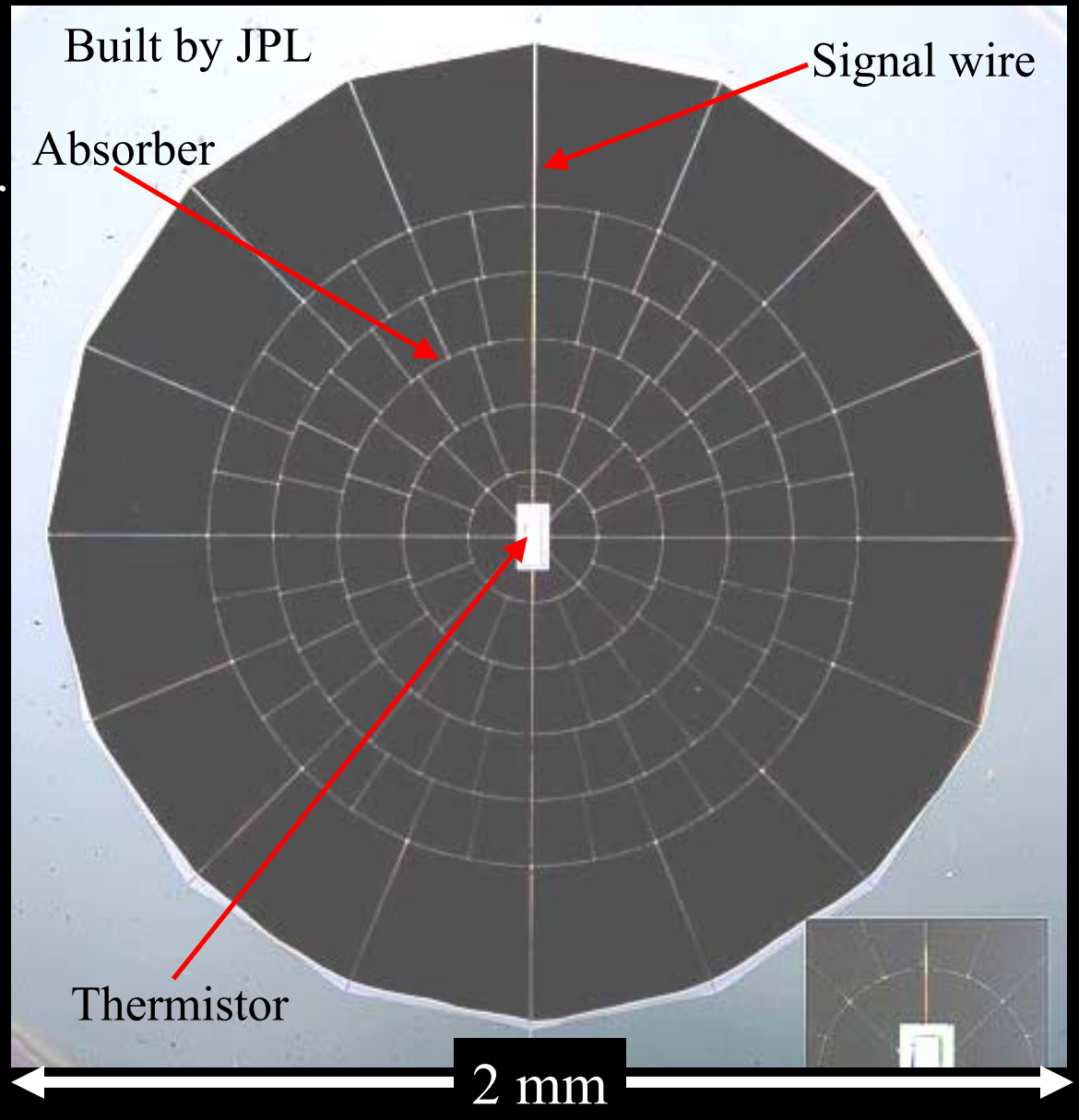
Development of thermal detectors for far IR and mm-waves

time required to make a measurement (seconds)

10^{17}

●Langley's bolometer

●Golay Cell

10^{12} ●Golay Cell

●Boyle and Rodgers bolometer

1year ●F.J.Low's cryogenic bolometer

10^7

●Composite bolometer

1day

1 hour ●Composite bolometer at 0.3K

10^2

1 second ●Spider web bolometer at 0.3K

●Spider web bolometer at 0.1K

Photon noise limit for the CMB

year

1900   1920   1940   1960   1980   2000   2020   2040   2060

Table 5.   In-flight bolometer performance

ν_0 (GHz)	τ (ms)	η_{opt}	G (pW K^{-1})	R (MΩ)	NEP (1 Hz) (10^{-17} W/$\sqrt{\text{Hz}}$)	NET$_{CMB}$ (μK$\sqrt{\text{s}}$)
90	22	0.30	82	5.5	3.2	140
150sm	12.1	0.16	85	5.9	4.2	140
150mm	15.7	0.10	88	5.5	4.0	190
240	8.9	0.07	190	5.7	5.7	210
410	5.7	0.07	445	5.4	12.1	2700

Note. — In-flight bolometer performance. The 150 GHz channels are divided into single mode (150sm) and multimode(150mm). The optical efficiency of the channels decreased significantly from the measured efficiency of each feed structure due to truncation by the Lyot stop. The NEP is that measured in flight, and includes contributions from detector noise, amplifier noise, and photon shot noise.

Crill et al., 2003 – BOOMERanG 1998 bolometers, 300 mK
The same kind of bolometer is used now in Planck @100mK

Measured performance of Planck HFI bolometers **(0.1K)**
(Holmes et al., Appl. Optics, **47**, 5997, 2008)

Multi-moded

= Photon noise limit

NEP attoW/Hz$^{1/2}$

857GHz

100

100GHz   143GHz   217GHz   353GHz   545GHz

10

P   P   P   P
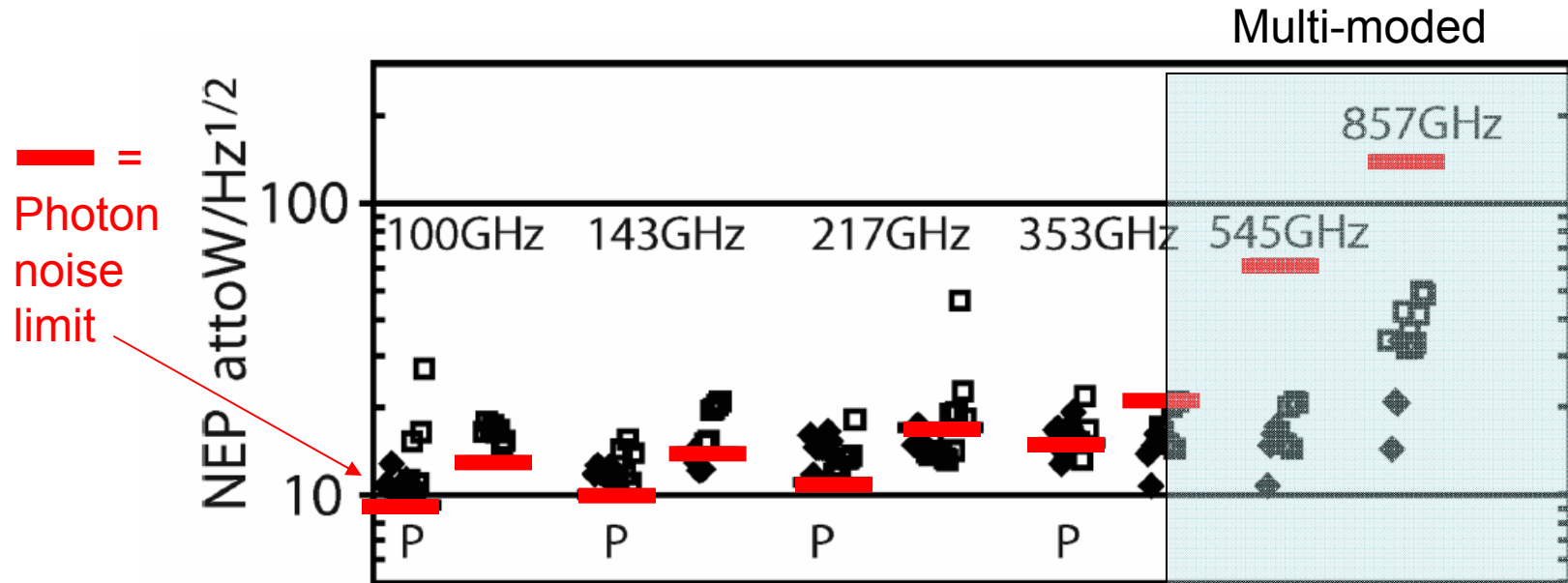
Fig. 1. Measured detector dark NEP including $6.5\,\mathrm{nV}/\sqrt{\mathrm{Hz}}$ amplifier noise at nominal bias for each frequency band. Solid symbols are the NEP for detectors installed in the focal plane. The open symbols are the NEP spare bolometers. The solid lines indicate the photon background limit from a 35 K telescope and astrophysical sources in each band for a 30% bandwidth and 30% in band optical efficiency. Unpolarized detectors at 100 GHz were made and delivered but were replaced by polarized detectors.

- This detector is sensitive enough to allow the detailed measurement of fluctuations in the otherwise isotropic cosmic microwave background

- These are linked to the fluctuations of the homogeneous isotropic model.

- They provide a new way to study structure formation, geometry and composition of the universe.

Perturbations

- Additional cosmological evidence comes from the study of perturbations of the homogeneous isotropic FRW metric.
- The hierarchy of structures (stars, galaxies, clusters of galaxies, superclusters…) in the visible universe marks important deviations from uniformity in the present universe.
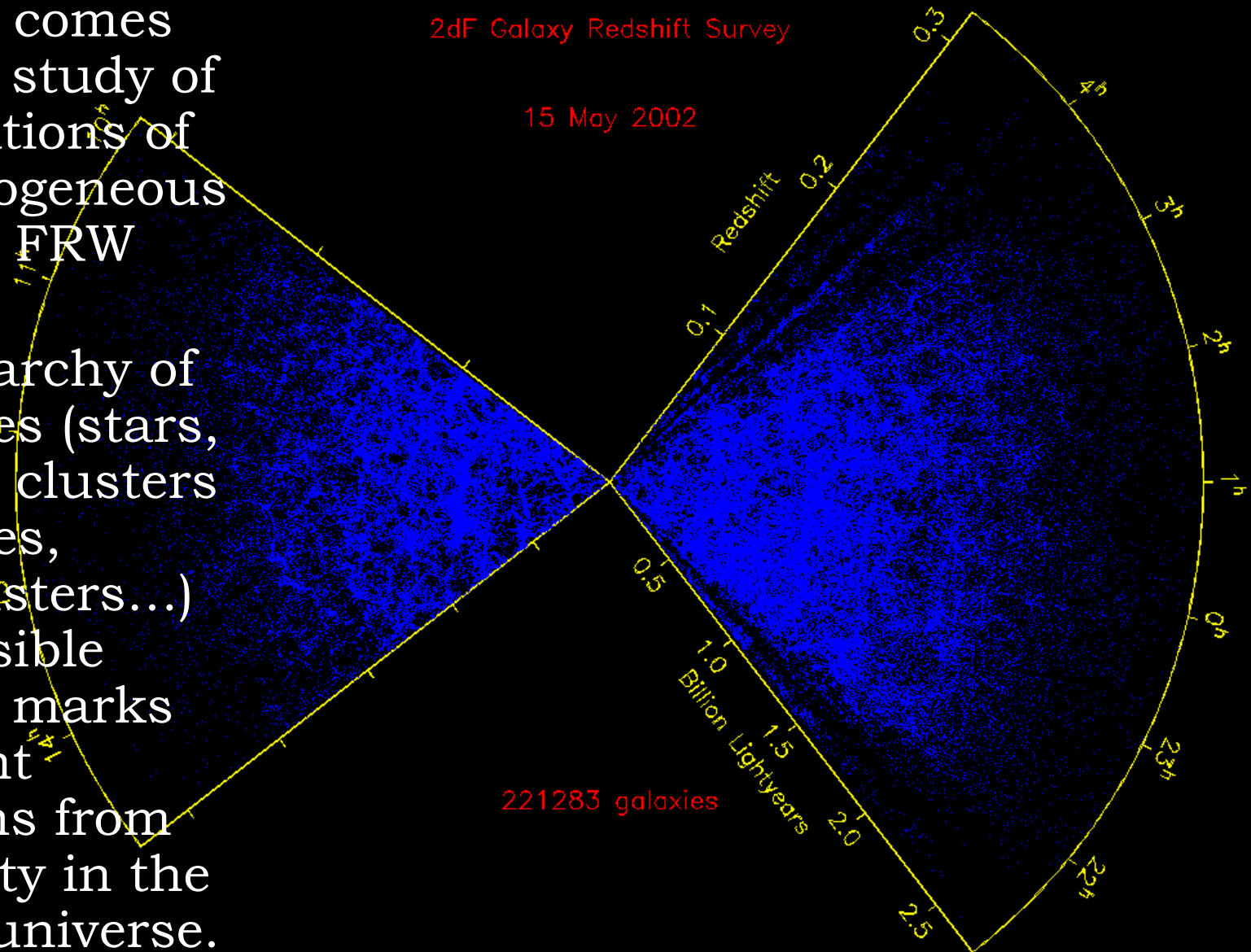
2dF Galaxy Redshift Survey

15 May 2002

221283 galaxies

Redshift

0.1
0.2
0.3

0.5
1.0
1.5
2.0
2.5
Billion Lightyears

- We believe that structures in the Universe derive from tiny density perturbations of the Primeval Fireball.
- These grow, under gravitational instability.
- In an expanding universe the growth is very slow.

Perturbation Theory

- Random Gaussian field:

$$\rho(\bar{x},t) = \rho(t)\left[1 + \delta(\bar{x},t)\right]$$
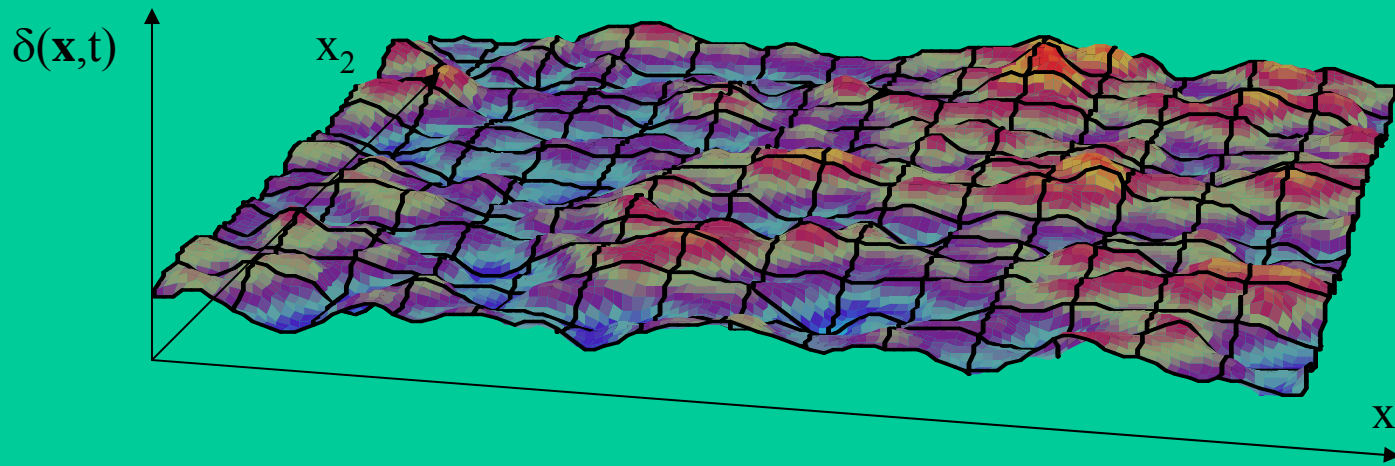
- Fourier Transform:

$$\delta(\bar{x},t) = \int \frac{d^3k}{8\pi}\,\delta_k(t)e^{i\bar{k}\cdot\bar{x}}$$

- Power Spectrum:

$$P(k) = \left\langle \left|\delta_k\right|^2 \right\rangle$$

Perturbation Theory

- Compute :
  - The response of the Primeval Plasma of photons, baryons and dark matter, to a primordial spectrum of density perturbations
  - The resulting **Anisotropy** of the Cosmic Microwave Background
  - The growth of structures and the development of the **Large Scale Structure** of the Universe

- Initial conditions:

$$P(k) = Ak^n$$

  either
  - Adiabatic :

$$\frac{\delta n_b}{n_b} = \frac{\delta n_{DM}}{n_{DM}} = \frac{\delta n_\gamma}{n_\gamma} \rightarrow \frac{\delta \rho_b}{\rho_b} = \frac{\delta \rho_{DM}}{\rho_{DM}} = \frac{4}{3}\frac{\delta \rho_\gamma}{\rho_\gamma} \rightarrow \frac{\delta \rho}{\rho} \neq 0$$

  or
  - Isocurvature :

$$\frac{\delta n_{DM}}{n_{DM}} \neq \frac{\delta n_\gamma}{n_\gamma} \quad ; \quad \frac{\delta \rho_b}{\rho_b} = 0 \quad ; \quad \frac{\delta \rho}{\rho} = 0$$

  or a mixture of the two ?

CMB anisotropy

- Different physical effects, all related to $\delta\rho/\rho$, produce CMB Temperature fluctuations:

$$\frac{\delta T}{T} = \frac{1}{3}\frac{\delta\varphi}{c^2} + \frac{1}{4}\frac{\delta\rho_\gamma}{\rho_\gamma} - \frac{\vec{v}}{c}\cdot\vec{n}$$

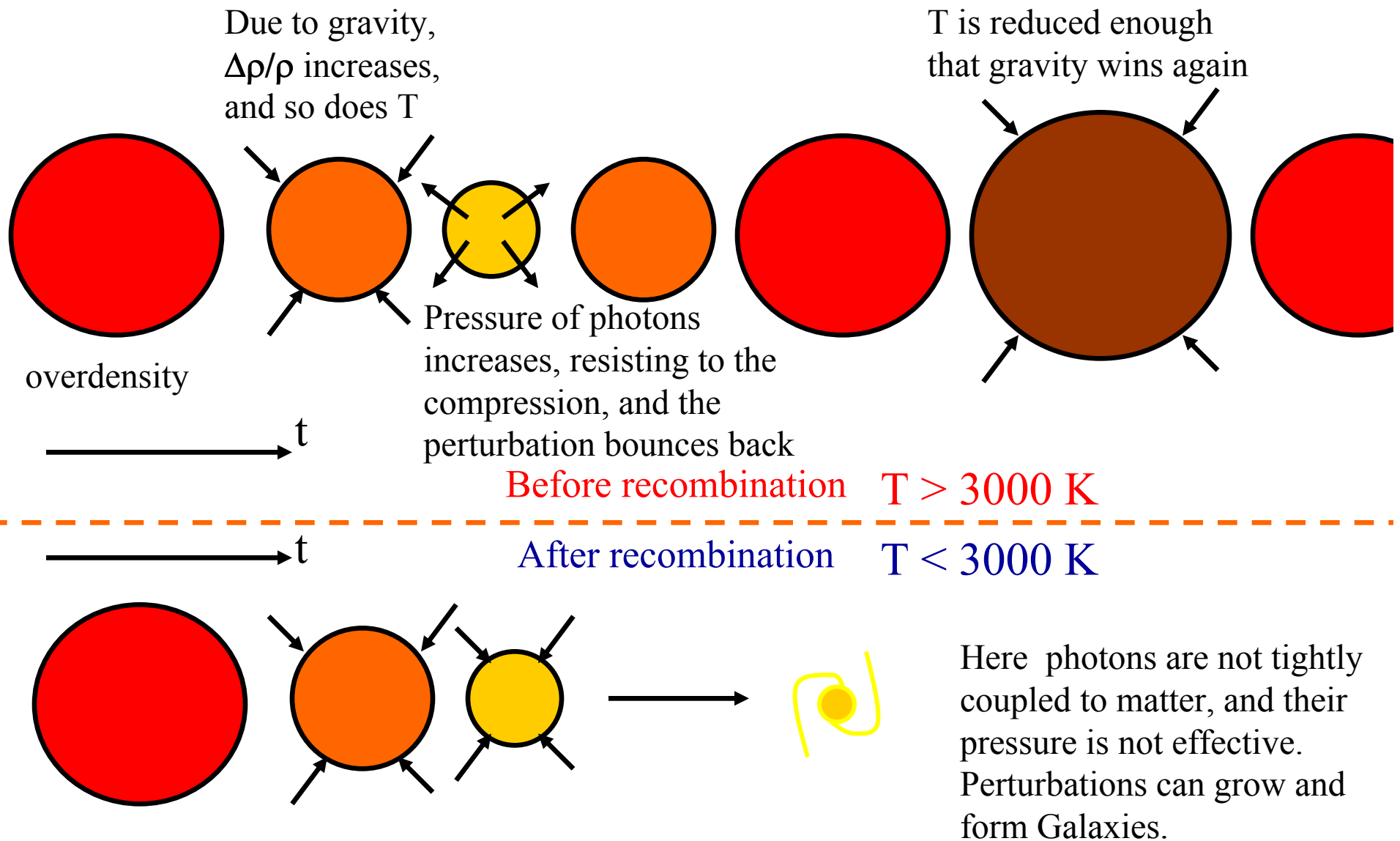Sachs-Wolfe (gravitational redshift)   Photon density fluctuations   Doppler effect from velocity fields

- Scales larger than the horizon are basically frozen in the pre-recombination era.
- If the power spectrum P(k) is scale-invariant (P(k)=Ak), a characteristic power spectrum of $\delta T/T$ is produced at large scales: $c_\ell \approx 1/[\ell(\ell+1)]$
- This has been detected in 1992 by COBE DMR

- Photons coming out of an overdensity loose some energy due to the gravitational potential gradient they have to climb (gravitational redshift):

$$\frac{\delta T}{T} = \frac{\delta \nu}{\nu} = \frac{\delta \Phi}{c^2}$$

- However, the same overdensity also produces a time delay, so these photons effetively come from an earlier epoch with respect to surrounding ones:

$$\frac{\delta t}{t} = \frac{\delta \Phi}{c^2}$$

- During matter domination

$$a \propto t^{2/3} \quad ; \quad T \propto 1/a \quad \rightarrow \quad \frac{\delta T}{T} = -\frac{\delta a}{a} = -\frac{2}{3}\frac{\delta t}{t} = -\frac{2}{3}\frac{\delta \Phi}{c^2}$$

- The sum of the two effects is called the Sachs-Wolfe (1967) effect, dominant at large angular scales

$$\frac{\delta T}{T} = \frac{1}{3}\frac{\delta \Phi}{c^2}$$

Large-Scale Anisotropy

- **1992**: COBE-DMR detects the small (10ppm) large-scale anisotropy of the CMB.

- The measured spectrum requires a scale invariant P(k) (n=1)

- Its incredible smoothness requires an inflationary process happening in the first split second after the Big Bang.

31.5 GHz

53 GHz

90 GHz

$-100\ \mu K$ ▮▮▮ $+100\ \mu K$

G. Smoot et al. 1992

$$\Delta T(\theta, \varphi) = \sum_{\ell, m} a_{\ell m} Y_\ell^m (\theta, \varphi)$$

$$c_\ell = \left\langle a_{\ell m}^2 \right\rangle$$

$$\left\langle \Delta T^2 \right\rangle = \frac{1}{4\pi} \sum_\ell (2\ell + 1) c_\ell$$

c_ℓ

I(I+1)c/2π (μK²)
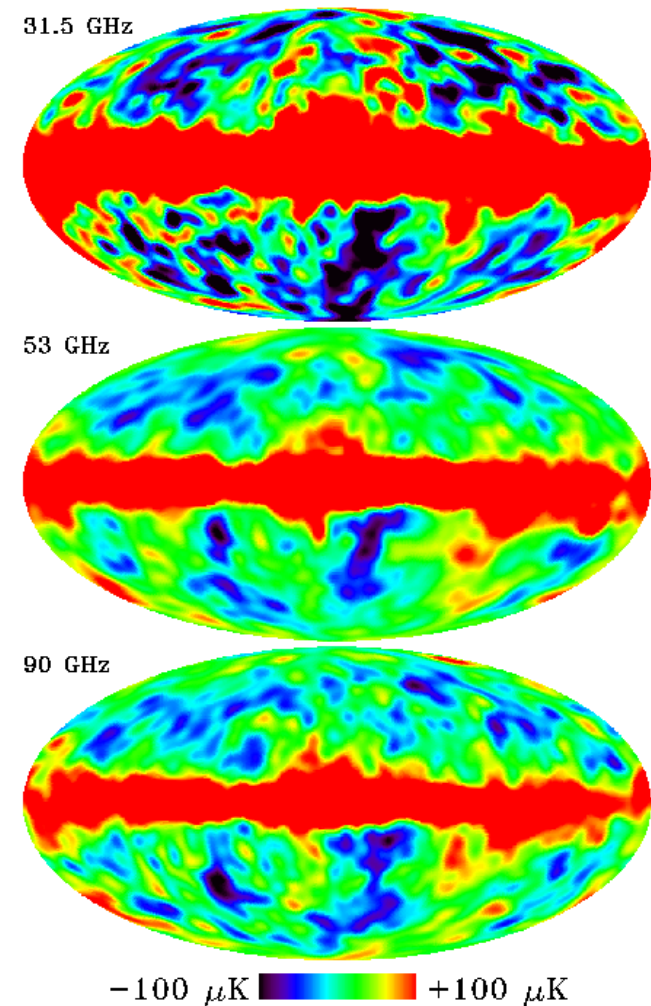
multipole I

- The **rms anisotropy** has contributions from many angular scales
- The **angular power spectrum** c_ℓ of the anisotropy defines the contribution to the rms from the different multipoles
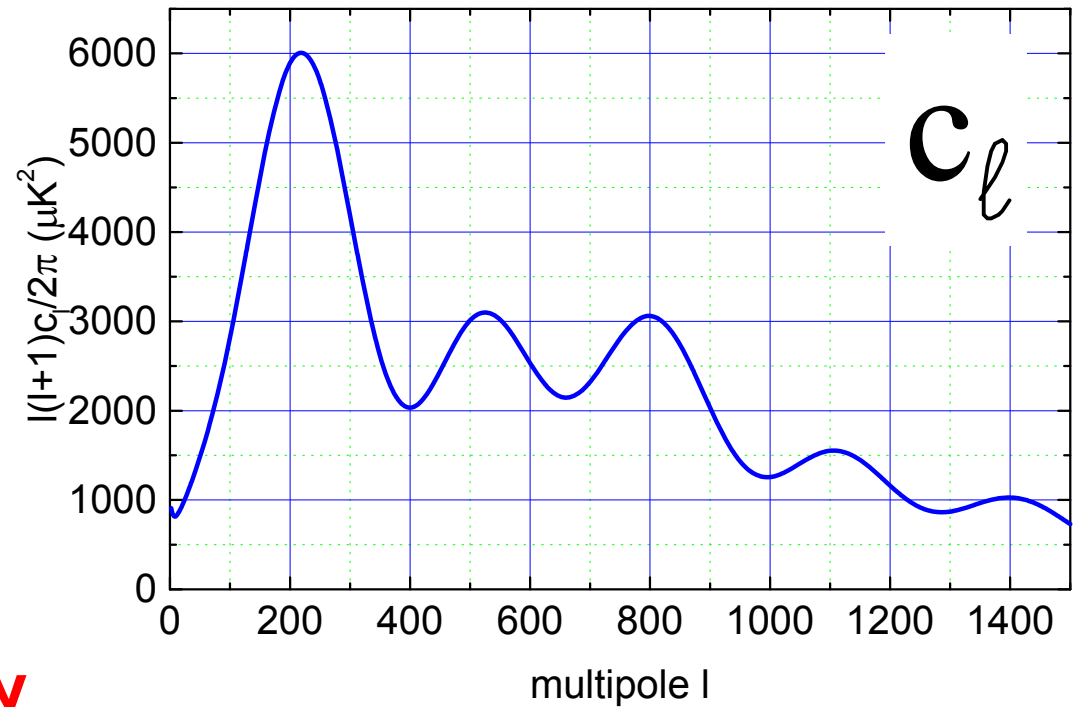
Why this way ?

Horizons

- At recombination (t=380000 years), only regions of the Universe closer than 380000 light years have had the possibility (enough time) to interact.

- That length, as seen from a distance of >10 billion light years, has an angular size of about 1 degree.

14 000 000 000 ly

1°

1°

10°

T₁

T₂

380000 ly

380000 ly
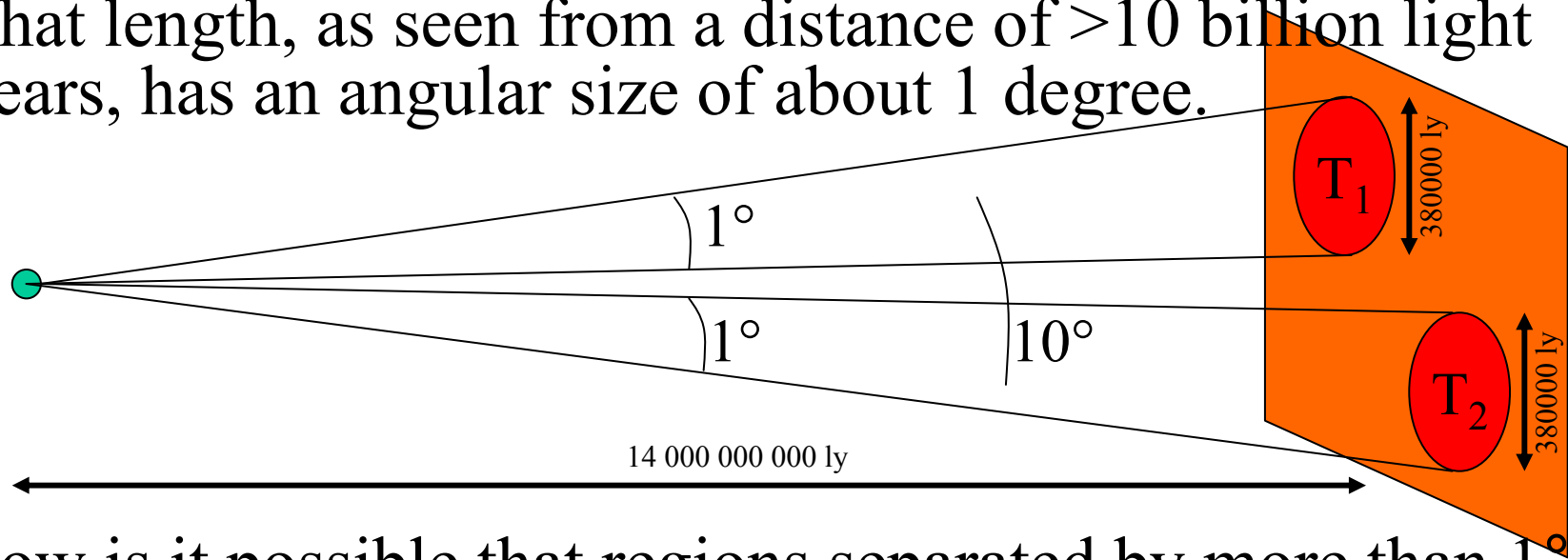
- How is it possible that regions separated by more than 1° are seen in the COBE map to have the same temperature, within 1 part in 10000 ? They could not interact in all the history of the Universe, from the Big Bang to recombination ! (the "Paradox of Horizons")

Inflation ?

- At recombination, the causal horizon ct subtends an angle of about 1°.

- In the original Hot Big Bang scenario, regions separated by more than 1° are not causally connected, and have not been causally connected before.

- They are, however, highly isotropic. How can this be ?

- Idea: an ultrafast **inflation** of space, happening at around the grand-unification energy, can separate regions that had been in causal contact before. All the sky we can see today has been in causal contact in a microscopic region before inflation.

- Can we test inflation experimentally ?

Inflation ?

- Inflation is a predictive theory:

  1. Any initial curvature is flattened by the huge expansion: we expect a Euclidean universe.
  2. Adiabatic, gaussian density perturbations are produced from quantum fluctuations. This is the physical origin for density fluctuation.
  3. The power spectrum of scalar perturbations is approximately scale invariant, $P(k)=Ak^n$ with n slightly less than 1.
  4. Tensor perturbations produce a background of gravitational waves, inducing a characteristic polarization pattern in the CMB

- 1,2,3 can be tested measuring CMB anisotropy
- 4 can be tested measuring CMB polarization

CMB anisotropy

- Different physical effects, all related to $\delta\rho/\rho$, produce CMB Temperature fluctuations:

$$\frac{\delta T}{T} = \frac{1}{3}\frac{\delta\varphi}{c^2} + \frac{1}{4}\frac{\delta\rho_\gamma}{\rho_\gamma} - \frac{\vec{v}}{c}\cdot\vec{n}$$

Sachs-Wolfe (gravitational redshift)   Photon density fluctuations   Doppler effect from velocity fields

- Scales larger than the horizon are basically frozen in the pre-recombination era. Flat power spectrum of $\delta T/T$ at large scales.

- Scales smaller than the horizon undergo acoustic oscillations from horizon-crossing to recombination. Acoustic peaks in the power spectrum of $\delta T/T$ at sub-degree scales.

Density perturbations (Δρ/ρ) were **oscillating** in the primeval plasma (as a result of the opposite effects of gravity and photon pressure).

Due to gravity,
Δρ/ρ increases,
and so does T

T is reduced enough
that gravity wins again

overdensity

Pressure of photons
increases, resisting to the
compression, and the
perturbation bounces back

Before recombination   T > 3000 K

After recombination   T < 3000 K

Here photons are not tightly
coupled to matter, and their
pressure is not effective.
Perturbations can grow and
form Galaxies.

After recombination, density perturbation can **grow** and create the hierarchy of structures we see in the nearby Universe.

In the primeval plasma, photons/baryons density perturbations start to oscillate only when the sound horizon becomes larger than their linear size . Small wavelength perturbations oscillate faster than large ones.
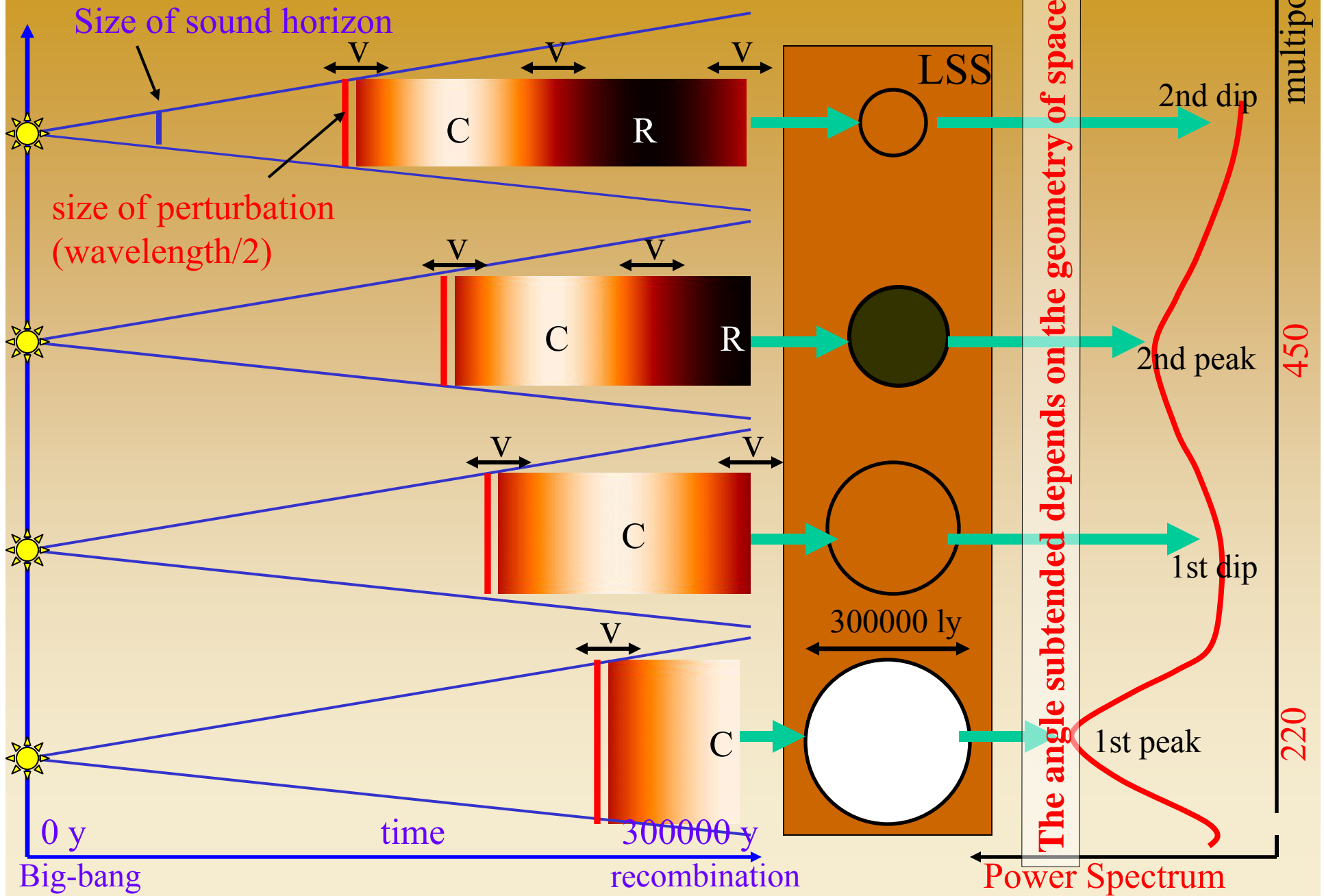
Size of sound horizon

size of perturbation (wavelength/2)

V   V   V

C   R

LSS

2nd dip

V   V

C   R

2nd peak

V   V

C

1st dip

V

C

300000 ly

1st peak

multipole

450

220

The angle subtended depends on the geometry of space

0 y   time   300000 y

Big-bang   recombination   Power Spectrum

USE THE SLIDERS TO MATCH THE **BLUE LINE** TO THE **RED LINE**

CMB Analyzer
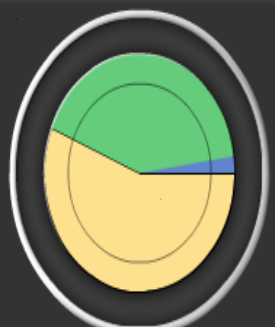
Universe Content

Atoms
4 %

Cold Dark Matter
22 %

Dark Energy
74 %

Additional Properties

Hubble Constant
73

Reionization redshift
11

Spectral Index
0.95

Answer Button:

I Give Up!

No! Don't give up yet! Play some more...

or... if you must:

Set the model components to the WMAP values.
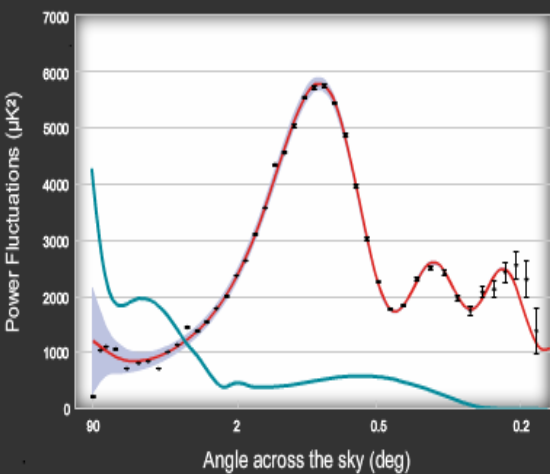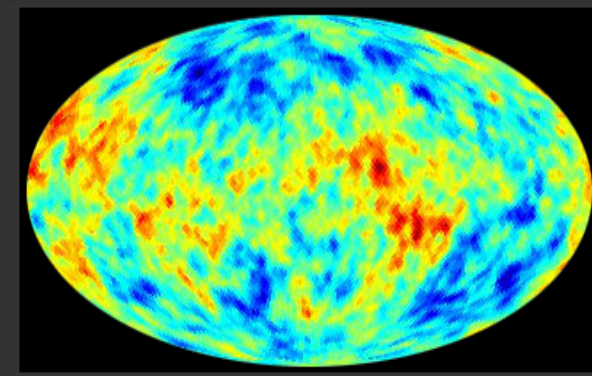
Age: 13.7 billion years

Flatness: 1.00

ANSWER   RESET

LSS

14 Gly

1° Critical density Universe Ω=1

horizon

Ω>1

2°
High density Universe

horizon

0.5°
Low density Universe Ω<1

horizon
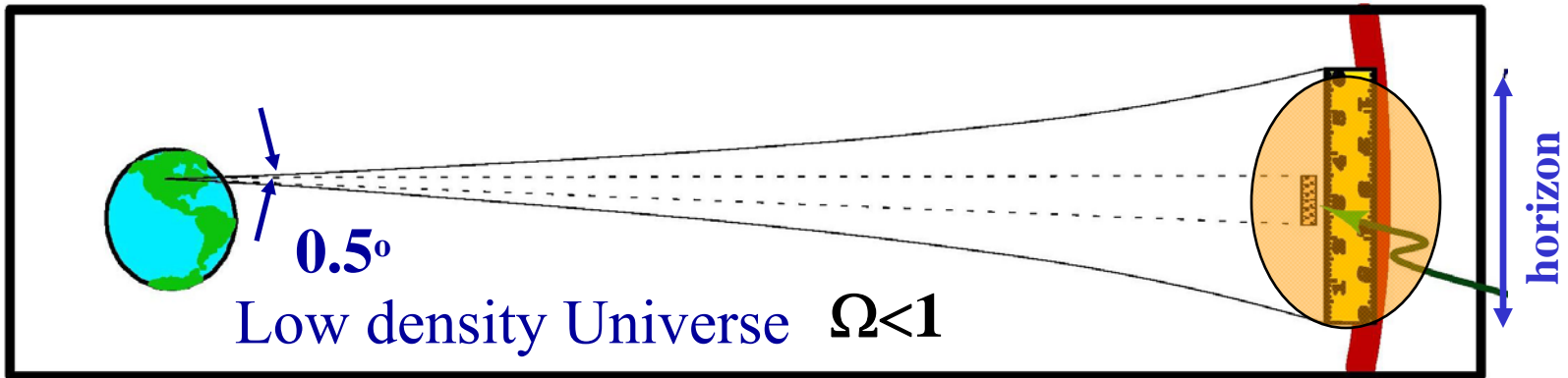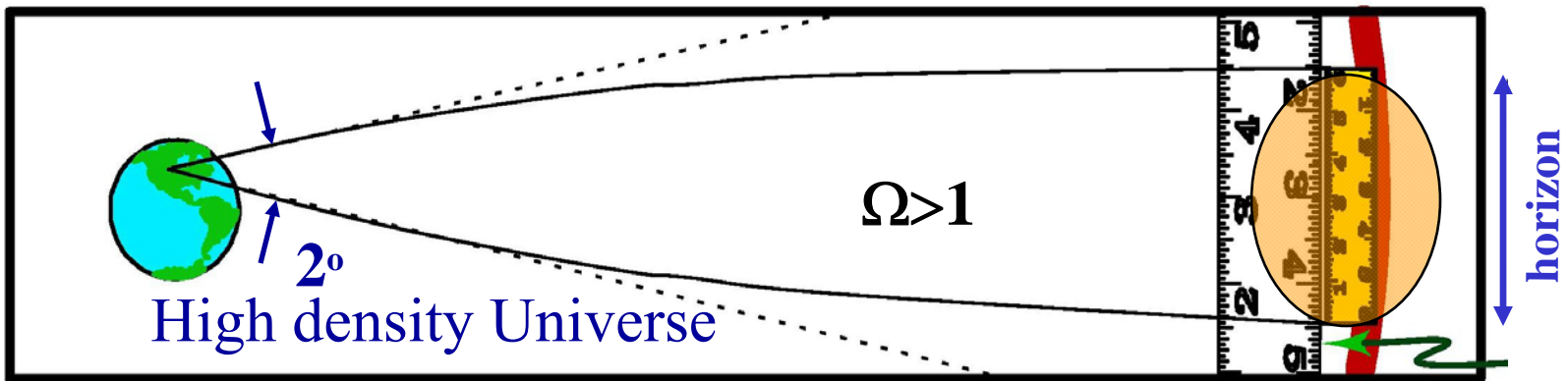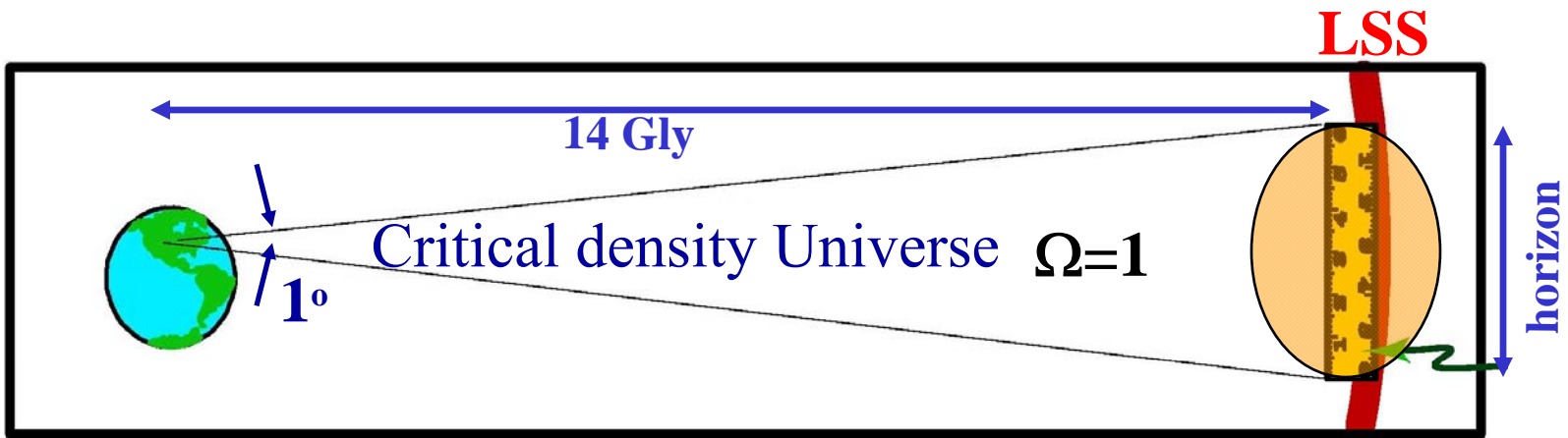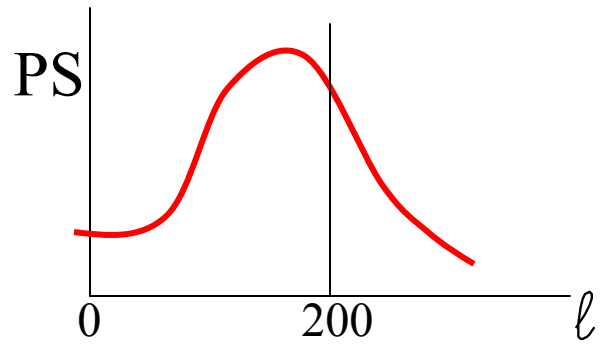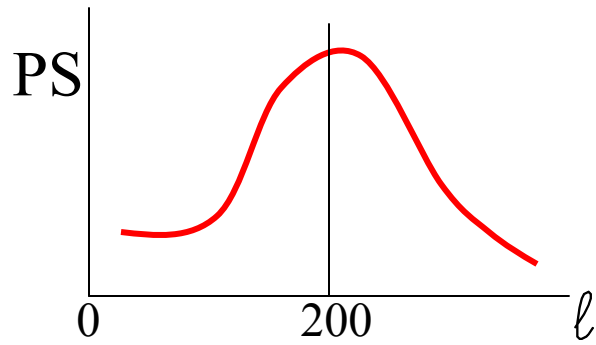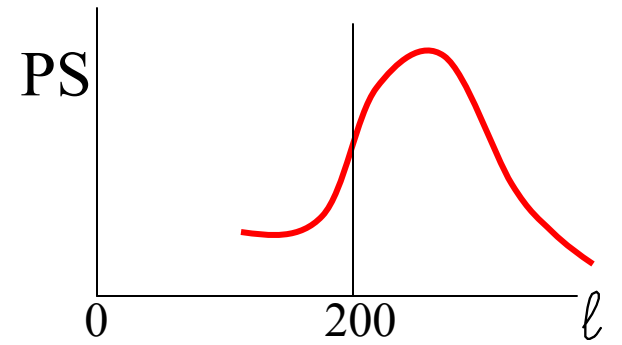
PS	PS	PS
0 200 ℓ	0 200 ℓ	0 200 ℓ
High density Universe	Critical density Universe	Low density Universe
$\Omega > 1$	$\Omega = 1$	$\Omega < 1$
2°	1°	0.5°
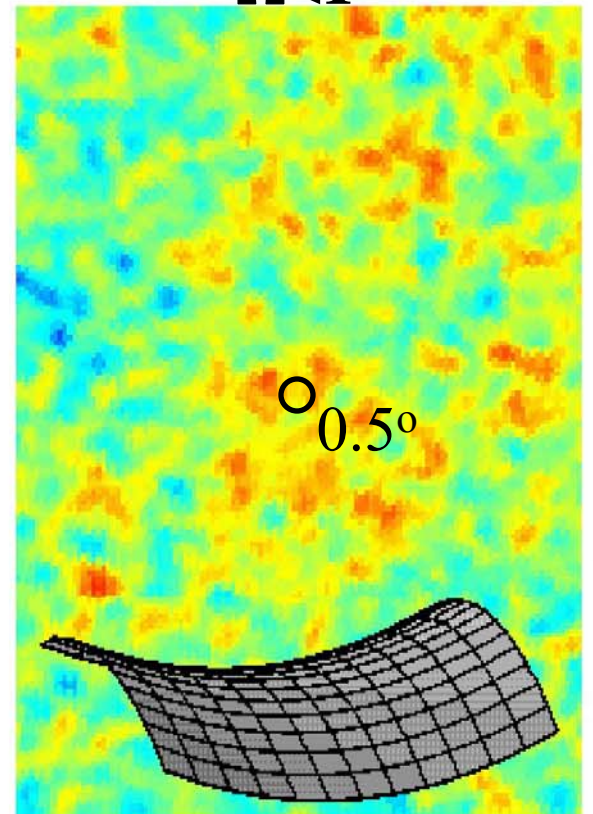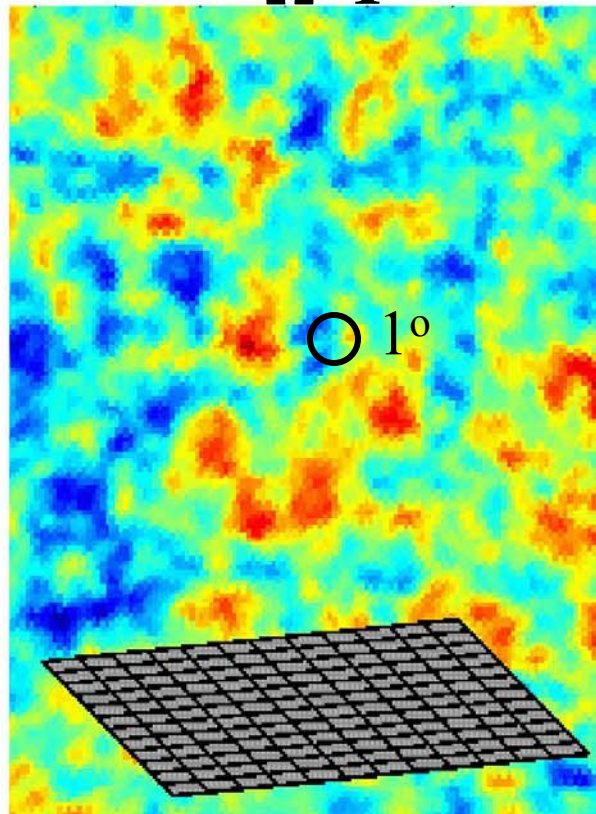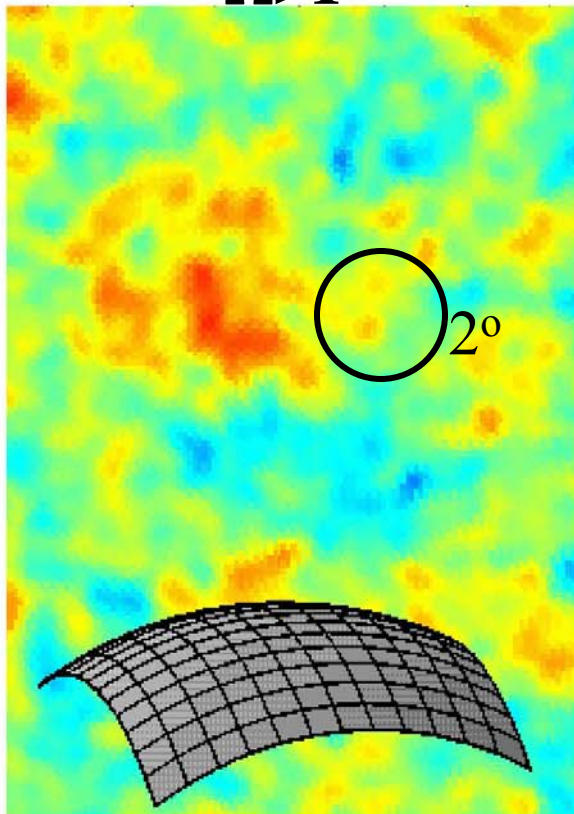
Expected power spectrum:

$$\Delta T(\theta, \varphi) = \sum_{\ell, m} a_{\ell m} Y_\ell^m(\theta, \varphi)$$

$$c_\ell = \left\langle a_{\ell m}^2 \right\rangle$$

$$\left\langle \Delta T^2 \right\rangle = \frac{1}{4\pi} \sum_\ell (2\ell + 1) c_\ell$$

See e.g. http://camb.info to compute c_ℓ for a given cosmological model

An instrument with finite angular resolution is not sensitive to the smallest scales (highest multipoles). For a gaussian beam with s.d. σ:

$$w_\ell^{LP} = e^{-\ell(\ell+1)\sigma^2}$$

c_ℓ

Quest for high angular resolution

- 20' FWHM
- 10' FWHM
- 5' FWHM
- 7° FWHM

Expected power spectrum:

$$\Delta T(\theta, \varphi) = \sum_{\ell, m} a_{\ell m} Y_\ell^m(\theta, \varphi)$$

$$c_\ell = \left\langle a_{\ell m}^2 \right\rangle$$

$$\left\langle \Delta T^2 \right\rangle = \frac{1}{4\pi} \sum_\ell (2\ell + 1) c_\ell$$

c_ℓ

rms signal in an instrument with gaussian beam σ :

$$\left\langle \Delta T^2 \right\rangle_{meas} = \frac{1}{4\pi} \sum_\ell (2\ell + 1) w_\ell^{LP} c_\ell$$

$$w_\ell^{LP} = e^{-\ell(\ell+1)\sigma^2}$$

$$\left.\frac{\Delta T}{T}\right|_{rms} = 4.2 \times 10^{-5}$$
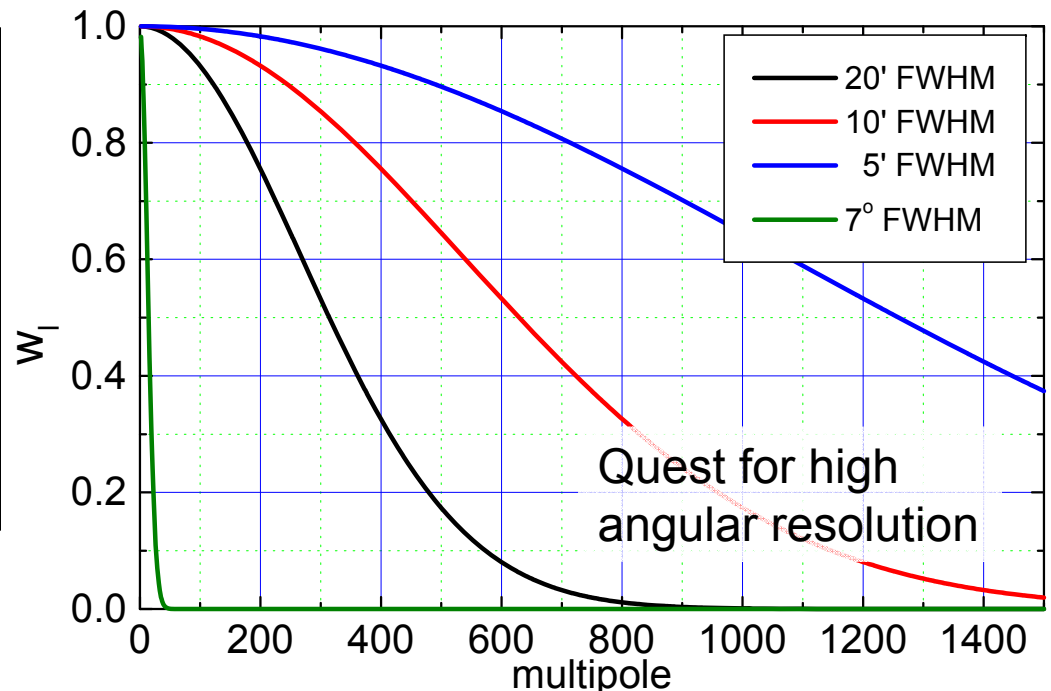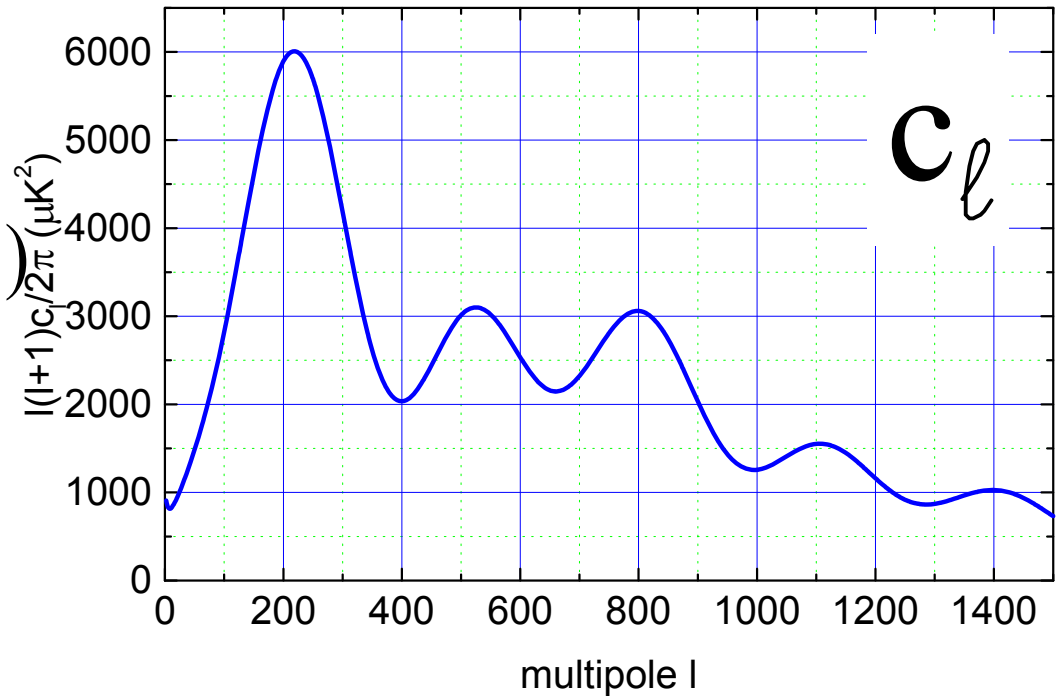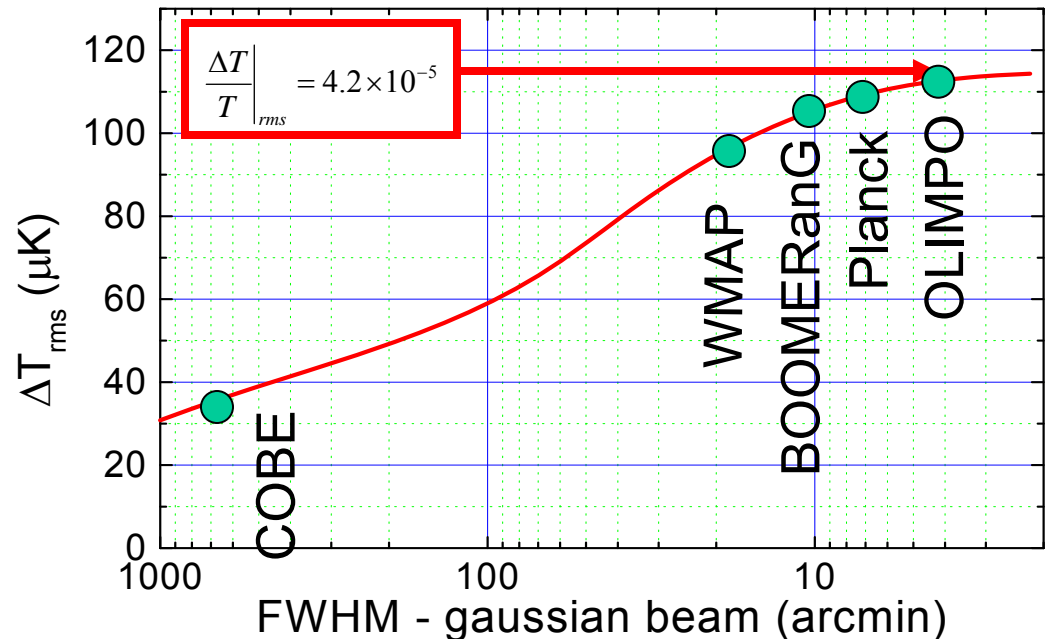
Did Inflation really happen ?

- **We do not know**. Inflation has not been proven yet. It is, however, a mechanism able to produce primordial fluctuations with the right characteristics.

- Four of the basic predictions of inflation have been proven:
  - existence of super-horizon fluctuations
  - gaussianity of the fluctuations
  - flatness of the universe
  - scale invariance of the density perturbations

- One more remains to be proved: the stochastic background of gravitational waves produced during the inflation phase.

- **CMB can help** in this – see below.

CMB polarization

- CMB radiation is Thomson scattered at recombination.
- If the local distribution of incoming radiation in the rest frame of the electron has a *quadrupole moment*, the scattered radiation acquires some degree of linear polarization.

-10ppm +10ppm
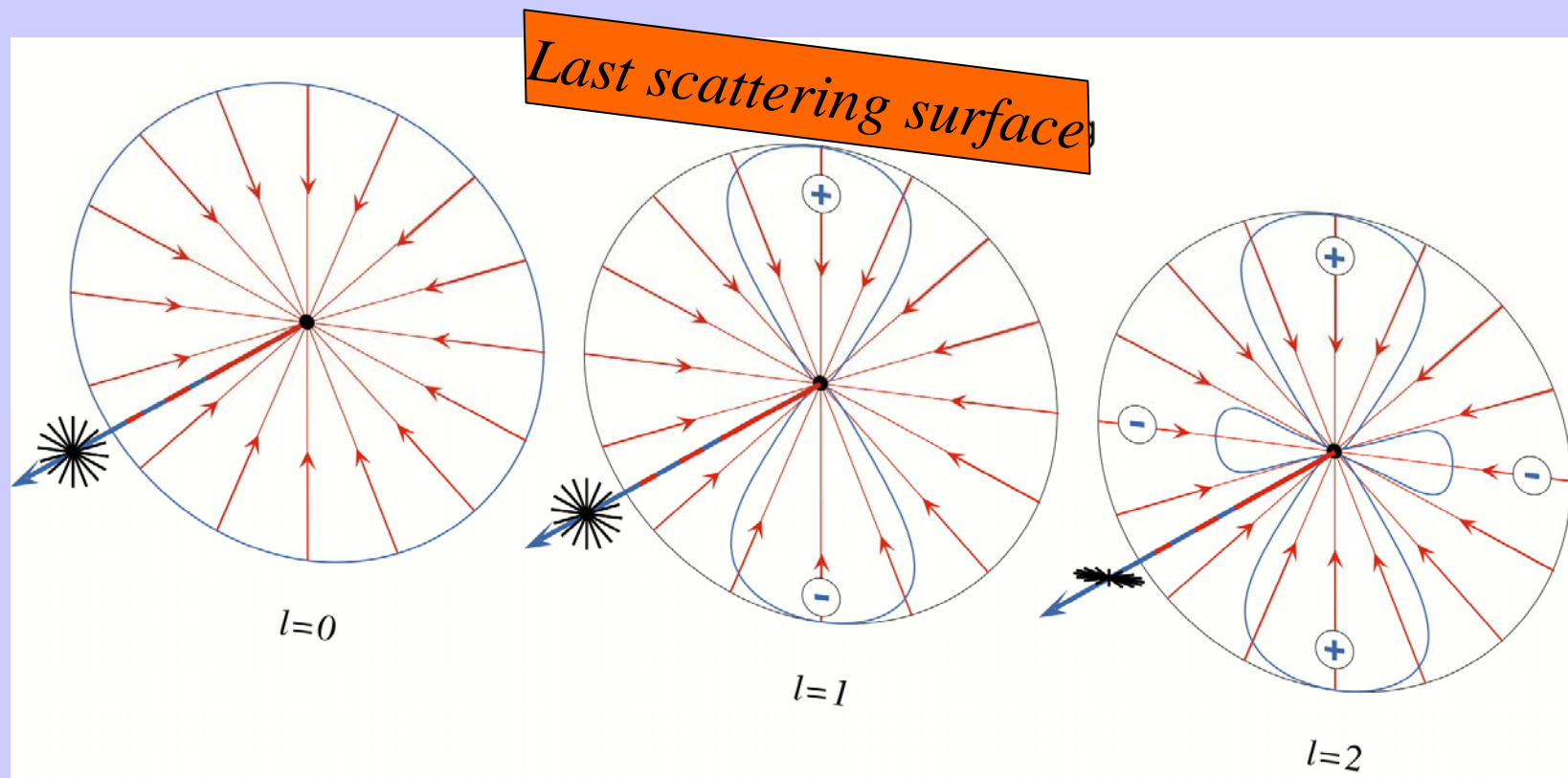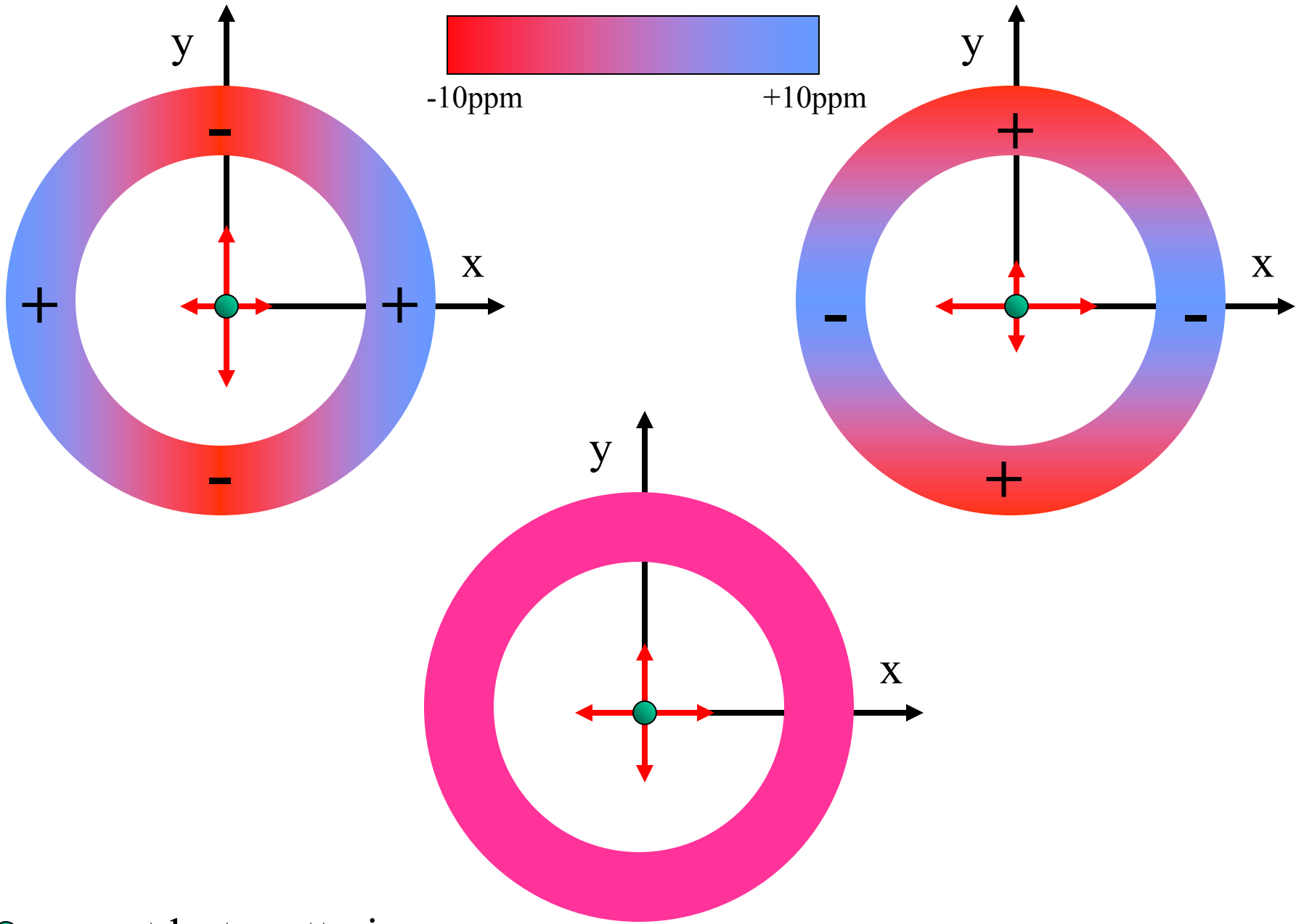
= e⁻ at last scattering
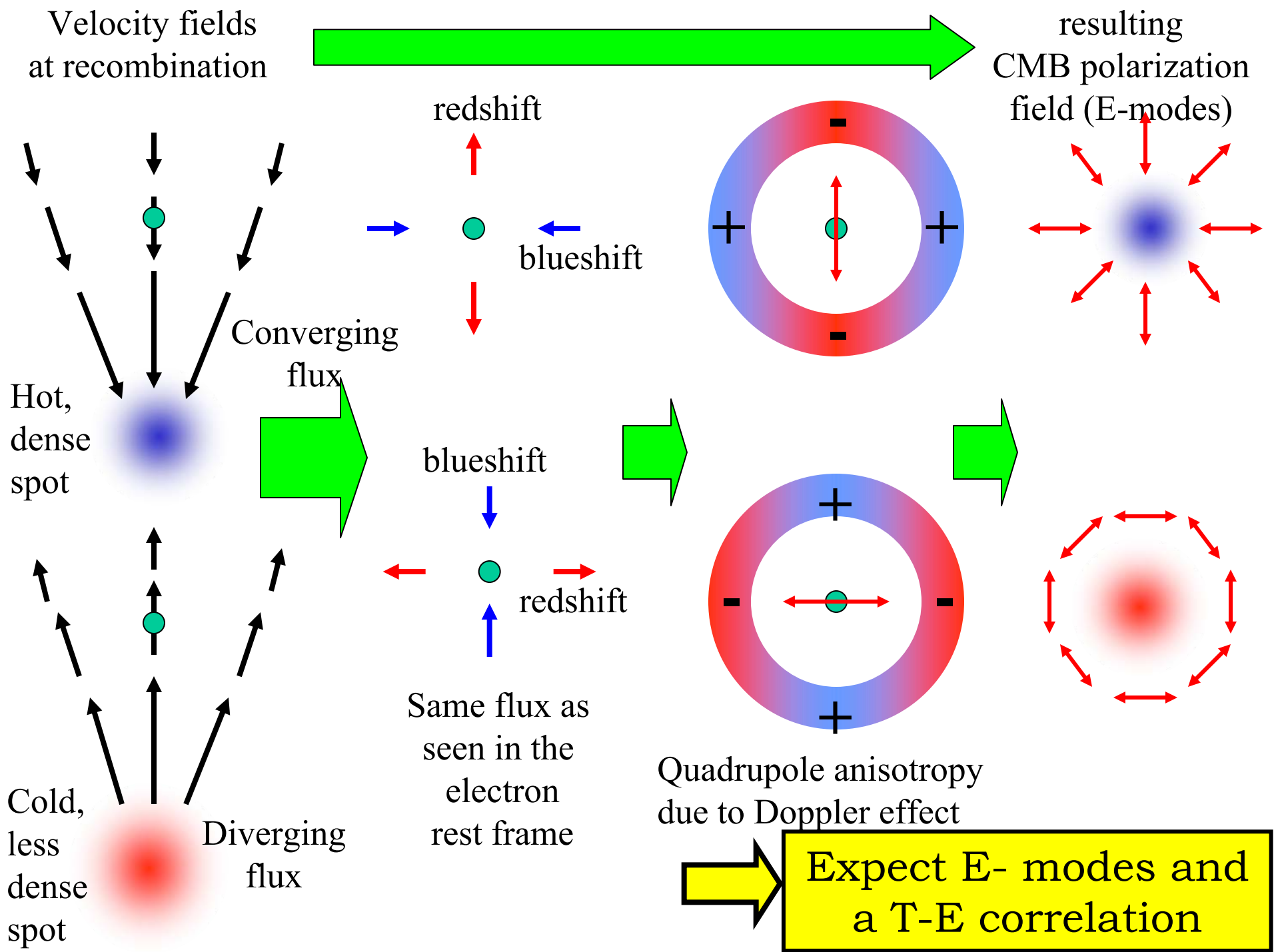
Velocity fields at recombination

resulting CMB polarization field (E-modes)

redshift

blueshift

Hot, dense spot

Converging flux

Cold, less dense spot

Diverging flux

blueshift

redshift

Same flux as seen in the electron rest frame
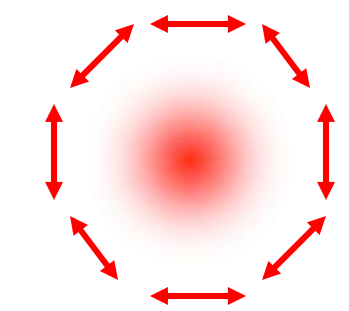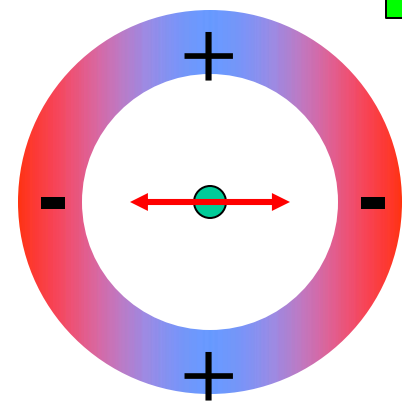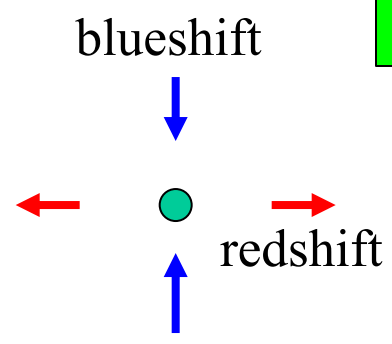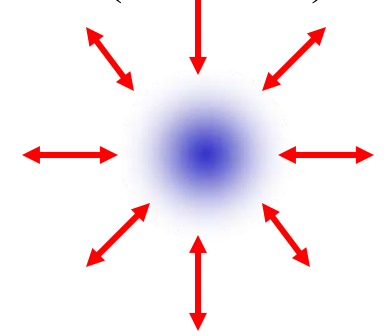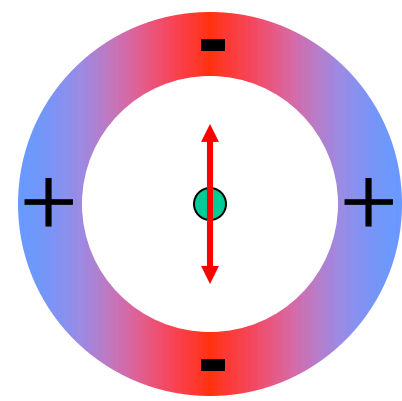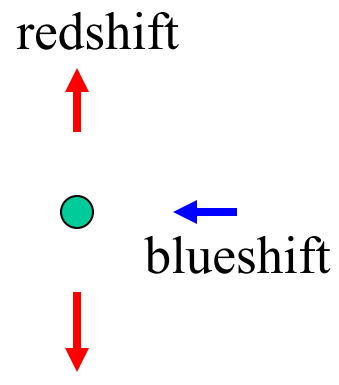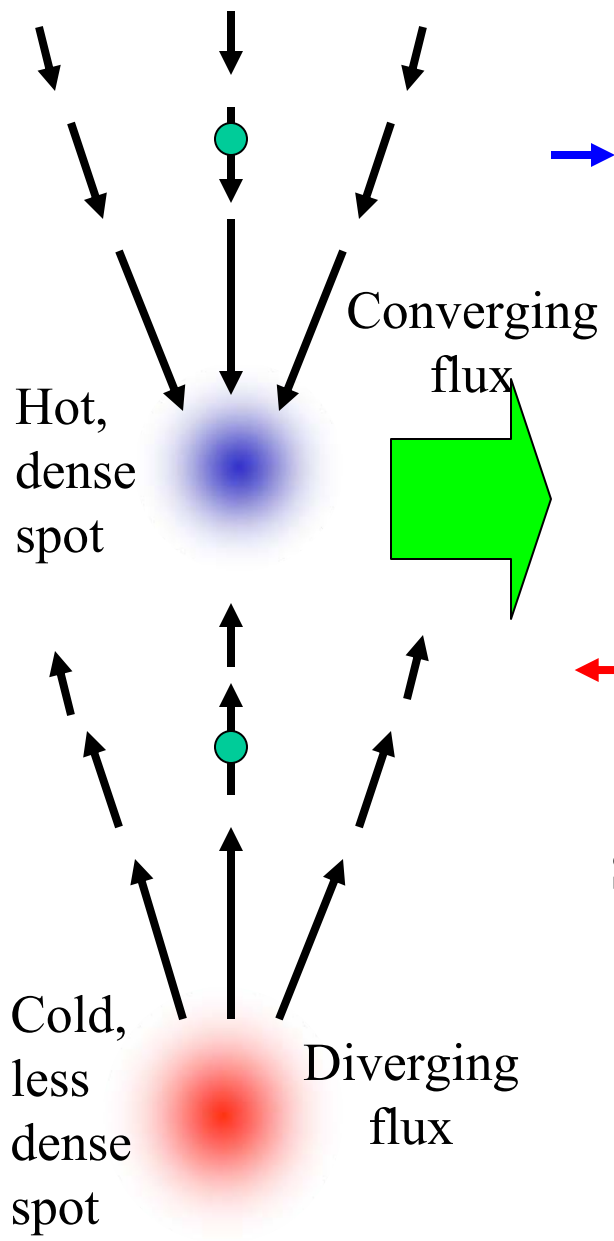
Quadrupole anisotropy due to Doppler effect

Expect E- modes and a T-E correlation

- E-modes are irrotational

- E modes are related to velocities, while T is related mainly to density

- We expect a power spectrum of the E-modes, <EE>, with maxima and mimina in quadrature with the anisotropy power spectrum <TT>.
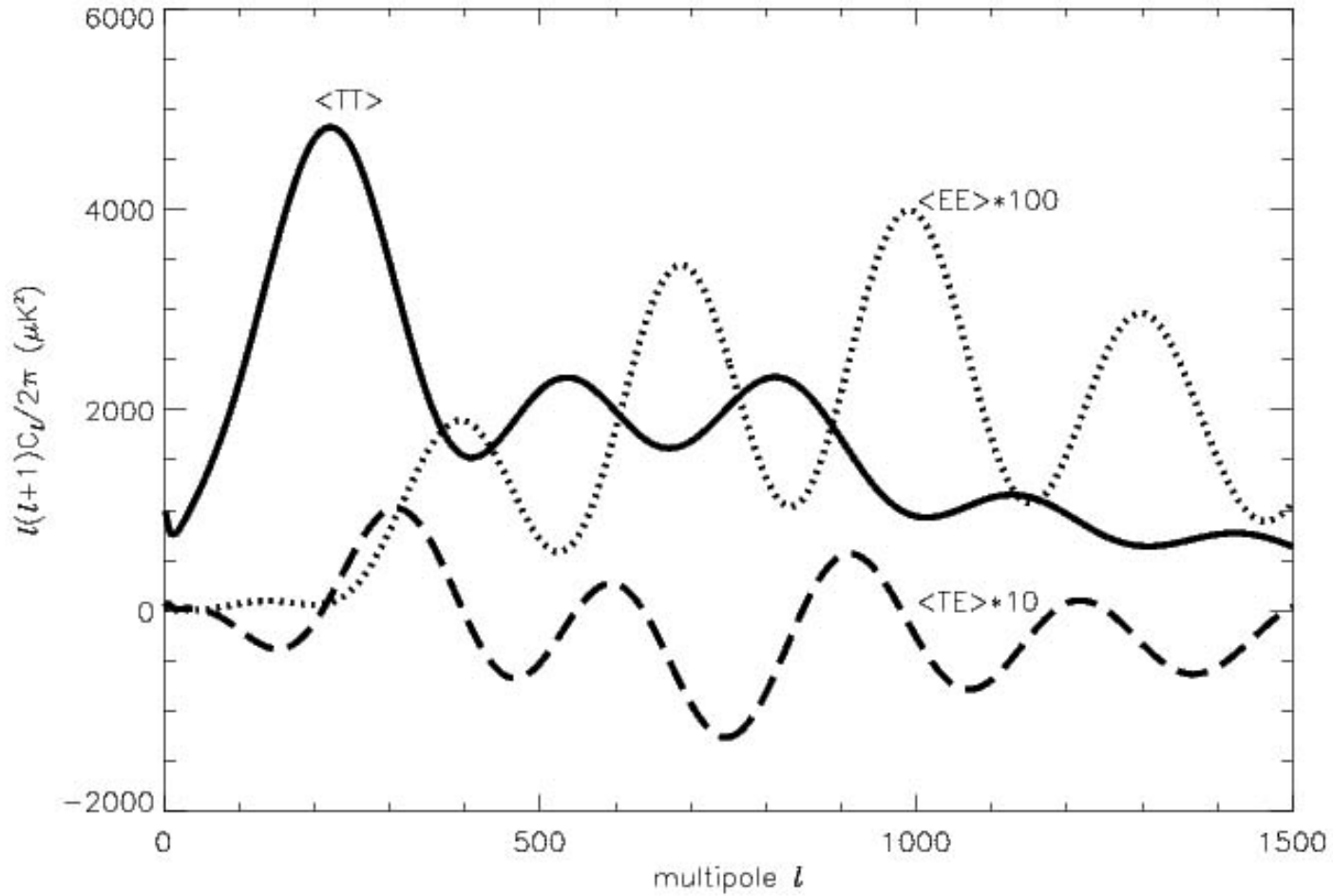
Figure 1.7: Estimated power spectra for the cosmological parameters: $\Omega_b = 0.05$, $\Omega_{cdm} = 0.3$, $\Omega_\Lambda = 0.65$, $\Omega_\nu = 0$, $H_0 = 65$ km/s/Mpc, $\tau = 0.17$. The temperature power spectrum, $\langle TT \rangle = C_\ell^T$, the E-modes power spectrum $\langle EE \rangle = C_\ell^E$ multiplied by a factor 100 to make it visible and the cross power spectrum between temperature and polarization, $\langle TE \rangle = C_\ell^{TE}$ multiplied by a factor 10. The spectra are computed using the publicly available code CMBFAST (http://www.cmbfast.org),

E-modes : 3 μK (2002…)

Temperature Polarization

1 deg.

Cold Spot Simulation

Cold Spot WMAP Data

Hot Spot Simulation

Hot Spot WMAP Data

Komatsu et al. 2010 – astro-ph/1001.4538

Velocity field near density fluctuation

Resulting anisotropy seen by e-

Resulting polarization pattern

WMAP7 measured data (stacked)

If inflation really happened...
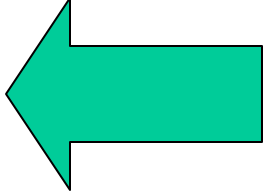
- It stretched geometry of space to nearly Euclidean ⟵ OK

- It produced a nearly scale invariant spectrum of density fluctuations ⟵ OK
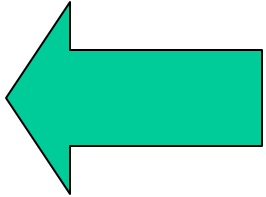
- It produced a stochastic background of gravitational waves. ⟵ ?
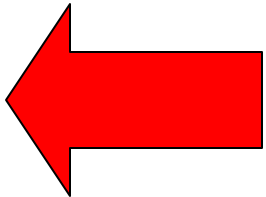
Quadrupole from P.G.W.

- If inflation really happened:
  - ✓ It stretched geometry of space to nearly Euclidean
  - ✓ It produced a nearly scale invariant spectrum of gaussian density fluctuations
  - ✓ It produced a stochastic background of gravitational waves: Primordial G.W. The background is so faint that even LISA will not be able to measure it.

- Tensor perturbations also produce quadrupole anisotropy. They generate irrotational (E-modes) **and rotational (B-modes) components** in the CMB polarization field.

- Since B-modes are not produced by scalar fluctuations, they represent a signature of inflation.
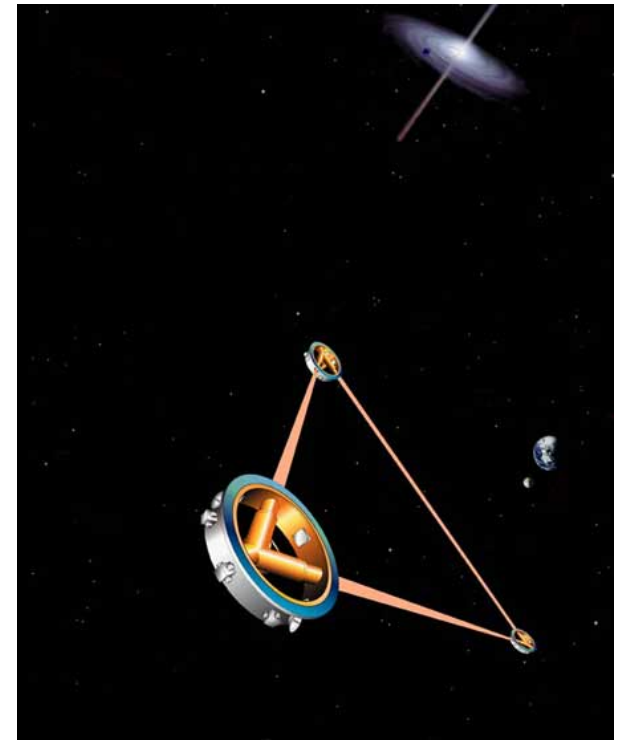
E-modes
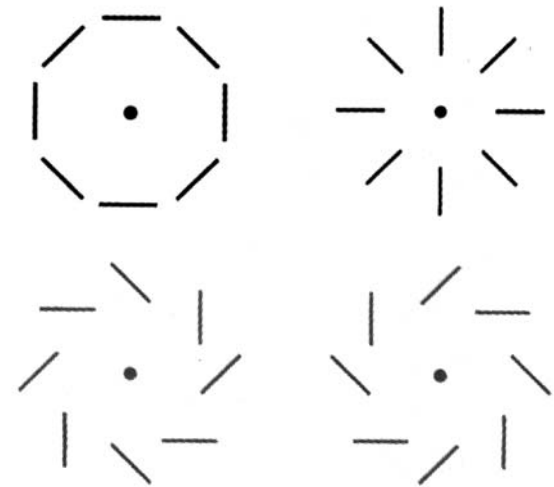
B-modes

B-modes from P.G.W.

- The amplitude of this effect is very small, but depends on the Energy scale of inflation. In fact the amplitude of tensor modes normalized to the scalar ones is:

$$\left(\frac{T}{S}\right)^{1/4} \equiv \left(\frac{C_2^{GW}}{C_2^{Scalar}}\right)^{1/4} \cong \frac{V^{1/4}}{3.7 \times 10^{16}\,\text{GeV}}$$ ⟵ Inflation potential

- and

$$\sqrt{\frac{\ell(\ell+1)}{2\pi} c_{\ell\,\text{max}}^B} \cong 0.1 \mu K \left[\frac{V^{1/4}}{2 \times 10^{16}\,\text{GeV}}\right]$$

- There are theoretical arguments to expect that the energy scale of inflation is close to the scale of GUT i.e. around 10^{16} GeV.

- The current upper limit on anisotropy at large scales gives T/S<0.5 (at 2σ)

- A competing effect is lensing of E-modes, which is important at large multipoles.

E-modes & B-modes

Spin-2 quantity   Spin-2 basis

$$(Q \pm iU)(\vec{n}) = \sum_{\ell,m} \left(a_{\ell m}^{E} \pm i a_{\ell m}^{B} \right)\, {}_{\pm 2}Y_{\ell m}(\vec{n})$$

- From the measurements of the Stokes Parameters **Q** and **U** of the linear polarization field we can recover both irrotational and rotational a_{lm} by means of modified Legendre transforms:

E-modes produced by scalar and tensor perturbations

$$a_{\ell m}^{E} = \frac{1}{2} \int d\Omega\, W(\vec{n}) \left[(Q+iU)(\vec{n})\, {}_{+2}Y_{\ell m}(\vec{n}) + (Q-iU)(\vec{n})\, {}_{-2}Y_{\ell m}(\vec{n}) \right]$$

B-modes produced **only** by tensor perturbations

$$a_{\ell m}^{B} = \frac{1}{2i} \int d\Omega\, W(\vec{n}) \left[(Q+iU)(\vec{n})\, {}_{+2}Y_{\ell m}(\vec{n}) - (Q-iU)(\vec{n})\, {}_{-2}Y_{\ell m}(\vec{n}) \right]$$

The signal is extremely weak

- Nobody really knows how to detect this.
  - Pathfinder experiments are needed
- Whatever smart, ambitious experiment we design to detect the B-modes:
  - It needs to be extremely sensitive
  - It needs an extremely careful control of systematic effects
  - It needs careful control of foregrounds
  - It will need independent experiments with orthogonal systematics.
- There is still a long way to go: …

Very difficult

- Everything (telescope, ground, …) is emitting copiously in the FIR range

- The earth atmosphere is opaque and emissive, and in addition is also unstable !

- Compared to these emissions, the astronomical signals in this range are tiny.

- Detector noise must be minimized (cryogenic cooling down to 0.3 or 0.1K).

Legend:
- 250K, $\varepsilon=1$
- 250K, $\varepsilon=0.1$
- Atmosphere 4 km, 0.5 mm pwv
- 250K, $\varepsilon=0.01$
- Atmosphere 41 km
- CMB
- CMB polarization

x-axis: wavenumber (cm^{-1})

y-axis: Brightness (W/cm^2/sr/cm^{-1})
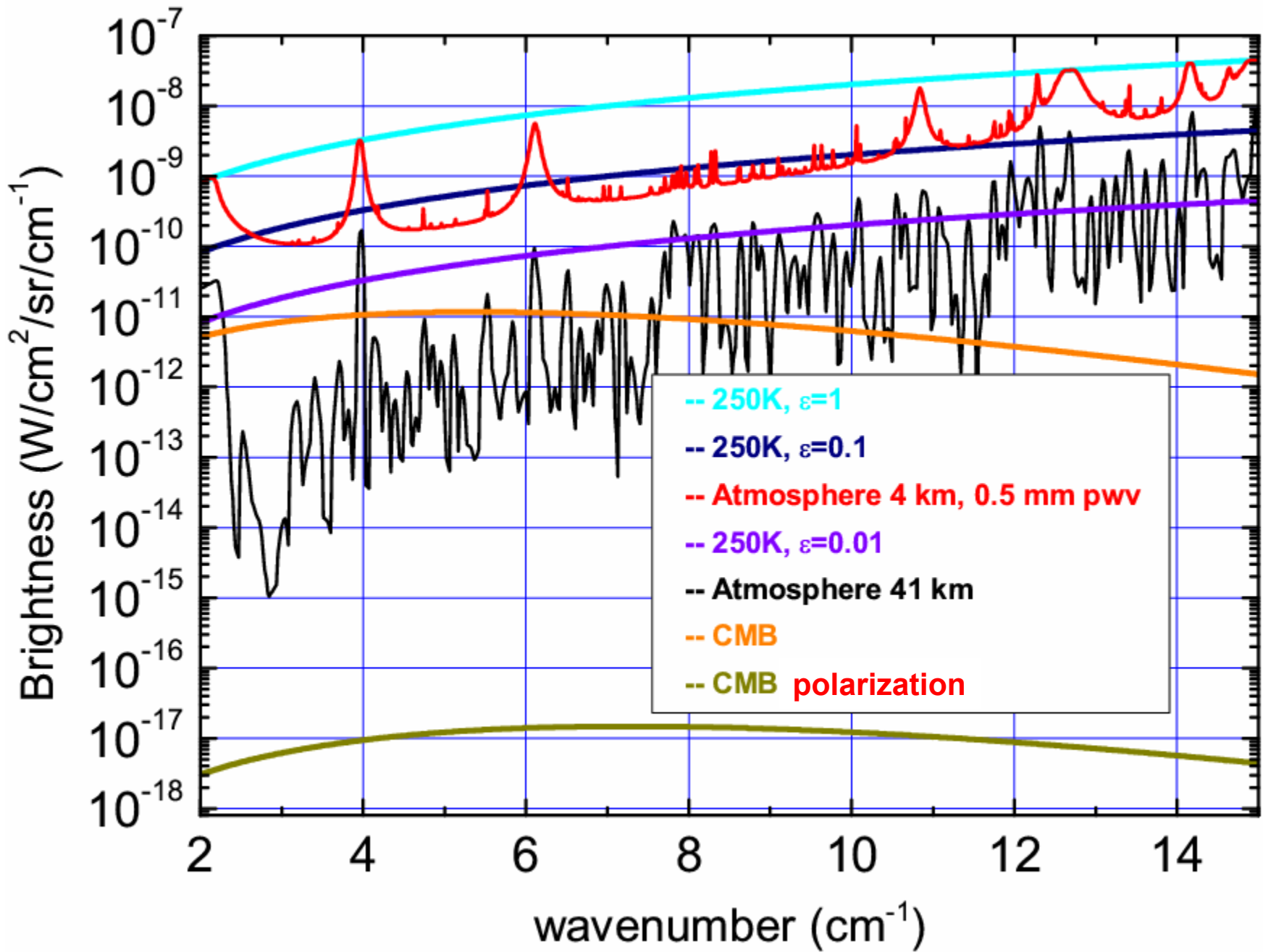
Radiation Noise

- The fundamental limit of any measurement.
- Photon noise reflects the particle-wave duality of photons.
- It is the sum of Poisson noise (particles) PLUS interference noise (waves)
- Poisson noise:

$$\left\langle \Delta E^2 \right\rangle = \left(h\nu \right)^2 \left\langle \Delta N^2 \right\rangle = \left(h\nu \right)^2 \left\langle N \right\rangle = \left(h\nu \right)^2 \frac{W}{h\nu} = h\nu Wt$$

This is a typical random-walk process (variance prop.to time).
Using Einstein's generalization $\left\langle \Delta\theta^2 \right\rangle = 2kBTt \Rightarrow \left\langle \dot{\theta}_f^2 \right\rangle df = 4kBTdf$
we get the power spectrum and the variance
of radiative power fluctuations:

$$\left\langle \Delta W_f^2 \right\rangle df = 2h\nu Wdf$$

Radiation Noise

- Orders of magnitude example: A He-Ne 1 mW laser beam has a perfect Poisson statistics, so

$$\sqrt{\left\langle \Delta W_f^2 \right\rangle} = \sqrt{2h\nu W} = 2.5 \times 10^{-11} \; \frac{W}{\sqrt{Hz}}$$

- Notice the power spectrum units (remember that the integral of the PS over frequency is the variance).

- In this case the intrinsic fluctuations per unit bandwidth are >7 orders of magnitude smaller than the signal.

- It is useless to build a complex detector with a noise of $10^{-15} \, W/\sqrt{Hz}$ for this measurement: the precision of the measurement will be limited at a level of $2.5 \times 10^{-11} \, W/\sqrt{Hz}$

Radiation Noise

- Thermal radiation (like the CMB) has also wave interference noise: the correct statistics is Bose-Einstein.

$$\langle N \rangle = \frac{g}{e^{(E-\mu)/kT} - 1} \quad ; \quad \langle \Delta N^2 \rangle = T \left. \frac{d\langle N \rangle}{d\mu} \right|_{T,V}$$

$$\Rightarrow \quad \boxed{\langle \Delta N^2 \rangle = \langle N \rangle + \frac{\langle N \rangle^2}{g}}$$

Poisson noise

Wave interference noise

Radiation Noise

- For a blackbody

$$\langle N \rangle = \frac{g}{e^{(E-\mu)/kT} - 1} \quad ; \quad g = 2\frac{v^2}{c^3} 4\pi V dv$$

$$\langle N \rangle = \frac{8\pi v^2}{c^3} \frac{1}{e^{hv/kT} - 1} V dv$$

$$\Rightarrow \quad \boxed{\langle \Delta N^2 \rangle = \langle N \rangle \left[1 + \frac{1}{e^{hv/kT} - 1} \right]}$$

Poisson noise, important at short wavelengths

Wave interference noise, Important at low frequencies

Radiation Noise

$$\left\langle \Delta N^2 \right\rangle = \left\langle N \right\rangle \left[1 + \frac{1}{e^{h\nu/kT} - 1} \right]$$

$$\left\langle \Delta E^2 \right\rangle = (h\nu)^2 \left\langle N \right\rangle \left[1 + \frac{1}{e^{h\nu/kT} - 1} \right] = h\nu Wt \left[1 + \frac{1}{e^{h\nu/kT} - 1} \right]$$

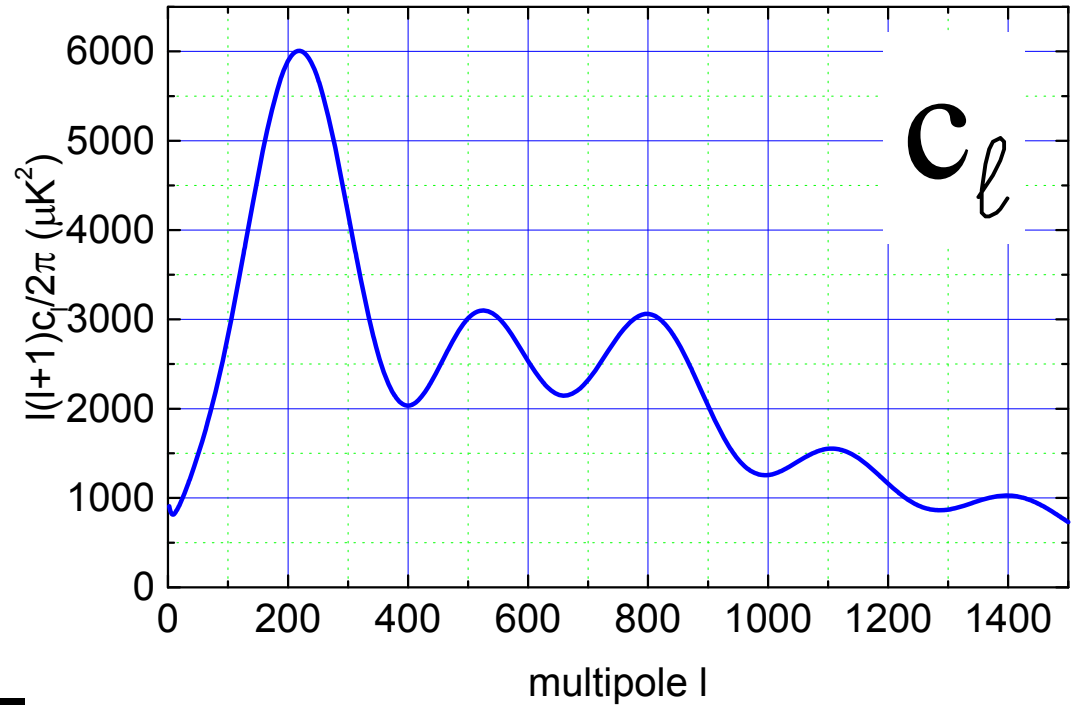$$\left\langle \Delta W^2 \right\rangle df = 2h\nu \left\langle W \right\rangle \left[1 + \frac{1}{e^{h\nu/kT} - 1} \right] df$$

$$\sqrt{\left\langle \Delta W^2 \right\rangle df} = \sqrt{\frac{4k^5}{c^2 h^3}} \sqrt{A\Omega T^5} \sqrt{\int_{x_1}^{x_2} \frac{x^4 e^x}{\left(e^x - 1 \right)^2} dx \ df}$$

$$\sqrt{\frac{4k^5}{c^2 h^3}} = 2.77 \times 10^{-18} \frac{W}{\sqrt{cm^2 \, sr \ Hz \ K^5}}$$

CMB observables

- **The spectrum**

$$B(\nu,T) = \frac{2h}{c^2}\frac{\nu^3}{e^x - 1} \qquad x = \frac{h\nu}{kT}$$

- **The angular distribution**

$$\Delta B(\nu,T) = \frac{xe^x}{e^x - 1} B(\nu,T)\frac{\Delta T}{T}$$

- **The polarization state**

$$\Delta B_P(\nu,T) = \frac{xe^x}{e^x - 1} B(\nu,T)\frac{\Delta T_P}{T}$$

- **The noise**

$$\sqrt{\langle \Delta W^2(\nu,T)\rangle}\,dx = \sqrt{\frac{4k^5 T^5}{c^2 h^3}\frac{x^4 e^x}{\left(e^x - 1\right)^2}\,dx}$$

T=2.725 K

W m^{-2} sr^{-1} Hz^{-1}

CMB (MKS units)

- average brightness
- anisotropy (rms)
- polarization (E rms)
- photon noise (rms)
- polarization (B rms)

W (m^2 sr Hz)$^{-1/2}$ Hz$^{-1/2}$

W m^{-2} sr^{-1} Hz^{-1}

W m^{-2} sr^{-1} Hz^{-1}
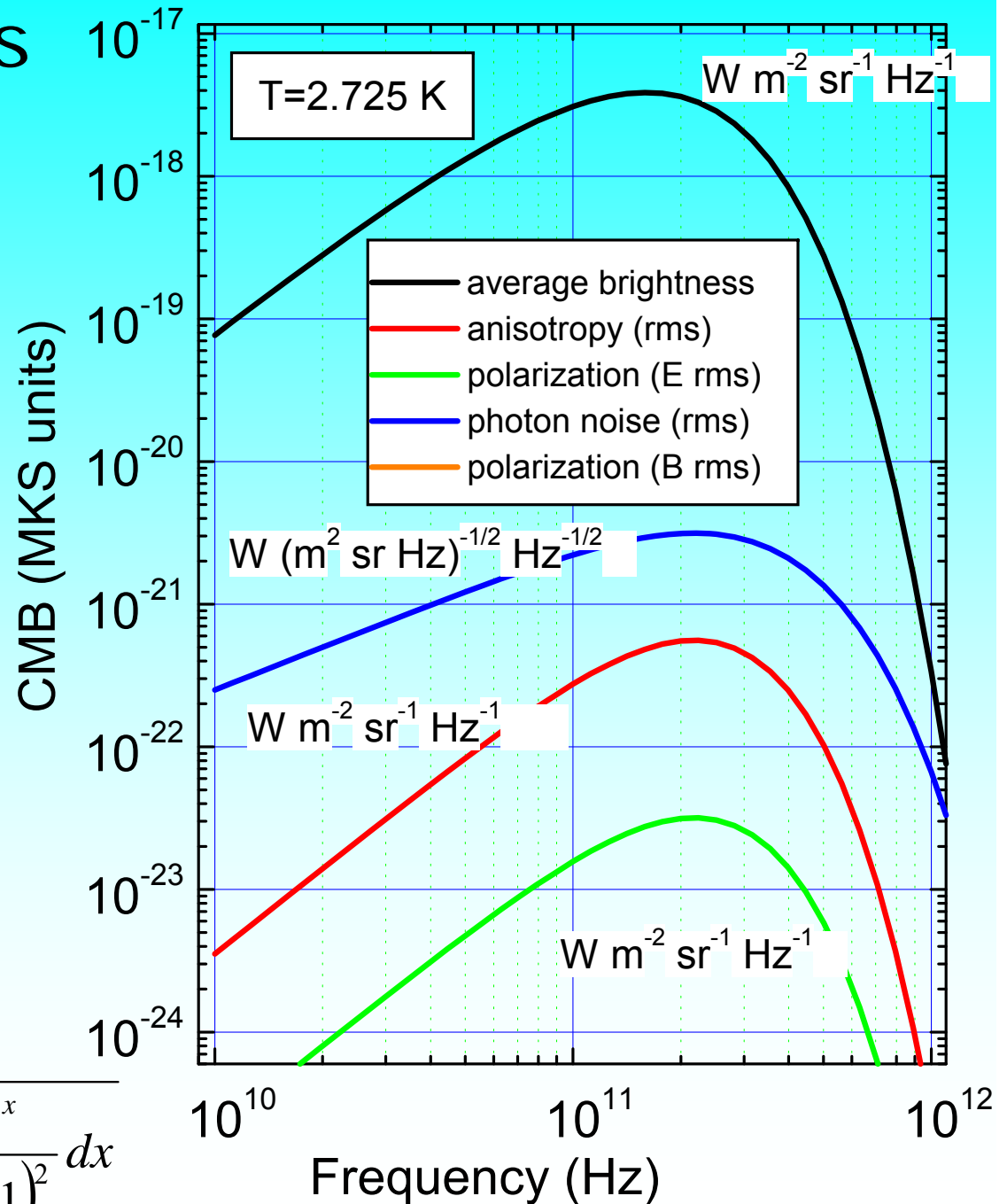
Frequency (Hz)

Noise and integration time

- Any detector has a response time τ which limits its sensitivity at high post-detection frequencies. Data taken at intervals shorter than τ will not be independent.

- The error on the estimate of $\langle W \rangle_t$, the average power in the observation time t, is

- $$\sigma_{\langle W \rangle_t} = \frac{\sigma_{\langle W \rangle}}{\sqrt{N}} = \frac{\sqrt{\int_{f_{min}}^{f_{max}} \langle \Delta W^2 \rangle df}}{\sqrt{N}}$$

- where N is the number of independent measurements. In the integration time t, it will be $N = t/\tau$.

Noise and integration time

- $$\sigma_{\langle W \rangle_T} = \frac{\sigma_{\langle W \rangle}}{\sqrt{N}} = \frac{\sqrt{\int_{f_{min}}^{f_{max}} \langle \Delta W^2 \rangle df}}{\sqrt{N}} = \frac{\sqrt{\int_{f_{min}}^{f_{max}} \langle \Delta W^2 \rangle df}}{\sqrt{t/\tau}} =$$

$$\cong \frac{\sqrt{\int_{1/T}^{1/\tau} \langle \Delta W^2 \rangle df}}{\sqrt{t/\tau}} = \frac{\sqrt{\langle \Delta W^2 \rangle \left[\frac{1}{\tau} - \frac{1}{t} \right]}}{\sqrt{t/\tau}} \cong \sqrt{\frac{\langle \Delta W^2 \rangle}{t}}$$

- The noise decreases as the square root of the integration time.
- Notice that this applies equally to detector noise and to intrinsic radiation noise.

Noise and integration time

- Numerical example: CMB anisotropy (or polarization) measurement limited only by radiation noise:

$$\Delta B (\nu, T) = \frac{\Delta T}{T} \int_{x_1}^{x_2} \frac{x e^{x}}{e^{x} - 1} B(x, T) \, dx$$

$$\sigma\left(\frac{\Delta T}{T}\right) = \frac{\sigma(\Delta B)}{\int_{x_1}^{x_2} \frac{x e^{x}}{e^{x} - 1} B(x, T) \, dx}$$

$$\sigma\left(\frac{\Delta T}{T}\right) = \frac{\sqrt{\frac{4 k^{5} T^{5}}{c^{2} h^{3}} A \Omega \int_{x_1}^{x_2} \frac{x^{4} e^{x}}{\left(e^{x} - 1\right)^{2}} \, dx}}{\frac{2 k^{4} T^{4}}{c^{2} h^{3}} A \Omega \int_{x_1}^{x_2} \frac{x^{4} e^{x}}{(e^{x} - 1)^{2}} \, dx} \sqrt{\frac{1}{t}}$$
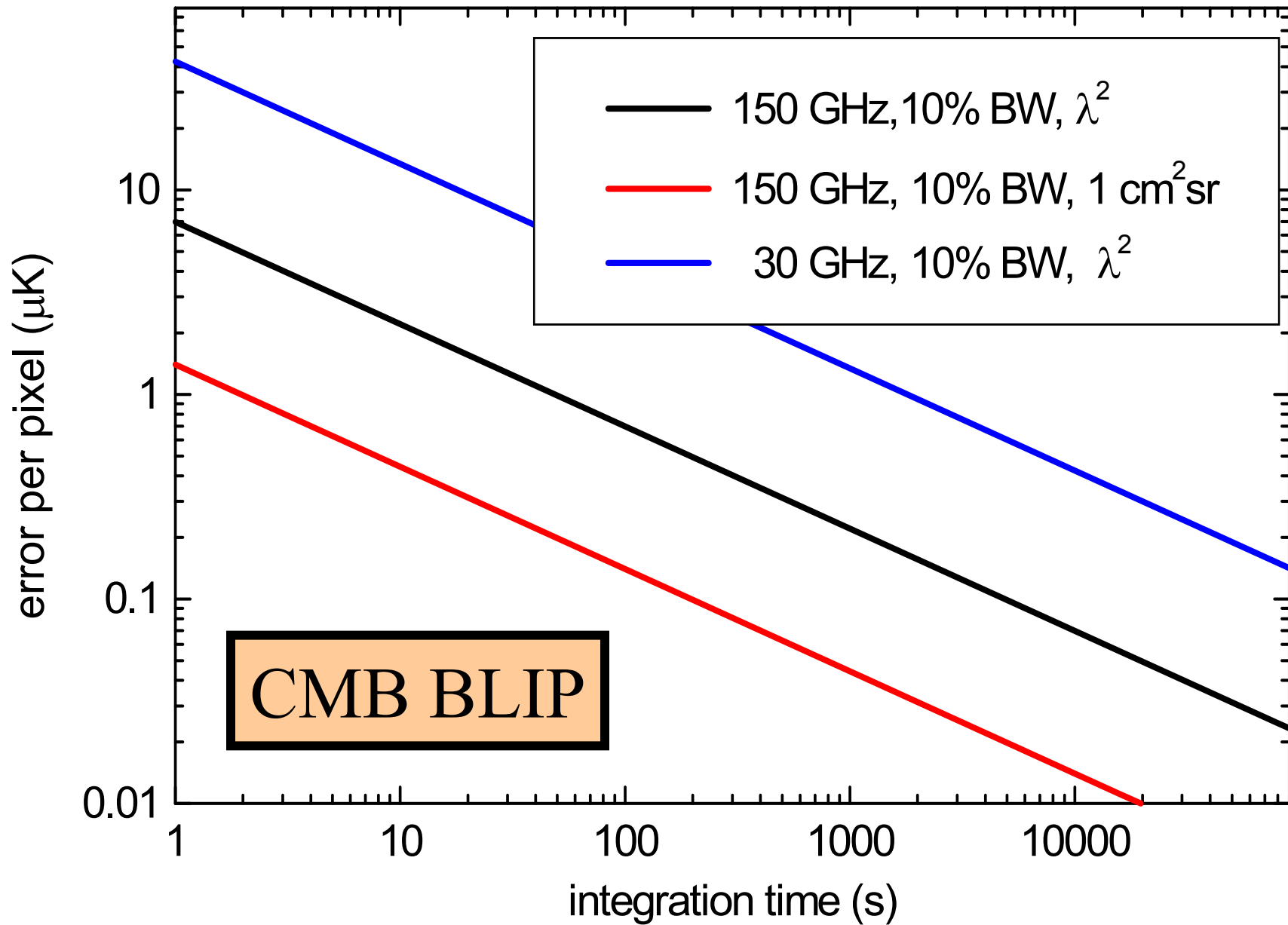
Radiation Noise

- For a grey-body with emissivity $\varepsilon < 1$
- relevant cases:
  - Detector with efficiency <1 (filters, and so on)
  - Radiation emitted by a mirror
  - Radiation emitted by the atmosphere in the atmospheric windows

$$N' = \varepsilon N$$

$$\left\langle \Delta N'^2 \right\rangle = \varepsilon \left\langle N' \right\rangle \left[1 + \frac{\varepsilon}{e^{h\nu/kT} - 1} \right]$$

$$\sqrt{\left\langle \Delta W^2 \right\rangle df} = \sqrt{\frac{4k^5}{c^2 h^3}} \sqrt{A\Omega T^5} \sqrt{\varepsilon \int_{x_1}^{x_2} \frac{x^4 (e^x - 1 + \varepsilon)}{e^x - 1} dx \, df}$$

Expected power spectrum:

$$\Delta T(\theta, \varphi) = \sum_{\ell, m} a_{\ell m} Y_\ell^m(\theta, \varphi)$$

$$c_\ell = \left\langle a_{\ell m}^2 \right\rangle$$

$$\left\langle \Delta T^2 \right\rangle = \frac{1}{4\pi} \sum_\ell (2\ell + 1) c_\ell$$

An instrument with finite angular resolution is not sensitive to the smallest scales (highest multipoles). For a gaussian beam with s.d. σ:

$$w_\ell^{LP} = e^{-\ell(\ell+1)\sigma^2}$$
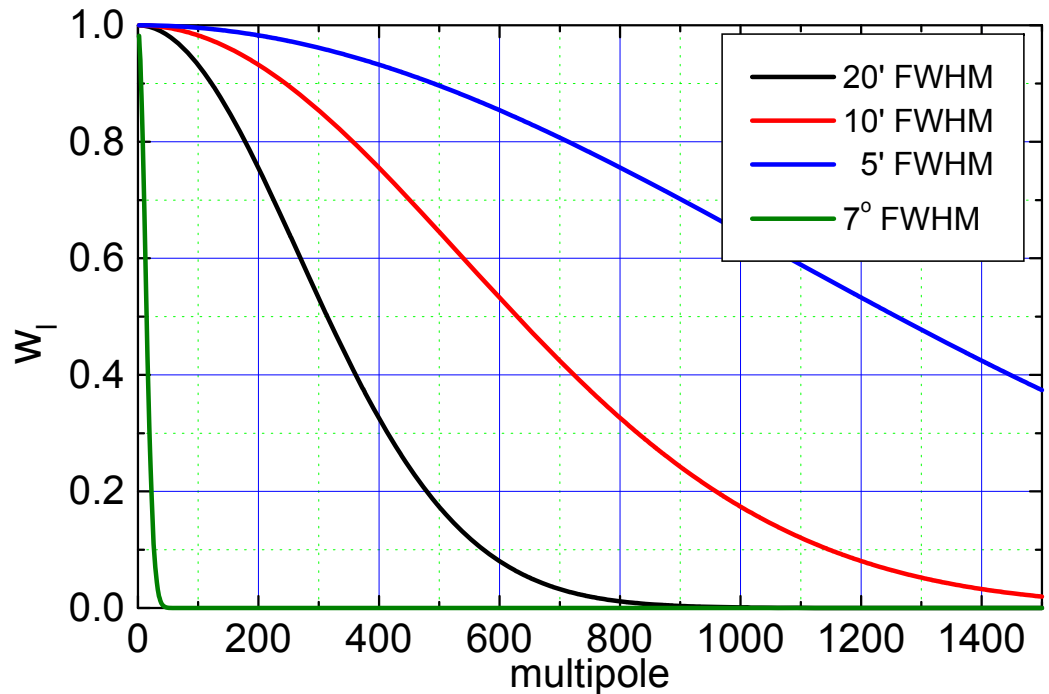
What is $RA(\theta,\phi)$?

- The intensity is the square of the field:

$$\frac{dI}{d\Omega} = I_o \left[\frac{2J_1(ak\theta)}{ak\theta} \right]^2$$

- The first zero is for

$$\theta_{10} = 1.22 \frac{\lambda}{2a}$$

- The FWHM is similar
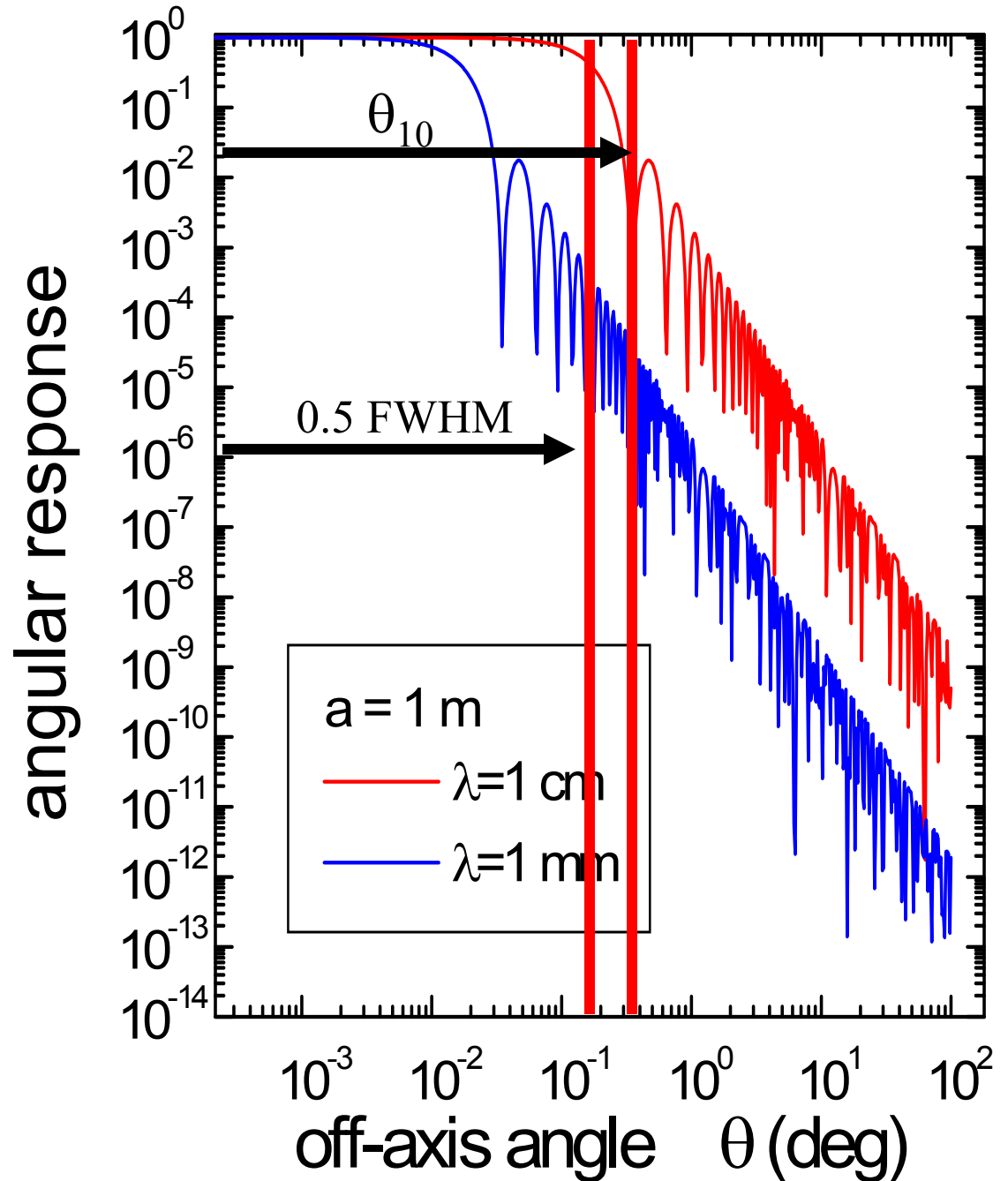
Mirror Diameter (mm)=	500	1000	2000	3000
λ(mm) / f(GHz)	FWHM(')	FWHM(')	FWHM(')	FWHM(')
10 / 30	83.89	41.94	20.97	13.98
3 / 100	25.17	12.58	6.29	4.19
1 / 300	8.39	4.19	2.10	1.40
0.5 / 600	4.19	2.10	1.05	0.70

1. Angular resolution better than 1° implies a primary mirror larger than 1 m
2. Sidelobes are an issue, expecially at long wavelengths.

Expected power spectrum:
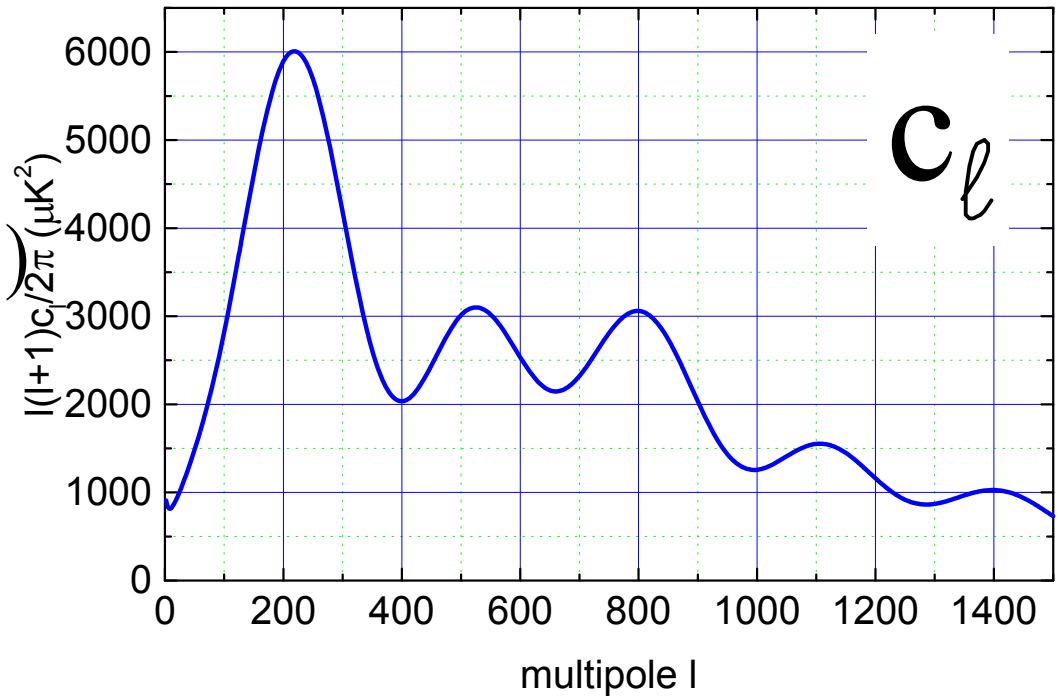
$$\Delta T(\theta, \varphi) = \sum_{\ell, m} a_{\ell m} Y_\ell^m(\theta, \varphi)$$

$$c_\ell = \left\langle a_{\ell m}^2 \right\rangle$$

$$\left\langle \Delta T^2 \right\rangle = \frac{1}{4\pi} \sum_\ell (2\ell + 1) c_\ell$$

rms signal in an instrument with gaussian beam σ :

$$\left\langle \Delta T^2 \right\rangle_{meas} = \frac{1}{4\pi} \sum_\ell (2\ell + 1) w_\ell^{LP} c_\ell$$

$$w_\ell^{LP} = e^{-\ell(\ell+1)\sigma^2}$$

$$\left. \frac{\Delta T}{T} \right|_{rms} = 4.2 \times 10^{-5}$$
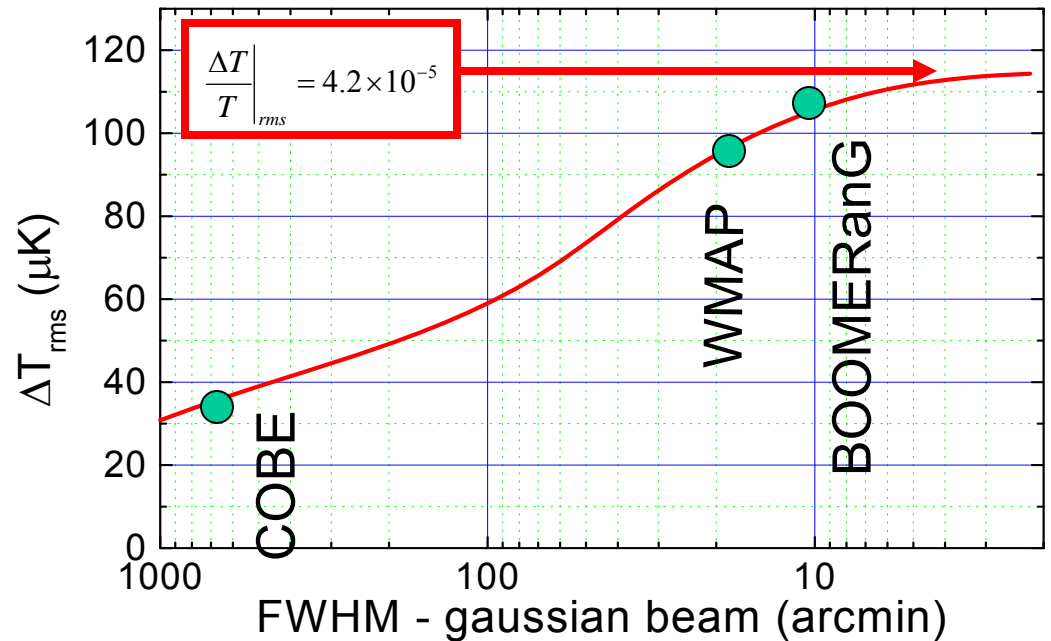
Importance of low sidelobes

- In the case of CMB observations, the detected brightness is the sum of the brightness from the sky (dominant for the solid angles directed towards the sky, in the main lobe) and the Brightness from ground (dominant for the solid angles directed towards ground, in the sidelobes).
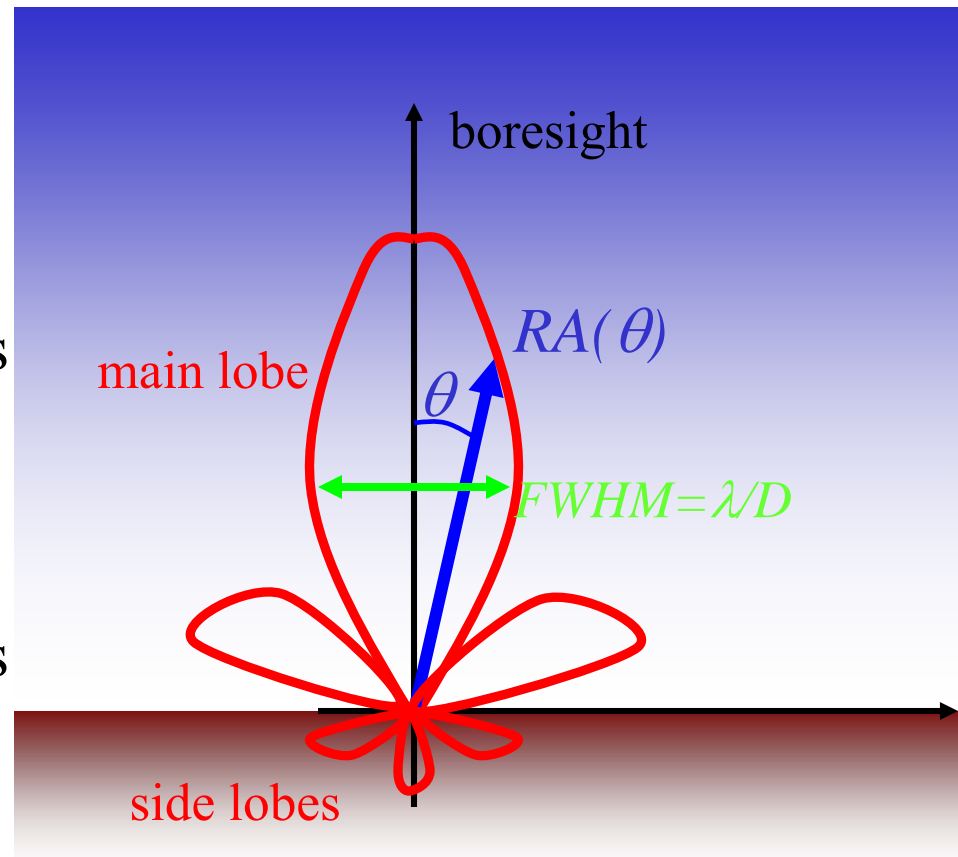
$$W = A \left[\int_{\substack{main \\ lobe}} B_{sky}(\theta, \varphi) RA(\theta, \varphi) d\Omega + \int_{\substack{side \\ lobes}} B_{Ground}(\theta, \varphi) RA(\theta, \varphi) d\Omega \right]$$

Importance of low sidelobes

$$W = A\left[\int_{\substack{main\\lobe}} B_{sky}(\theta,\varphi)RA(\theta,\varphi)d\Omega + \int_{\substack{side\\lobes}} B_{Ground}(\theta,\varphi)RA(\theta,\varphi)d\Omega\right]$$

signal of interest   disturbance signal

$$W \approx A\left[B_{sky}(\theta,\varphi)\left\langle RA_{\substack{main\\lobe}}(\theta,\varphi)\right\rangle\Omega_{\substack{main\\lobe}} + B_{Ground}(\theta,\varphi)\left\langle RA_{\substack{side\\lobes}}(\theta,\varphi)\right\rangle\Omega_{\substack{side\\lobes}}\right]$$

$$\approx 3K \qquad \approx 1 \qquad \ll 1\ srad \qquad \approx 300K \qquad \approx 2\pi\ srad$$

Obtaining : signal of interest >> disturbance signal

requires $\left\langle RA_{\substack{main\\lobe}}(\theta,\varphi)\right\rangle >>> \left\langle RA_{\substack{side\\lobes}}(\theta,\varphi)\right\rangle$

$$W \approx A \left[\underbrace{B_{sky}(\theta,\varphi) \left\langle RA_{\substack{main \\ lobe}}(\theta,\varphi) \right\rangle \Omega_{\substack{main \\ lobe}}}_{\text{signal of interest}} + \underbrace{B_{Ground}(\theta,\varphi) \left\langle RA_{\substack{side \\ lobes}}(\theta,\varphi) \right\rangle \Omega_{\substack{side \\ lobes}}}_{\text{disturbance signal}} \right]$$

$$\approx 3K \qquad \approx 1 \qquad <<1\ srad \qquad \approx 300K \qquad \approx 2\pi\ srad$$

$$\left\langle RA_{\substack{side \\ lobes}}(\theta,\varphi) \right\rangle << \left\langle RA_{\substack{main \\ lobe}}(\theta,\varphi) \right\rangle \left[\frac{\Omega_{\substack{main \\ lobe}}}{\Omega_{\substack{side \\ lobes}}} \right] \left[\frac{B_{sky}(\theta,\varphi)}{B_{Ground}(\theta,\varphi)} \right] \approx \frac{\Omega_{\substack{main \\ lobe}}(srad)}{600}$$

FWHM	$\Omega_{mainlobe}$	$<RA_{sidelobes}>$
10º	2×10^{-2} srad	$<<4\times10^{-5}$
1º	2×10^{-4} srad	$<<4\times10^{-7}$
10'	7×10^{-6} srad	$<<1\times10^{-8}$
1'	7×10^{-8} srad	$<<1\times10^{-10}$

!!!
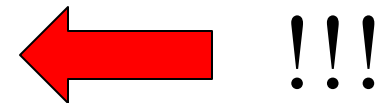
Low diffraction design

- Real world angular responses are worse than the one studied here.
- Sharp edges are in general important sources of diffraction, and must be avoided in low sidelobes design. Use smoothed edges.
- A trumpet has a slow transition to free space at the aperture to avoid diffraction of sound waves.
- The spider supporting the secondary mirror in a Cassegrain telescope is an important source of diffraction.
- Penzias and Wilson used an under-illuminated off-axis paraboloid, to get low sidelobes

10dB = a factor 10 in power

spillover lobe
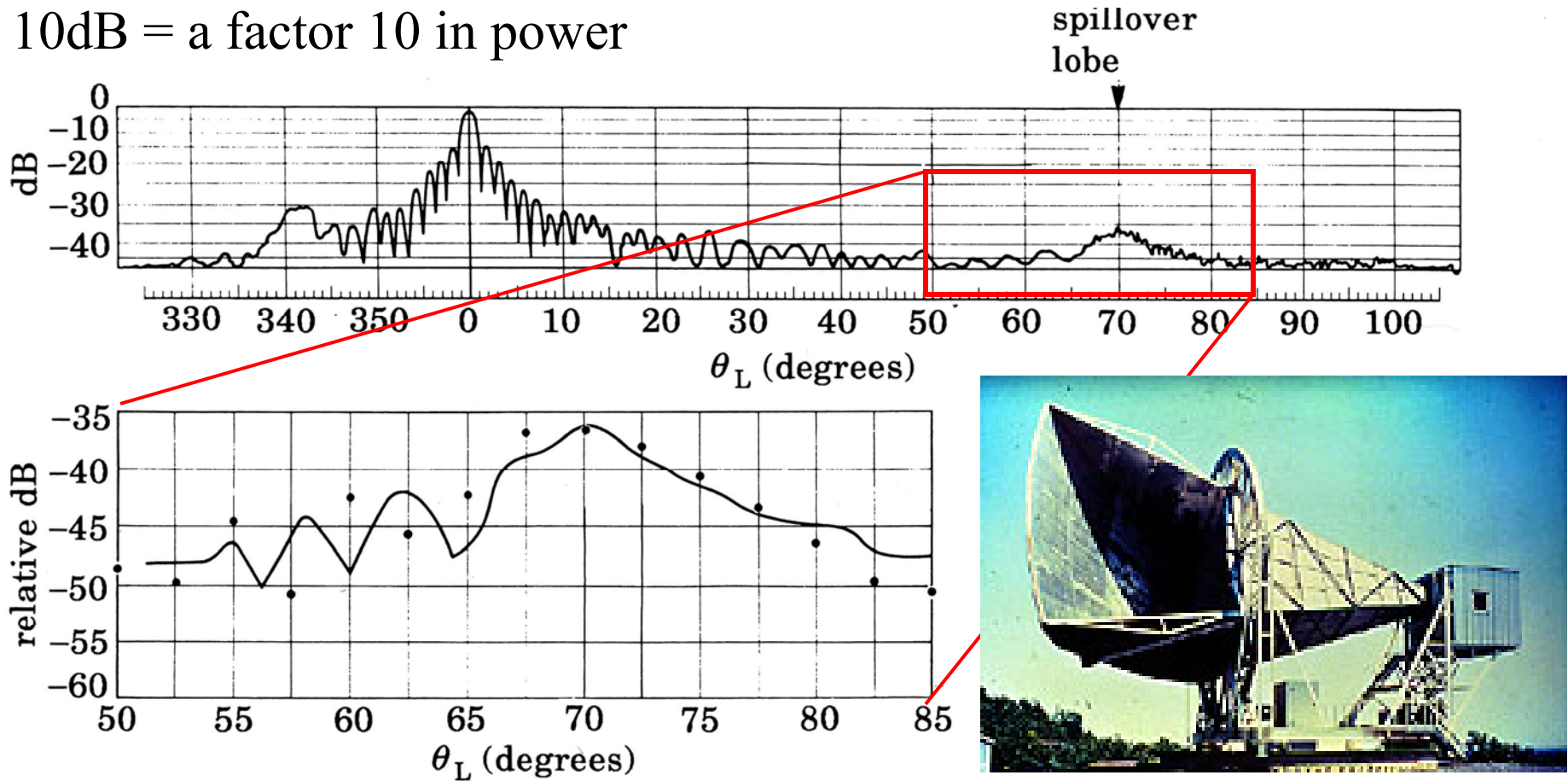
Fig. 12. – Upper panel: scheme of the horn-antenna. It is a part of a large paraboloid: lateral shields prevent spurious radiation entering in the system outside the nominal beam width. Isotropic level -43 dB. Lower panel: angular response of the antenna, as measured by means of a transmitter located in front of the antenna at different angles. The spillover lobe is studied in detail in the lowest part of the graph. Earth's radiation entering via the spillover lobe determines the antenna temperature noise. —— Measured data, ● computed data. (Adapted by Crawford *et al.* [34].)

Other example of low sidelobes design: Planck

STRAY LIGHT

Main Beam

Sub Spillover

Main Spillover

Main Spillover

F. Villa, LFI

Full Pattern of the LFI9 at 100 GHz, $\varphi = 45$ deg

COBE

WMAP,
Planck

L2

900km $\updownarrow$

1.5Mkm
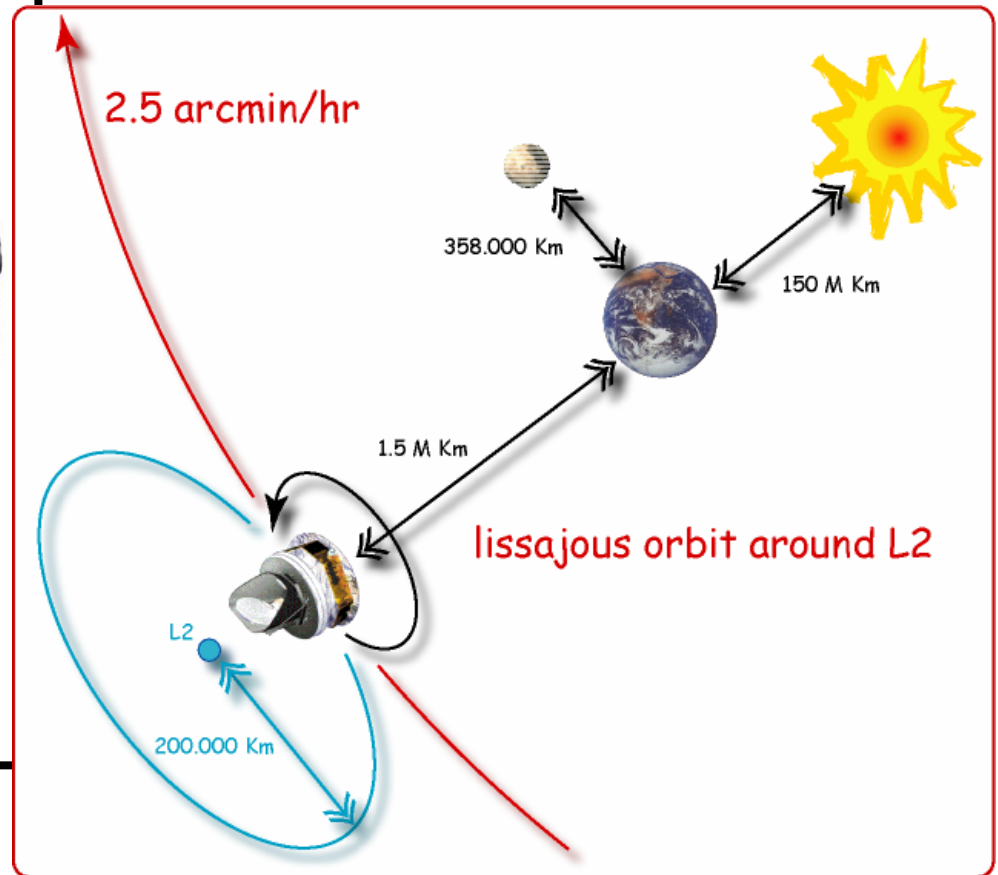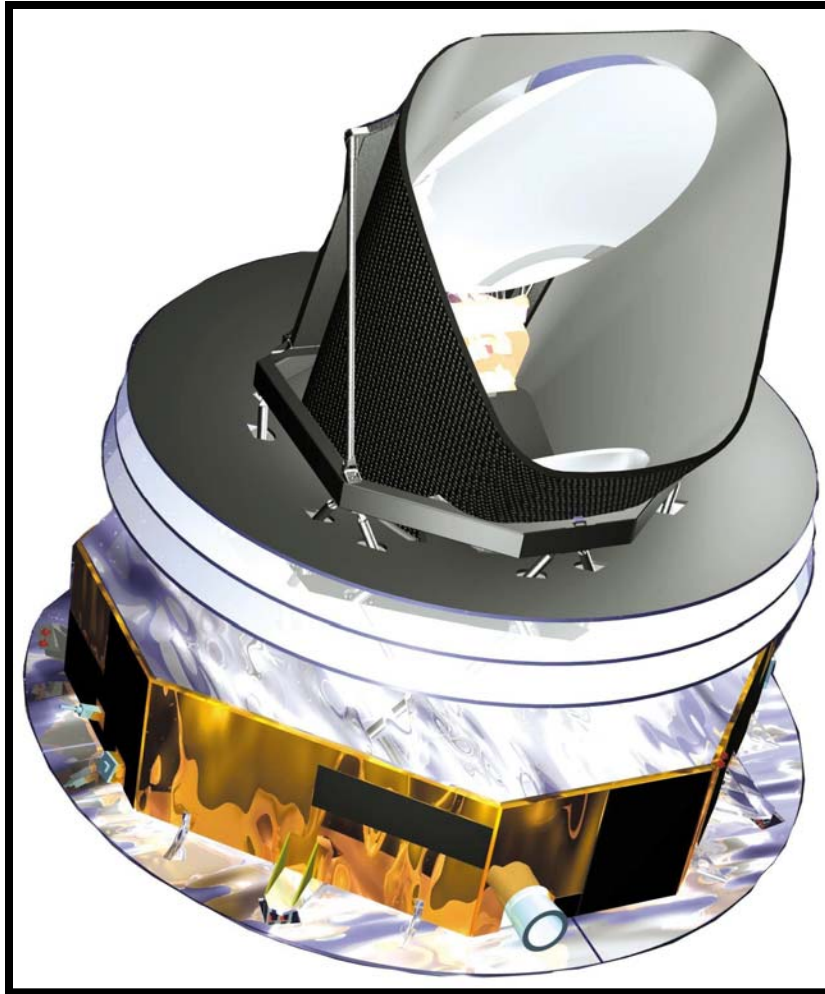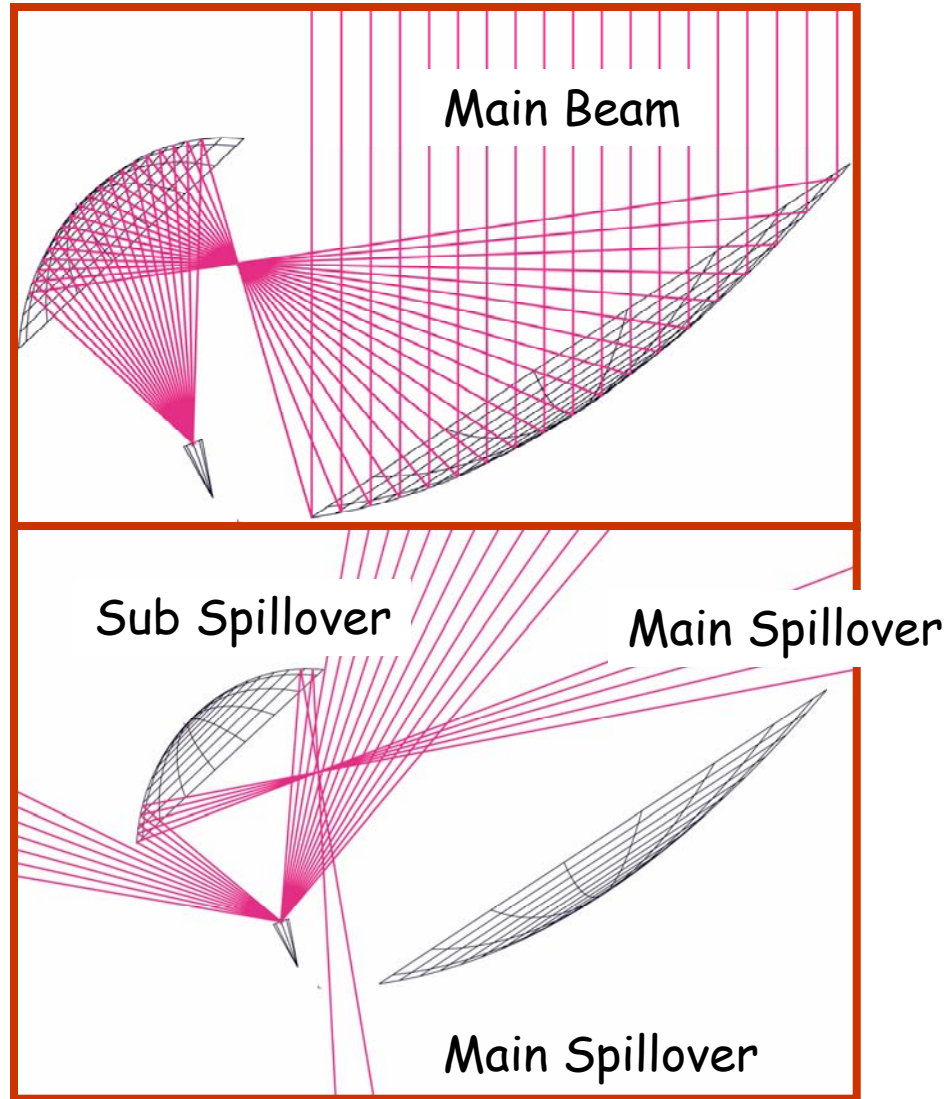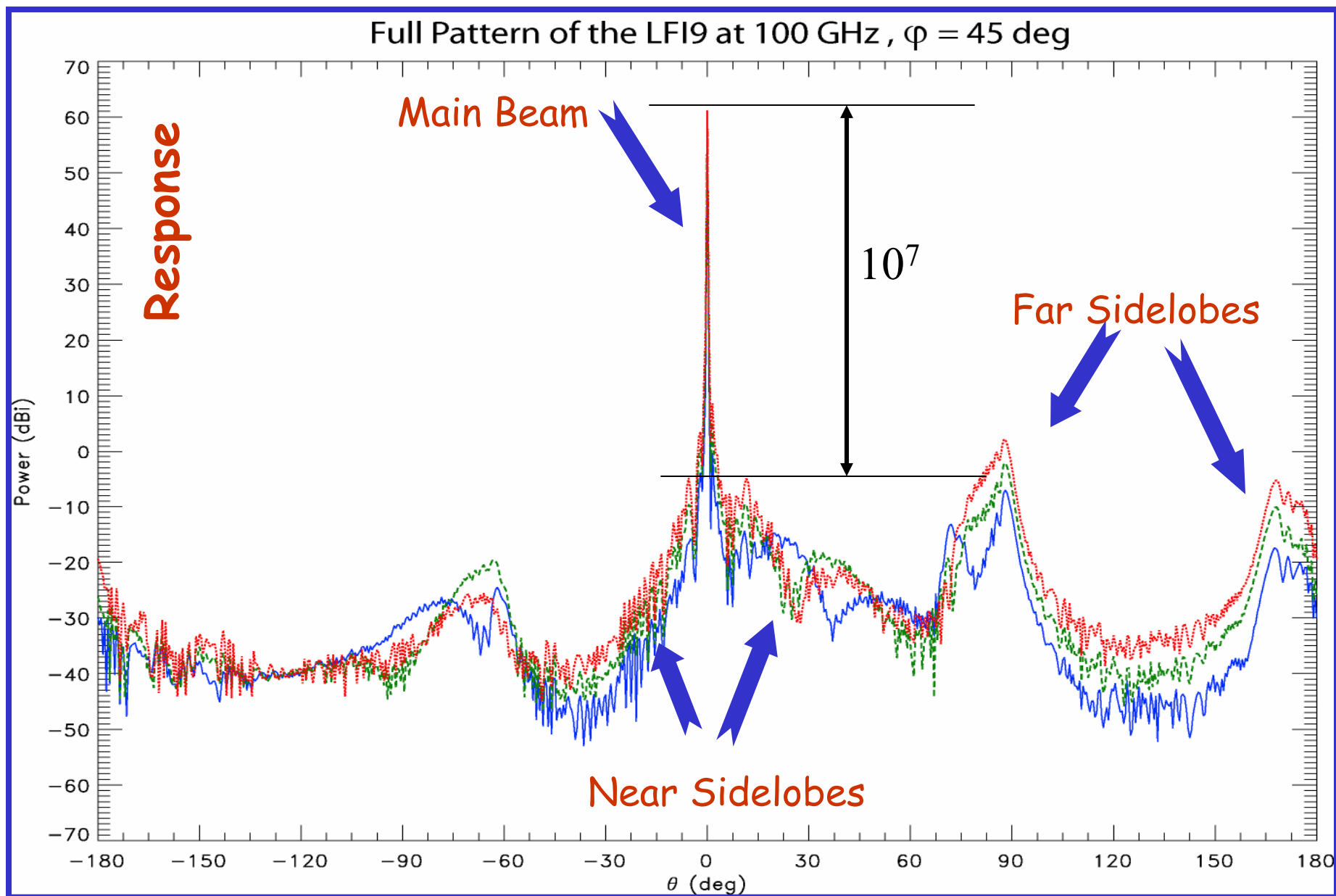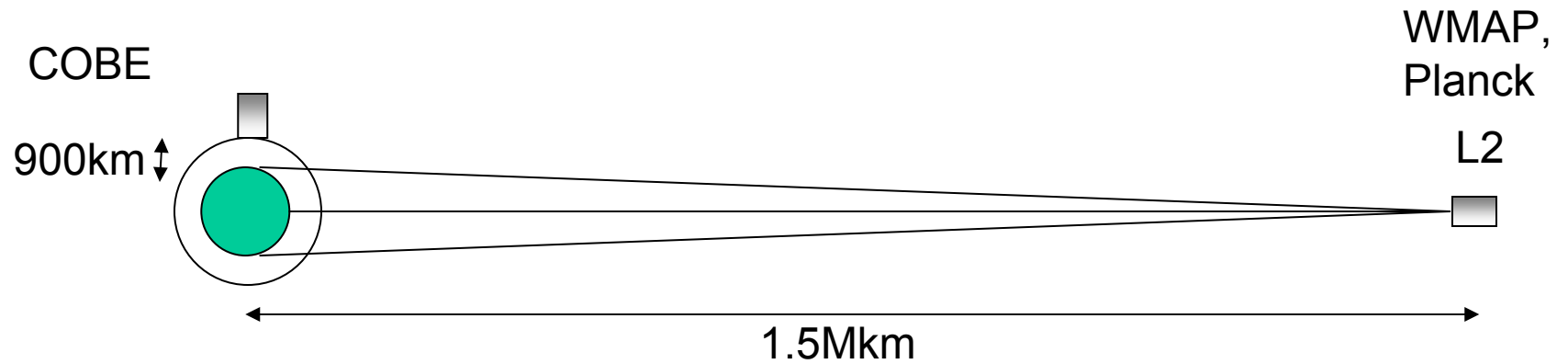
Going to L2 reduces the solid angle occupied by the Earth by a factor $2\pi/2\times10^{-4}=31000$, thus relaxing by the same factor the required off-axis rejection.

FWHM	$\Omega_{mainlobe}$	$<RA_{sidelobes}>$
10°	2×10^{-2} srad	$<<1$
1°	2×10^{-4} srad	$<<0.01$
10'	7×10^{-6} srad	$<<3\times10^{-4}$
1'	7×10^{-8} srad	$<<3\times10^{-6}$

BOOMERanG : launched from McMurdo (Antarctica) 1998

WMAP (lauched in 2001)
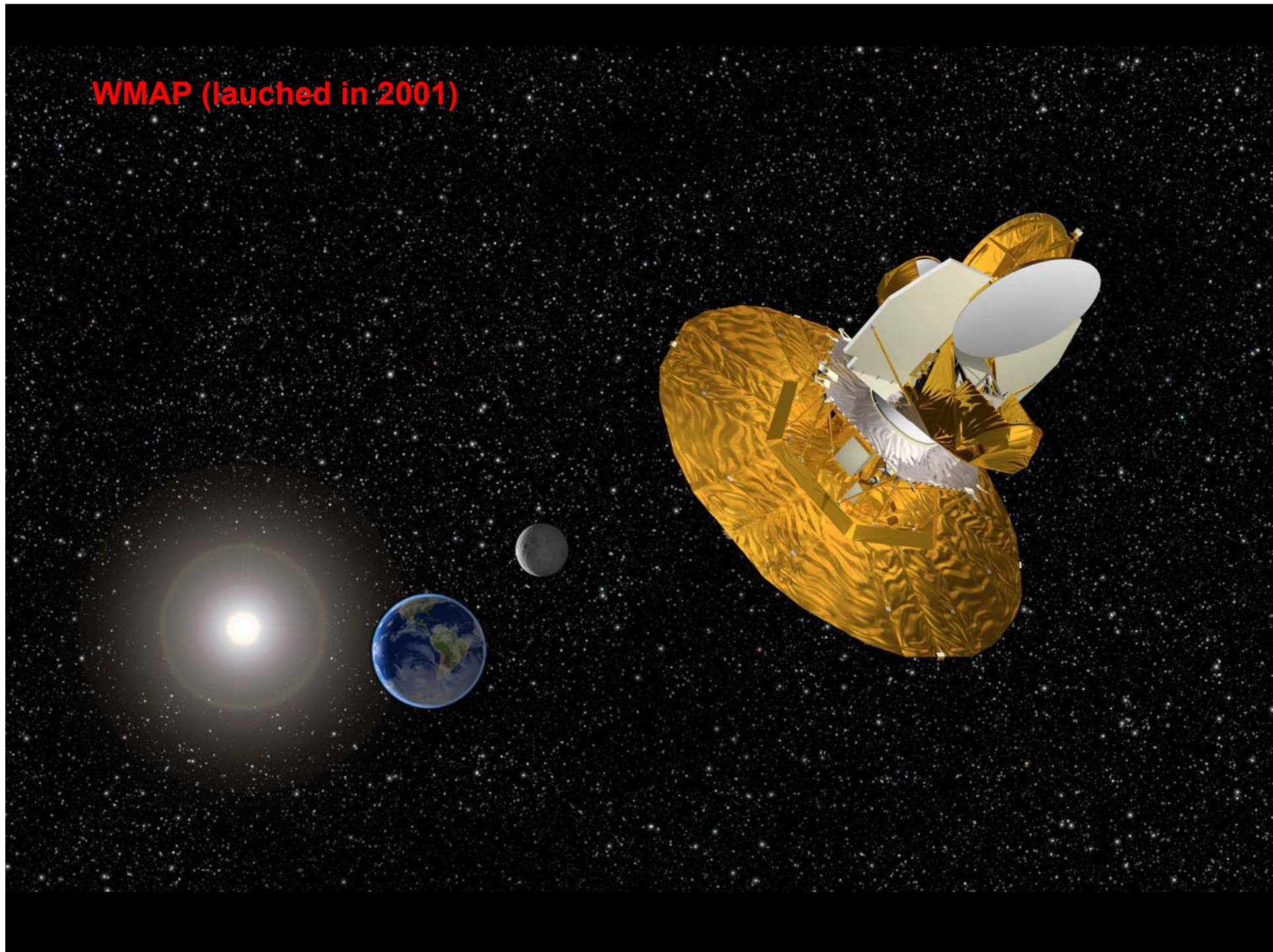
The last revolution …
ten years ago

- Large arrays of bolometers (2002 +)
- TES allow complete microfabrication of bolometers : large arrays possible
- e.g. Caltech/JPL, Berkeley, NIST, Goddard, Bonn, Paris, Grenoble …
- The mapping speed is boosted.
- Coupled to large (10m) telescopes, can explore the CMB with high angular resolution (arcmin)

Atacama Cosmology Telescope
6m diameter, 1 deg^2 FOV
5190 m osl
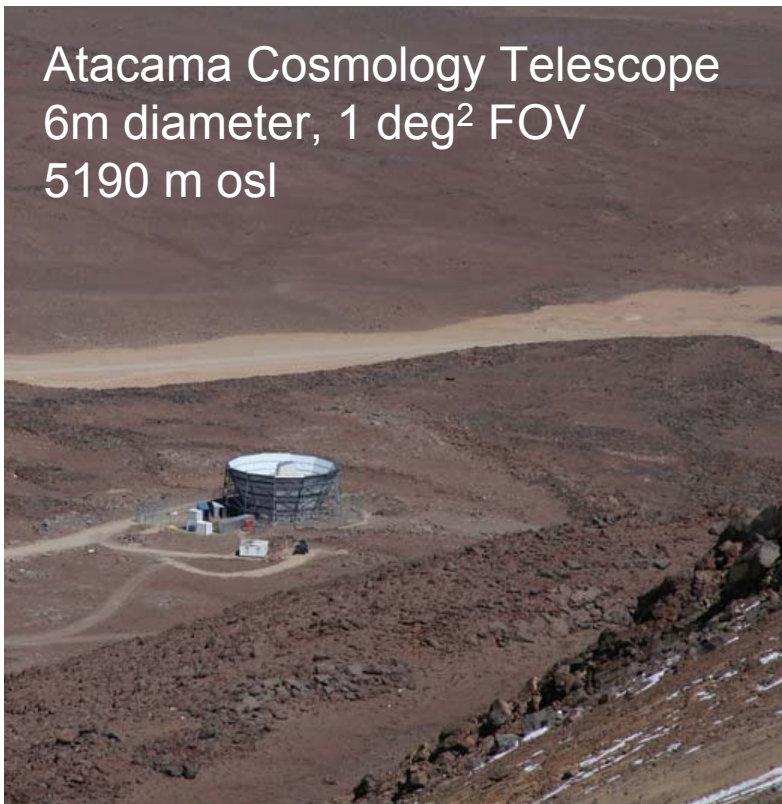
South Pole Telescope
10m diameter, 1 deg^2 FOV
2800 m osl
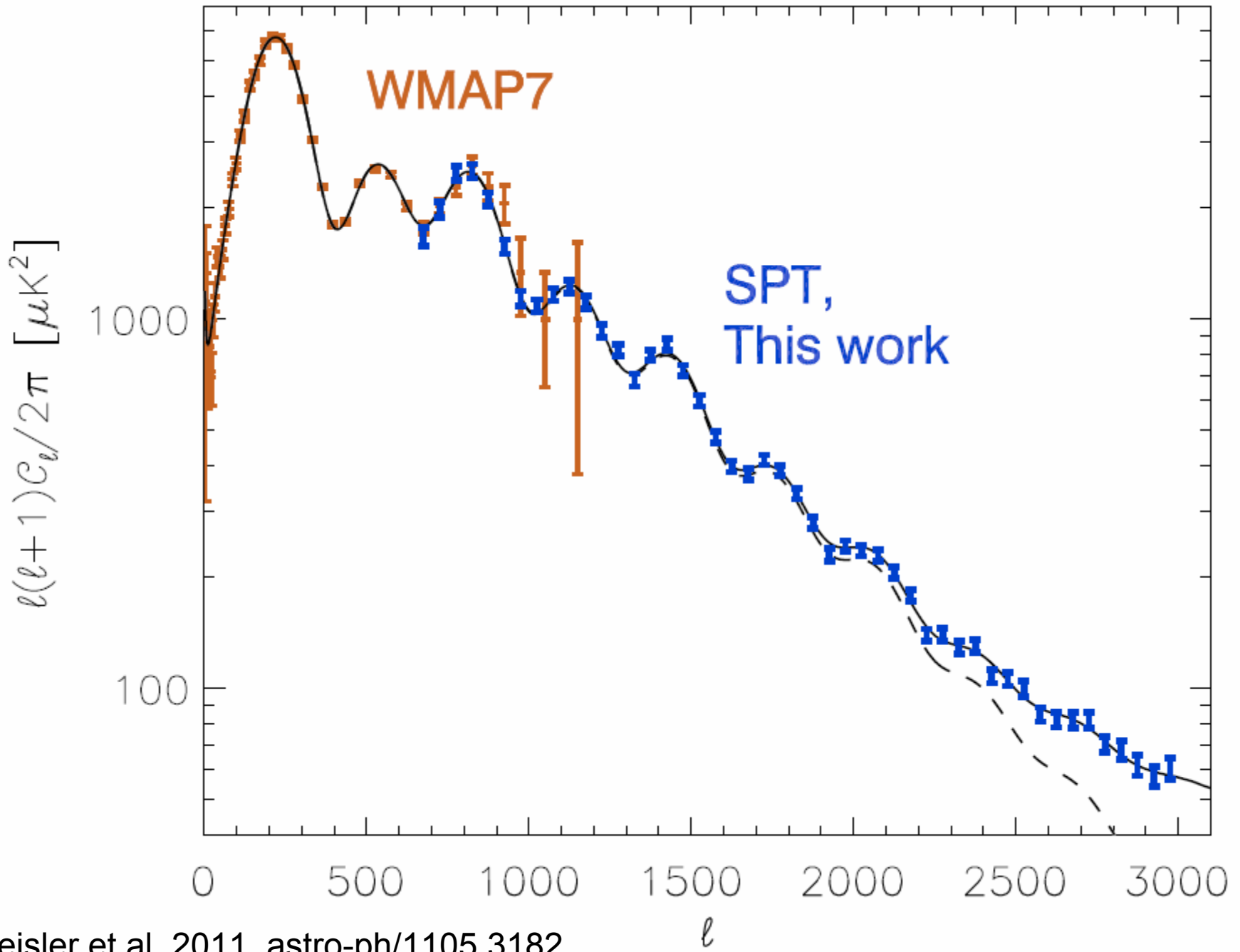
Keisler et al. 2011, astro-ph/1105.3182

**Radiazione
< 0.3%**

**Materia
Normale
4%**

Baryons

**Materia
Oscura
22%**

Dark Matter

**Energia
Oscura
74%**

Dark Energy
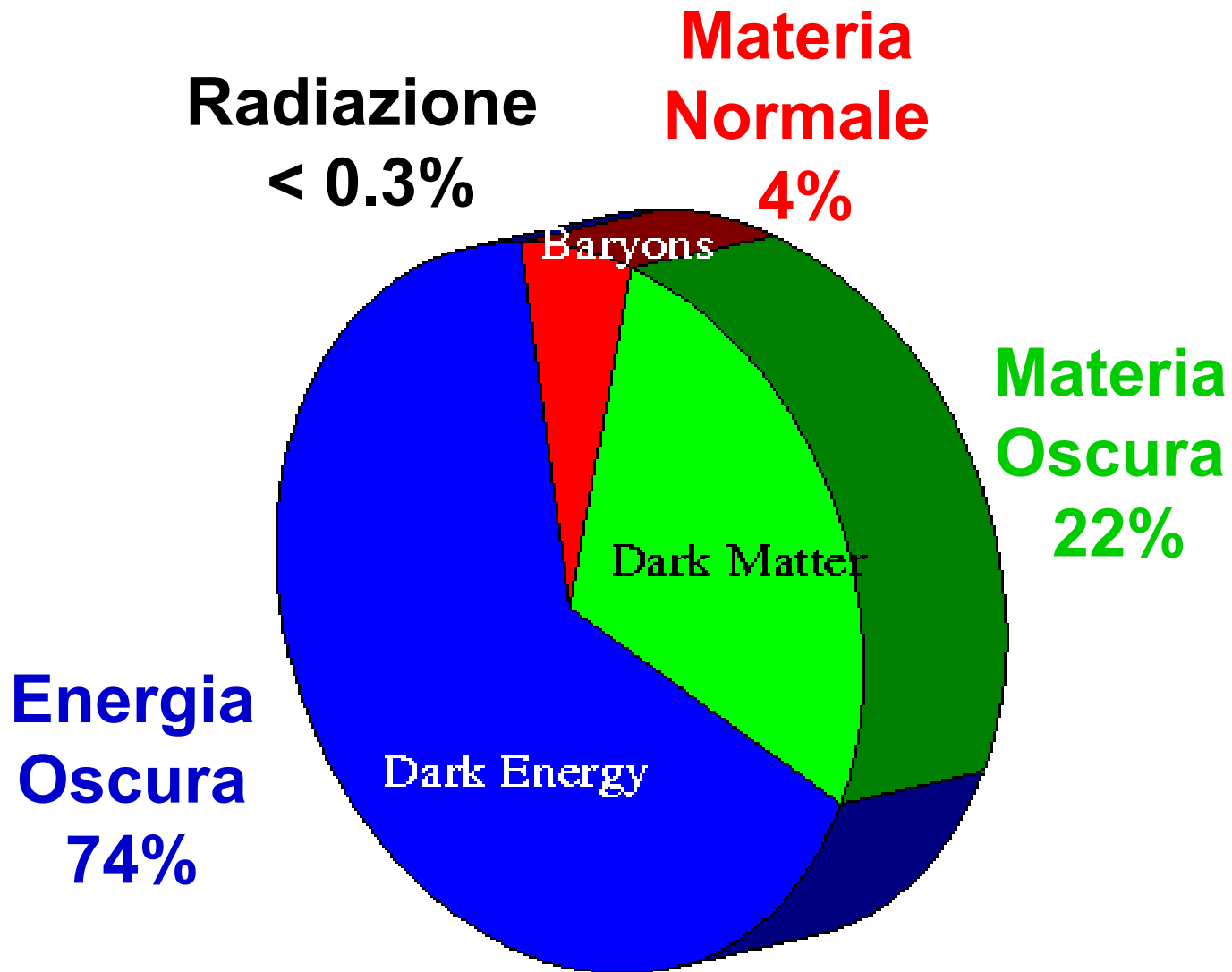
Planck

Current Trends & Requirements for new detectors

- CMB Anisotropy for neutrino mass, dark matter, etc.

- Sunyaev-Zeldovich effect

- Spectroscopy of the CMB

- Polarization Measurements

ALL THESE MEASUREMENTS REQUIRE ARRAYS OF DETECTORS LIMITED BY PHOTON NOISE, TO BOOST THE MAPPING SPEED

MOST OF THESE MEASUREMENTS REQUIRE SPACE MISSIONS TO REDUCE THE RADIATIVE BACKGROUND

Neutrinos and the CMB

- Structures present between us and the CMB act as lenses on CMB anisotropy and polarization.
- The formation of structures depends on the presence of cosmological neutrinos and their masses.. so does their effect on CMB spectra
- This effect acts in epochs when structures are more linear than those sampled by direct galaxy surveys like Euclid, which are affected by non-linear effects.
- So CMB data extend and complement optical data. The combination of Euclid + Planck data will have a sensitivity to $\Sigma m_\nu = 0.25$ eV (1σ) (see Galli et al. 2009)
- Using an optimized balloon mission we can reach $\Sigma m_\nu = 0.05$ eV (1σ) which ensures the determination of neutrino hierarchy.
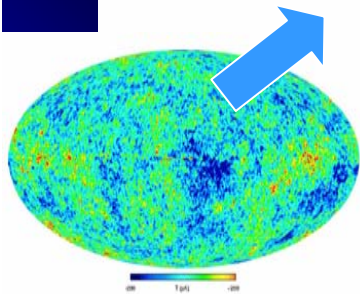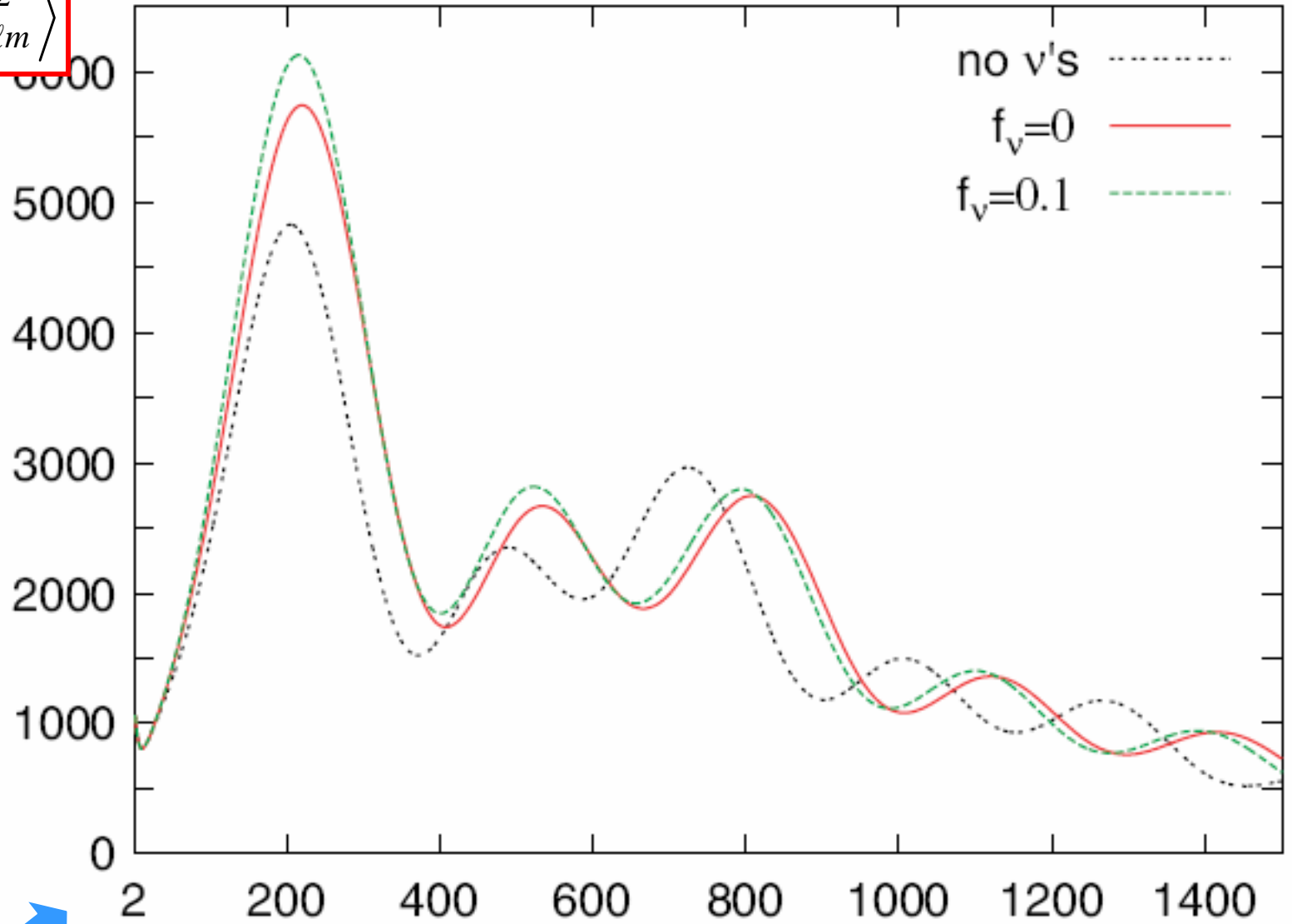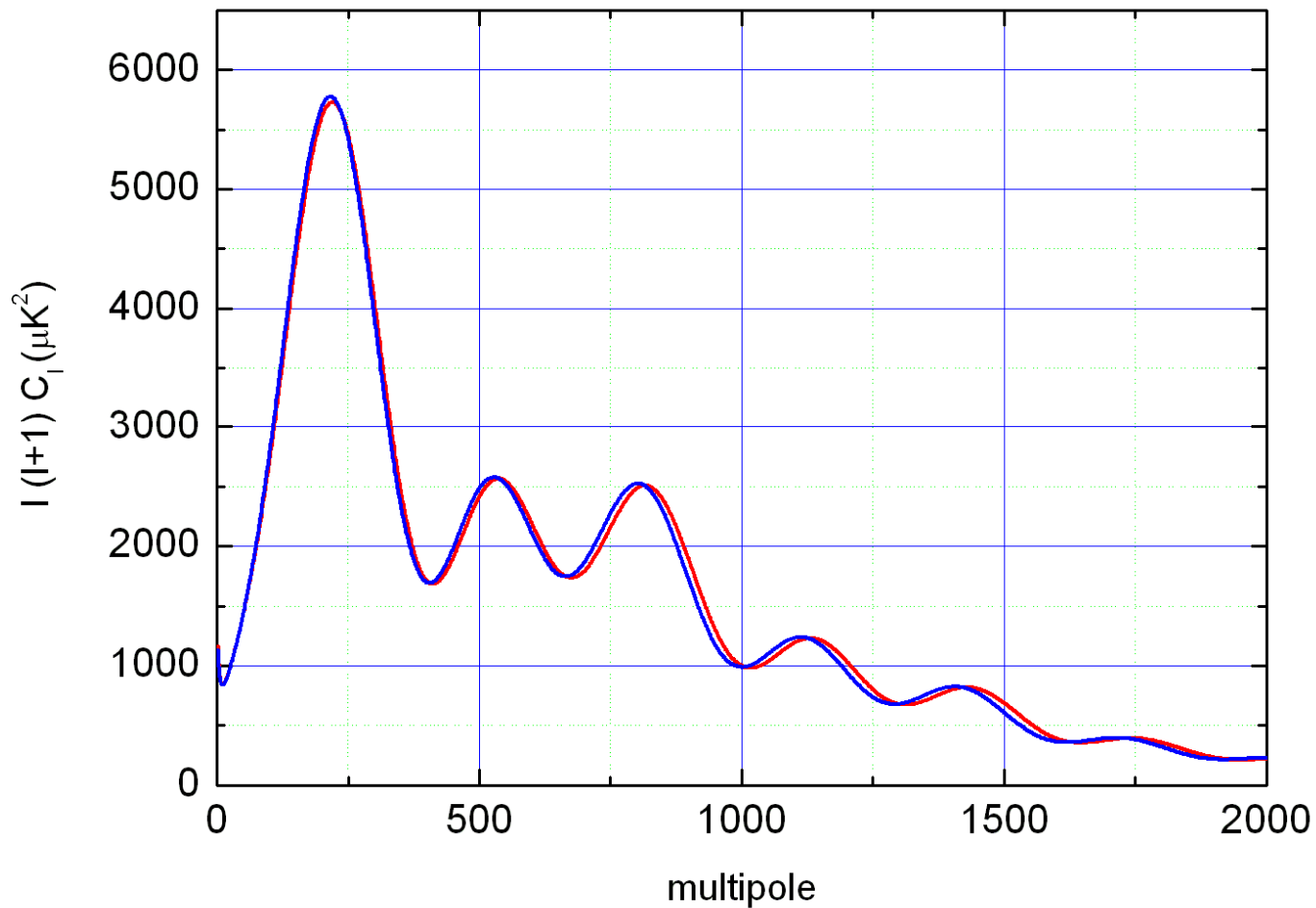
- Effect on massive neutrinos on CMB anisotropy power spectrum (red: $N\nu=3$, $\Sigma m\nu=0.65$ eV)
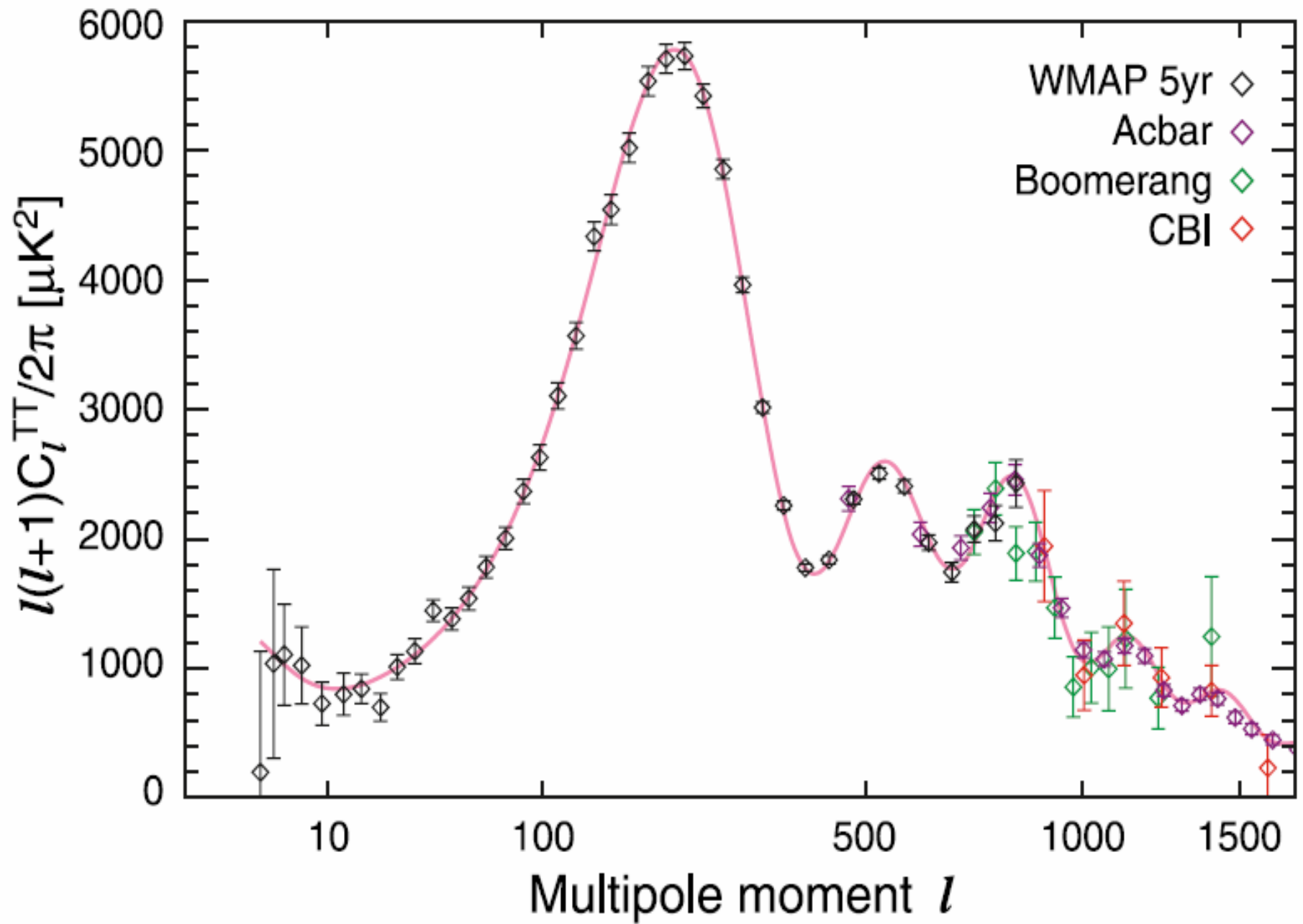
TABLE II: Representative cosmological data sets and corresponding 2σ (95% C.L.) constraints on the sum of ν masses Σ.

Case	Cosmological data set	Σ (at 2σ)
1	CMB	< 1.19 eV
2	CMB + LSS	< 0.71 eV
3	CMB + HST + SN-Ia	< 0.75 eV
4	CMB + HST + SN-Ia + BAO	< 0.60 eV
5	CMB + HST + SN-Ia + BAO + Lyα	< 0.19 eV

From Fogli et al. 2008, Astro-ph/0805.2517

With Planck : < 0.2 eV
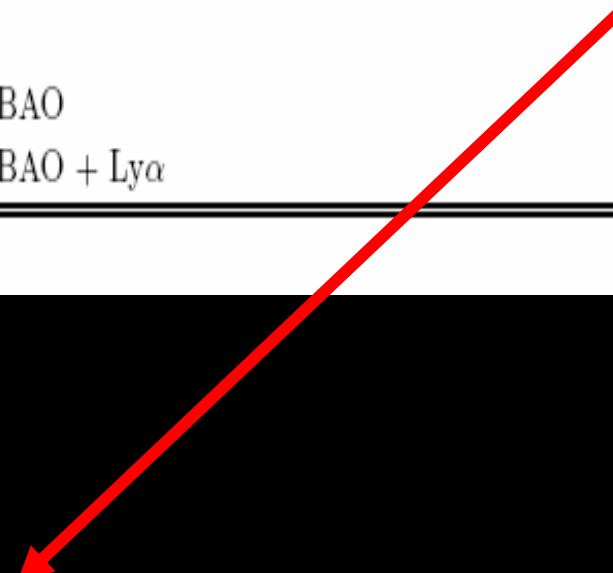
a large CMB telescope can be used to measure neutrino masses

- High sensitivity, angular resolution and sky coverage are all needed simultaneously.
- Large, shielded telescope (4m diam.) with large focal plane. Difficult to accomodate on a rocket.
- Can be done with current technology on a balloon:
  - 1000 KIDs detectors @ 220 GHz (RIC INFN group V)
  - OLIMPO – like telescope with 4m carbon-fiber mirror
  - Resolution 1.5' FWHM (single mode)
  - Pointing instrument (not scanning) for improved calibration.
  - Polar-night flight for large sky coverage.
  - Total cost below 3M€, realization 3 years
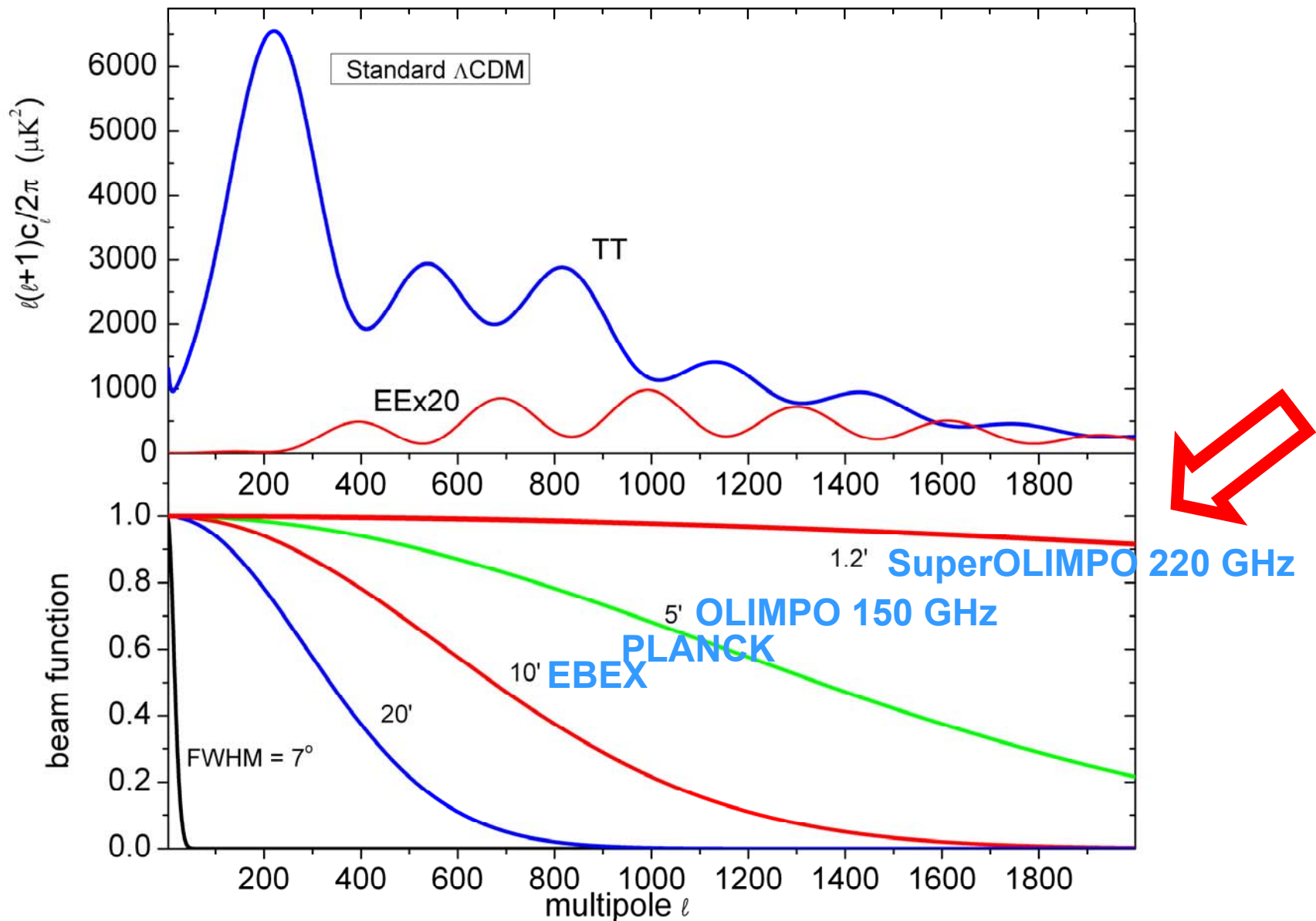
Angular resolution is the key !

Super-OLIMPO: performance
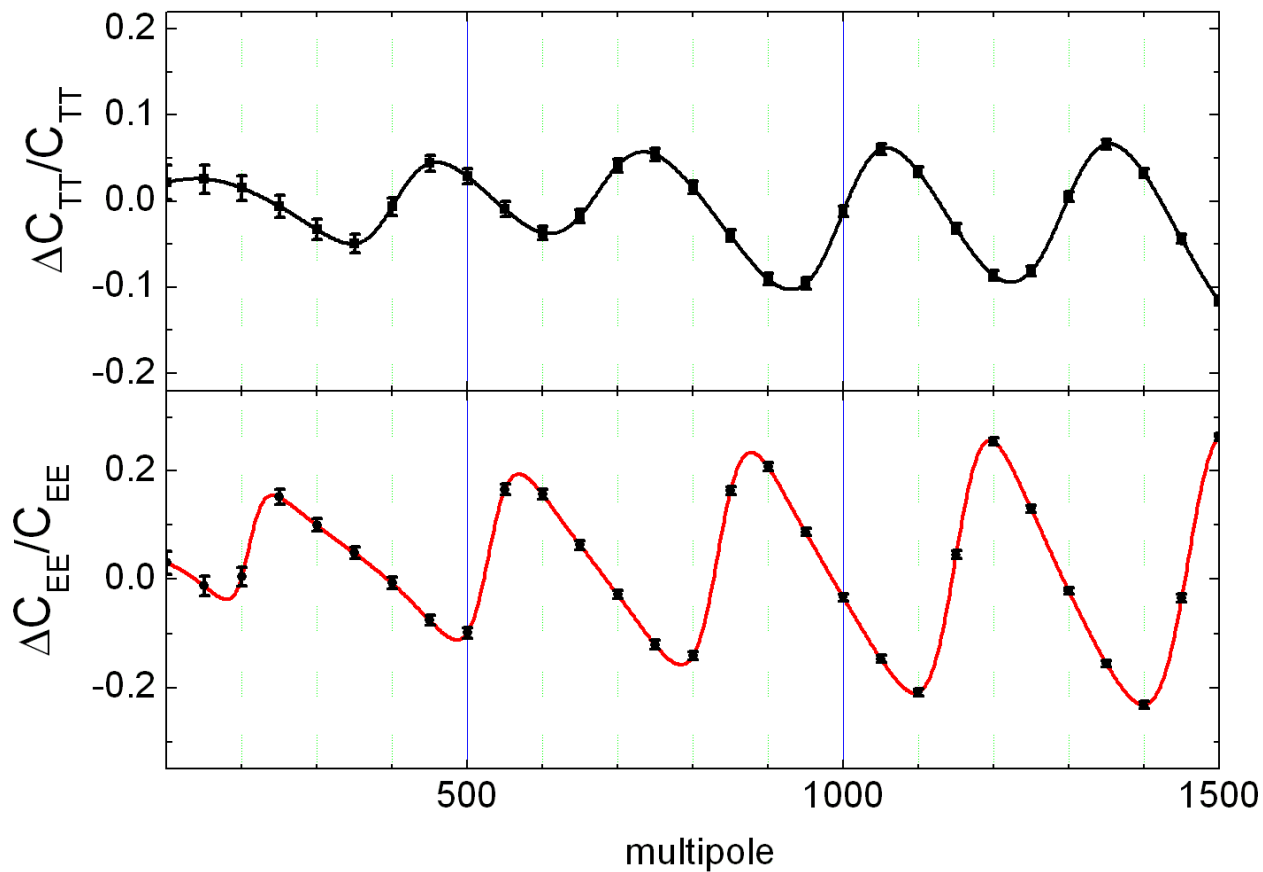
- **Effect on massive neutrinos on CMB anisotropy and polarization spectra (Nν=3, Σmν=0.65 eV)**

Super-OLIMPO: performance

Combining a new CMB experiment to Planck coud improve the bounds on the neutrino mass by a factor 3 (without any other prior). This would falsify Degenerate Hierarchy and probe the Inverted Hierarchy
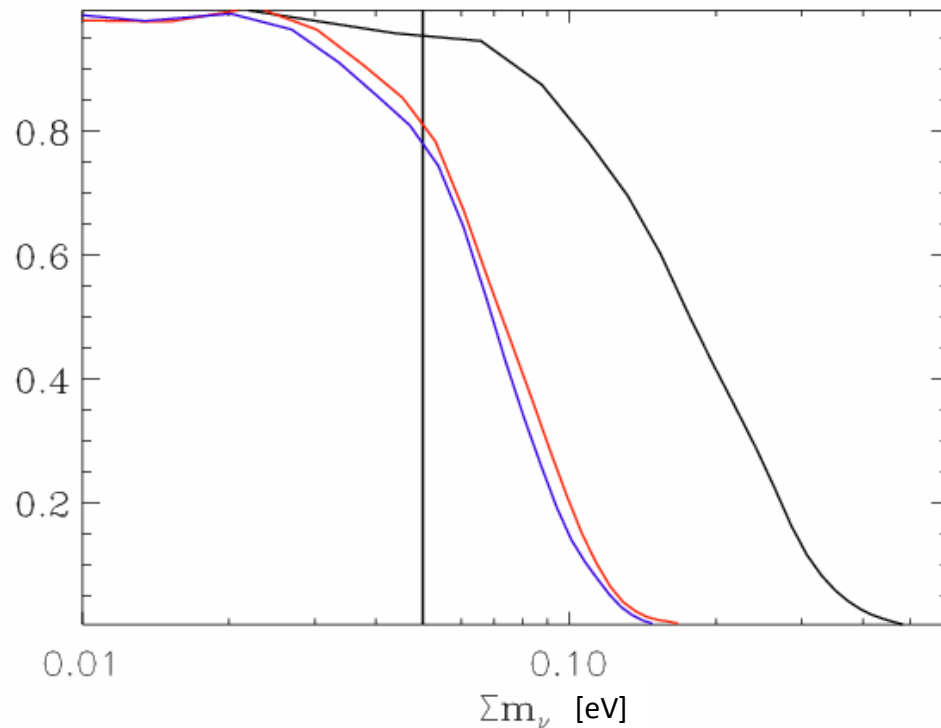
Limits at 95% c.l.:

Black: Planck

$$\sum m_n < 0.28\ eV$$

Red: Planck+1000 bol.

$$\sum m_n < 0.098\ eV$$

Blue: Planck+5000 bol

$$\sum m_n < 0.093\ eV$$

- **constraints on neutrino masses (from Pagano & Melchiorri)**

Constraints on Neutrino Masses from CMB + Priors

Limits at 95% c.l.:
Red: 1000 riv+
    Prior 1% H_0+
    Priori 2% Ω_m

$$\sum m_n < 0.057\ eV$$

Blue: 5000 riv+
    Prior 1% H_0+
    Priori 2% Ω_m

$$\sum m_n < 0.054\ eV$$

Red Dashed: 1000 riv+
    Prior 0.5% H_0+
    Priori 1% Ω_m

$$\sum m_n < 0.040\ eV$$

Blue Dashed: 5000 riv+
    Prior 0.5% H_0+
    Priori 1% Ω_m

$$\sum m_n < 0.035\ eV$$
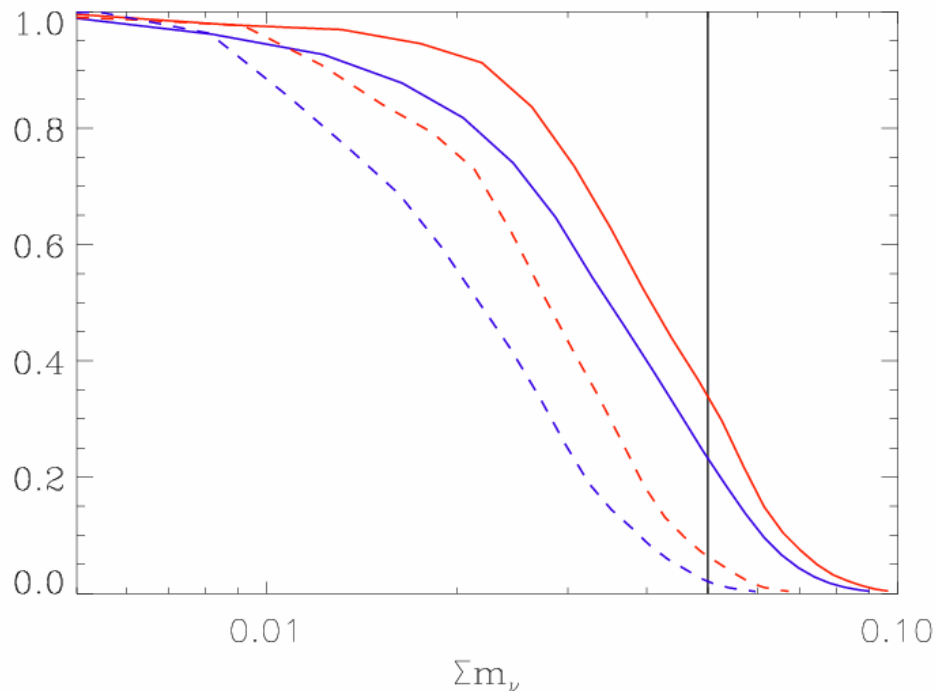
With external priors on the Hubble parameter
And the matter density also the Normal
Hierarchy can be probed: safe detection of
a neutrino mass.

● **constraints on neutrino masses (from Pagano & Melchiorri)**

Parameter uncertainty	Planck	Planck +SuperOlimpo	Planck +SO+Euclid
$\sigma(\sum m_\nu)$	< 0.28 eV	< 0.09 eV (3.1)	< 0.05 eV (5.6)

TABLE I.   errors on cosmological parameters in the case of massive neutrinos. The numbers in brackets show the improvement factor σ_{Planck}/σ respect to the Planck experiment. The entries for $\sigma(\sum m_\nu)$ are upper limits $(<)$ at 95% c.l..

Parameter uncertainty	Planck	Planck +SuperOlimpo	Planck +SO+Euclid
$\sigma(N_\nu^{\mathrm{eff}})$	0.18	0.044　　(4.1)	0.034　　(5.3)

TABLE II. 68% c.l. errors on cosmological parameters in the case of extra background of relativistic particles N_ν^{eff}. The numbers in brackets show the improvement factor σ_{Planck}/σ respect to the Planck experiment.

Parameter uncertainty	Planck	Planck +SuperOlimpo		Planck +SO+Euclid	
$\sigma(Y_p)$	0.010	0.0033	(3.0)	0.0025	(4.0)

TABLE III. 68% c.l. errors on cosmological parameters in the case of helium abundance. The numbers in brackets show the improvement factor σ_{Planck}/σ respect to the Planck experiment.

CMB & galaxy clusters (..and dark matter ..)
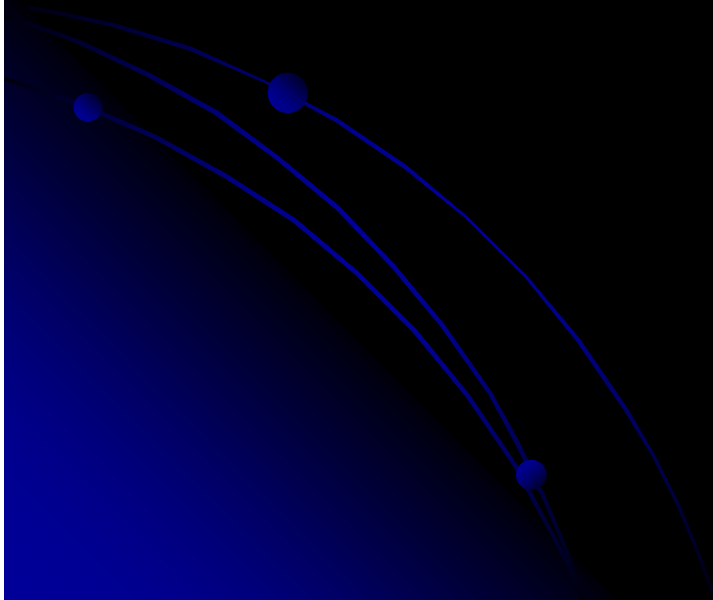
S-Z

- Inverse Compton Effect for CMB photons against charged particles in the hot gas of clusters
- Cluster optical depth: $\tau = n\sigma\ell$

  ℓ = a few Mpc = 10^{25} cm

  $n < 10^{-3}$ cm^{-3}

  $\sigma = 6.65 \times 10^{-25}$ cm^2

- So $\tau = n\sigma\ell < 0.01$: there is a 1% likelihood that a CMB photon crossing the cluster is scattered by an electron

- Eelectron >> Ephoton, so the electron transfers energy to the photon. To first order, the energy gain of the photon is

$$\frac{\Delta\nu}{\nu} = \frac{kT_e}{m_e c^2} \approx \frac{5keV}{500keV} = 0.01$$

- The resulting CMB temperature anisotropy is

$$\frac{\Delta T}{T} \approx \tau \frac{\Delta\nu}{\nu} \approx 0.01 \times 0.01 = 10^{-4}$$

CMB photons

cluster

Birkinshaw M., 1999, Physics Reports, 310, 97-195
Sunyaev R., Zeldovich Y.B., 1972, Comm. Astrophys. Space Phys., 4, 173
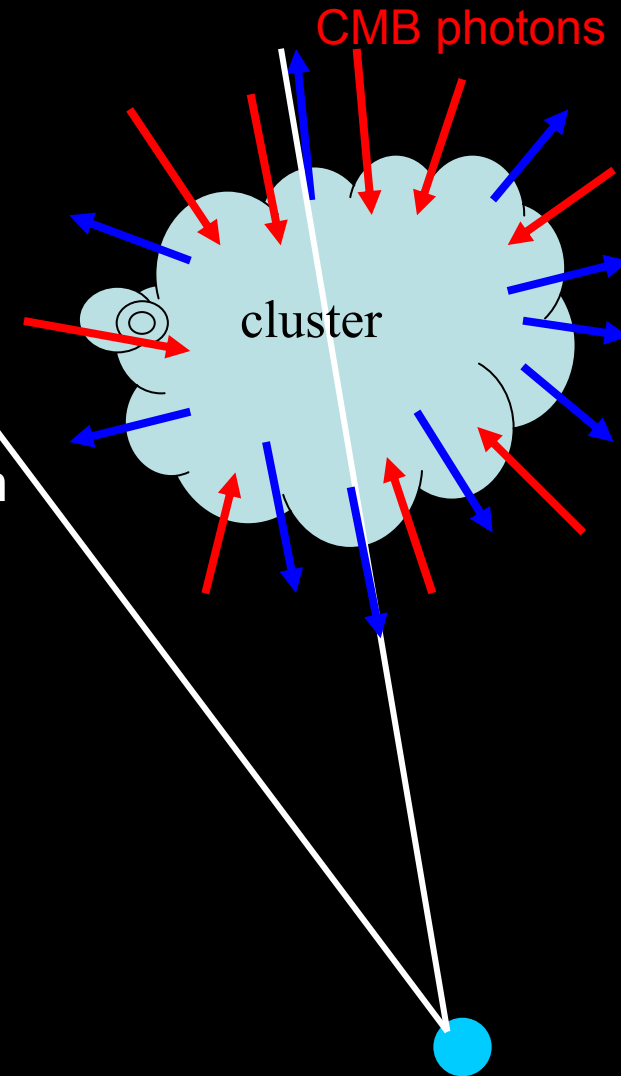
The Sunyaev-Zeldovich Effect

- The S-Z Effect does not depend on the distance (redshift) of the cluster, and depends linearly on the density of the gas

- X-ray brightness decreases significantly with distance and gas density (depends on the square of the density).

X-ray   S-Z   X-ray   S-Z   X-ray   S-Z

Sunyaev-Zeldovich Effect

All photons increase their energy. The result is a distortion of the spectrum of the CMB in the direction of rich clusters

Brightness

frequency

A decrement at low frequencies (<217GHz)

An increment at high frequencies (> 217GHz)

best ground-based photometers: 4 bands

Atmospheric transmission, pwv=0.5mm

ISD Δ emission, 18K
6 kJy/sr @ 150 GHz

Thermal SZ

Non-Thermal SZ

Kinematic SZ

Thermal SZ

transmission

1.0
0.8
0.6
0.4
0.2
0.0

0   200   400   600   800   1000

Brightness (MJy/sr)

0.15
0.10
0.05
0.00
-0.05
-0.10

0   200   400   600   800   1000
frequency (GHz)

EC0   EC1, EC2   EC3   EC4   EC5

Dynamically Relaxed Clusters

X-ray
Images
(Chandra)

| ABELL 2029 | MS2137 | MS1137 |
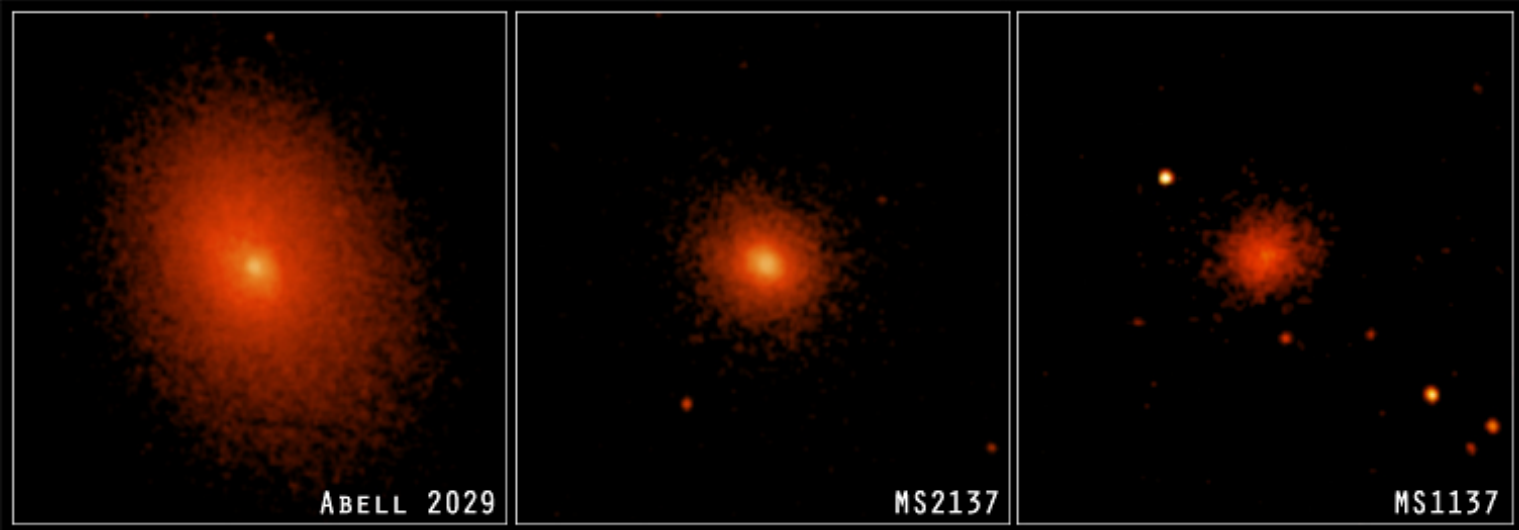
D = 1 GLy   3.5 GLy   6.7 GLy

● 0.4' FWHM beam (λ = 1.1 mm D = 12000 mm)

● 0.5' FWHM beam (λ = 1.4 mm D = 12000 mm)

● 0.7' FWHM beam (λ = 2.0 mm D = 12000 mm)

Not all clusters are dynamically relaxed and well beheaved, like the ones above.
So we need large telescopes to study the internal structure,
and/or spectroscopic observations to detect non-thermal effects.

Perseus Cluster
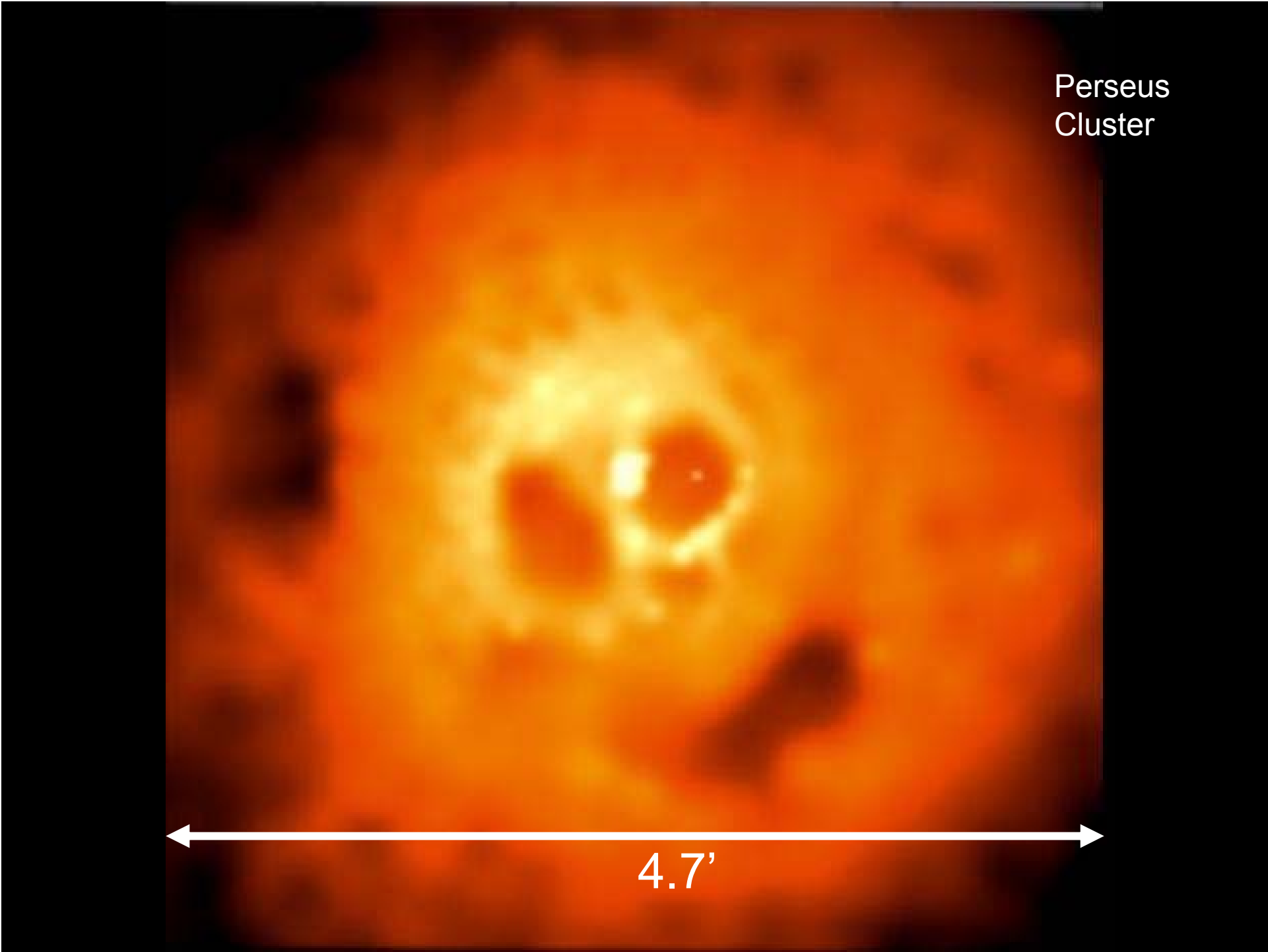
4.7'

large telescopes (10m class)

….

and large arrays
of detectors (1000 or more)

Atacama Cosmology telescope (ACT)
APEX – SZ
South Pole Telescope
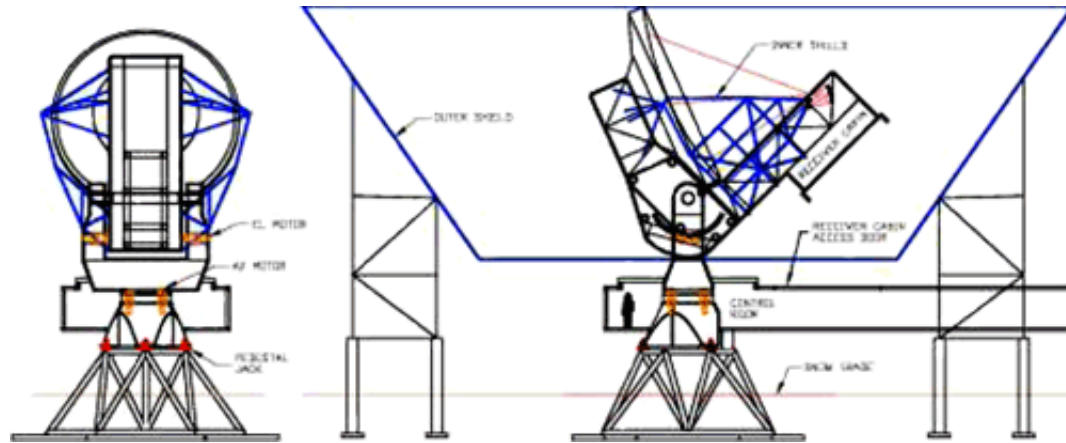
2003   *The South Pole Telescope*

SPT

2006

2007: first light

(1) FROM SKY

(3) Secondary Mirror

(4) Focal Plane

(2) Primary Mirror

1m

10K

10K

0.3K
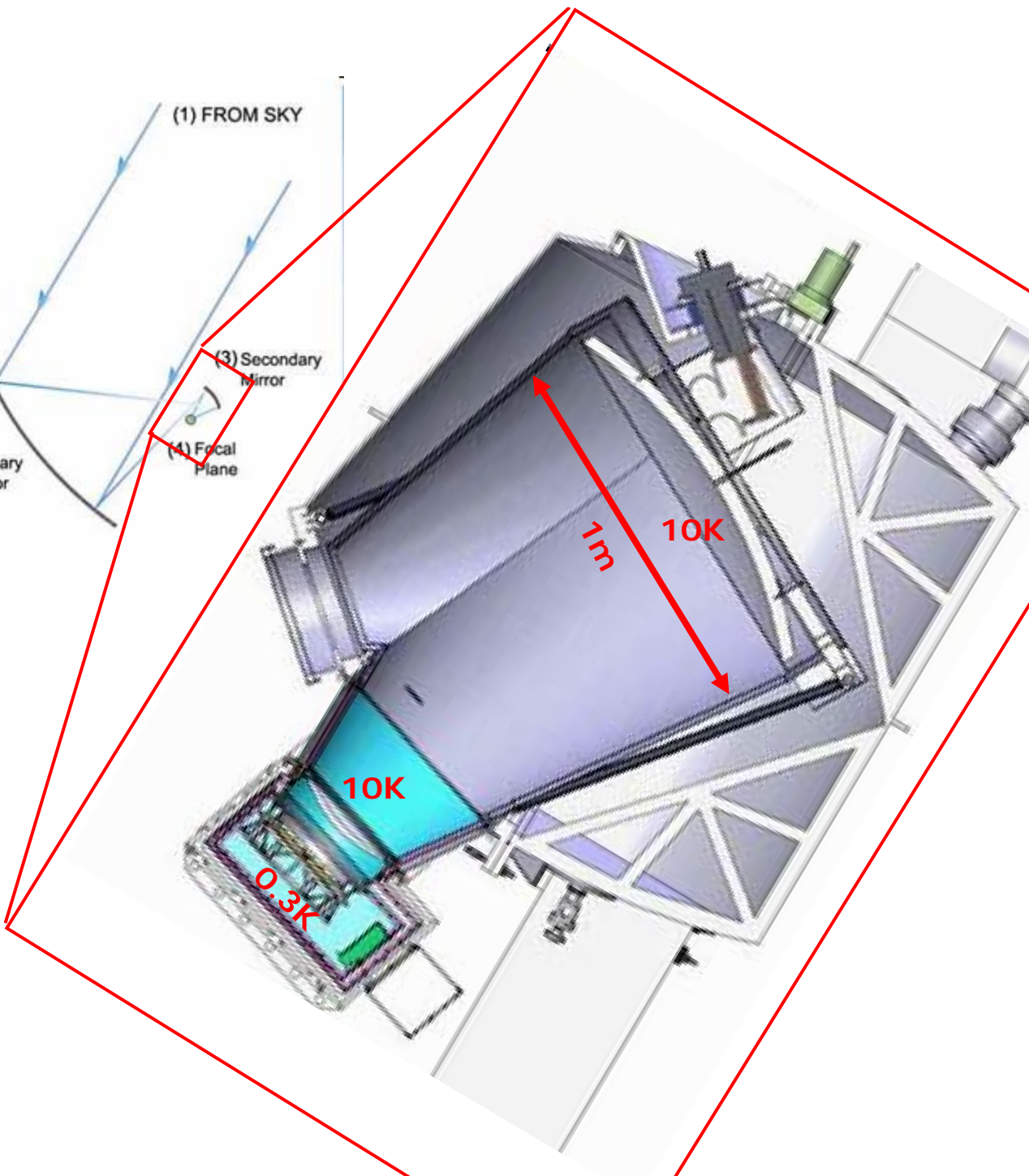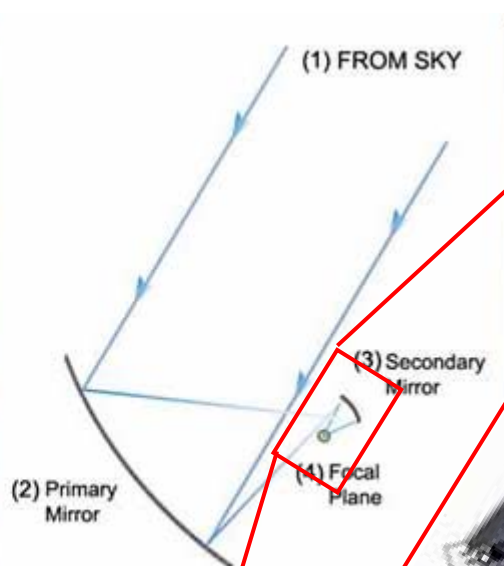
Optics Cryostat + Receiver

Receiver Array

180 mm = 1 degree diameter (on sky)
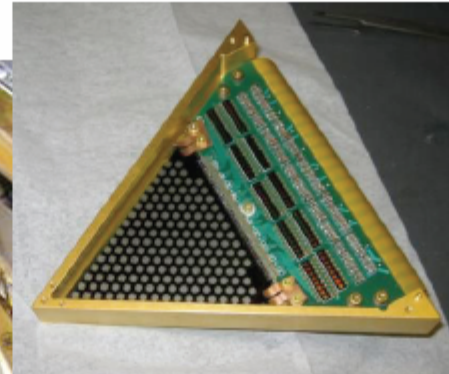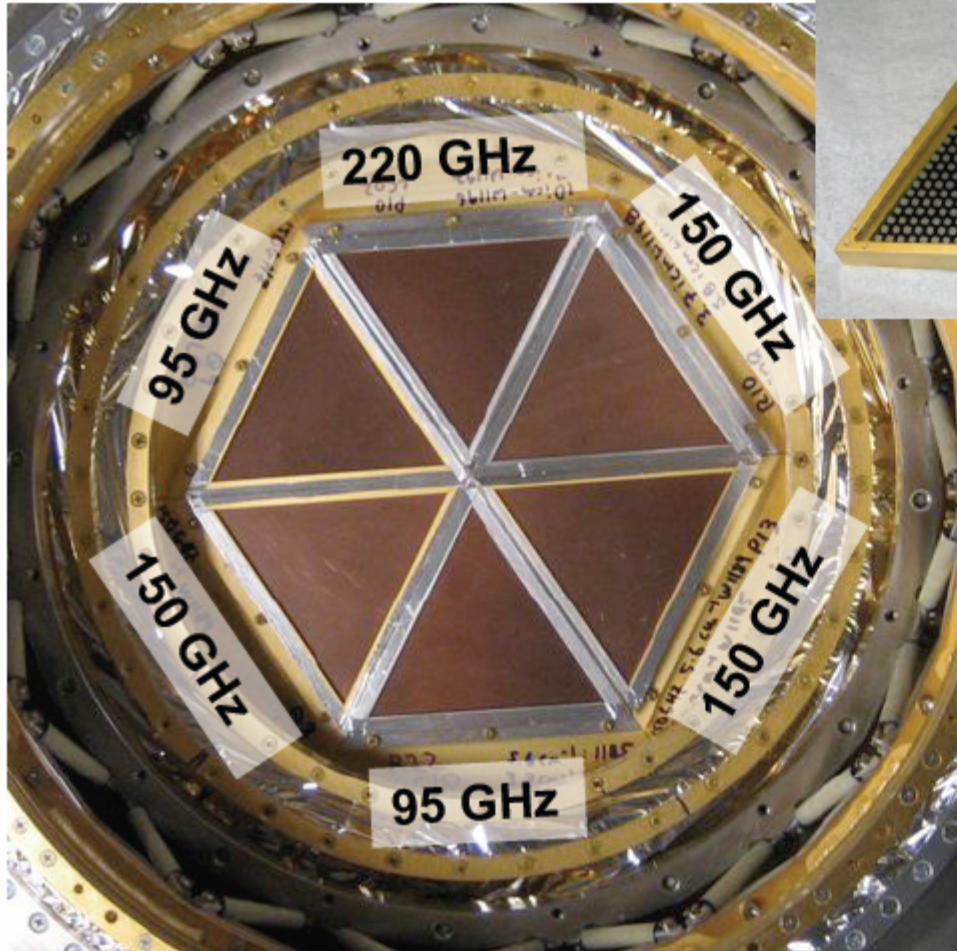
- 6 wedges * 160 bolometers per wedge = 960 channels

- 8 bolometers read out by a single SQUID using frequency-domain multiplexing

- Three bands: 90 GHz, 150 GHz, 220 GHz
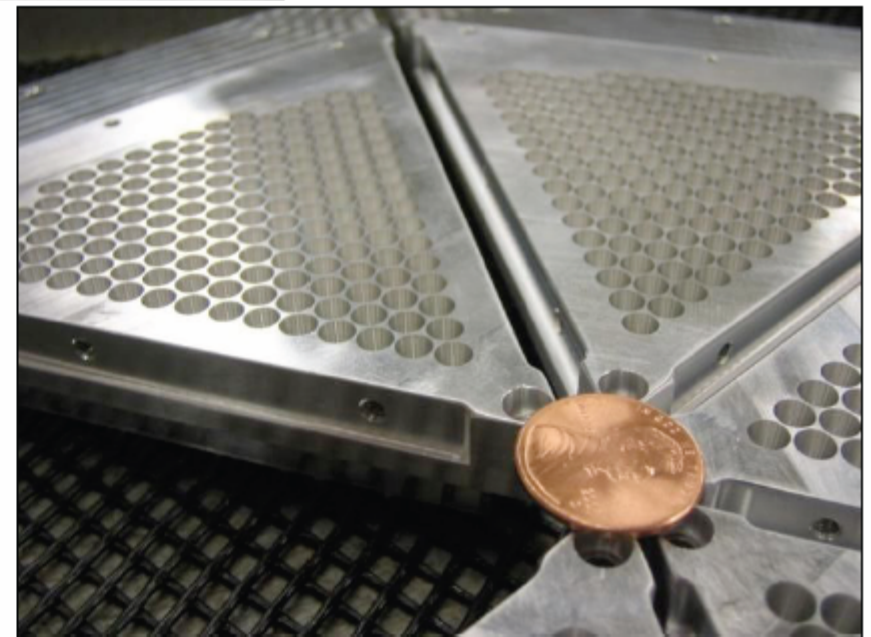
Bolometers

Suspended gold spiderweb bolometer read out with a TES
and frequency domain multiplexing (like an AM radio)
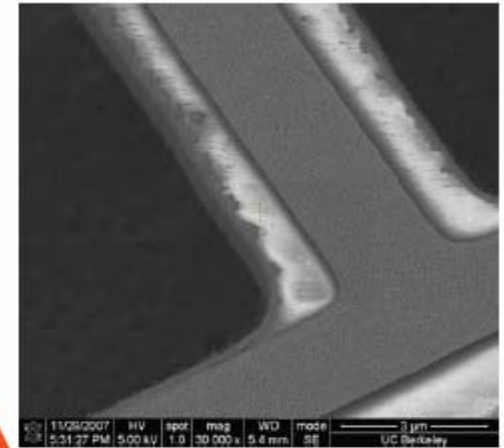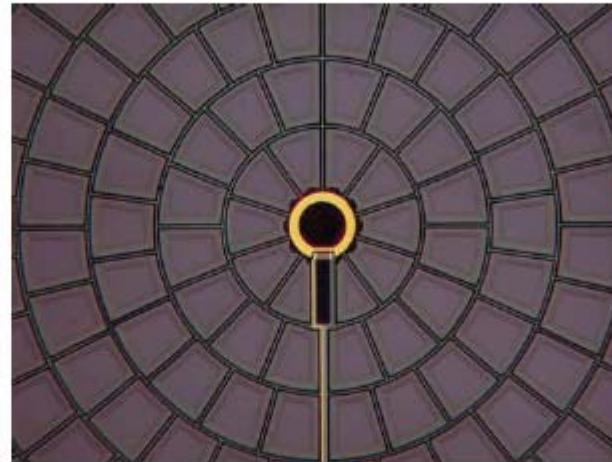
Al/Ti TES
Tc ~ 600mK

Six 160 pixel
wedges are the
heart of the SPT
camera

30 Jan 2008

30 μm   12
TES detector
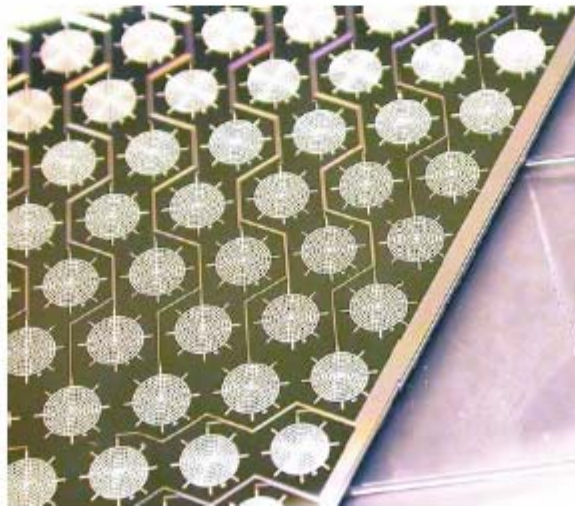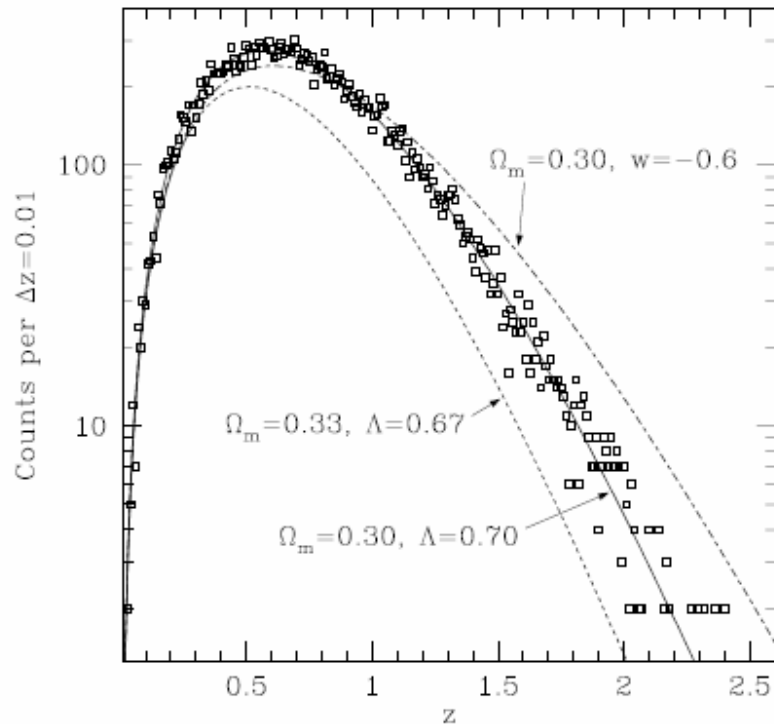
Figure 11. An illustration of the effect of cosmology on the expected number of SZE detected galaxy clusters as a function of redshift. The data points are appropriate for a 4000 square degree SPT survey with idealized sensitivity. The data points and the line passing through them were generated assuming a canonical $\Omega_M = 0.3, \Omega_\Lambda = 0.7, \sigma_8 = 1$ cosmology. The other two lines show the large effect in the expected cluster counts due to slight changes in the cosmology. The value of σ_8 was adjusted to give the same normalization for the local cluster abundance in each model. The bottom curve is for a model with more matter and correspondingly less dark energy. The top curve at shows the effect of only a change in the equation of state of the dark energy in the canonical model. (Figure courtesy of G. Holder)
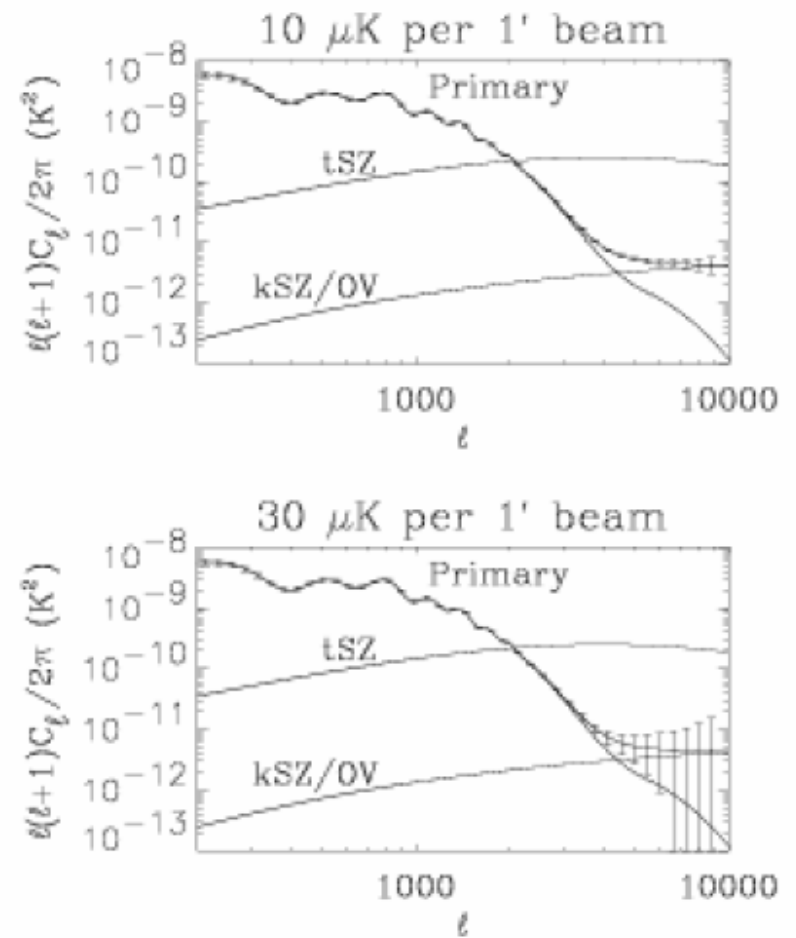
Figure 12. An illustration of the potential of the SPT to measure fine-scale CMB anisotropy. The two panels show statistical errors on the high-ℓ CMB power spectrum from 500 deg^2 of sky measured at two different levels of noise per $1'$ beam. Both panels assume perfect subtraction of the thermal SZE signal and other astrophysical contaminants; achieving the required accuracy in this subtraction will be a significant challenge. (Spectra courtesy of W. Hu.)
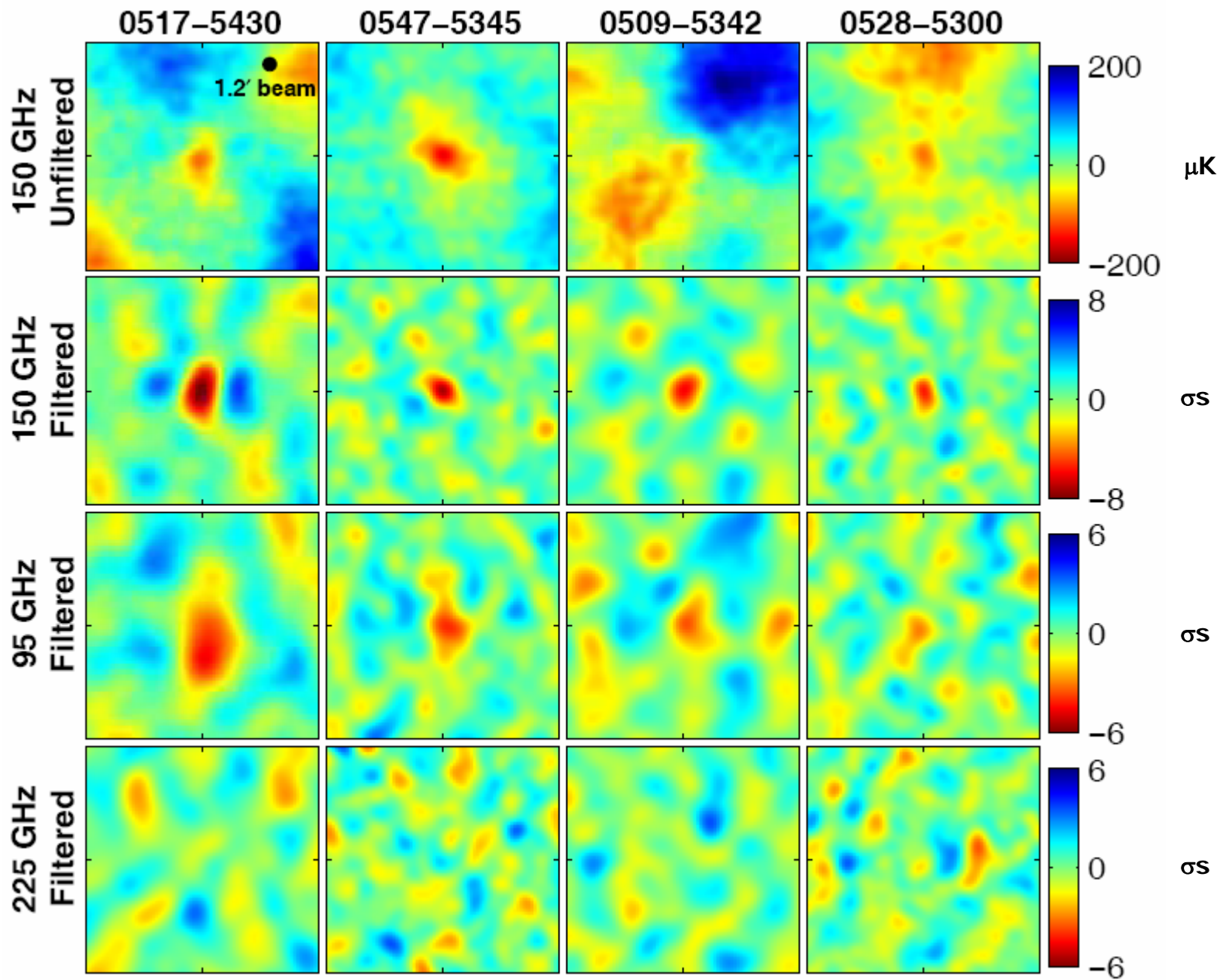
Galaxy clusters discovered with a Sunyaev-Zel'dovich effect survey - astro-ph/0810.1578

295 bolometers LABOCA (345 GHz) Bonn

APEX 12m telescope
Atacama (ALMA site)
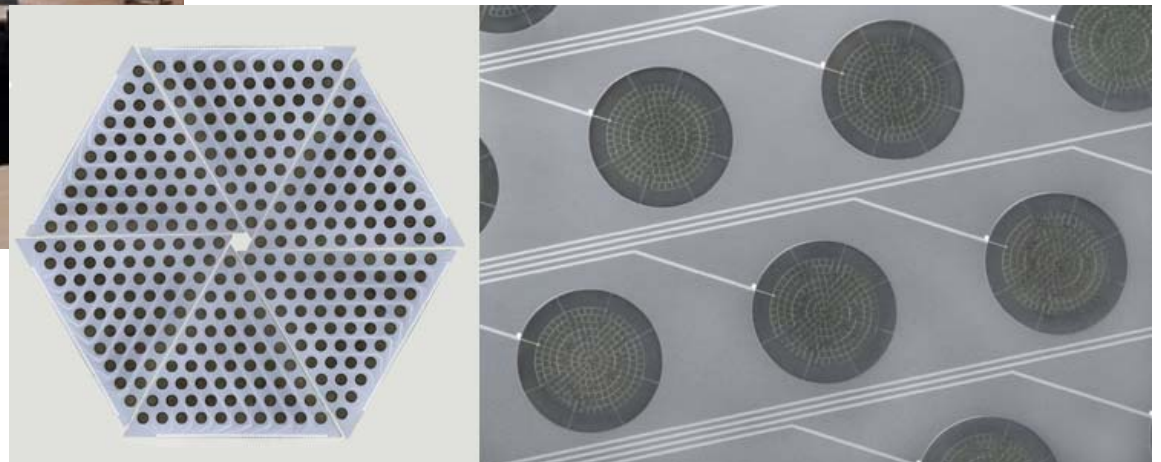
330 bolometers APEX-SZ (150 GHz) Berkeley
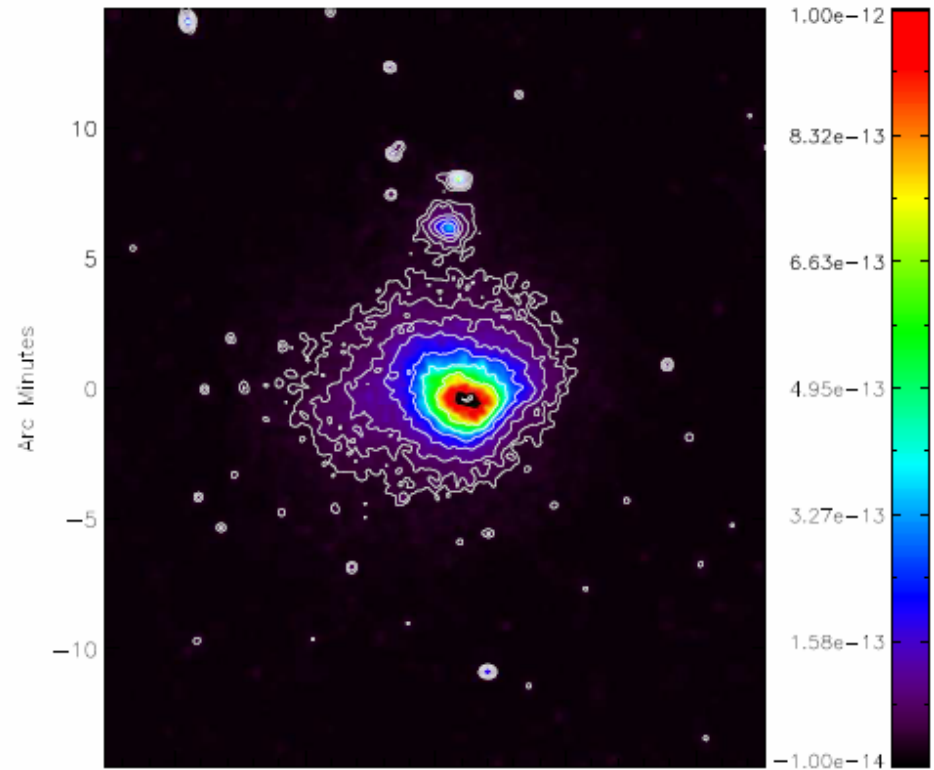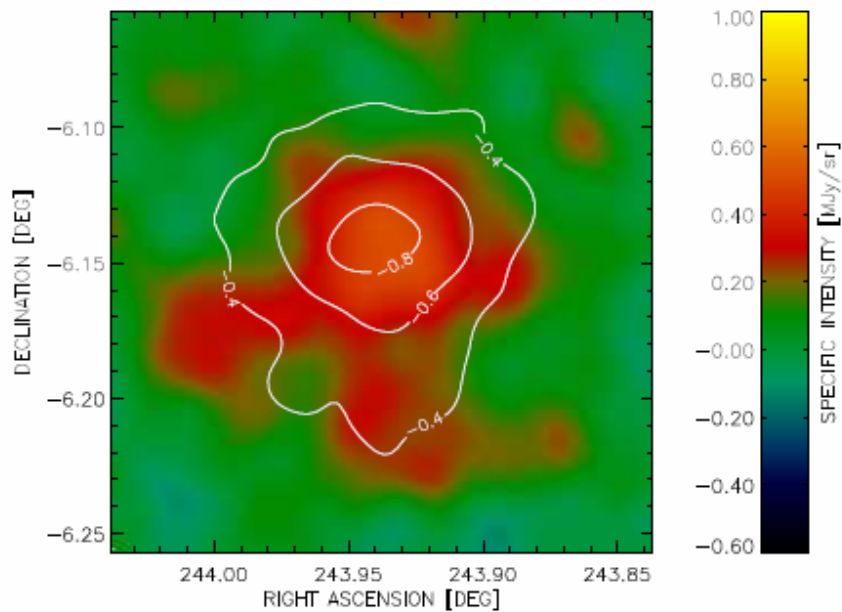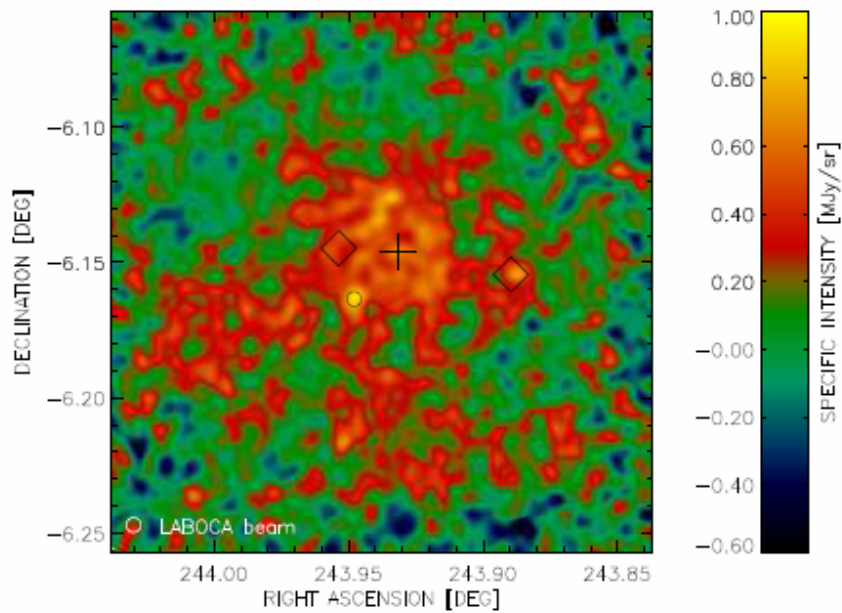
Fig. 3. Smoothed, background subtracted, X-ray map of Abell 2163 in the [0.5-2] keV band (see text for details). Logarithmically spaced contours highlight the large dynamical range of the cluster emission. The unit of the color scale is $\mathrm{erg\, s^{-1} cm^{-2} arcmin^{-2}}$.

Fig. 2. *Top:* Final 345 GHz LABOCA map of Abell 2163, smoothed with the 19.5″ beam. The cross marks the position of a bright flat-spectrum radio source (Cooray et al. 1998). The diamonds mark the positions of two BCGs (Maurogordato et al. 2008). The circle marks the position of the bright point source found in the present data. *Bottom:* LABOCA map smoothed to the APEX-SZ resolution of 1 arcminute. The bright point source described in the text has been removed. The APEX-SZ 150 GHz map is shown as contours.

ACT : Atacama Cosmology Telescope
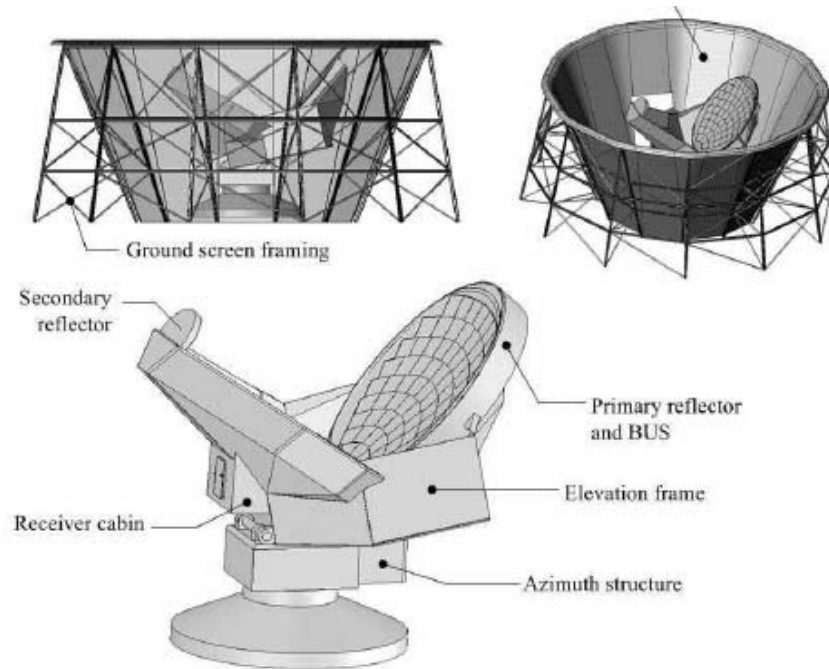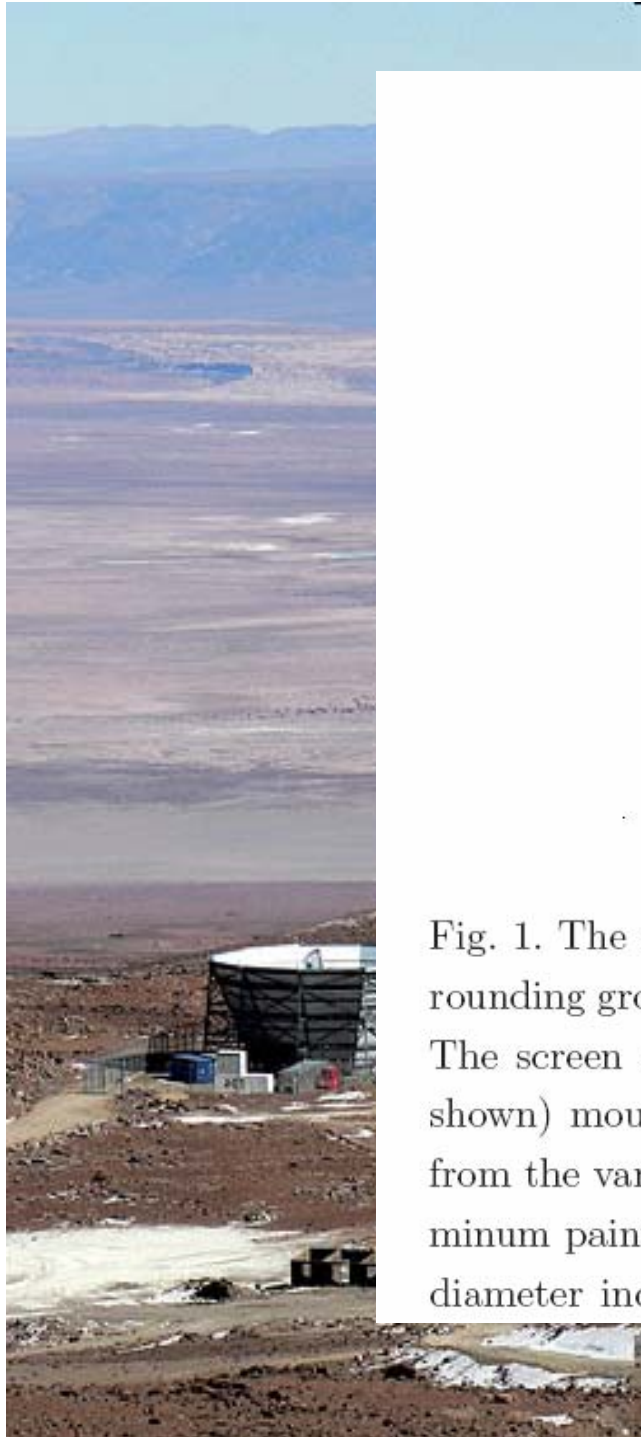
Fig. 1. The ACT telescope. The mechanical design has a low profile; the surrounding ground screen completely shields the telescope from ground emission. The screen also acts as a weather shield. An additional ground screen (not shown) mounted on the telescope hides the secondary and half the primary from the vantage point of the lower diagram. This inner ground screen is aluminum painted white to reduce solar heating. The primary mirror is $\sim 7\,\mathrm{m}$ in diameter including its surrounding guard ring. "BUS" refers to the mirror's

Abell S0592

Difference

1E 0657-56 (Bullet)

Difference
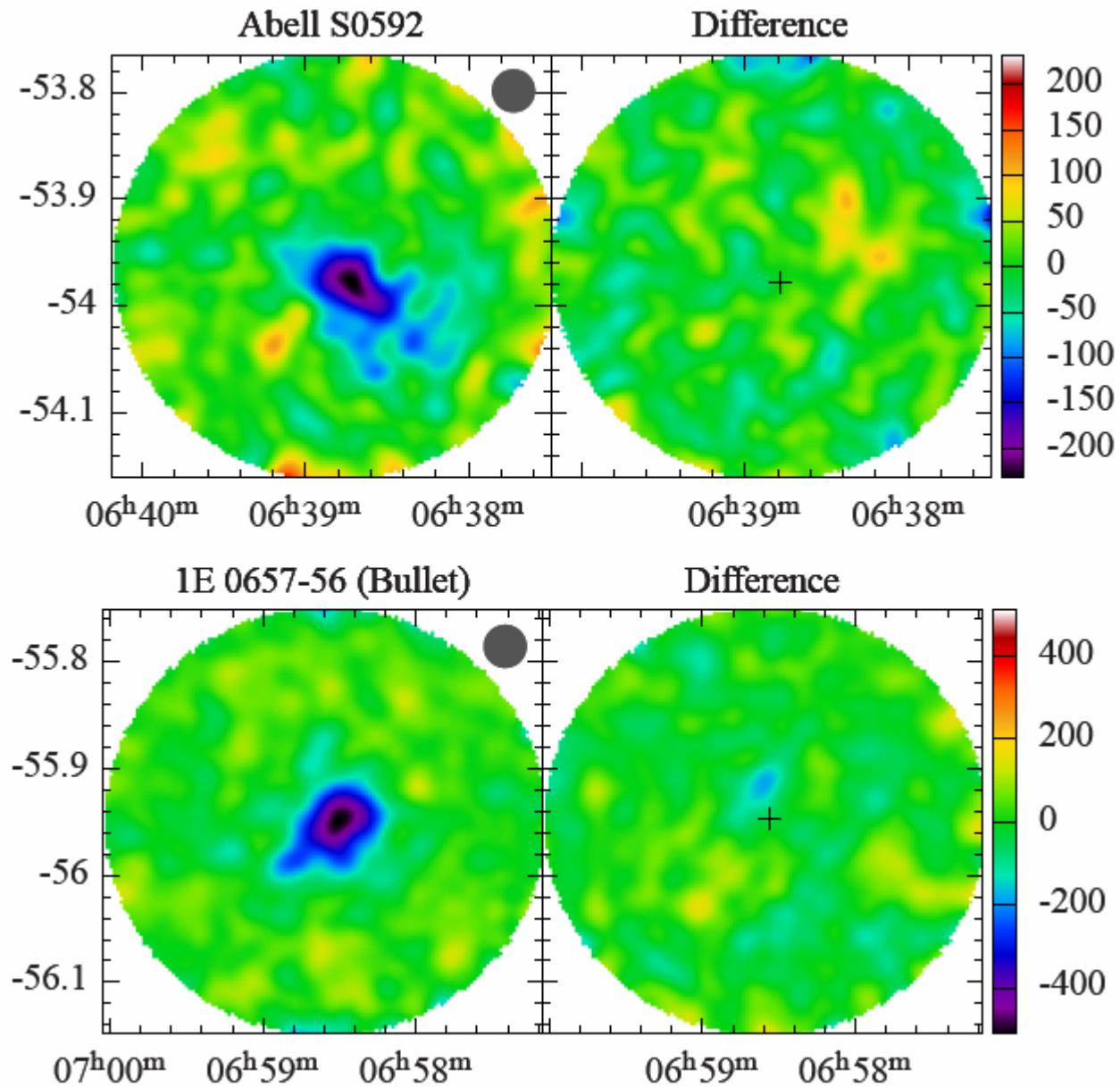
Detections during regular ACT survey , with 3 to 11 minutes of observation (!)

TABLE 2
SELECTION OF SZ CLUSTERS DETECTED BY ACT

ACT Descriptor	Catalog Name	J2000 Coordinates[a]		rms[b] [μK]	t_{int}[c] [min]	$SNR\,(\theta)$[d]	ΔT_{SZ}[e] [μK]	$10^{10} \times Y(\theta)$[f]		
		RA	Dec.					$\theta \leq 2'$ (± 0.2)	$\theta \leq 4'$ (± 0.6)	$\theta \leq 6'$ (± 1.2)
Previously Detected										
ACT-CL J0245−5301	Abell S0295	$02^h45^m28^s$	$-53°01'36''$	44	10.1	15.2 (6.8′)	−250	0.89	2.36	3.91
ACT-CL J0330−5228	Abell 3128 (NE)	$03^h30^m50^s$	$-52°28'38''$	49	10.3	12.8 (4.3′)	−260	0.94	2.69	4.34
ACT-CL J0509−5345	SPT-CL 0509−5342	$05^h09^m20^s$	$-53°45'00''$	47	10.1	7.7 (5.2′)	−70	0.33	1.07	1.50
ACT-CL J0516−5432	Abell S0520	$05^h16^m31^s$	$-54°32'42''$	55	6.8	4.2 (4.1′)	−110	0.19	-0.11	-0.55
ACT-CL J0546−5346	SPT-CL 0547−5345	$05^h46^m35^s$	$-53°46'04''$	46	9.5	13.9 (5.8′)	−250	0.91	2.36	3.67
ACT-CL J0638−5358	Abell S0592	$06^h38^m46^s$	$-53°58'40''$	55	7.5	8.1 (3.1′)	−230	0.70	1.40	2.07
ACT-CL J0645−5413	Abell 3404	$06^h45^m29^s$	$-54°13'52''$	59	9.3	2.8 (2.0′)	−120	0.12	-0.18	-0.69
ACT-CL J0658−5556	1E 0657−56 (Bullet)	$06^h58^m33^s$	$-55°56'49''$	80	3.4	12.1 (2.7′)	−510	1.60	2.95	3.56
Previously Undetected										
ACT-CL J0329−5226	—	$03^h29^m27^s$	$-52°26'26''$	50	11.3	14.8 (7.9′)	−230	0.71	1.91	3.30
ACT-CL J0447−5107	—	$04^h47^m50^s$	$-51°07'09''$	57	7.9	13.4 (7.4′)	−250	0.75	2.60	4.02

[a] Position of the deepest point in 2′ FWHM Gaussian smoothed map, except for ACT-CL J0509−5345 which has a position which gives a maximal SNR (see text). [b] Map rms measured outside a 6′ mask and reported for a one square arcminute area. [c] Integration time, defined as the approximate total time (in minutes) that the telescope was pointed in the map region. [d] Maximum signal-to-noise ratio (Eq. 29) and the radius θ at which it was obtained. [e] Cluster depth, as measured in a 2′ FWHM Gaussian smoothed map at the listed coordinates; intended as a guide to the magnitude of the decrement. [f] See Eq. 32 and following discussion.

- Photometric observations of the SZ can be significantly biased, when there are
- less spectral channels than free parameters.
- Components, LOS through a rich cluster:

ThSZ $\quad \dfrac{\Delta I_t}{I_{CMB}} = y\dfrac{x^4 e^x}{(e^x - 1)^2}[x\coth(x/2) - 4], \qquad y = \displaystyle\int_{LOS}\dfrac{kT_e}{m_e c^2}n_e\sigma_T \mathrm{d}\ell,$

NThSZ $\qquad p_{min}, \; Amp$

KSZ $\quad \dfrac{\Delta I_v}{I_{CMB}} \sim -\tau_t\dfrac{v_{LOS}}{c}\dfrac{xe^x}{(e^x - 1)}$

CMB $\quad \dfrac{\Delta I_{CMBi}}{I_{CMB}} = \dfrac{xe^x}{(e^x - 1)}\dfrac{\Delta T}{T}$

ISD $\qquad T_d, \; \tau_d \; ....(\beta)$

- Photometric observations of the SZ can be significantly biased, when there are
- less spectral channels than free parameters.
- Components, LOS through a rich cluster:

ThSZ $\quad \dfrac{\Delta I_{\mathrm{t}}}{I_{\mathrm{CMB}}} = y \dfrac{x^4 \mathrm{e}^x}{(\mathrm{e}^x - 1)^2} [x \coth(x/2) - 4], \quad y = \int_{\mathrm{LOS}} \dfrac{kT_{\mathrm{e}}}{m_{\mathrm{e}} c^2} n_{\mathrm{e}} \sigma_T \mathrm{d}\ell,$

NThSZ $\quad p_{min} , Amp$

KSZ $\quad \dfrac{\Delta I_{\mathrm{v}}}{I_{\mathrm{CMB}}} \sim -\tau_t \dfrac{v_{\mathrm{LOS}}}{c} \dfrac{x\mathrm{e}^x}{(\mathrm{e}^x - 1)}$

CMB $\quad \dfrac{\Delta I_{\mathrm{CMBi}}}{I_{\mathrm{CMB}}} = \dfrac{x\mathrm{e}^x}{(\mathrm{e}^x - 1)} \dfrac{\Delta T}{T}$

ISD $\quad T_d , \tau_d \ldots.(\beta)$

At least, 8 independent parameters !

best ground-based photometers: 4 bands
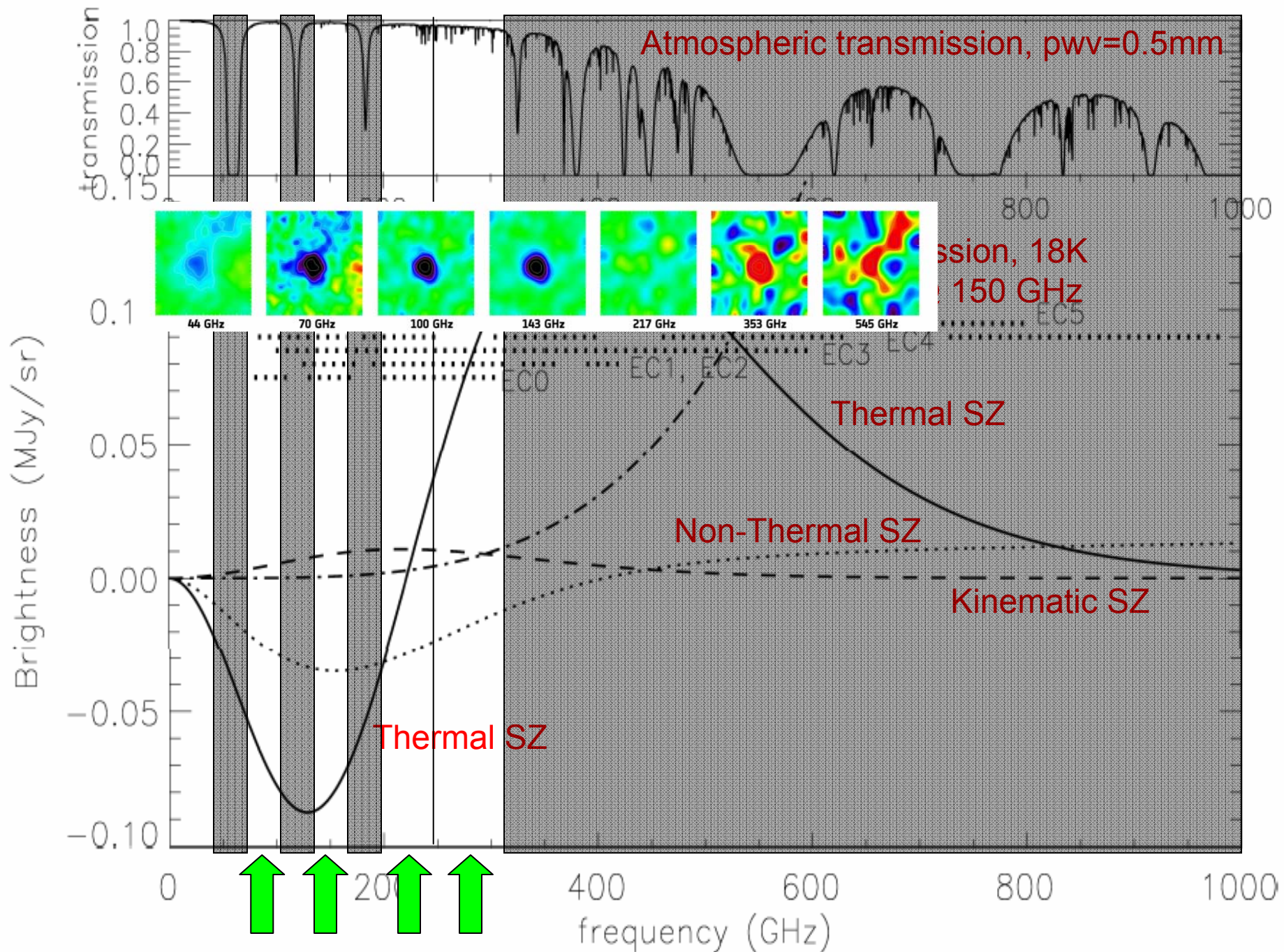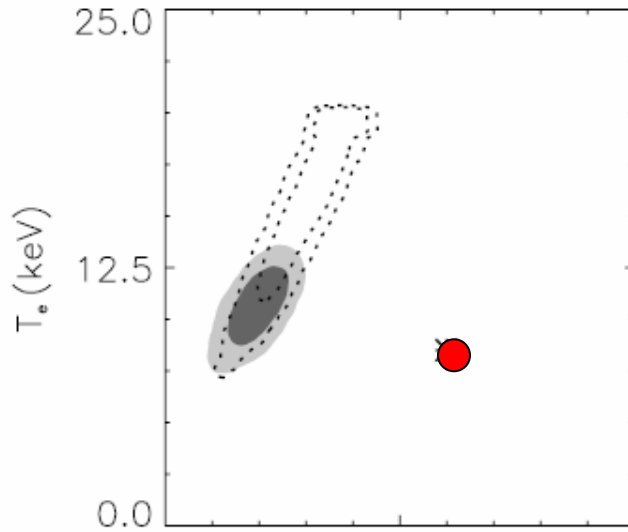
Atmospheric transmission, pwv=0.5mm

...ssion, 18K
... 150 GHz

44 GHz   70 GHz   100 GHz   143 GHz   217 GHz   353 GHz   545 GHz

Thermal SZ

Non-Thermal SZ

Kinematic SZ

Thermal SZ

EC0   EC1, EC2   EC3   EC4   EC5

Example : bias in the determination of LOS parameters, for a ground-based telescope with 4 photometric channels (75-115 ; 125-175 ; 200-240 ; 240-300) GHz
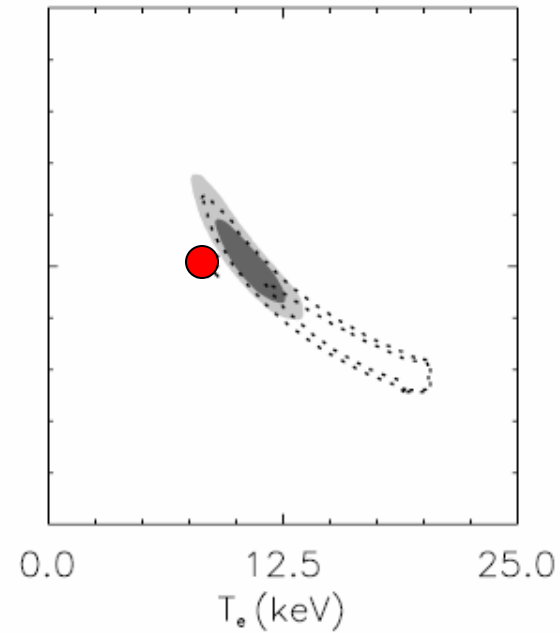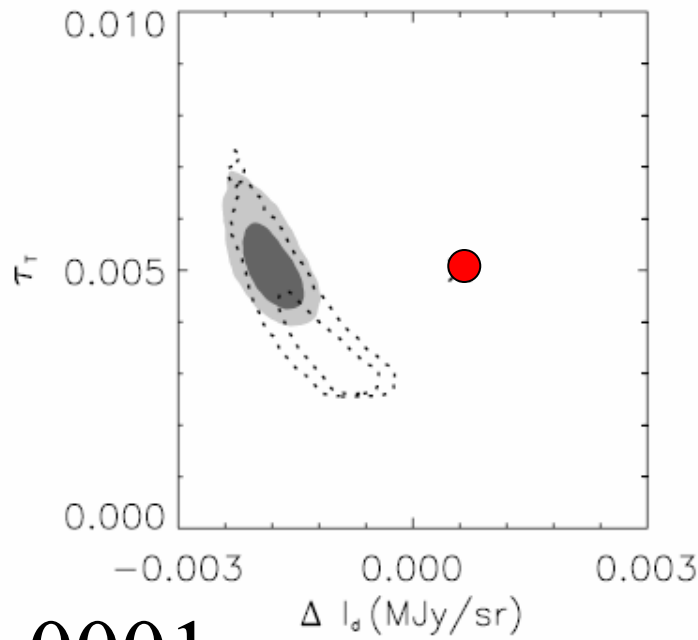
$$\tau_{nt} = 0.0001$$
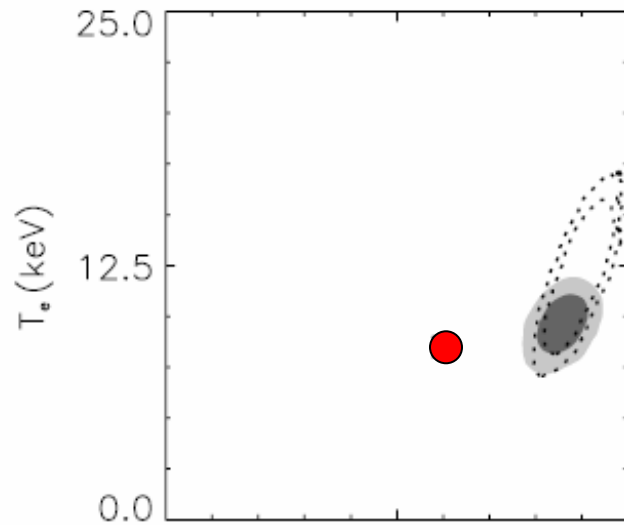
Example : bias in the determination of LOS parameters, for a ground-based telescope with 4 photometric channels (75-115 ; 125-175 ; 200-240 ; 240-300) GHz
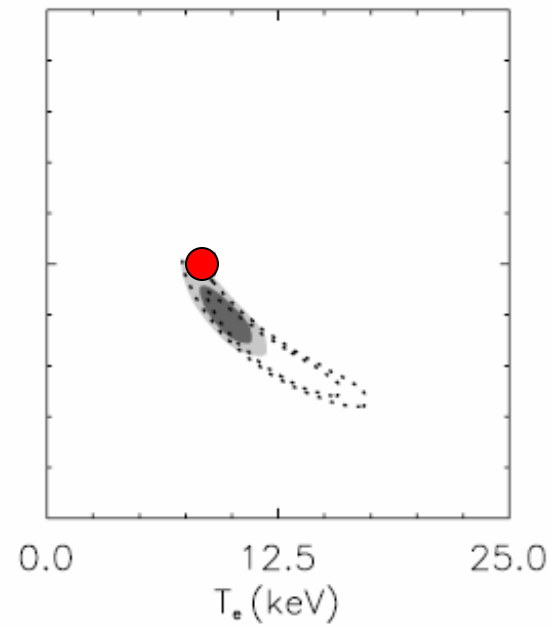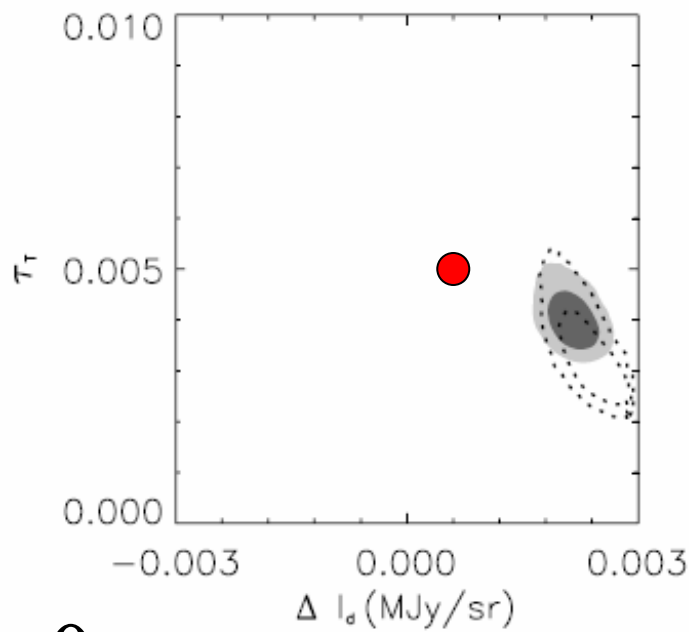
$\tau_{nt} = 0$
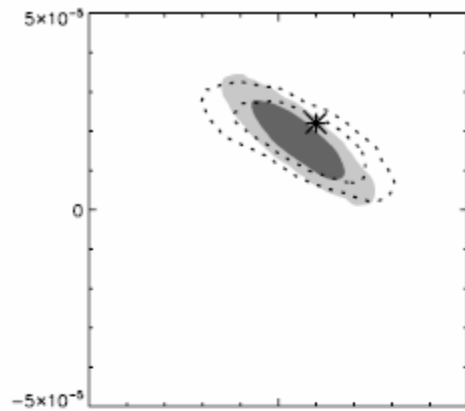
Example : bias in the determination of LOS parameters, for a ground-based telescope with 4 photometric channels (75-115 ; 125-175 ; 200-240 ; 240-300) GHz
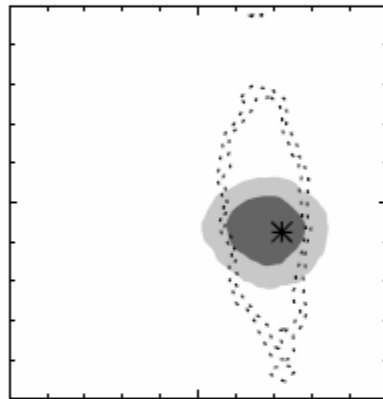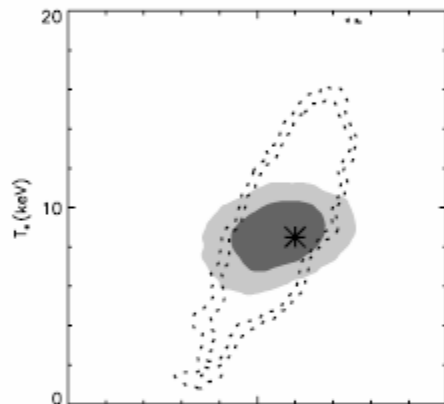
Fitting also ΔT_{CMB} : bias removed, but larger errors
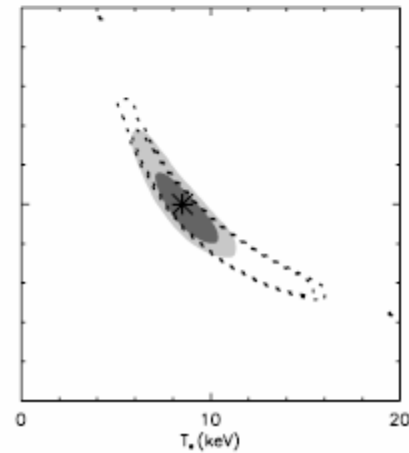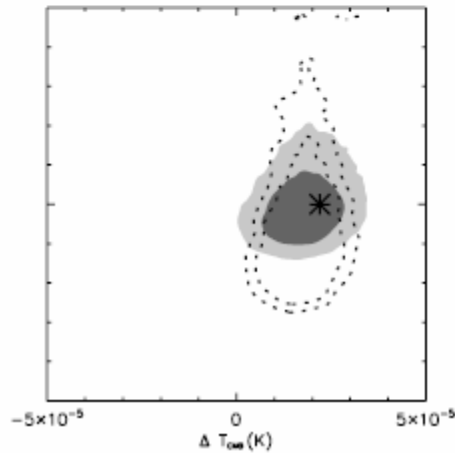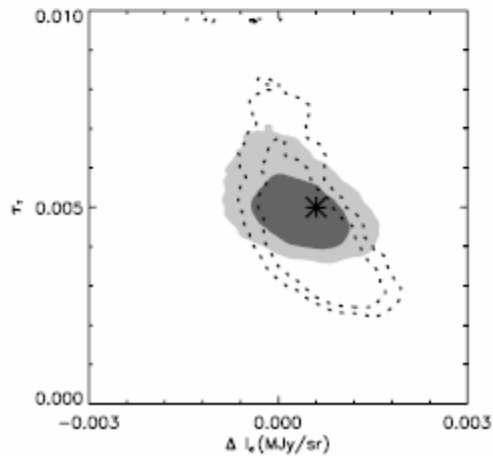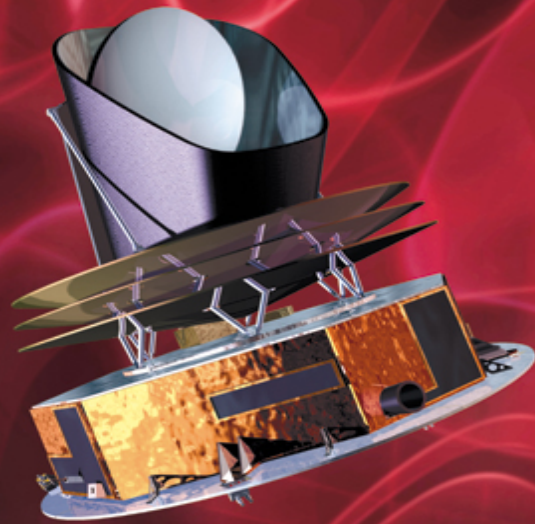
Planck is a very ambitious experiment.

It carries a complex CMB experiment (the state of the art, a few years ago) all the way to L2,

improving the sensitivity wrt WMAP by at least a factor 10,

extending the frequency coverage towards high frequencies by a factor about 10

A2319
As seen by
Planck

44 GHz 70 GHz 100 GHz 143 GHz 217 GHz 353 GHz 545 GHz
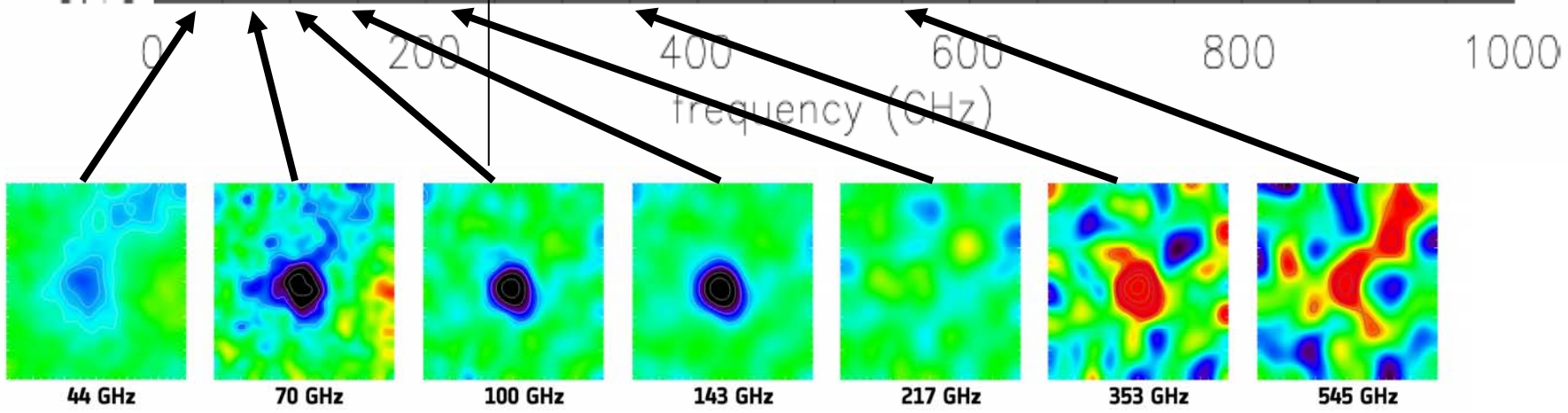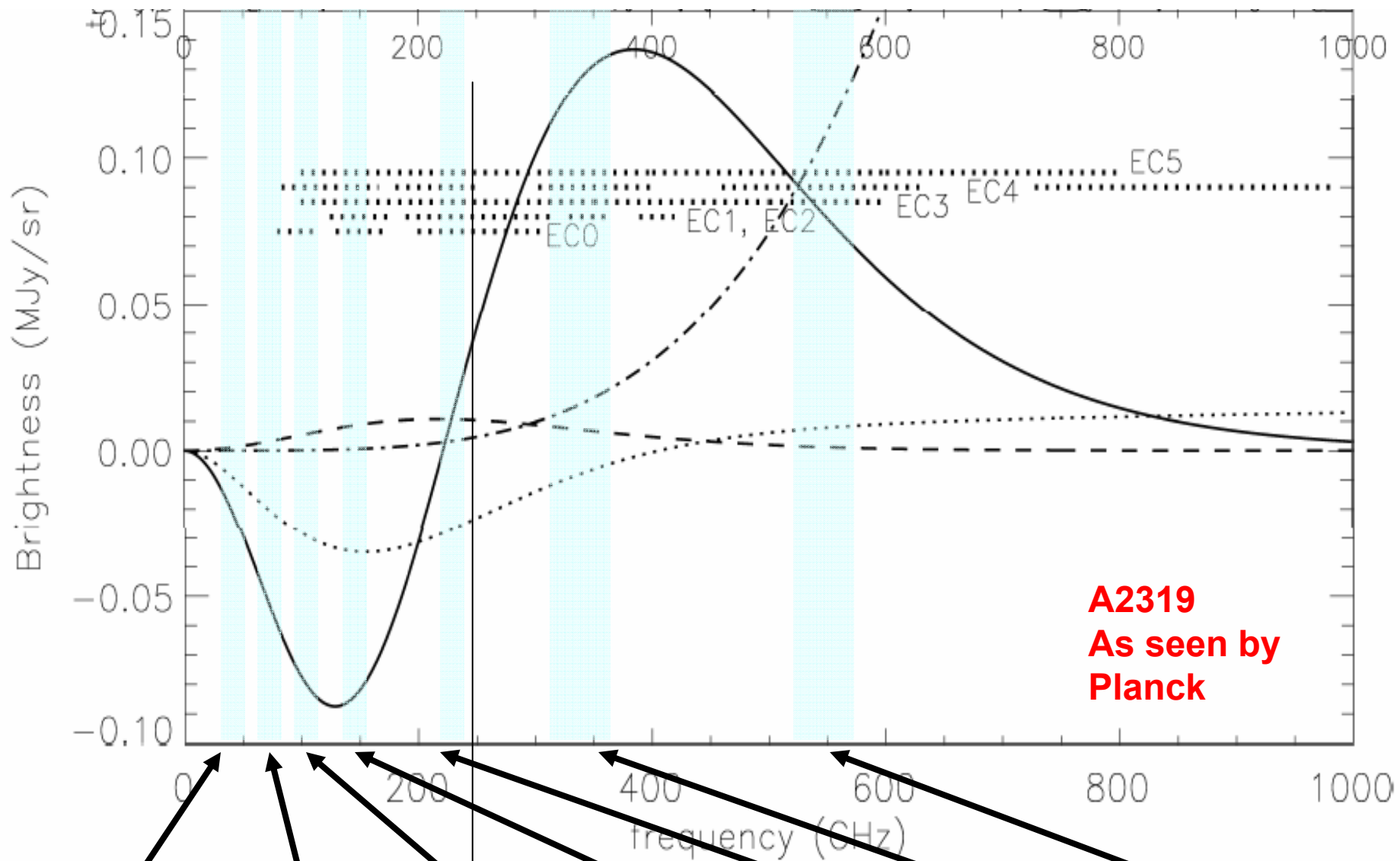
All-sky Sunyaev-Zeldovich clusters

- Planck multiband observations of SZ clusters (ESZ) over the full sky: 189 high quality cluster candidates detected
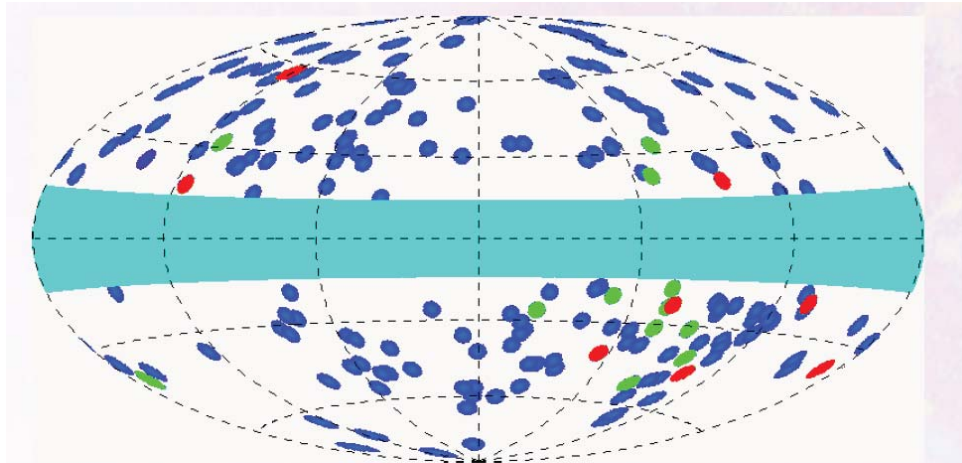
Fig.2 Distribution of ESZ clusters and candidate clusters on the sky (Galactic projection).

Known clusters	169
X-ray only	30
Optical Only	5
NEDSimbad only	1
X-ray + Optical	128
X-ray + SZ	1
SZ + Optical	1
X-ray + Optical + SZ	3
New Planck Clusters	20
XMM confirmed	11
AMI confirmed	1
Candidate new clusters	8

Discovered by Planck

- The clusters in the ESZ sample are mostly at moderate redshifts lying between z=0.01 and z=0.55, with 86% of them below z=0.3. The ESZ-cluster masses span over a decade from 0.9 to 15 × 10^{14} M_{sol} , i.e. up to the highest masses.

Clusters : Planck collaboration: astro-ph/1101:2024

All-sky Sunyaev-Zeldovich clusters

- SZ emission is extracted from multifrequency maps by filtering (matching multifrequency filter) and components separation.

Fig. 3 *Planck* observation of A2256 (S/N~29). The upper panel shows the raw (1°x1°) maps at 100, 143, 217, 353, and 545GHz. The lower panel shows the corresponding cleaned maps.
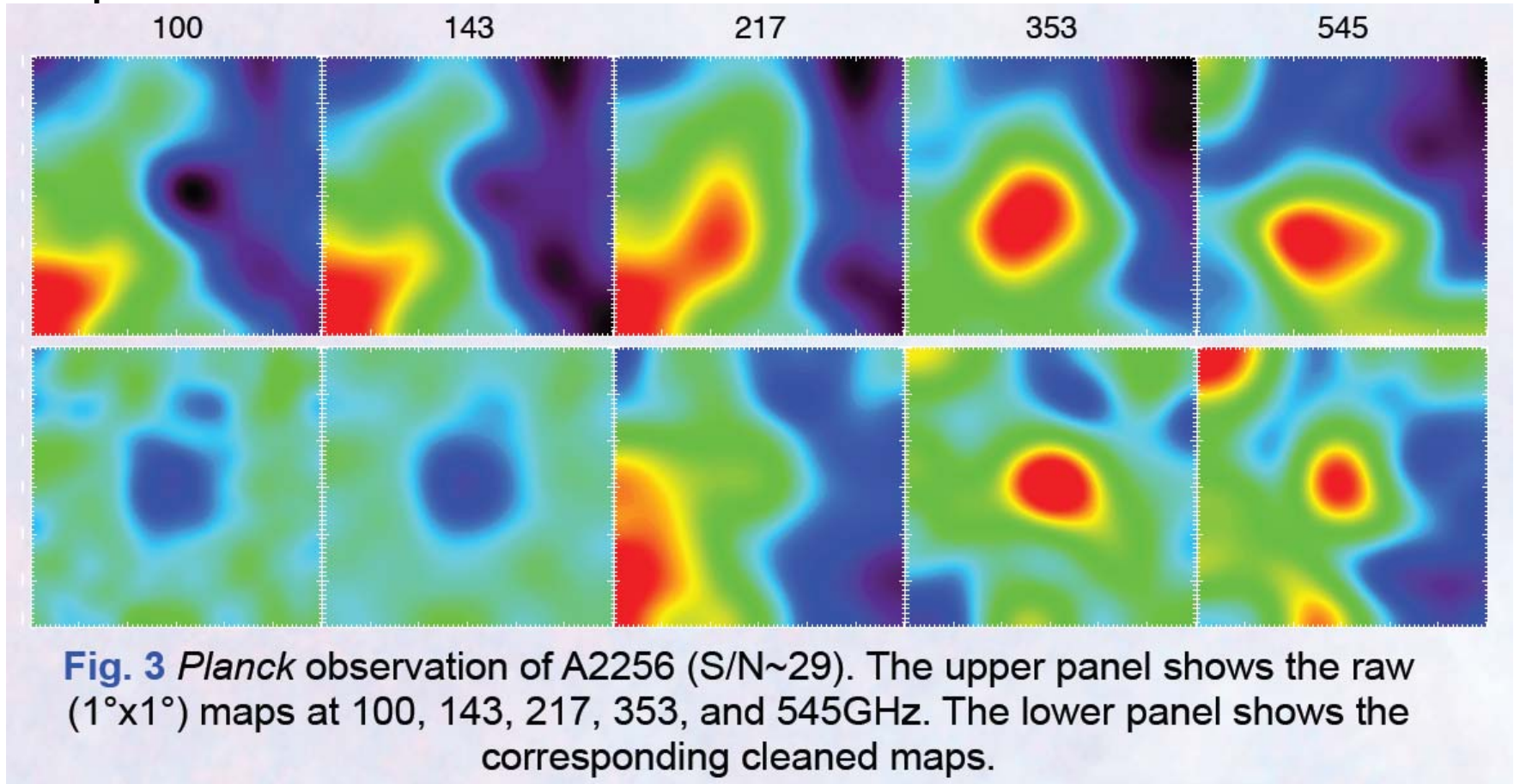
- Candidates are then validated comparing to Planck sources lists and other datasets (X-ray, optical, NED, etc.)

All-sky Sunyaev-Zeldovich clusters

- Thanks to its all-sky coverage, *Planck* has a unique capability to detect the rarest and most massive clusters in the exponential tail of the mass function.

-

- As a matter of fact, two of the newly-discovered clusters in the ESZ and confirmed by XMM-Newton have estimated total masses larger than $10^{15} M_{sun}$.
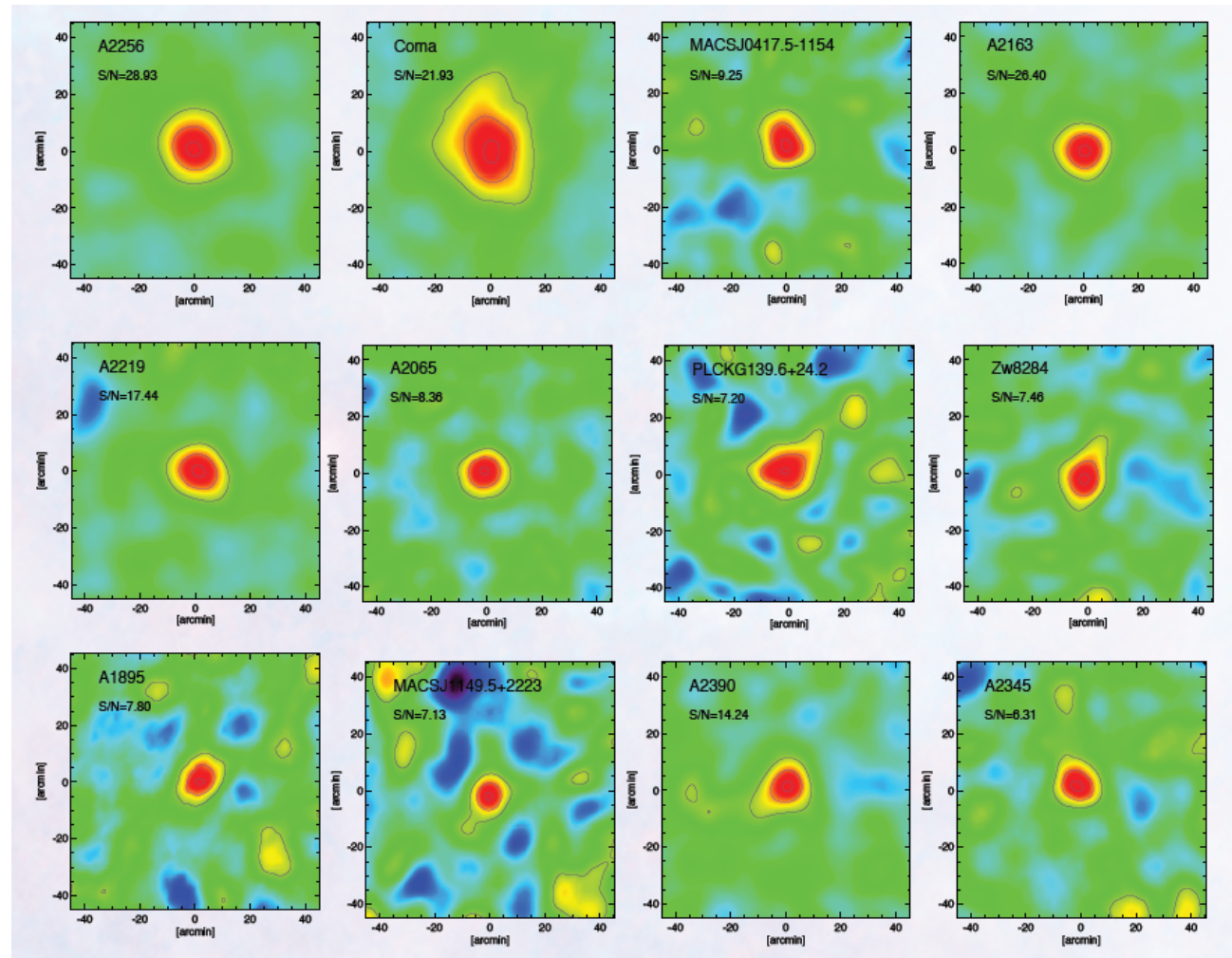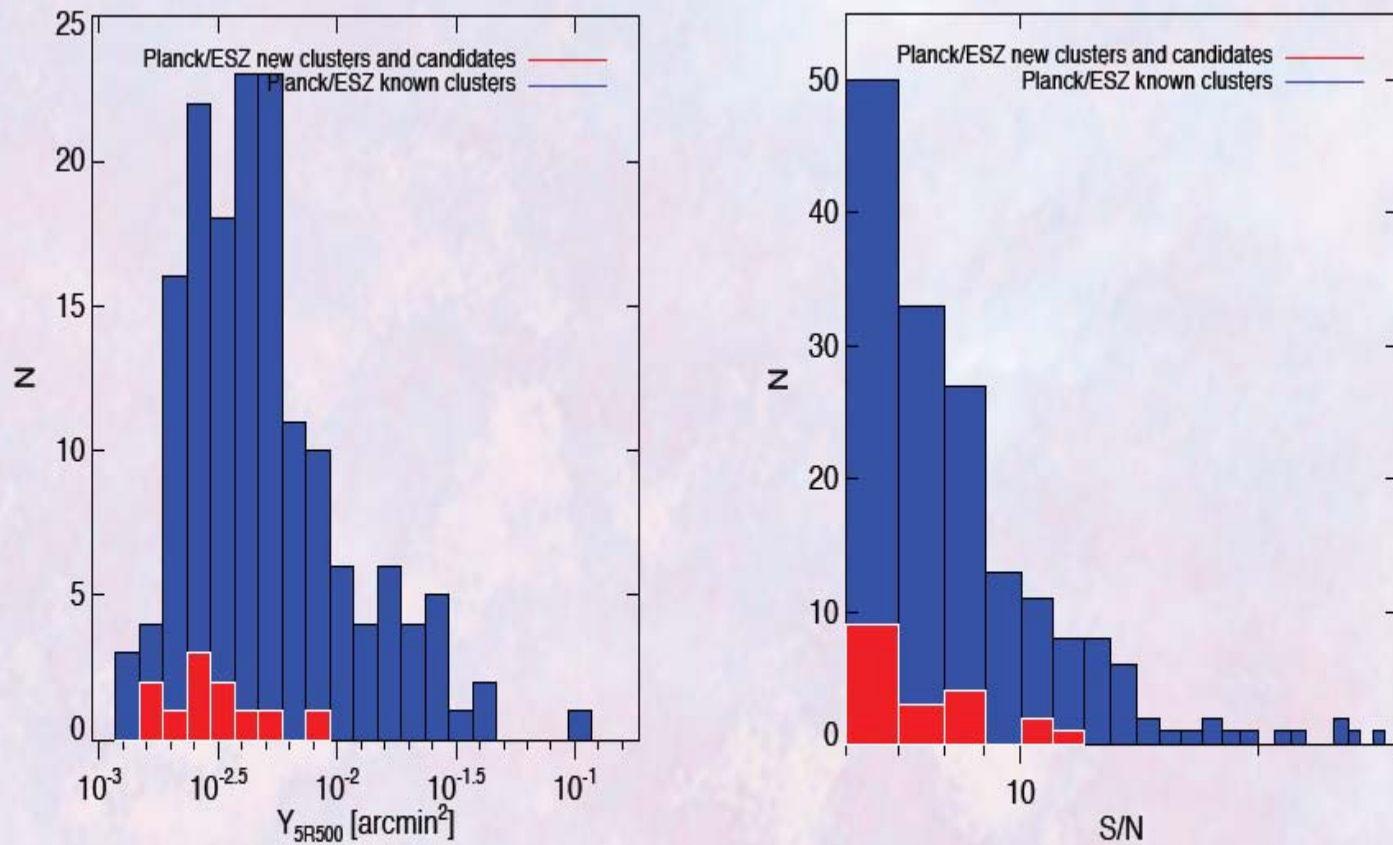
Fig.4 Distribution of the S/N and integrated Compton parameter values for the ESZ clusters and candidate new clusters

All-sky Sunyaev-Zeldovich clusters

Multiple Systems
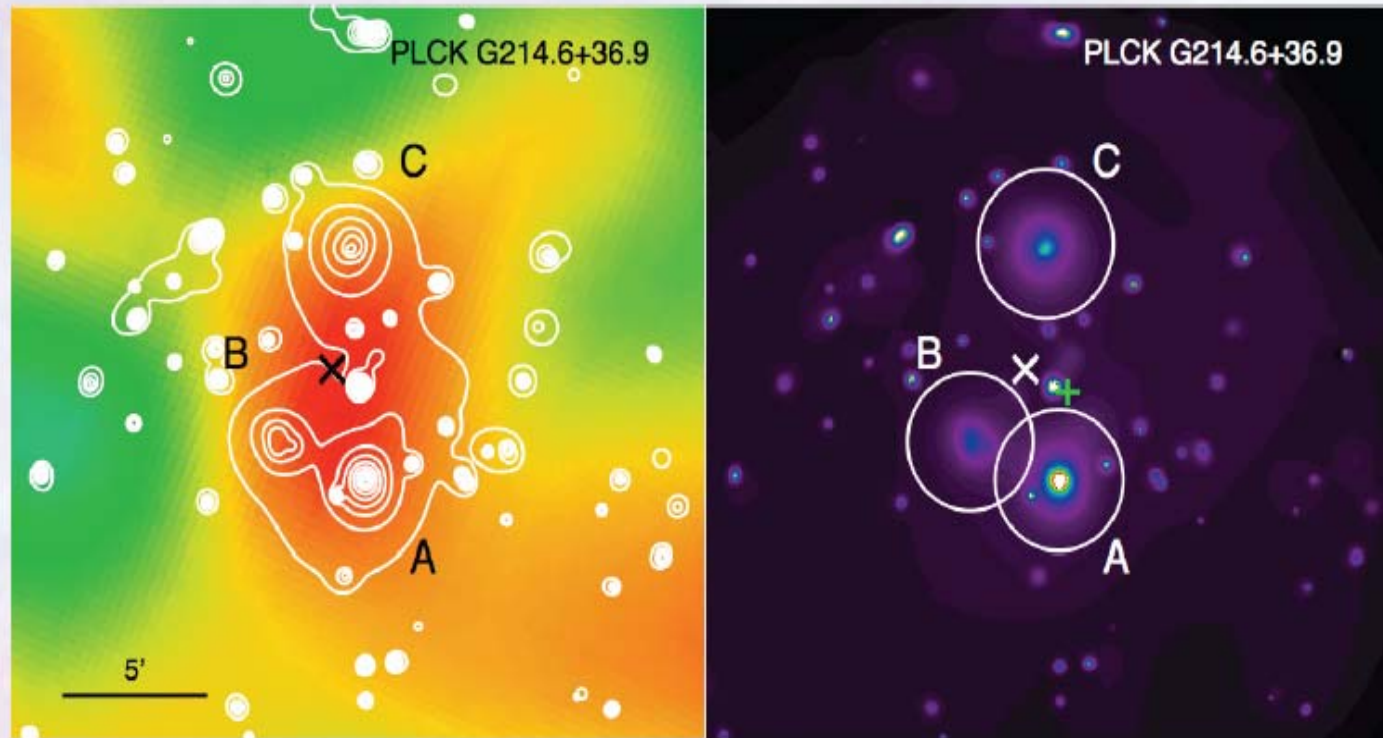
Example of the triple system PLCK G214.6+37.0. *Planck Y_{SZ} map (left)* with contours from the *XMM-Newton* wavelet filtered [0.3 − 2] keV image (right) overlaid in white. Extended components found in the *XMM-Newton* image are marked with letters. The circles in each *XMM-Newton* image denote the estimated R_{500} radius for each component.

The final solution: spectroscopic measurements of the SZ

- Requirements:

  - Wide spectral coverage
    (in principle 100 to 1000 GHz)
  - Modest spectral resolution ($\lambda/\Delta\lambda$ = 100 to 1000)
  - Differential input, high rejection of common mode signal (CMB is common mode and is 2750000 μK, cluster signal is differential and can be as low as 10 μK).
  - Imaging instrument
  - Wide field of view to image the whole cluster and have a clean reference area to compare

Comparison among Spectrometers solutions

ITEM	FTS	Grating	Fabry-Perot
Spectral coverage	YES	NO: 4 D-G needed	NO: 3 F-P needed
Simultaneous measurements	YES	YES	NO
Imaging capability	YES	NO: linear array per pixel	YES
Spectral resolution	Variable	Fixed	Fixed
Differential measurement capability	YES	NO	NO
Background / noise	Large: but relaxes detectors sensitivity and mirrors temperature	Small	Small
Technology readiness	OK	OK	OK: but constraint on mirrors planarity and movement

DFTS

- The differential fourier transform spectrometer (DFTS) is the best option.
- We decided to produce a prototype to be used (warm) on the **OLIMPO** balloon-borne telescope to proof the concept and get preliminary science.
- Scientific targets:
  - SZ
  - High redshift galaxies (C^+)
  - Galactic survey (study of CO, also as a contaminant)
  - Spectral-Spatial anisotropies
  - ….

OLIMPO

- *The OLIMPO experiment is a mm-wave balloon-borne telescope, optimized for high-frequency measurements of the Sunyaev-Zeldovich effect. The instrument uses four bolometer arrays, for simultaneous observations at 150, 210, 350, 480 GHz, coupled to a 2.6 m diameter Cassegrain telescope, achieving a resolution of 4,3,2,2 arcmin FWHM respectively.*

- *OLIMPO is a polar long-duration flight launched from Svalbard islands. The current observation plan includes deep integrations on a selected sample of 40 clusters, plus a wide blind survey of an empty sky area.*

- *We have recently upgraded the instrument adding* **spectroscopic capabilities** *within the 4 bands above, and discuss here the scientific potential of this innovative configuration.*

- In fig. 1 we show the OLIMPO balloon payload (Masi et al. 2008), with solar panels, ground shield and sun shield removed.

- Note the tiltable 2.6m primary mirror and the lightweigth secondary.

- Pointing is obtained rotating the payload around an azimuth pivot and changing the elevation of the inner frame, including the telescope, the FTS and the detector's cryostat

- The total mass of the payload is 1.5 tons.

The Payload
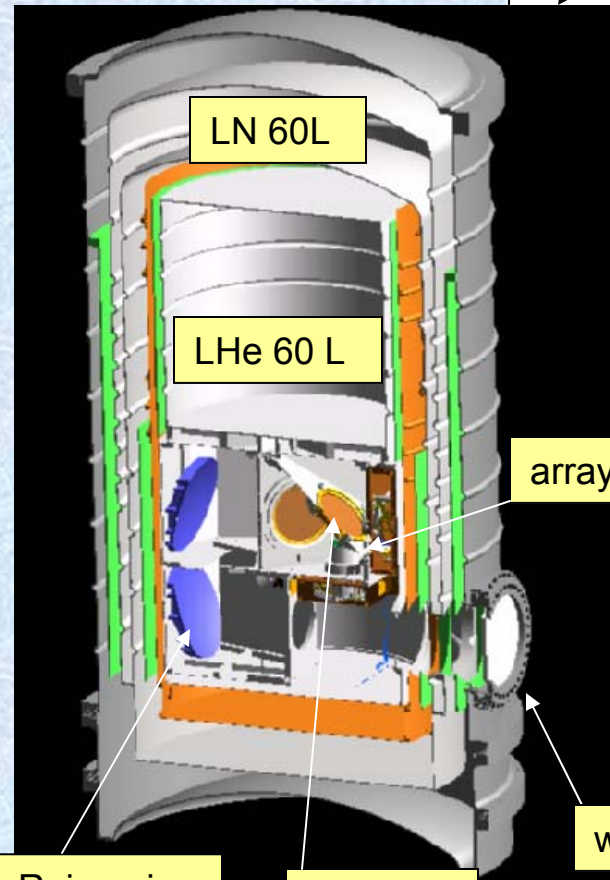
Cryostat with cold optics and detector arrays

Azimuth pivot

FTS

Readout electronics

Elevation motor

LN 60L

LHe 60 L

arrays

Reimaging optics

dichroics

window
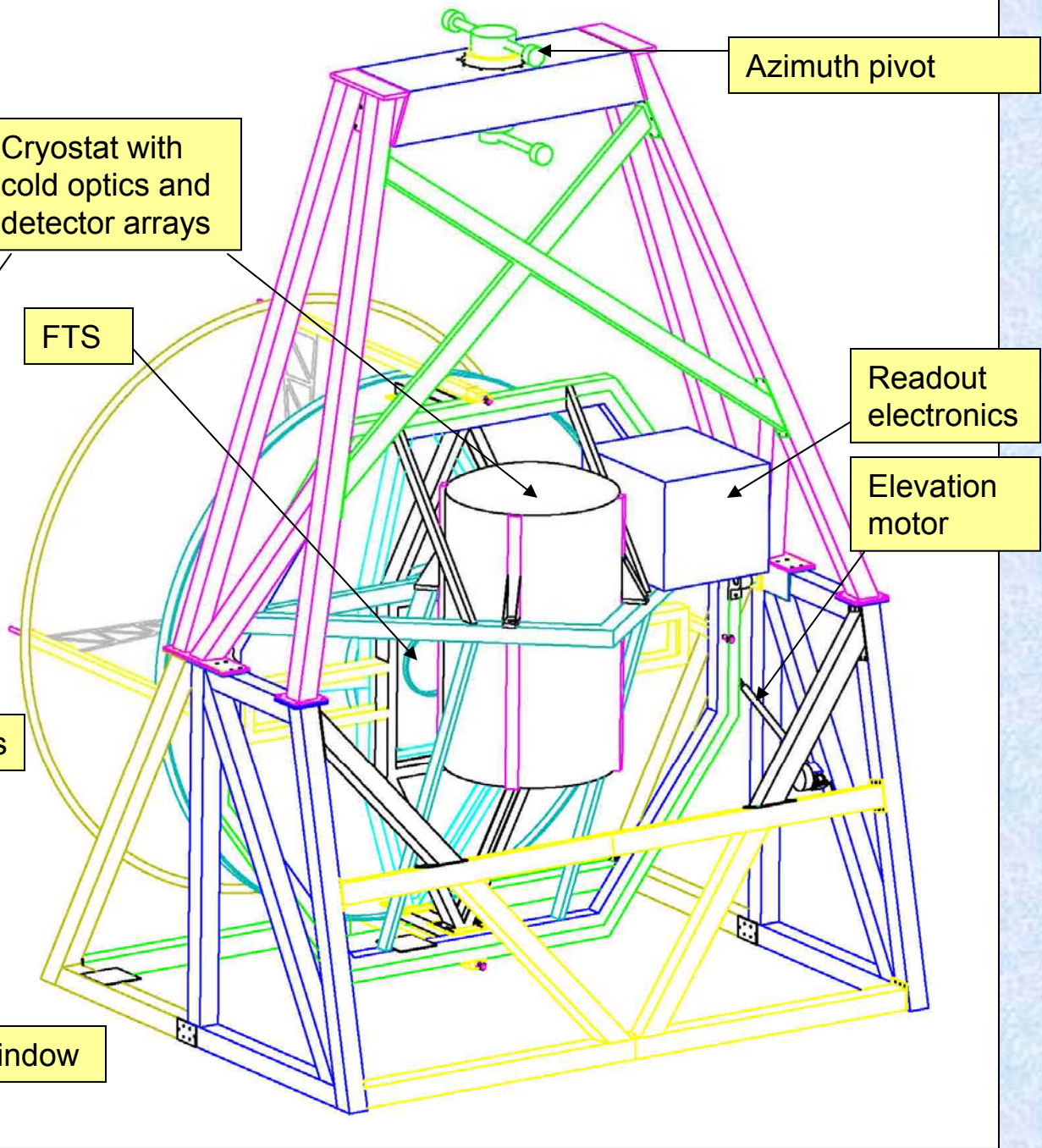
Low frequency arrays (TES

- **Buffer: Si$_3$N$_4$**
- **Thermistor: Ti (60nm) + Au (10/20 nm)**
- **Absorber/heater: spiderweb 1 (10 nm) + Au (5 nm), filling factor 5%**
- **NET150GHz=145 µK√s**
- **NET220GHz=275 µK√s**
- **Univ. Of Cardiff (Mauskopf)**

High frequency arrays

- NbxSi1-x (x=0.085)
- SiN 3x3 mm2
- Palladium absorber
- NET340GHz=430 µK√s
- NET450GHz=4300 µK√s
- Inst. Neel Grenoble (Camus)
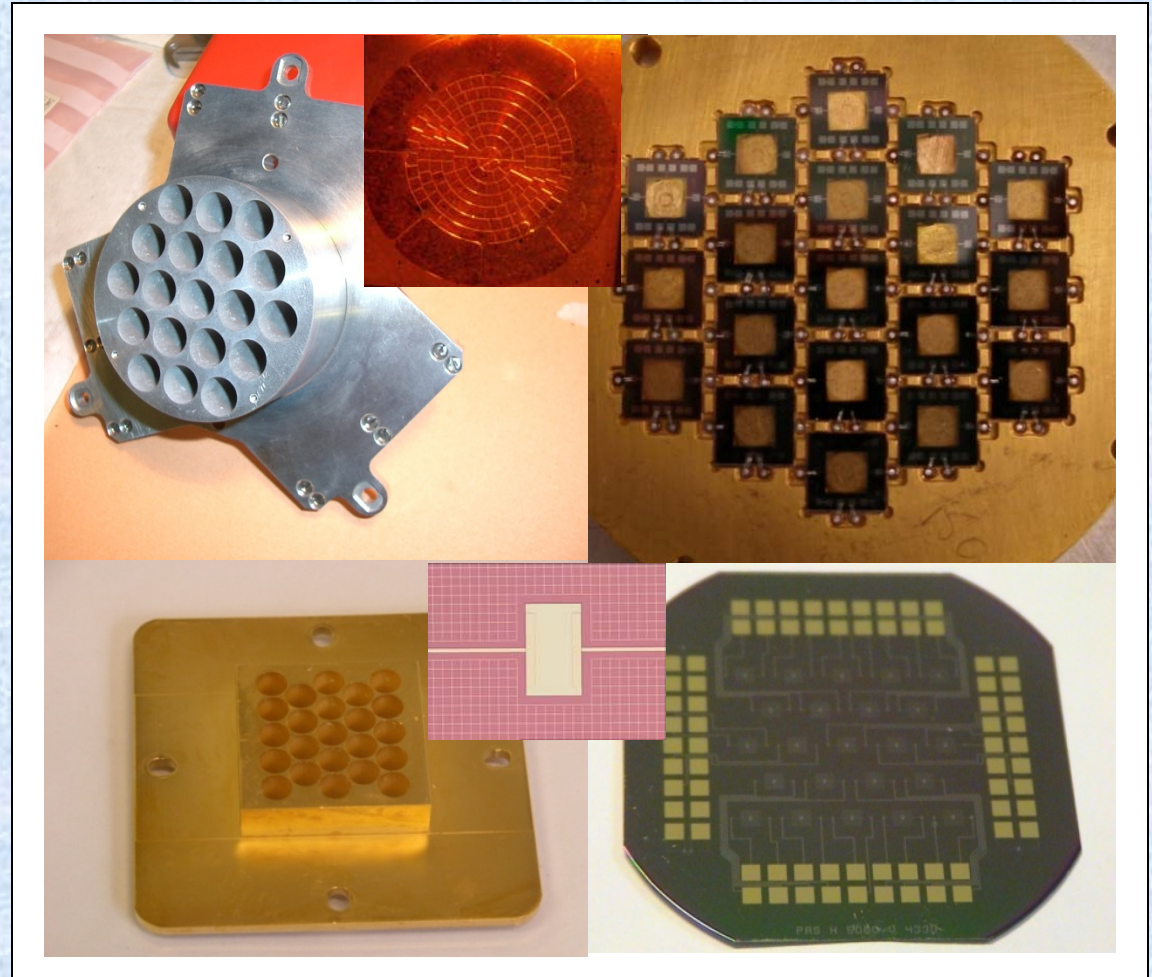
Filters Stacks (Ade, Tucker, Cardiff)

Bol.	ν_{eff} [GHz]	$\Delta\nu_{FWHM}$ [GHz]	Res. [']
19	148.4	21.5	4.2
19	215.4	20.6	2.9
23	347.7	33.1	1.8
23	482.9	54.2	1.8
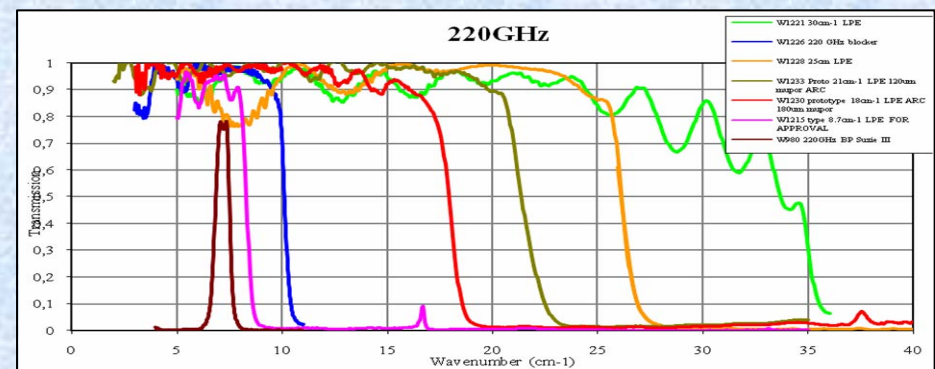
The spectroscopic instrument

- SZ studies can benefit significantly from spectroscopic measurements, which are required to break degeneracies between the parameters describing cluster and foreground emissions along the line of sight (see below).
- In 2008 we have studied for ASI a spectroscopic SZ space-mission (SAGACE, see de Bernardis et al. 2010).
- As a pathfinder, we are building a plug-in **D**ifferential **FTS** for OLIMPO.
- The **DFTS** configuration offers
  - an imaging spectrometer with very high throughput,
  - wide spectral coverage,
  - medium to high spectral resolution,
  - rejection of common-mode signals, like instrument emission and most of the ground pickup.
- The main problem is the high radiative background on the bolometers, which is solved splitting the observed frequency range in several bands with independent detector arrays. In the case of OLIMPO, this was already implemented in the 4-bands photometer.

The instrument is based on a double Martin Pupplett Interferometer configuration to avoid the loss of half of the signal.

A wedge mirror splits the sky image in two halves I_A and I_B, used as input signals for both inputs of the two FTS's.

Olimpo Telescope

Olimpo Cryostat

outgoing fields :

$$E^{FTSII} = \begin{pmatrix} B_x \cos(\delta/2) + i\,A_y \sin(\delta/2) \\ 0 \end{pmatrix}$$

$$E^{FTSI} = \begin{pmatrix} 0 \\ B_y \cos(\delta/2) + i\,A_x \sin(\delta/2) \end{pmatrix}$$

OLIMPO Primary Mirror

DFTS

Cold optics
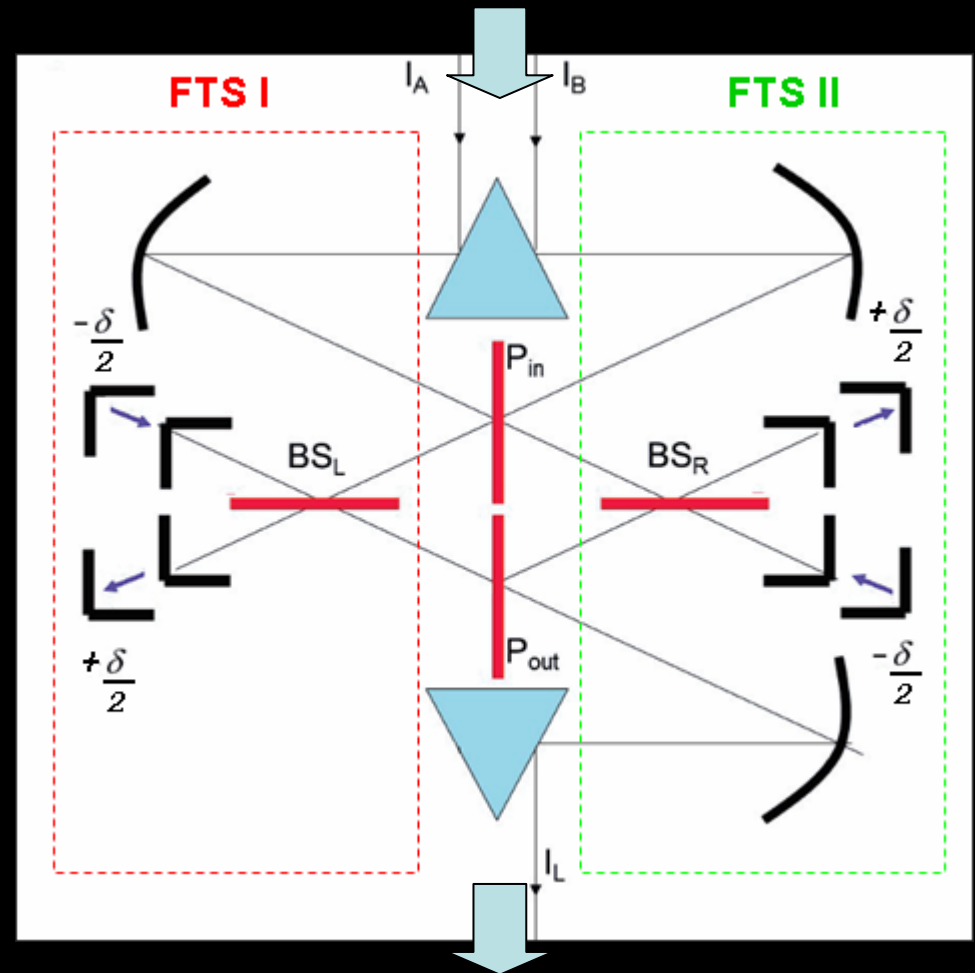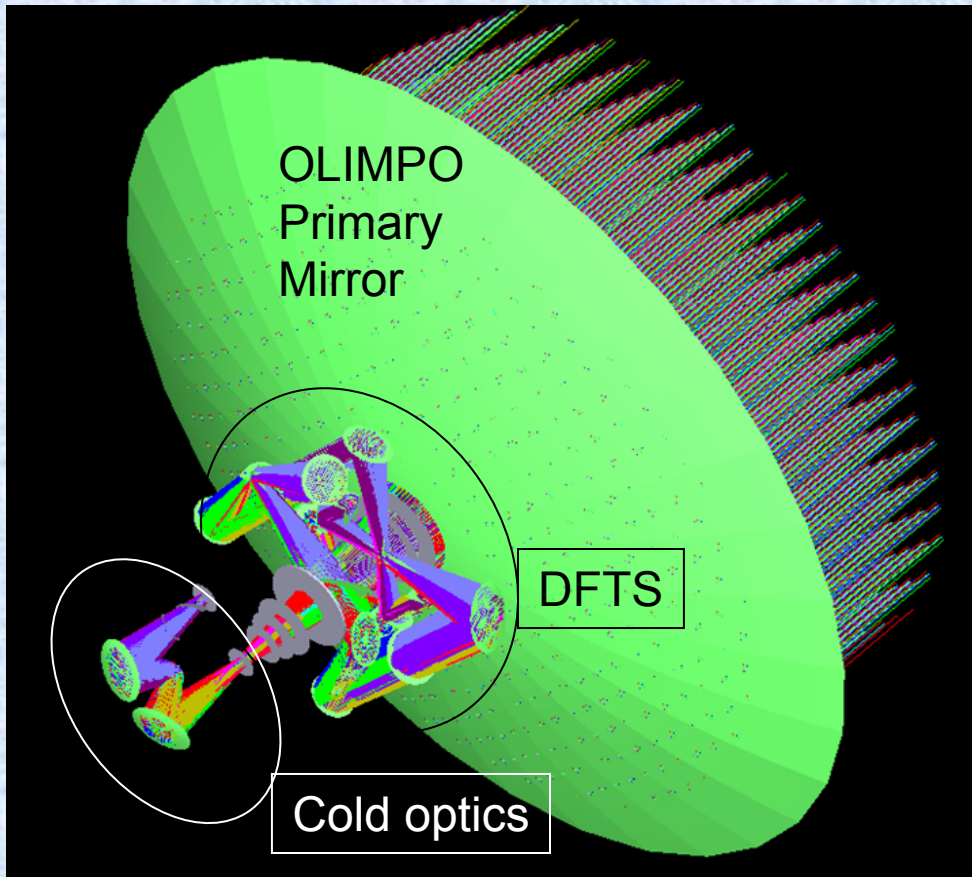
Global design of the optical system
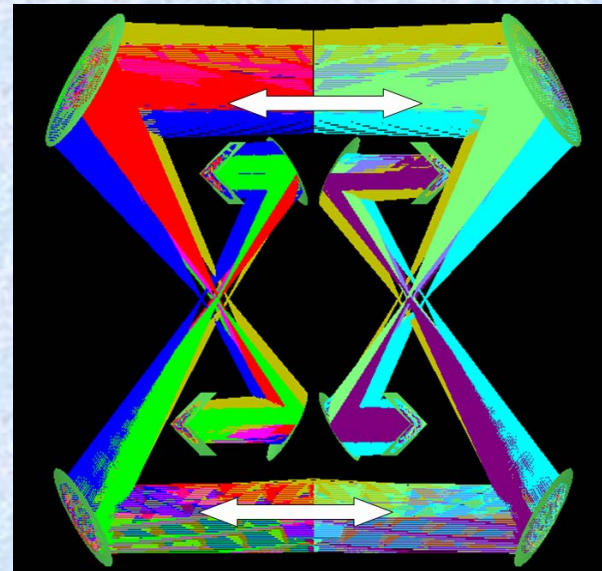
Optical layout of the doublel Martin-Puplett FTS
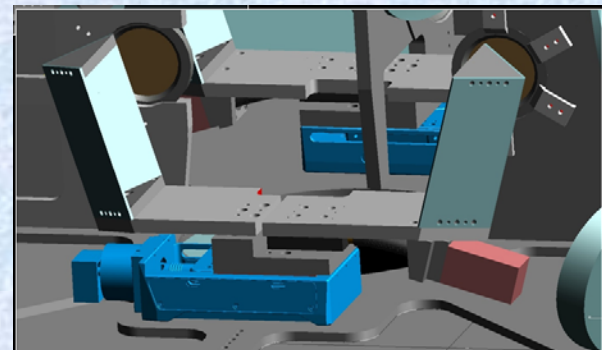
Mechanical arrangement of the translation stages

The OLIMPO Martin-Puplett Differential Fourier Transform Spectrometer

SKY IMAGE ON THE WEDGE MIRROR

A   B

C   D

FTS FOCAL PLANE

A-B

C-D
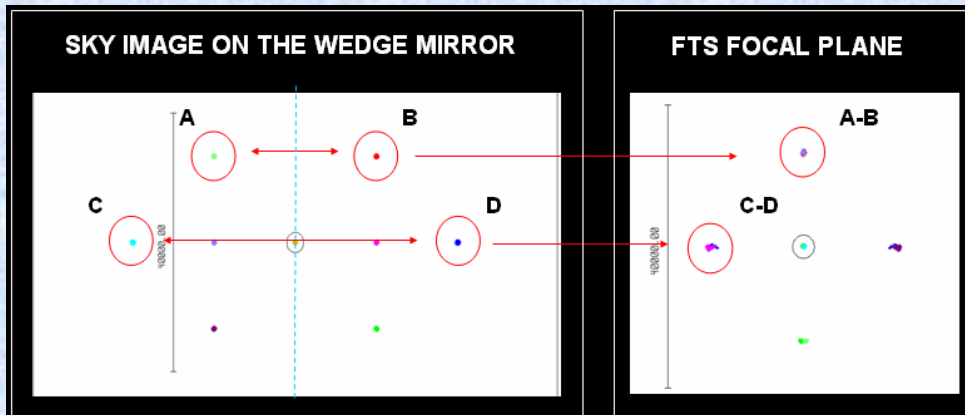
Differential field of view

Simulated OLIMPO measurement of a cluster l.o.s. with

τ_{th}=0.005,
T_e=10 keV,
τ_{nonth}=0.0001,
v_{pec}=500 km/s,
I_{dust}=6kJy/sr@150GHz

The data with the error bars are simulated observations from a single pixel of the OLIMPO-FTS, for an integration time of 3 hours. The two lines through the data points represent the input theory (thin) and the best fit for the plotted data realization (thick). The other thin lines represent thermal plus non-thermal SZE, and dust emission.

The high-frequency excess is due to a modest amount of dust

thermal + non-thermal

dust

this shift is due to the peculiar velocity of the cluster
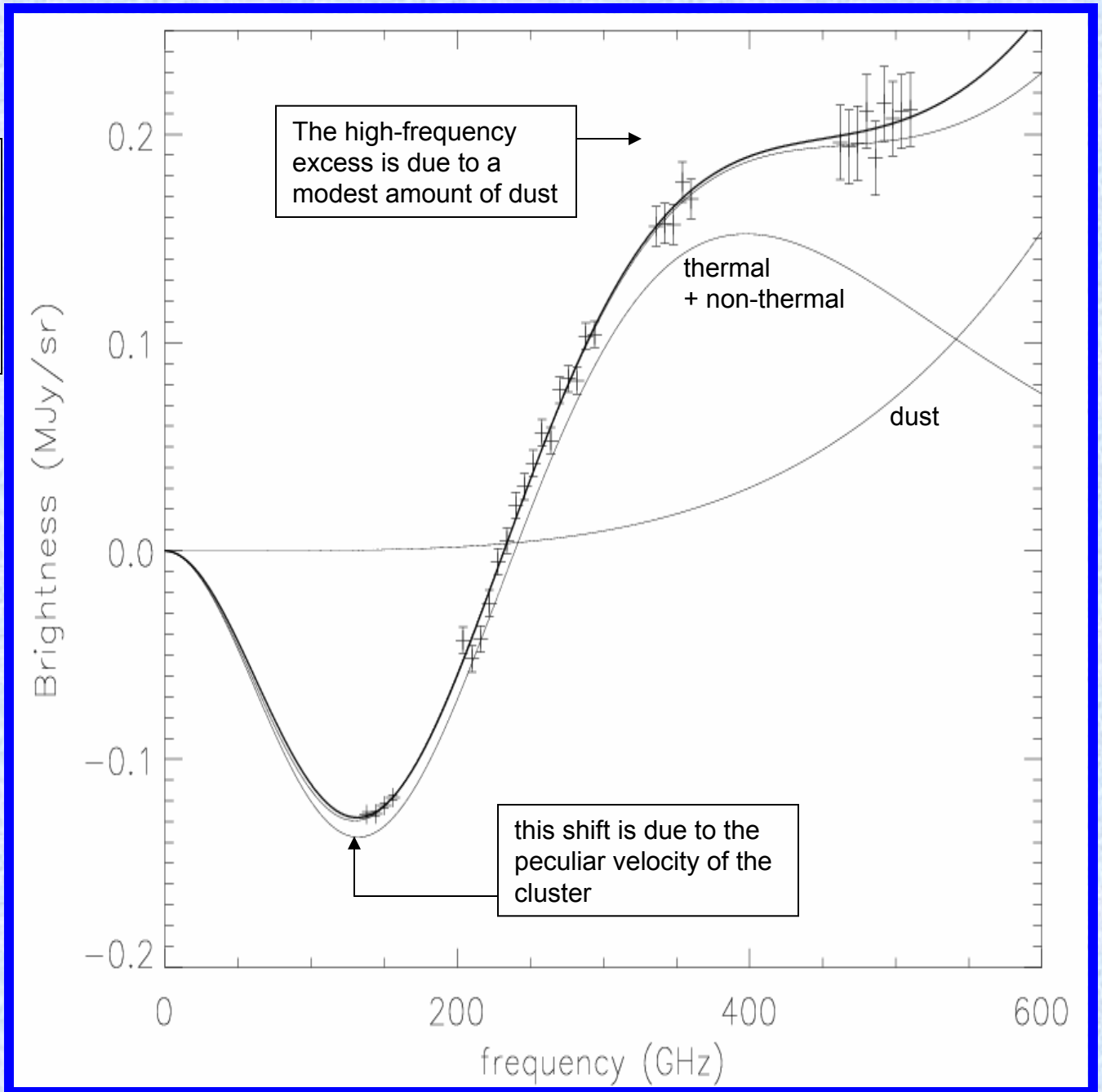
Parameters Determination

- In the presence of peculiar velocities, non-thermal populations (from AGNs in the cluster), and foreground dust, there are simply *too many free parameters* to be determined with the observation of a few frequency bands, like in ground-based measurements.

- We have carried out detailed simulations of OLIMPO observations in the spectroscopic configuration with an extended 200-300 GHz band.

- The spectroscopic configuration has superior performance in converging to the correct estimate of thermal optical depth and dust parameters, while the photometric configuration, *in the absence of priors*, tends to converge to biased estimates of the parameters. See de Bernardis et al. A&A **583**, A86 (2012).

Input parameters	OLIMPO	• No priors	• Prior T=(10±3) keV
τ_{th} =50x10^{-4}	FTS	τ_{th} =(63±27)10^{-4}	τ_{th} =(49±6)10^{-4}
T = 10 keV	3h integ.	T = (9.0±4.1) keV	T = (9.6±0.5)keV
τ_{non-th}=1x10^{-4}	one	τ_{non-th}=(14±9)10^{-5}	τ_{non-th}=(11±9)10^{-5}
ΔT_{CMB}=22μK	detector	ΔT_{CMB}=(24±43)μK	ΔT_{CMB}=(22±43)μK
$\Delta I_{dust150}$=6 kJy/sr		$\Delta I_{dust150}$=(5.7±1.6)kJy/sr	$\Delta I_{dust150}$=(5.8±0.9)kJy/sr

Observation Program

OLIMPO – CLUSTERS

- In a circumpolar summer long duration flight (>200h) we plan to observe 40 selected clusters and to perform a blind deep integration on a clean sky region
- We have optimized the observation plan distributing the integration time among the different targets according to their brightness and diurnal elevation.

ind	ID	RA	Dec	TIME	frac	NAME
0	1	212.83	52.2	18000	1	3C295CLUSTER
1	40	194.95	27.98	3600	0	ABELL1656
2	43	203.13	50.51	3600	1	ABELL1758
3	44	205.48	26.37	3600	1	ABELL1775
4	45	207.25	26.59	3600	1	ABELL1795
5	48	216.72	16.68	18000	1	ABELL1913
6	49	223.18	16.75	11360.88	1.27	ABELL1983
7	50	223.63	18.63	18000	1	ABELL1991
8	51	223.21	58.05	5640.53	1.28	ABELL1995
9	53	227.56	33.53	18000	1	ABELL2034
10	54	229.19	7	3600	1	ABELL2052
11	55	230.76	8.64	3600	1	ABELL2063
12	56	234.95	21.77	3600	1	ABELL2107
13	57	236.25	36.06	18000	1	ABELL2124
14	58	239.57	27.23	3600	1	ABELL2142
15	59	240.57	15.9	3600	1	ABELL2147
16	61	247.04	40.91	18000	1	ABELL2197
17	62	247.15	39.52	3600	1	ABELL2199
18	63	248.19	5.58	3600	1	ABELL2204
19	65	250.09	46.69	3600	1	ABELL2219
20	66	255.68	34.05	7230	1.49	ABELL2244
21	69	260.62	32.15	18000	1	ABELL2261
22	70	290.19	43.96	3600	1	ABELL2319
23	71	328.39	17.67	3600	1	ABELL2390
24	98	241.24	23.92	13045.75	1.1	AWM4
25	100	299.87	40.73	18000	1	CYGNUSA
26	101	201.2	30.19	18000	1	GHO1322+3027
27	102	241.11	43.08	18000	1	GHO1602+4312
28	107	230.46	7.71	3600	1	MKW03S
29	120	228.61	36.61	18000	1	MS1512.4+3647
30	121	245.9	26.56	13147.05	1.1	MS1621.5+2640
31	128	201.15	13.93	18000	0	NGC5129GROUP
32	134	199.34	29.19	18000	1	RDCSJ1317+2911
33	143	231.17	9.96	18000	1	RXJ1524.6+0957
34	150	211.73	28.57	18000	1	WARPJ1406.9+2834
35	151	213.8	36.2	18000	1	WARPJ1415.1+3612
36	161	194.02	25.95	18000	0	[VMF98]128
37	162	203.74	37.84	18000	1	[VMF98]139
38	163	205.71	40.47	18000	1	[VMF98]148
39	164	214.12	44.78	18000	1	[VMF98]158
40	165	250.47	40.03	18000	1	[VMF98]184

Mission Profile

SORA LAUNCH: July 1st 2009 (1.5 ton)

Pegaso—E trajectory 02/07 10:14   (double click to enlarge)
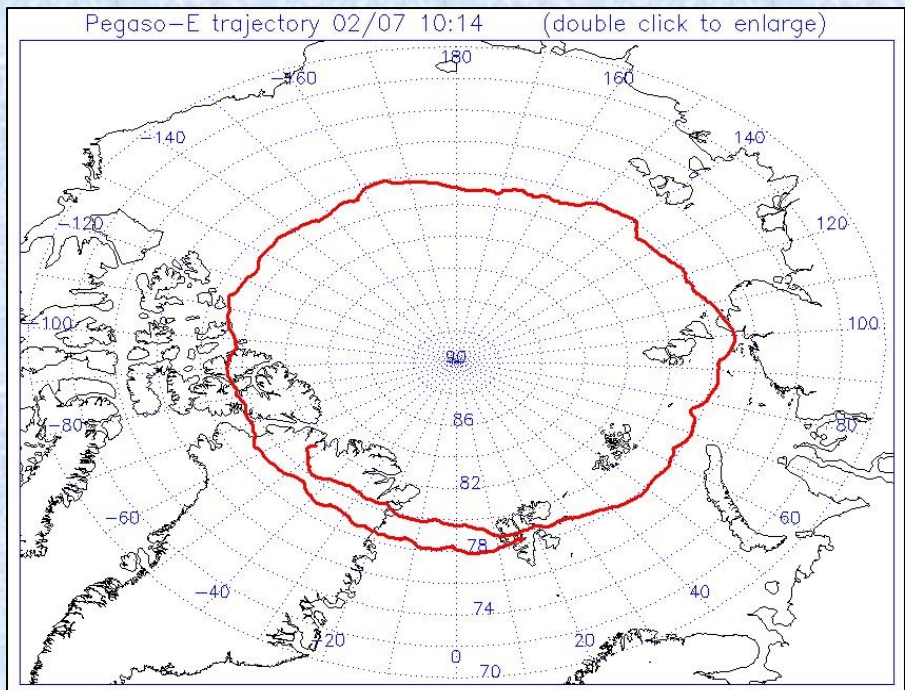
- We will use a long-duration circumpolar flight launched from Svalbard Islands (June 2013).
- We have tested these flights in collaboration with ASI, and demonstrared the feasibility of launching heavy payloads from the Longyearbyen airport, performing 2-3 weeks flights around the north pole during the Arctic summer.
- Backup-plan: Antarctica, 2014

millimetron
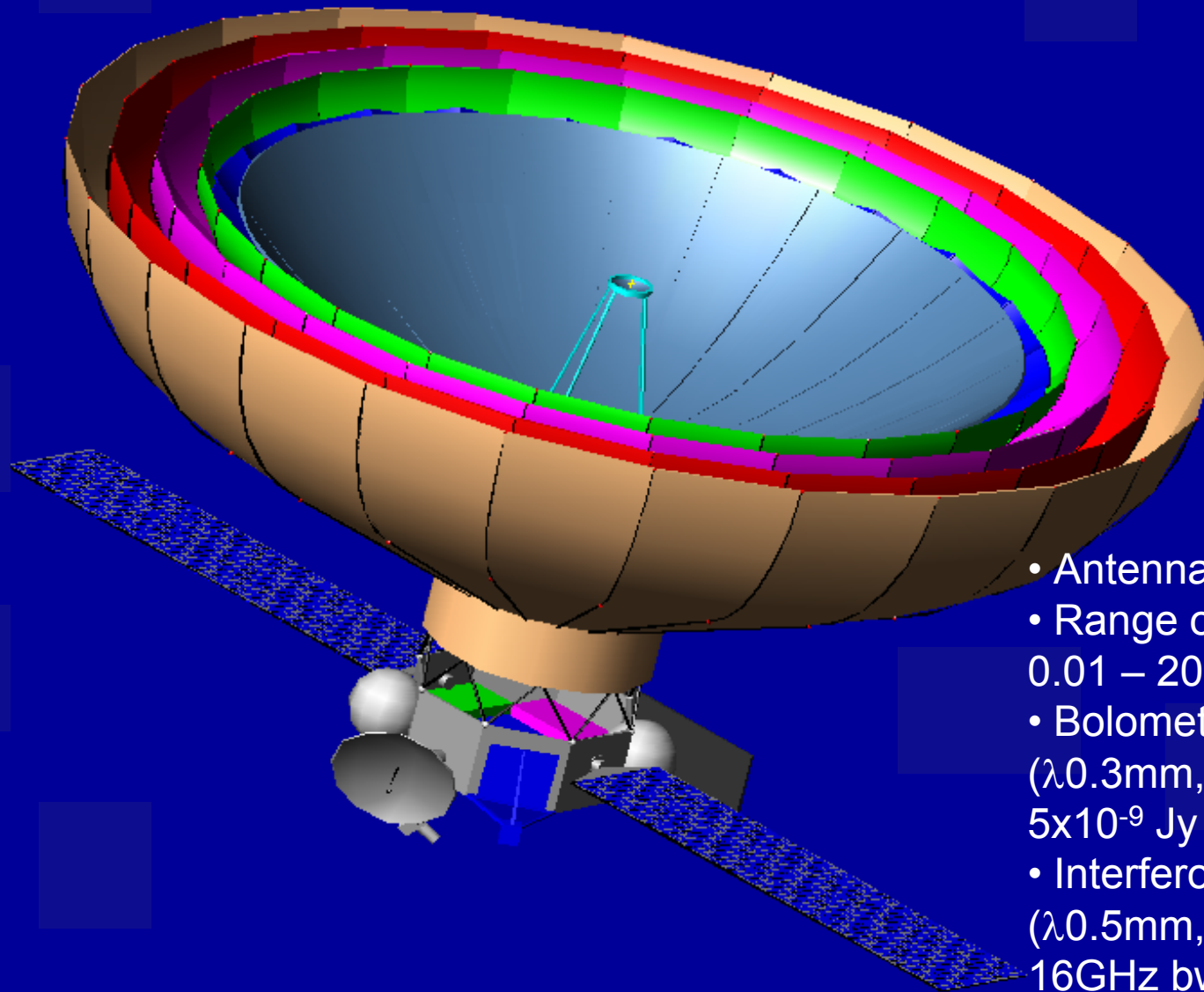
- Antenna diameter: 10 m
- Range of wavelengths: 0.01 – 20 mm
- Bolometric sensitivity (λ0.3mm, 1h integration): 5×10^{-9} Jy
- Interferometry sensitivity (λ0.5mm, 300s integration, 16GHz bw) : 10^{-4} Jy
- Interferometer beam: 10^{-9} arcsec

Cryo contr-reflector
(D=0.6m, T=4K)

Main reflector
(D=12m, F=3m, T=4K)

Flat mirror

Cryo container
D=3m,h=1m,T= 0.1-4K

Radiation screens

Deployable
truss

Solar arrays

Service module
(D=3.5m, h=1.5,m T=300K)

Radio and laser
TM antenna
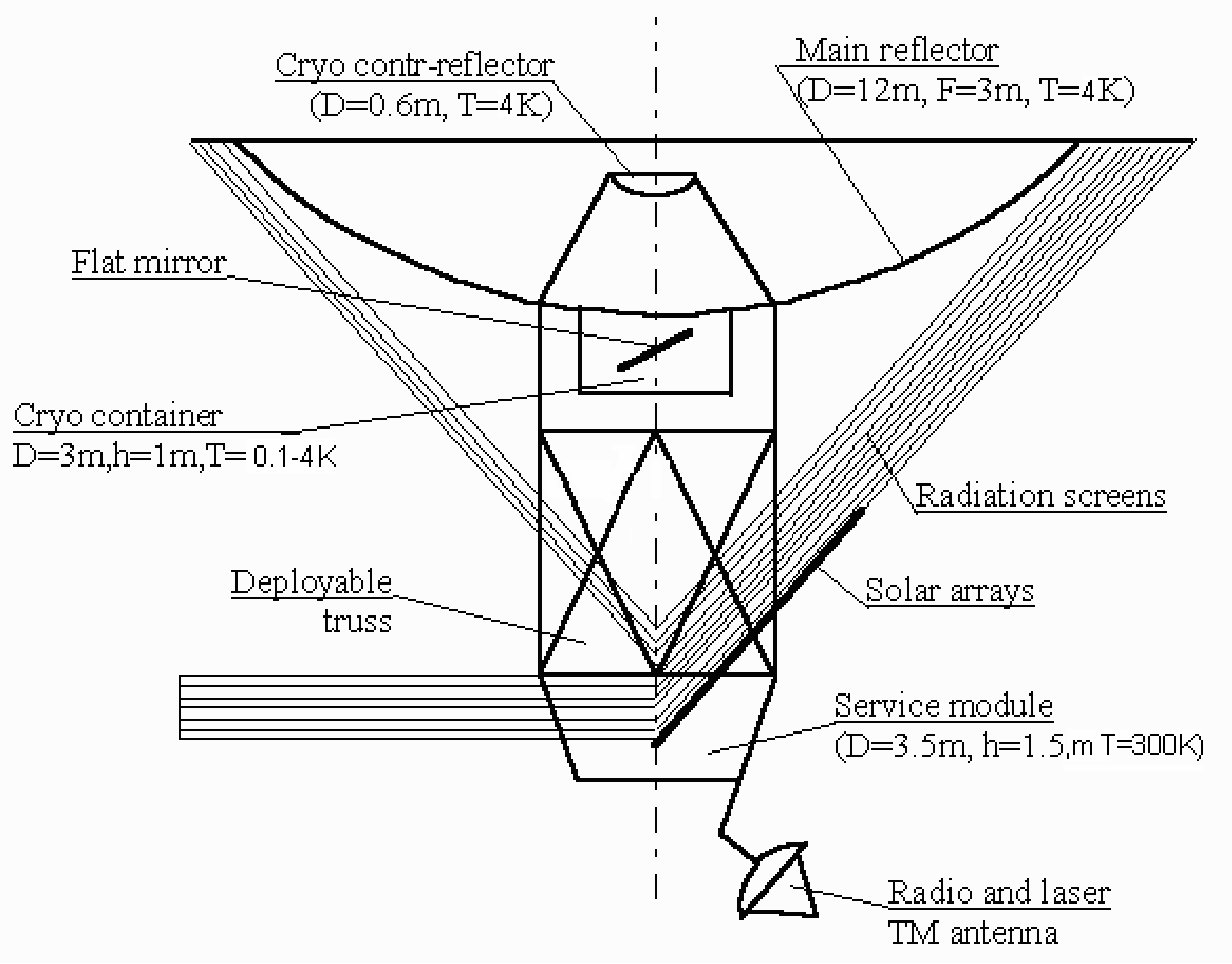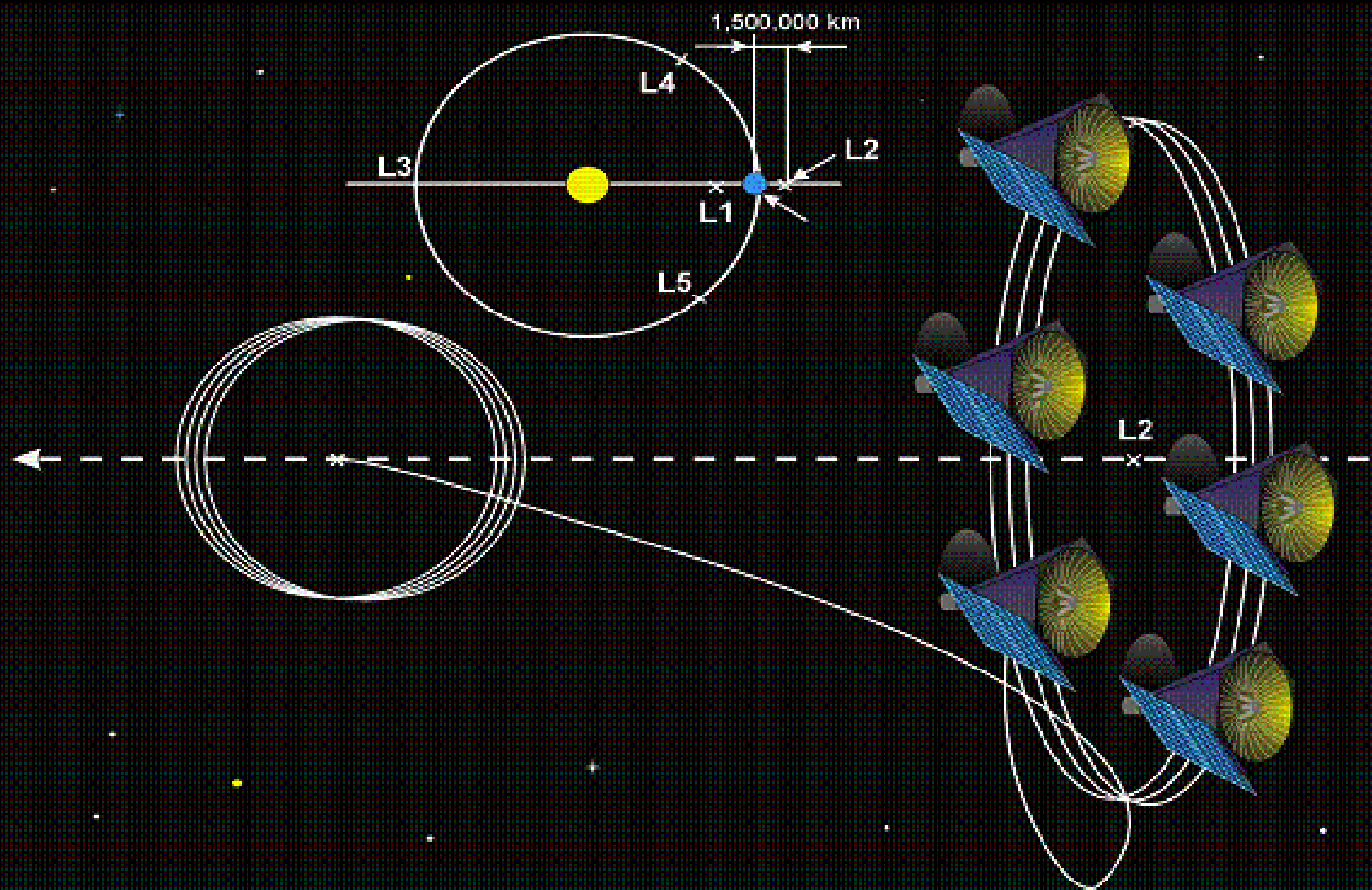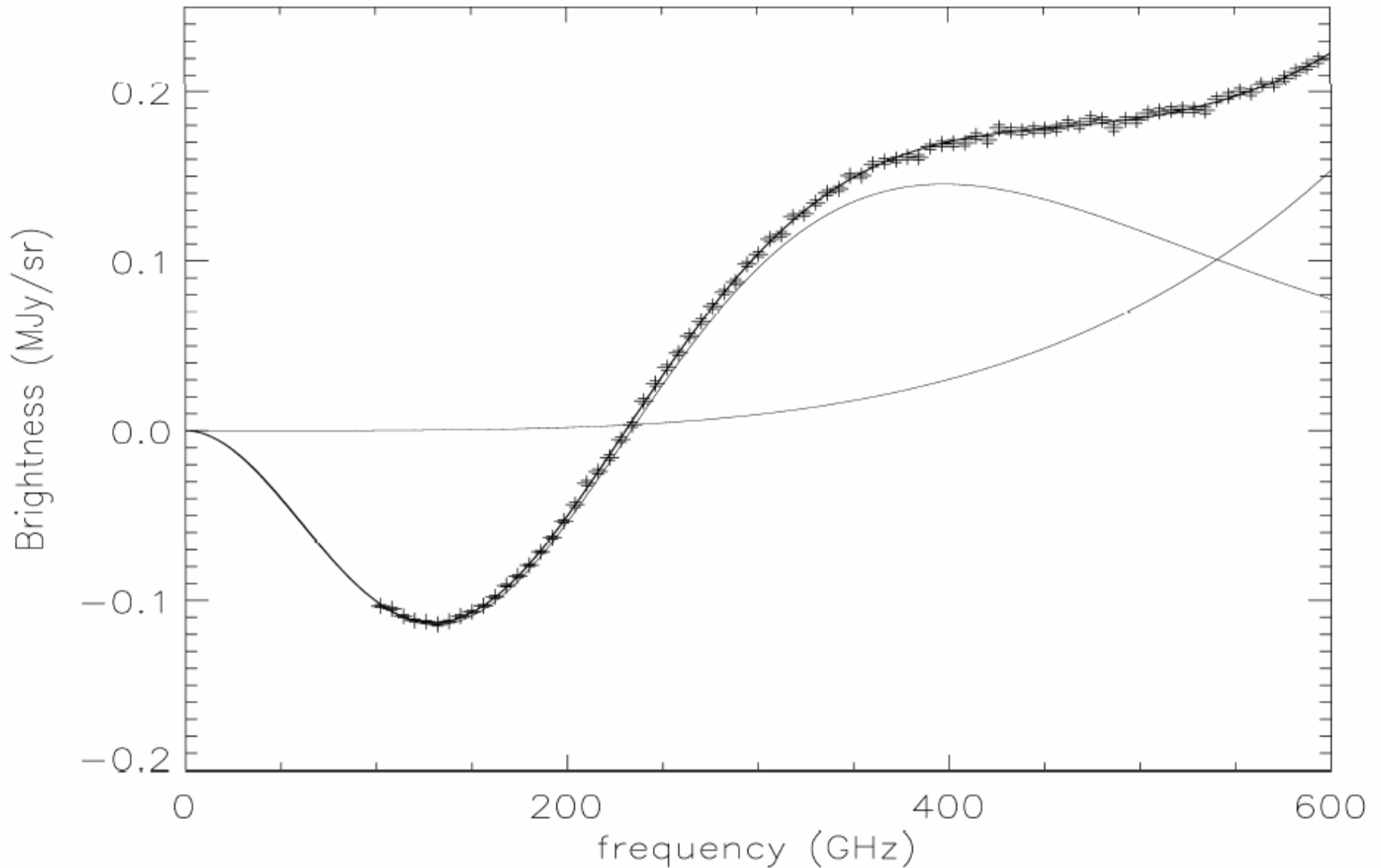
3 hours of observations of a rich cluster with a DFTS on Millimetron
Absolutely outstanding. USING A PHOTON NOISE LIMITED BOLOMETER IN
THE COLD ENVIRONMENT OF L2 WITH 4K TELESCOPE
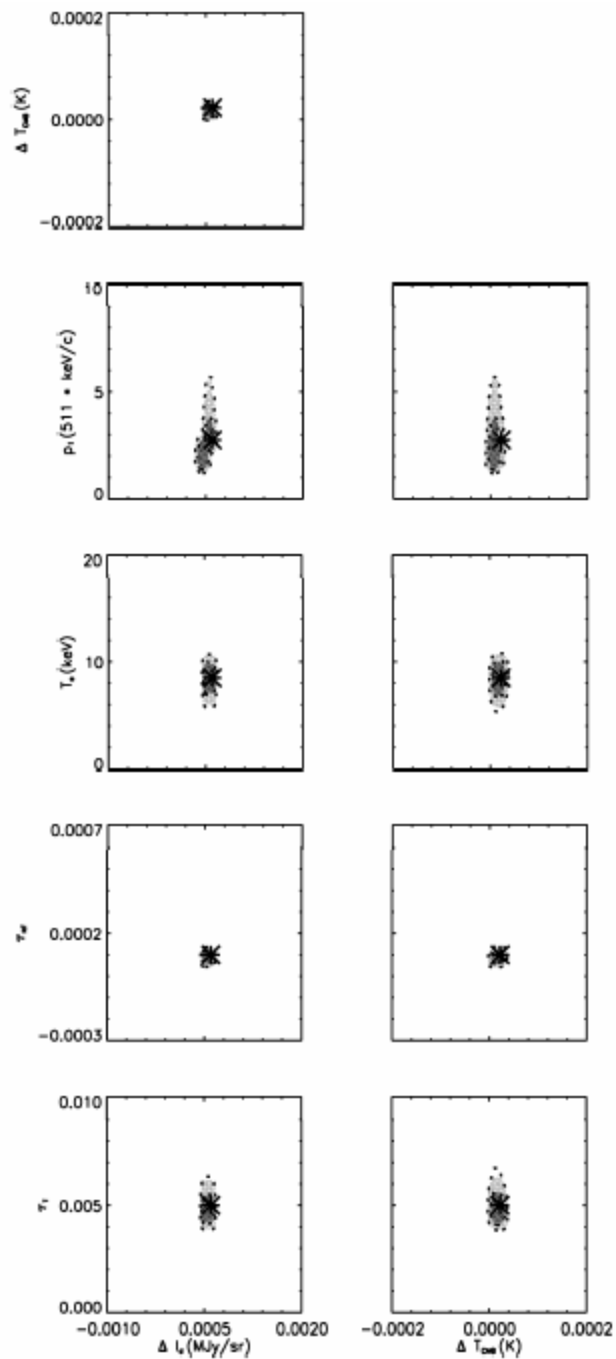
Parameter	input	best fit EC2 balloon - warm spec. prior $\sigma = 8$ keV	best fit EC2 balloon - warm spec. prior $\sigma = 3$ keV	best fit EC3 EO - cold spec. prior $\sigma = 8$ keV	best fit EC3 EO - cold spec. prior $\sigma = 3$ keV	best fit EC5 L2 - cold spec. prior $\sigma = 8$ keV	best fit EC5 L2 - cold spec. prior $\sigma = 3$ keV
$\tau_t \times 10^3$	5	5.0 ± 0.9	4.9 ± 0.8	5.8 ± 2.6	5.2 ± 0.6	5.1 ± 0.6	5.1 ± 0.5
$T(keV)$	8.5	8.4 ± 0.8	8.5 ± 0.1	7.7 ± 2.0	8.1 ± 0.8	8.5 ± 1.2	8.5 ± 1.0
$\Delta T_{CMB}(\mu K)$	22	20 ± 50	20 ± 50	23 ± 8	22 ± 8	22 ± 4	22 ± 4
$\Delta I_d (Jy/sr)$	600	570 ± 270	560 ± 270	590 ± 40	590 ± 40	600 ± 4	600 ± 4
$\tau_{nt} \times 10^3$	0.1	0.1 ± 0.1	0.1 ± 0.1	0.12 ± 0.03	0.11 ± 0.02	0.10 ± 0.01	0.10 ± 0.01
$p_1(511\,keV/c)$	2.75	2.6 ± 0.7	2.5 ± 0.7	2.5 ± 0.9	2.7 ± 1.1	3.0 ± 1.0	2.9 ± 0.9
$\langle \chi^2 \rangle / DOF$	-	$34.9/34$	$34.9/34$	$77.8/78$	$78.0/78$	$110.0/110$	$110.1/110$
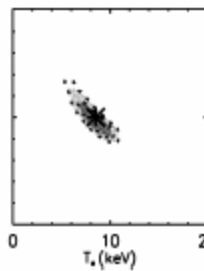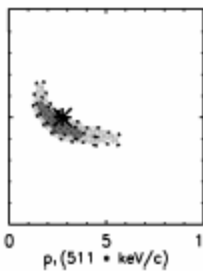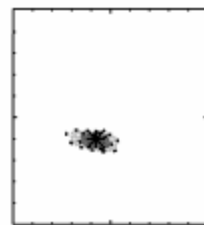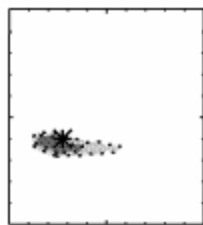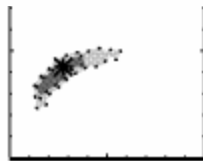
3h integration on the same LOS through a rich cluster

P. de Bernardis, et al., Astronomy and Astrophysics, **538,** A86 (2012)

1ES0657-556

Oscuro ammasso speciale

7.5'
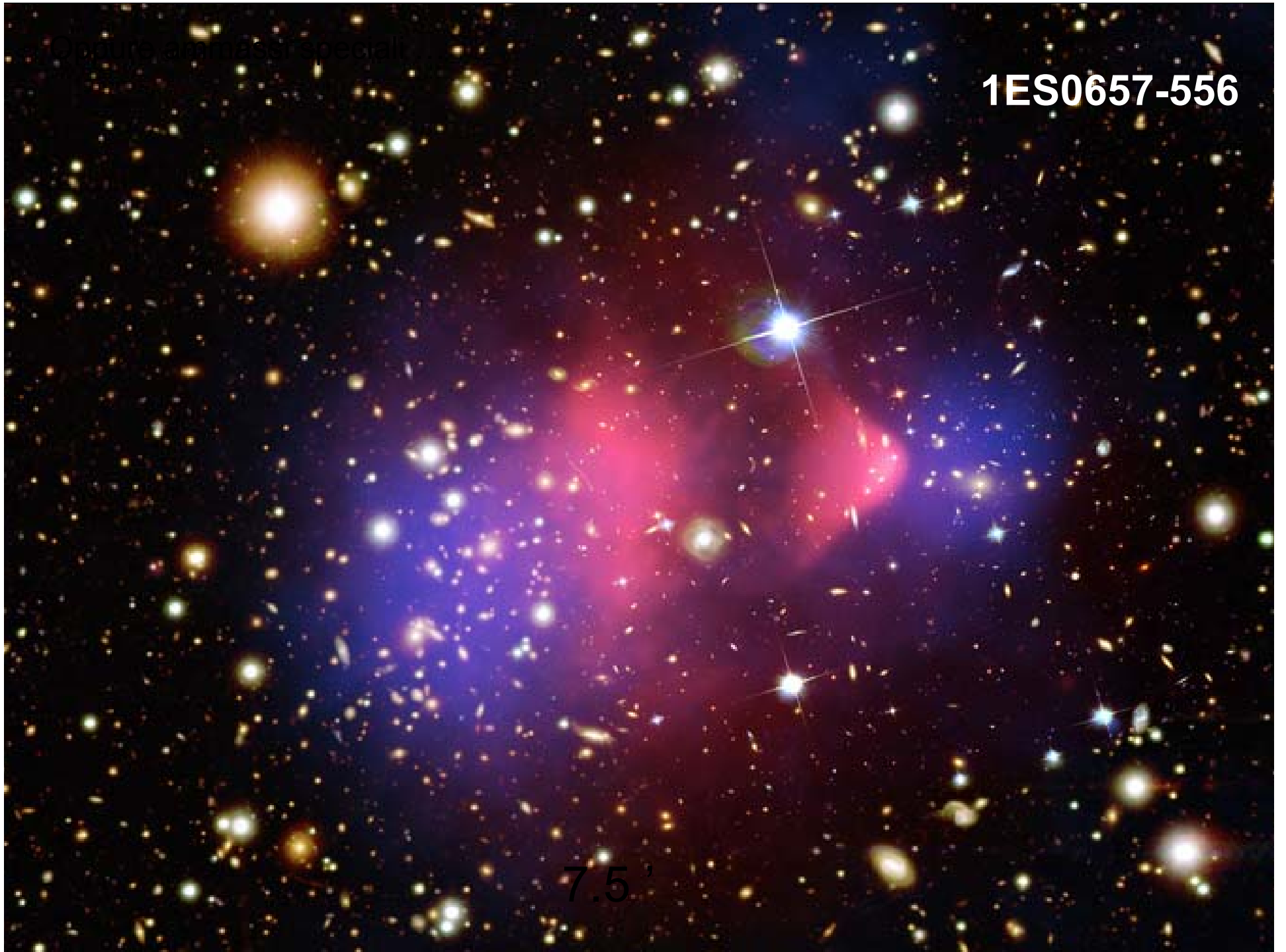
1ES0657-556: DM + thermal gas

Gas clump A)
T = 14 keV

Gas clump B)
T = 6 keV
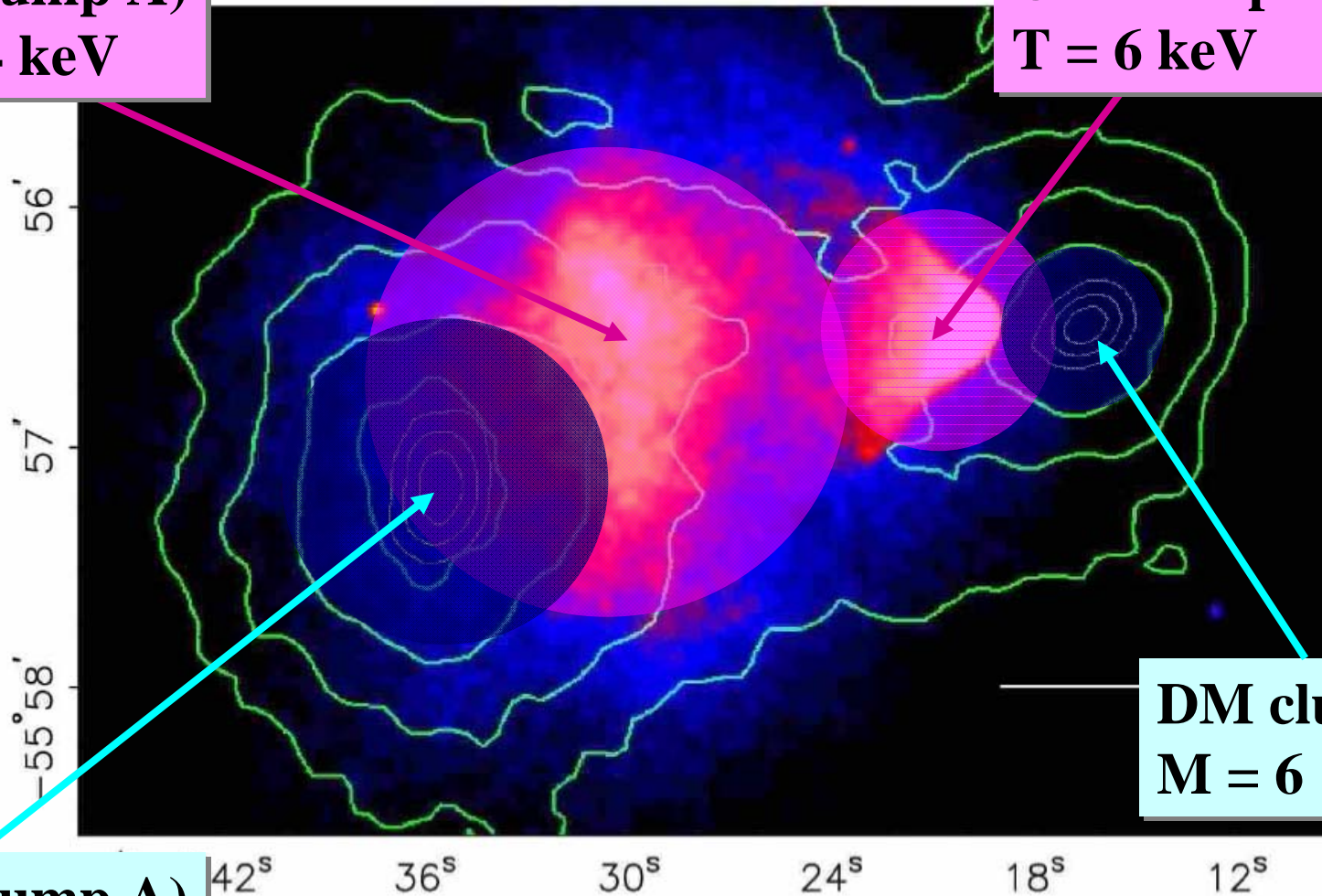
DM clump B)
M = $6 \cdot 10^{13}$ M$_\odot$

DM clump A)
M = 10^{15} M$_\odot$

[Clowe et al. 2006, and refs. therein]

SZ effect from DM

The SZ Effect
Compton Scattering of CMB photons
by IS/IC electrons

$$\Delta I(x) = I(x) - I_0(x)$$

I_{CMB}

Halo

$I_{CMB} + \Delta I_{SZ}$

γ

γ' e^-

$z \sim 1100$

Last scattering surface

$I_0(x)$

$I_{th}(x)$

$I_{DM}(x)$

I(x)

x=hν/kT

Radio Infrared Ultraviolet Gamma Rays

Microwave Visible X-Rays Cosmic Rays

thermal e⁻

$$\frac{\nu'}{\nu} = \frac{4}{3}$$
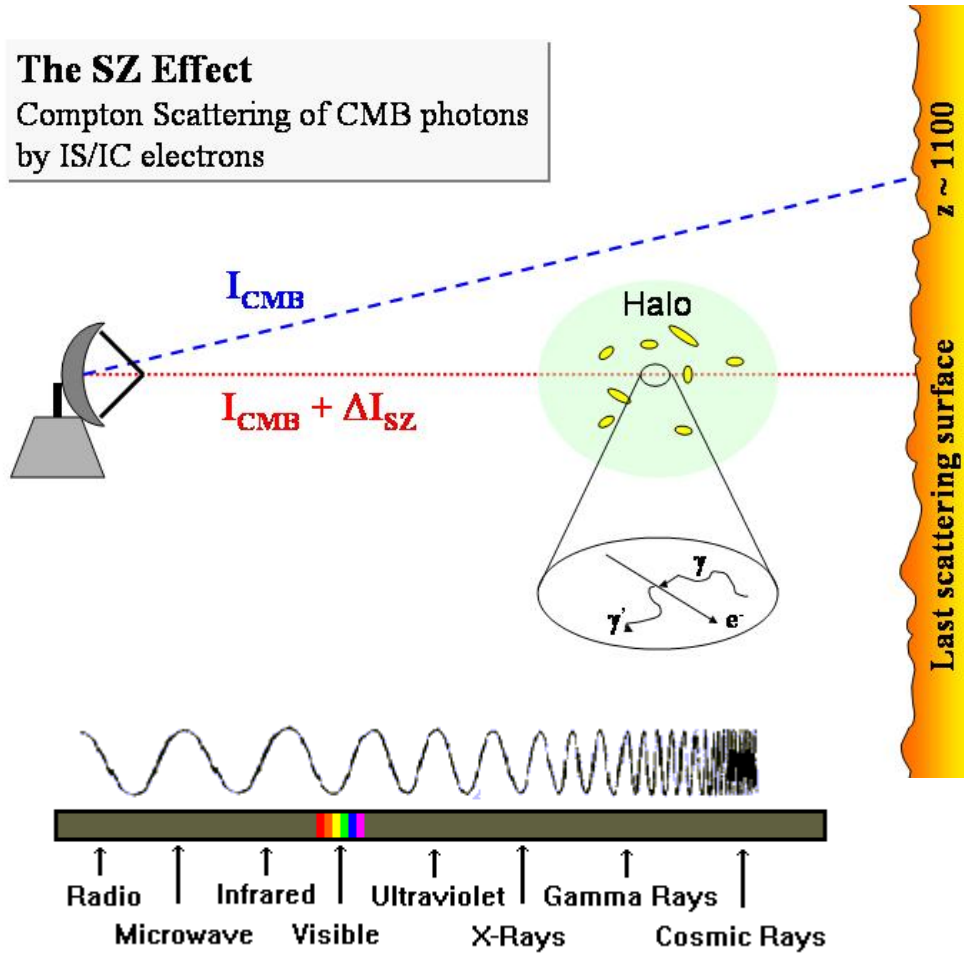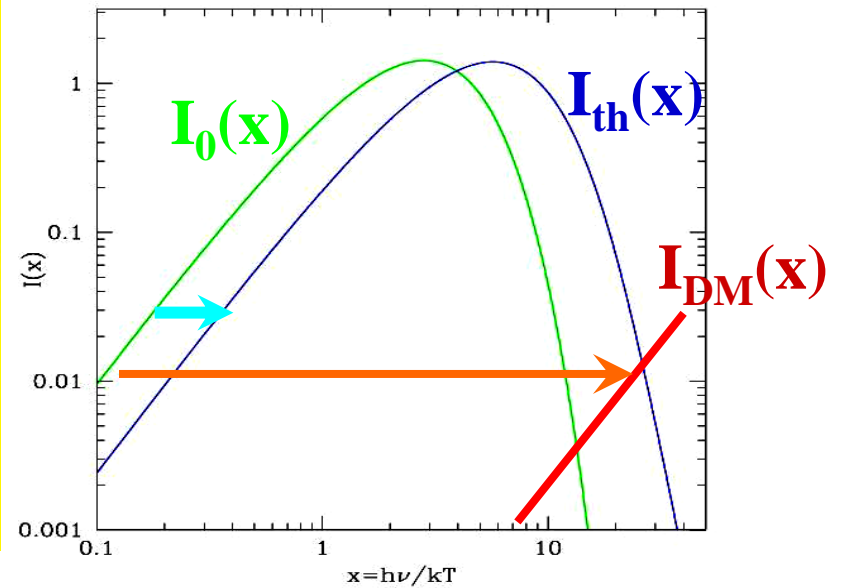
relativistic e⁻

$$\frac{\nu'}{\nu} = \frac{4}{3}\gamma^2 - 1$$

SZ effect at clump centres
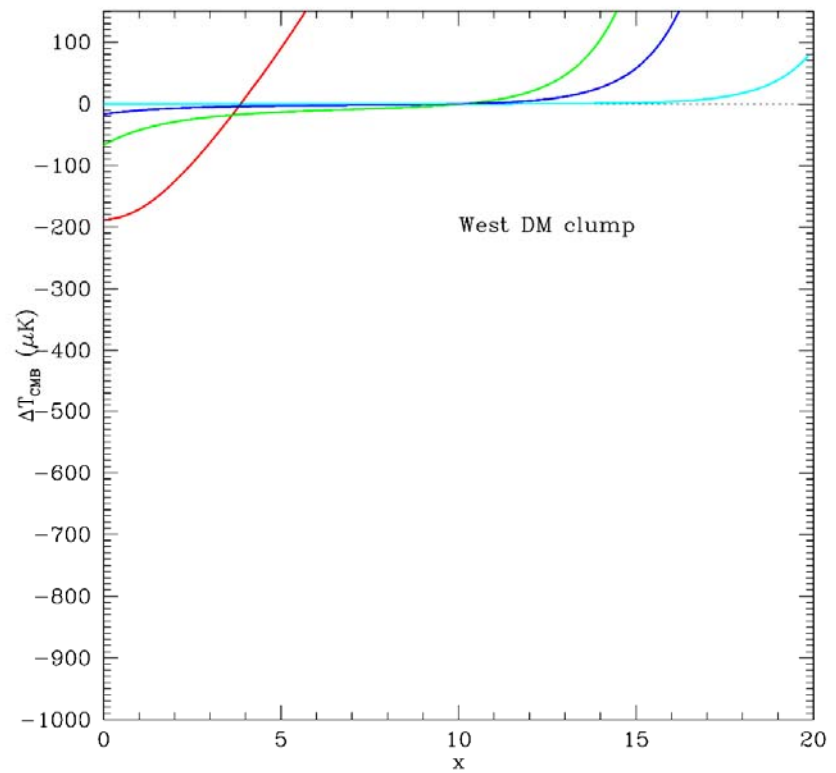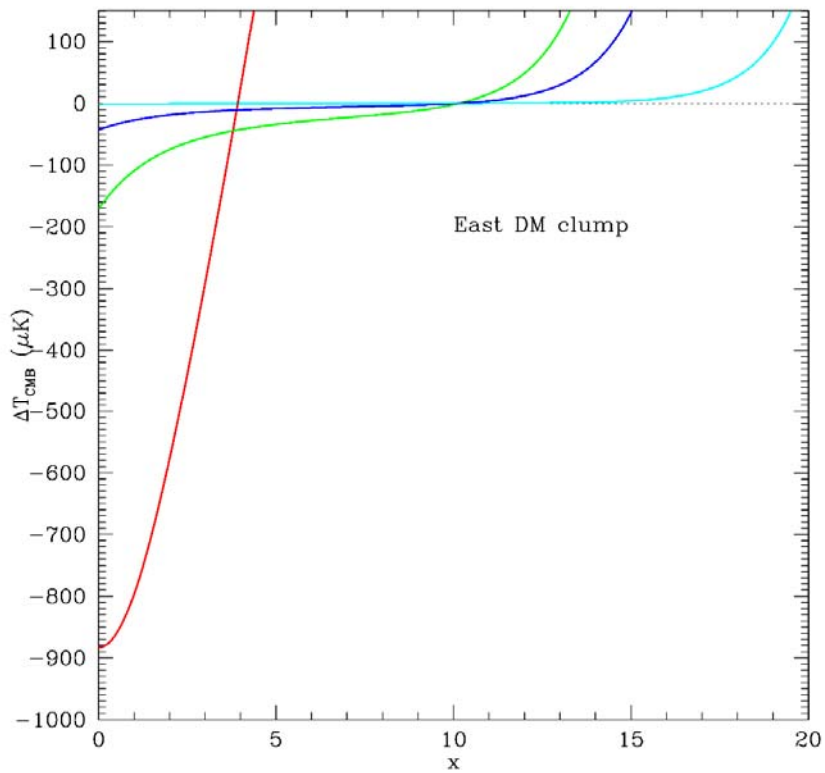
[Colafrancesco, de Bernardis, Masi, Polenta & Ullio 2006]

150 GHz   **220 GHz**   **350 GHz**
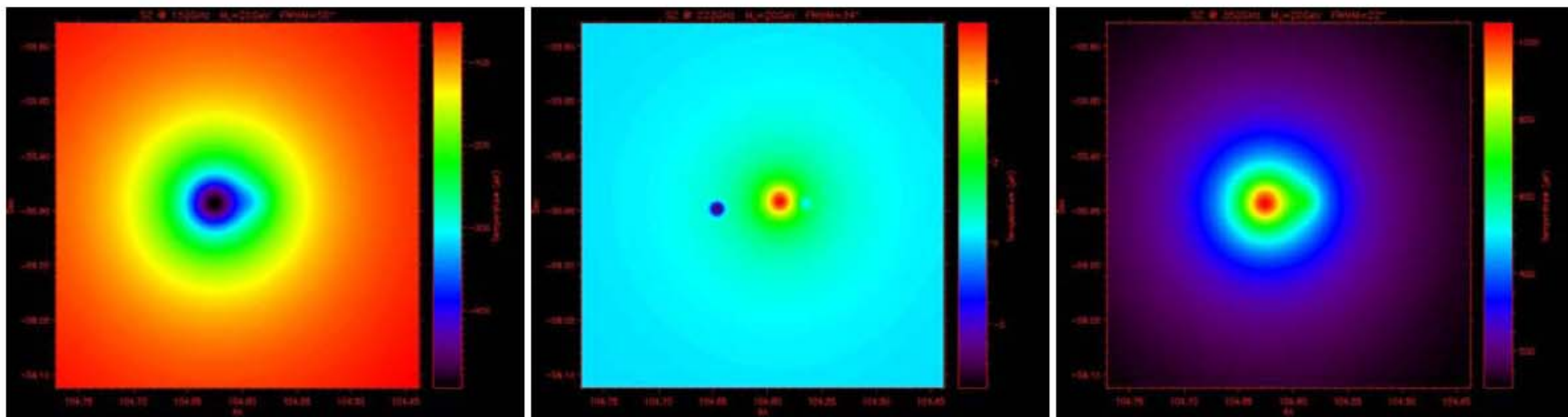
Fig. 2. The simulated SZ maps of the cluster 1ES0657-556 as observable with the SPT telescope at three frequencies: $\nu = 150$ GHz (left panel), $\nu = 223$ GHz (mid panel), $\nu = 350$ GHz (right panel). A neutralino mass of $M_\chi = 20$ GeV has been adopted here. Note that choosing the frequency of 223 GHz where the thermal SZE from the E baryonic clump vanishes maximizes the detectability of the SZ_{DM} effect from the two DM clumps.

Colafrancesco, de Bernardis, Masi, Polenta & Ullio *"Direct probes of Dark Matter in the cluster 1ES0657-556 through microwave observations"*, Astronomy and Astrophysics, 467, 1, (2007), L1-L5 ; astro-ph/0702568

Isolating SZ_{DM} (at 223 GHz)

$M_\chi = 20$ GeV $M_\chi = 40$ GeV $M_\chi = 80$ GeV
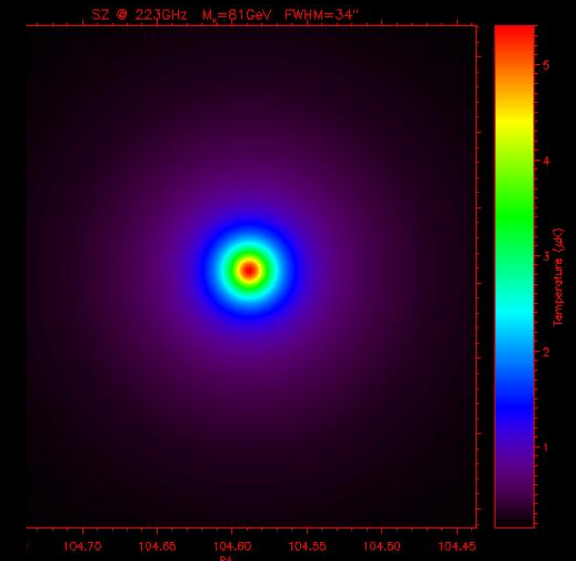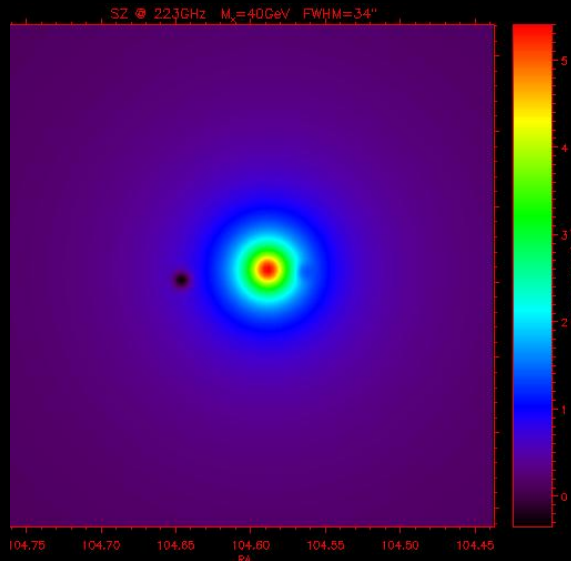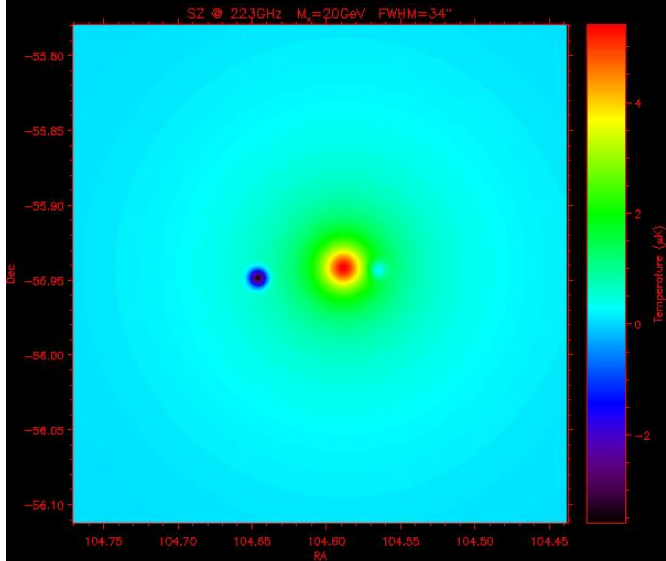
The SZE from the hot gas disappears at $x_{0,th}$ (~ 220-223 GHz) while the SZ_{DM} expected at the locations of the two DM clumps remains negative and with an amplitude and spectrum which depend on M_χ.

[Colafrancesco, de Bernardis, Masi, Polenta & Ullio 2006]
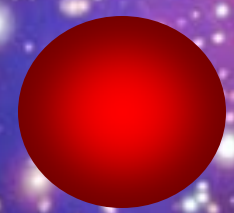
**Beam of
Super-OLIMPO
@220GHz**

7.5 '

Inflation & polarization
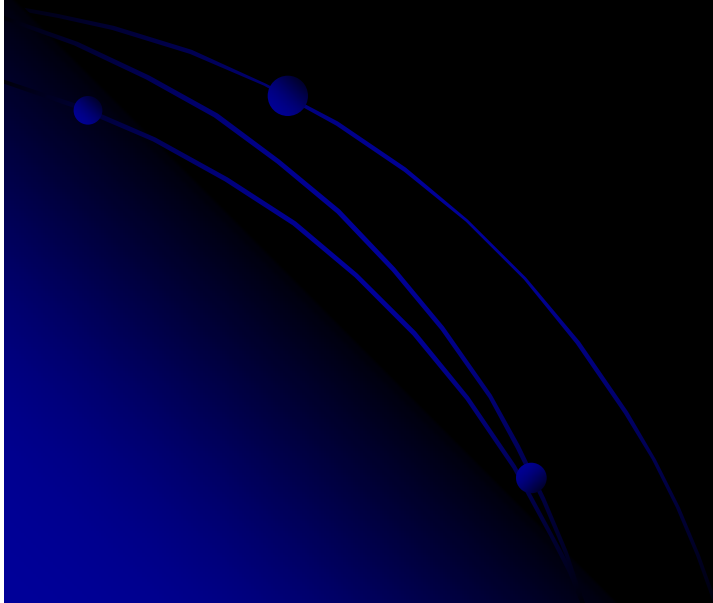
EBEX

Secondary Mirror

Star Camera

Primary Mirror

Cryostat

ACS Crate

Reaction Wheel

Magnetometer

Battery Table

pivot

dGPS, Sun sensor (not installed)

Suspension Cables (4)

Bolometer readout crate (2)

Elevation Actuator

Flight Computer Crate

EBEX Focal Plane

738 element array **141 element hexagon** **Single TES**

250 150

150 420 150

150 250

Lee, UCB

3 mm

5 cm
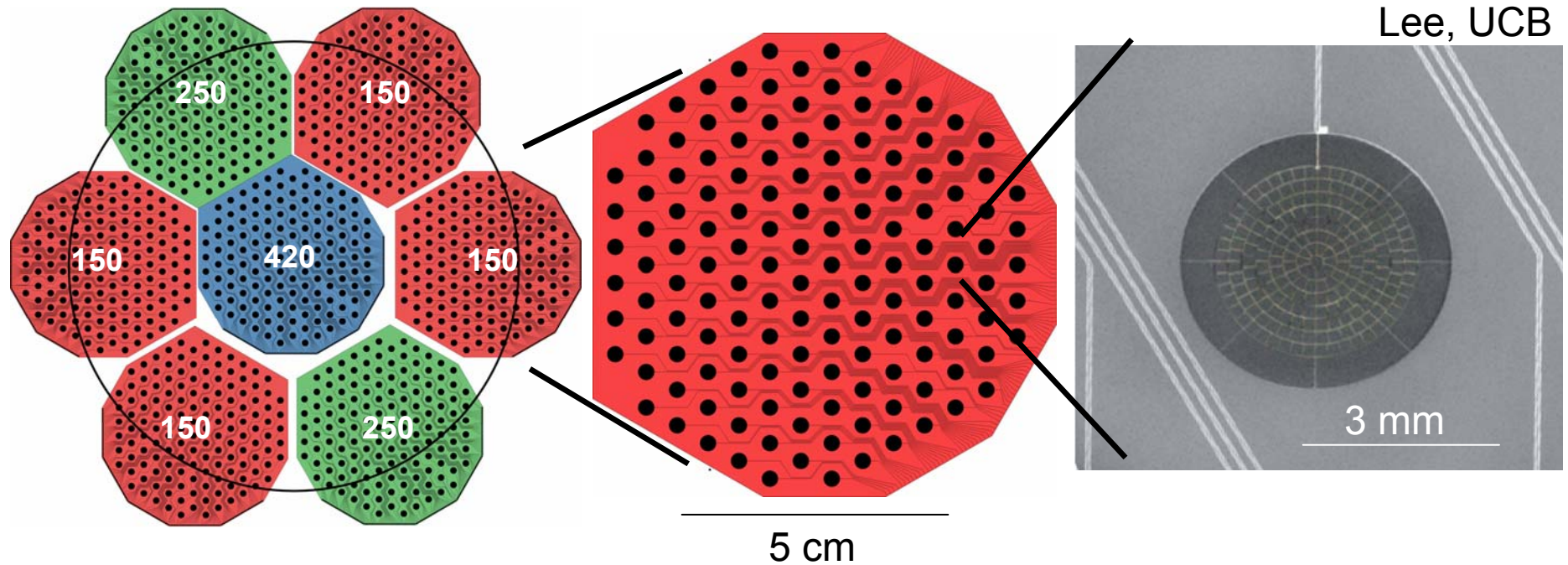
- Total of 1476 detectors
- Maintained at 0.27 K
- 3 frequency bands/focal plane

- G=15-30 pWatt/K
- NEP = 1.4e-17 (150 GHz)
- NEQ = 156 μK*rt(sec) (150 GHz)
- $\tau = 3$ msec,

Slide: Hanany

Science Goals

• Detect or set upper bound on inflation B-mode

• Measure lensing B-mode

• Understand Polarized Dust

• Improve estimation of cosmological parameters

Planck 1 year

EBEX 14 days
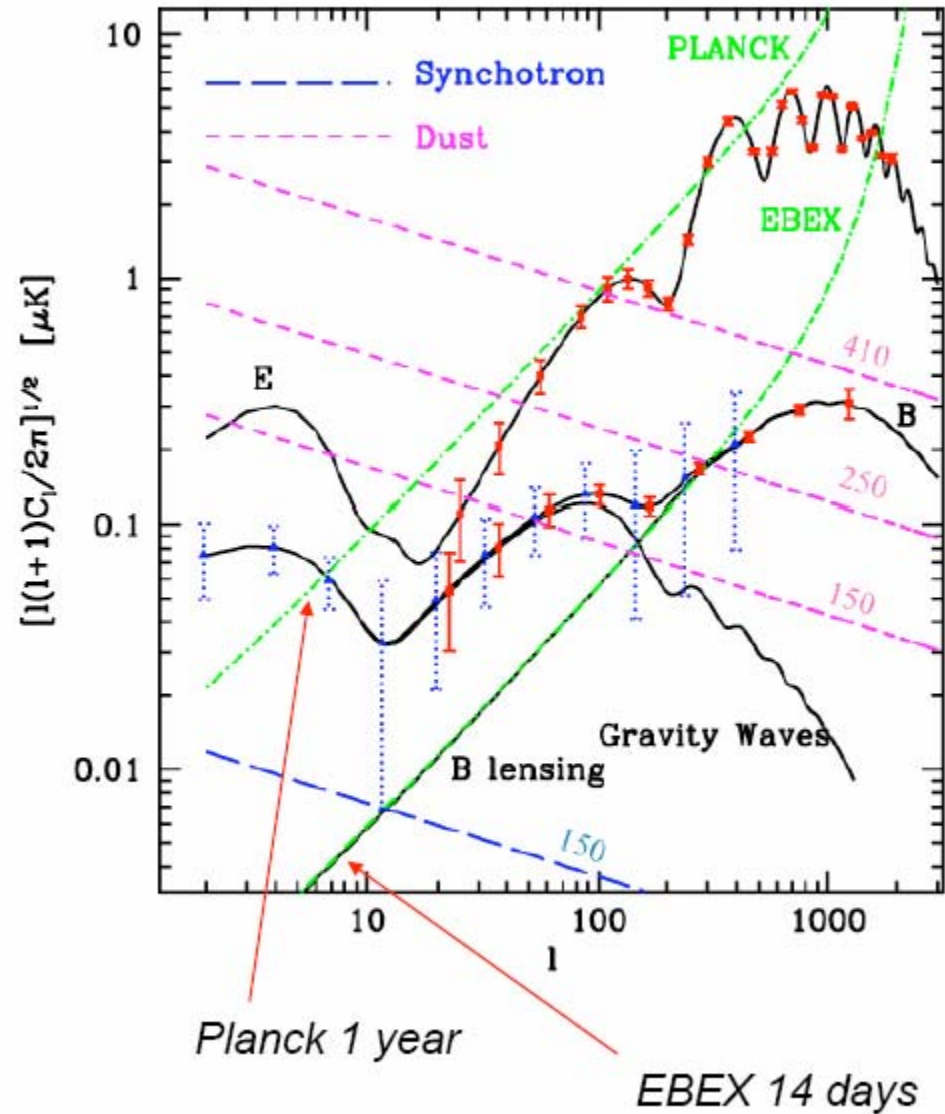
Focal Plane Hardware

36 cm

SPIDER

Suborbital Polarimeter for Inflation Dust and the Epoch of Reionization
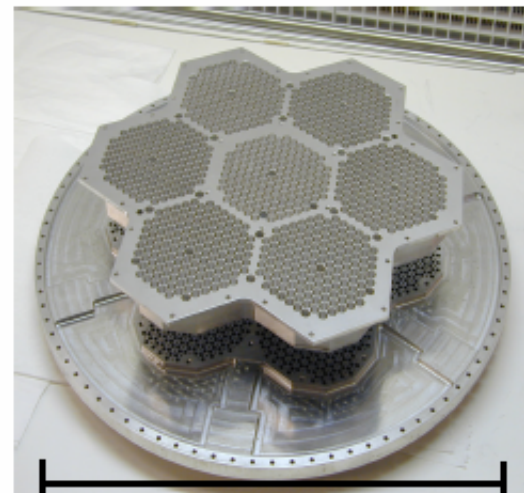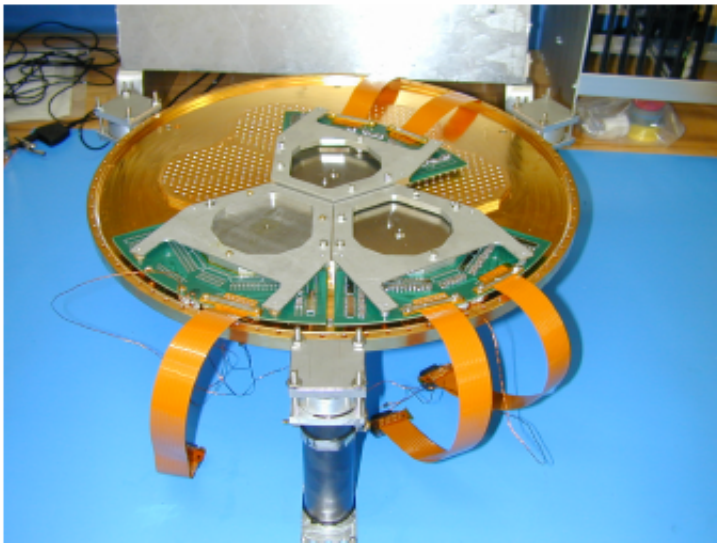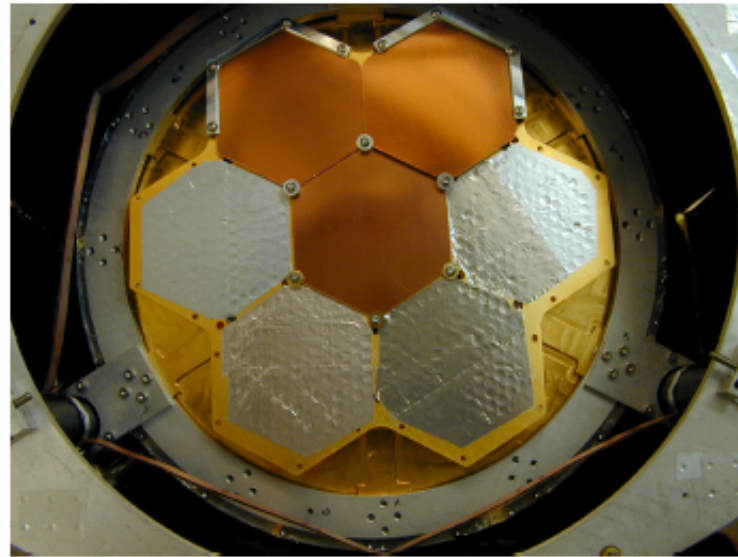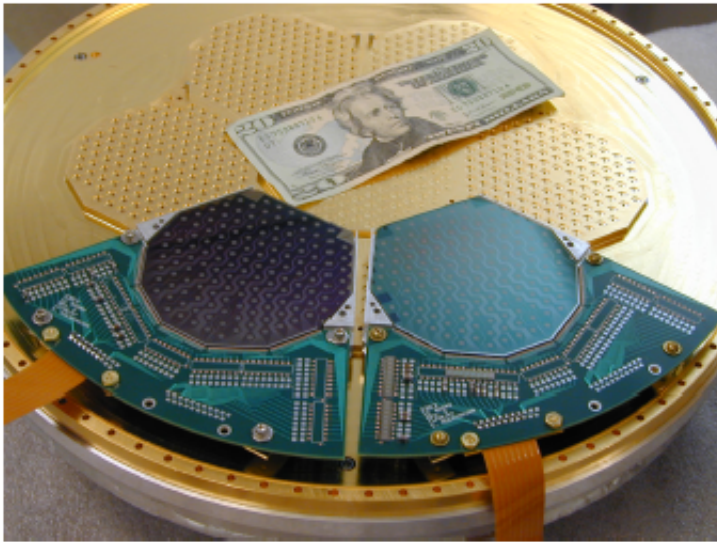
William Jones
Princeton University
for the
Spider Collaboration

The Path to CMBpol
June 31, 2009

Spider: A Balloon Borne CMB Polarimeter

Suborbital **P**olarimeter for **I**nflation **D**ust and the **E**poch of **R**eionization

• Long duration (~30 day cryogenic hold time) balloon borne polarimeter

• Surveys 60% of the sky each day of the flight, with ~0.5 degree resolution

• Broad frequency coverage to aid in foreground separation

• Will extract nearly all the information from the CMB E-modes

• Will probe B-modes on scales where lensing does not dominate

• Technical Pathfinder: solutions appropriate for a space mission
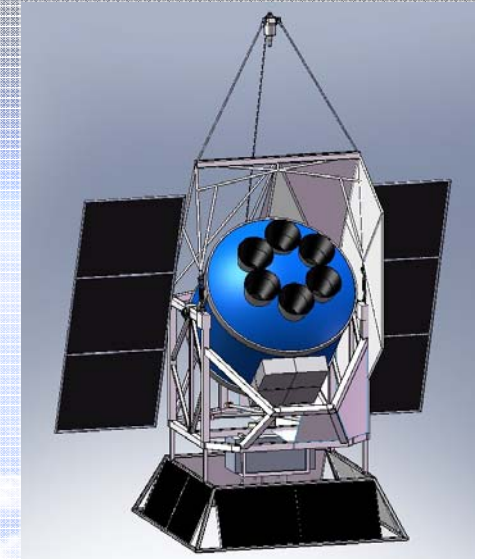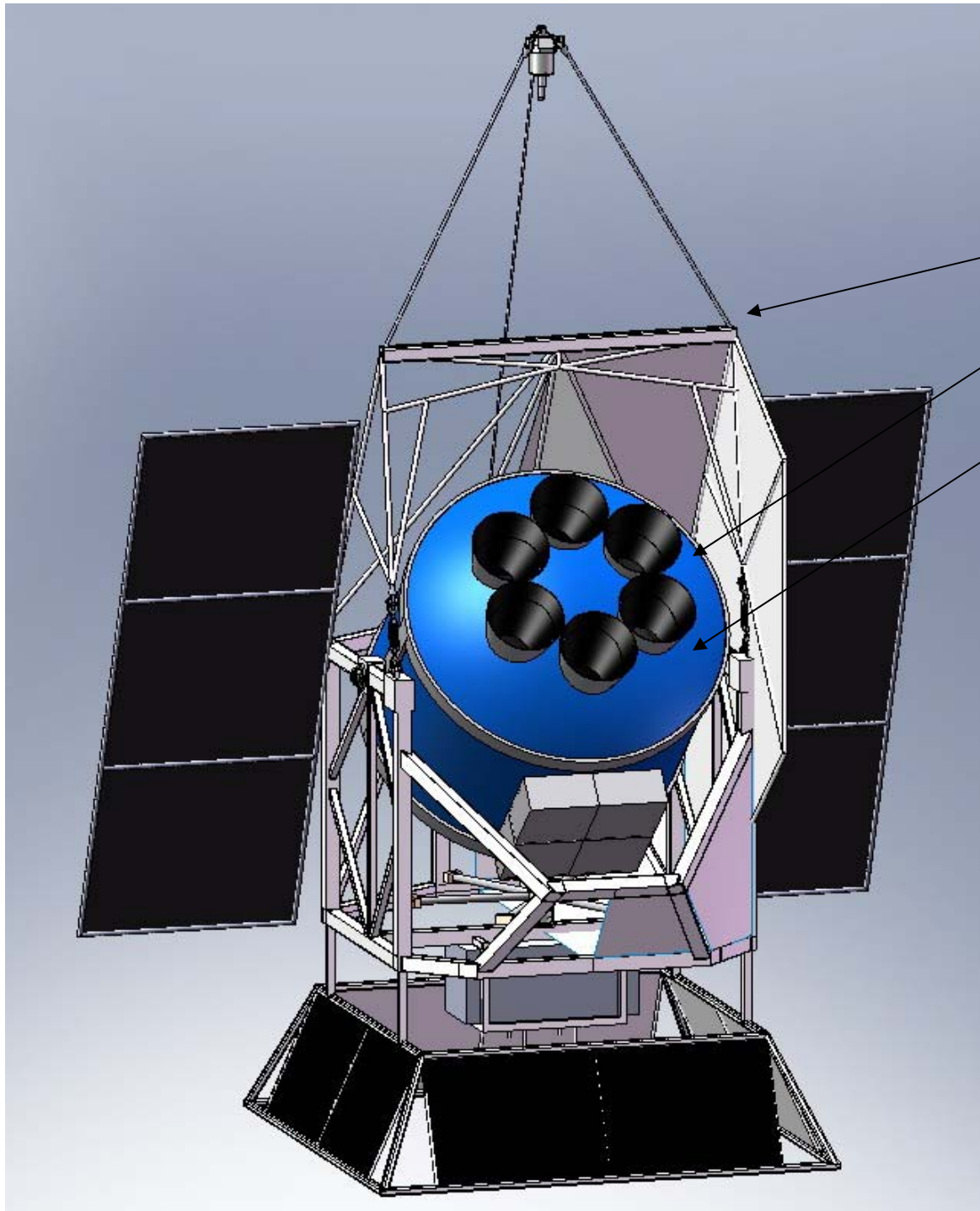
Carbon Fiber Gondola

Six single freq. telescopes

30 day, 1850 lb, 4K / 1.4 K cryostat

Attitude Control
- flywheel
- magnetometer
- rate gyros
- sun sensor

Pointing Reconstruction
- 2 pointed cameras
- boresight camera
- rate gyros

Flight Computers/ACS
- 1 TB for turnaround
- 5 TB for LDB
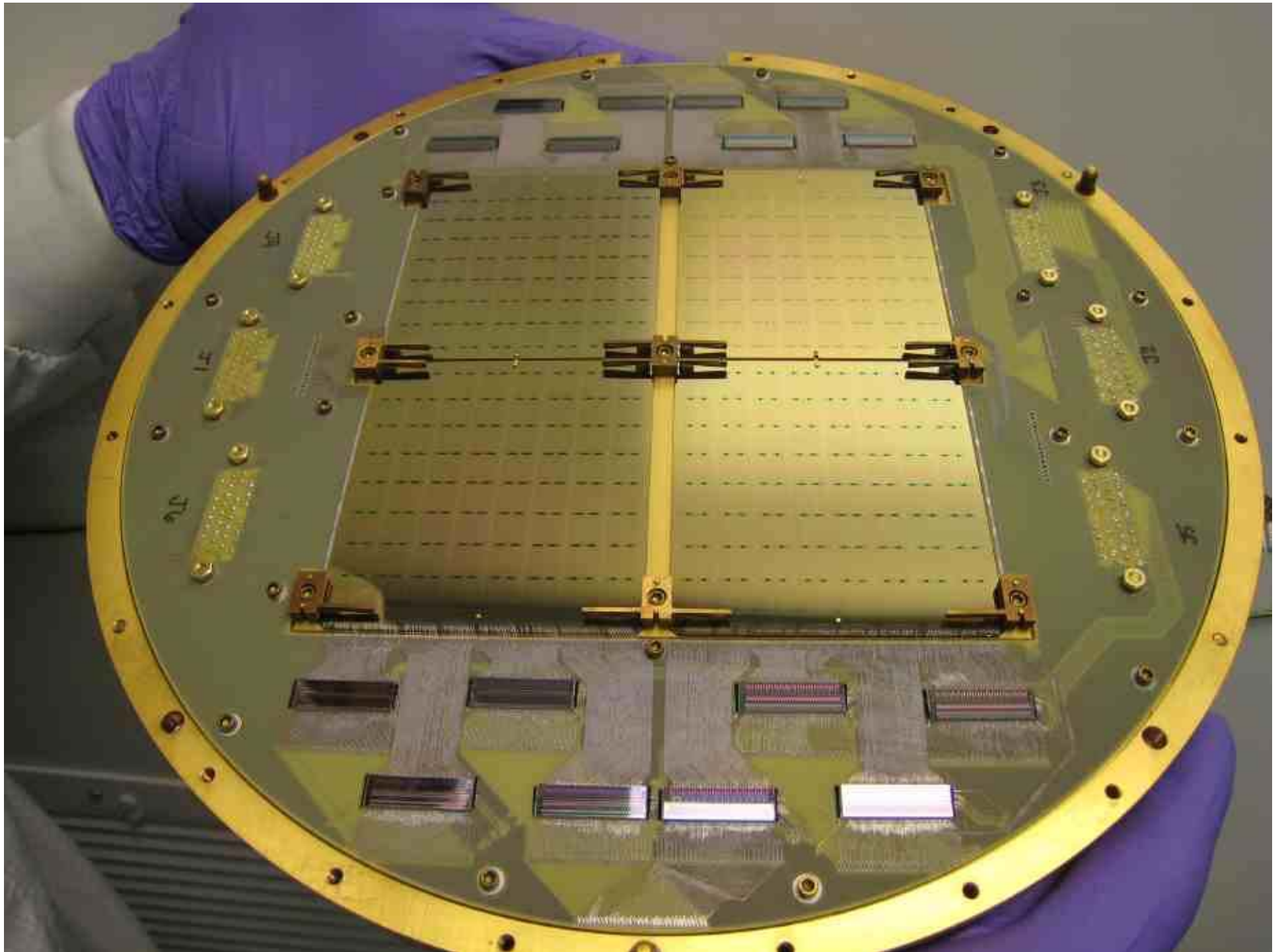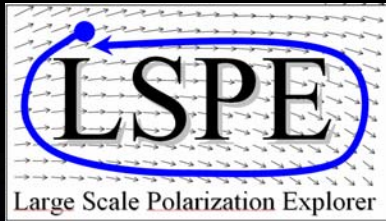
The Large Scale Polarization Explorer
P. de Bernardis, for the LSPE collaboration
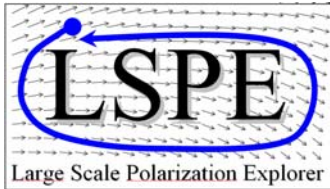
The LSPE collaboration

Giorgio Amico, Elia Battistelli, Alessandro Baù, Paolo de Bernardis, Marco Bersanelli, Andrea Boscaleri, Francesco Cavaliere, Alessandro Coppolecchia, Angelo Cruciani, Francesco Cuttaia, Antonio D' Addabbo, Giuseppe D'Alessandro, Simone De Gregori, Francesco Del Torto, Marco De Petris, Lorenzo Fiorineschi, Cristian Franceschet, Enrico Franceschi, Massimo Gervasi, David Goldie, Anna Gregorio, Vic Haynes, Luca Lamagna, Bruno Maffei, Davide Maino, Silvia Masi, Aniello Mennella, Ng Ming Wah, Gianluca Morgante, Federico Nati, Luca Pagano, Andrea Passerini, Oscar Peverini, Francesco Piacentini, Lucio Piccirillo, Giampaolo Pisano, Sara Ricciardi, Paolo Rissone, Giovanni Romeo, Maria Salatino, Maura Sandri, Alessandro Schillaci, Luca Stringhetti, Andrea Tartari, Riccardo Tascone, Luca Terenzi, Maurizio Tomasi, Fabrizio Villa, Giuseppe Virone, Stafford Withington, Andrea Zacchei, Mario Zannoni

Short **W**avelength **I**nstrument for the **P**olarization **E**xplorer (bolometers, 80-250 GHz) PI de Bernardis

STRatospheric **I**talian **P**olarimeter (radiometers, 40-90 GHz) PI Bersanelli

P. de Bernardis   Bologna   14 feb 2012
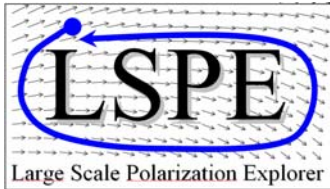
LSPE in a nutshell

- The Large-Scale Polarization Explorer is
  - a spinning stratospheric balloon payload
  - flying long-duration, in the polar night
  - aiming at CMB polarization at large angular scales
  - using polarization modulators to achieve high stability

- Frequency coverage: 40 – 250 GHz (5 channels)

- Angular resolution: 1.5 – 2.3 deg FWHM

- Sky coverage: 20-25% of the sky per flight

- Combined sensitivity: 10 $\mu K\ arcmin$ per flight
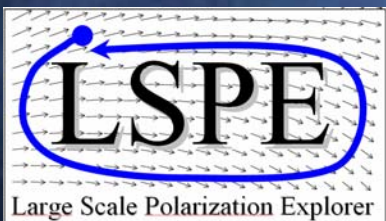
The LSPE payload

A spinning gondola, rotated by torque motors around an azimuth pivot

Stokes polarimeter with cold stepping HWP and arrays of large-throughput bolometers at 90, 145, 220 GHz; FWHM 2.4° to 1.4°

SWIPE

STRIP

Batteries (1GJ), telemetry, Attitude Control System, data storage
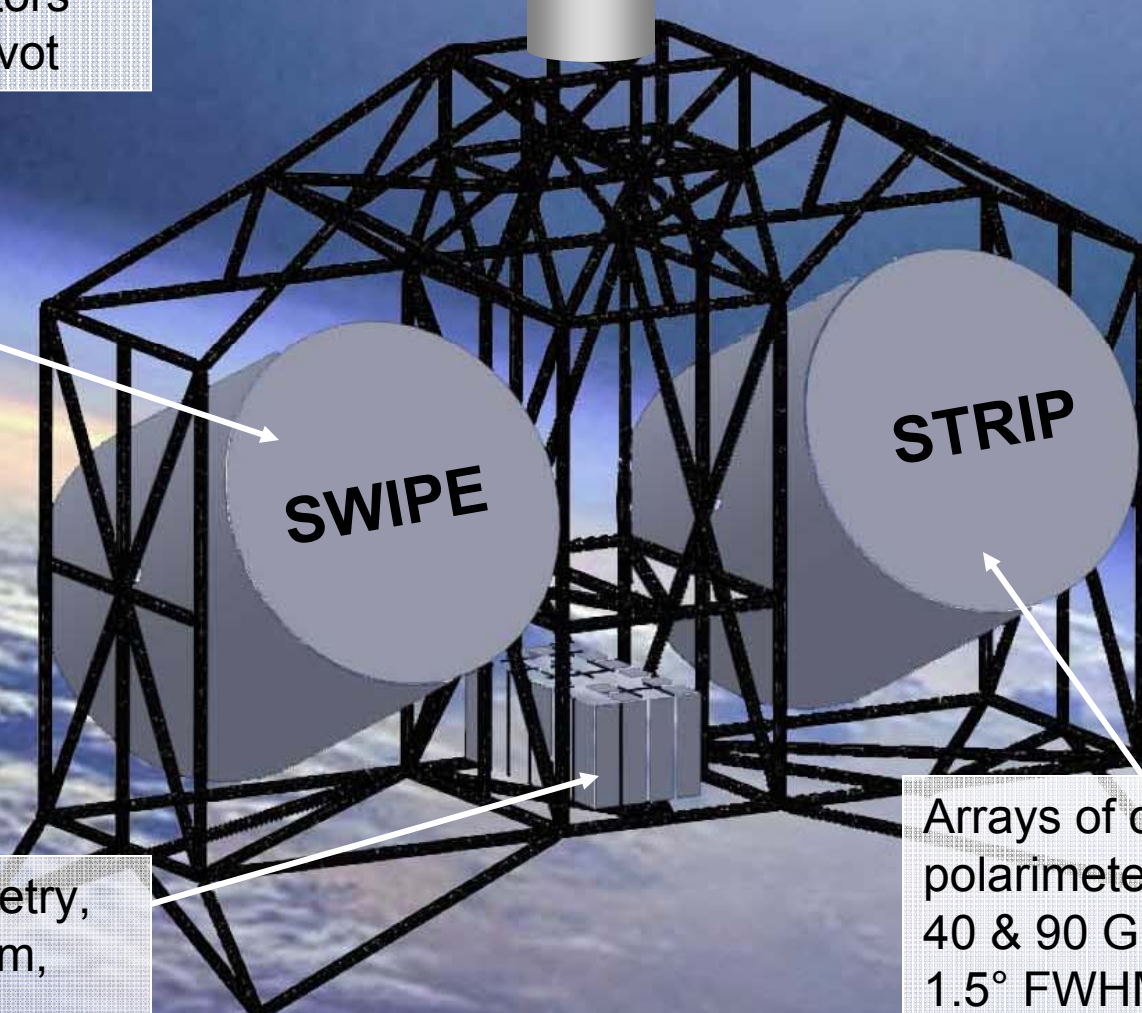
Arrays of coherent polarimeters at 40 & 90 GHz. 1.5° FWHM

- The instrument will be flown at 38 km of altitude by a 800000m³ balloon, at the end of 2014.
- Stratospheric balloons can be flown during the polar night despite of the low temperature of the air (see e.g. Archeops)
- The currently selected launch site is in the Svalbard islands (78° N), and the expected flight path will be a circle at approximately constant latitude.
- With recovery in Greenland, the flight can be 2-3 weeks long. This has been tested already in the summer.
- The site is easily reacheable (international airport) and large payloads have already been launched from there.

Mission profile

PEGASO circumpolar flight (2007) launched from Longyearbyen

Pegaso-E trajectory 02/07 10:14   (double click to enlarge)
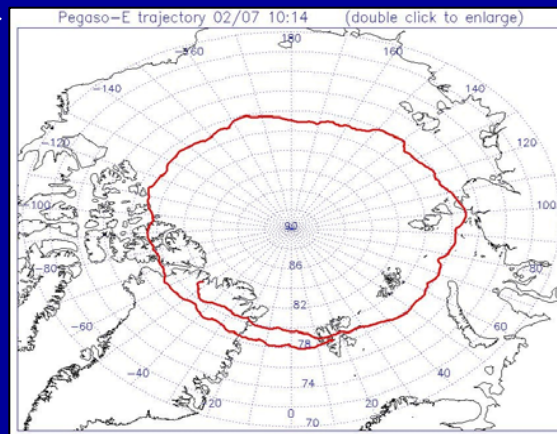
- The same thing can be done, with logistic complications, in Antarctica

Launch of the SORA experiment from the Longyearbyen airport (2009)

Sky Coverage

- The payload will just spin in azimuth during the flight.

- The telescopes of the two instruments will scan the sky at constant elevation. Performing a few elevation steps during the 2-3 weeks of the flight, more than 20% of the sky can be covered outside the galactic mask, with good cross-linking and significant integration time per pixel. (cfr. Farhang et al. astro-ph/1108.2043)

LSPE 145 GHz 10 deg elevation range

0 ▬▬▬▬▬▬▬ 1654 sec/pixel

LSPE – ACS
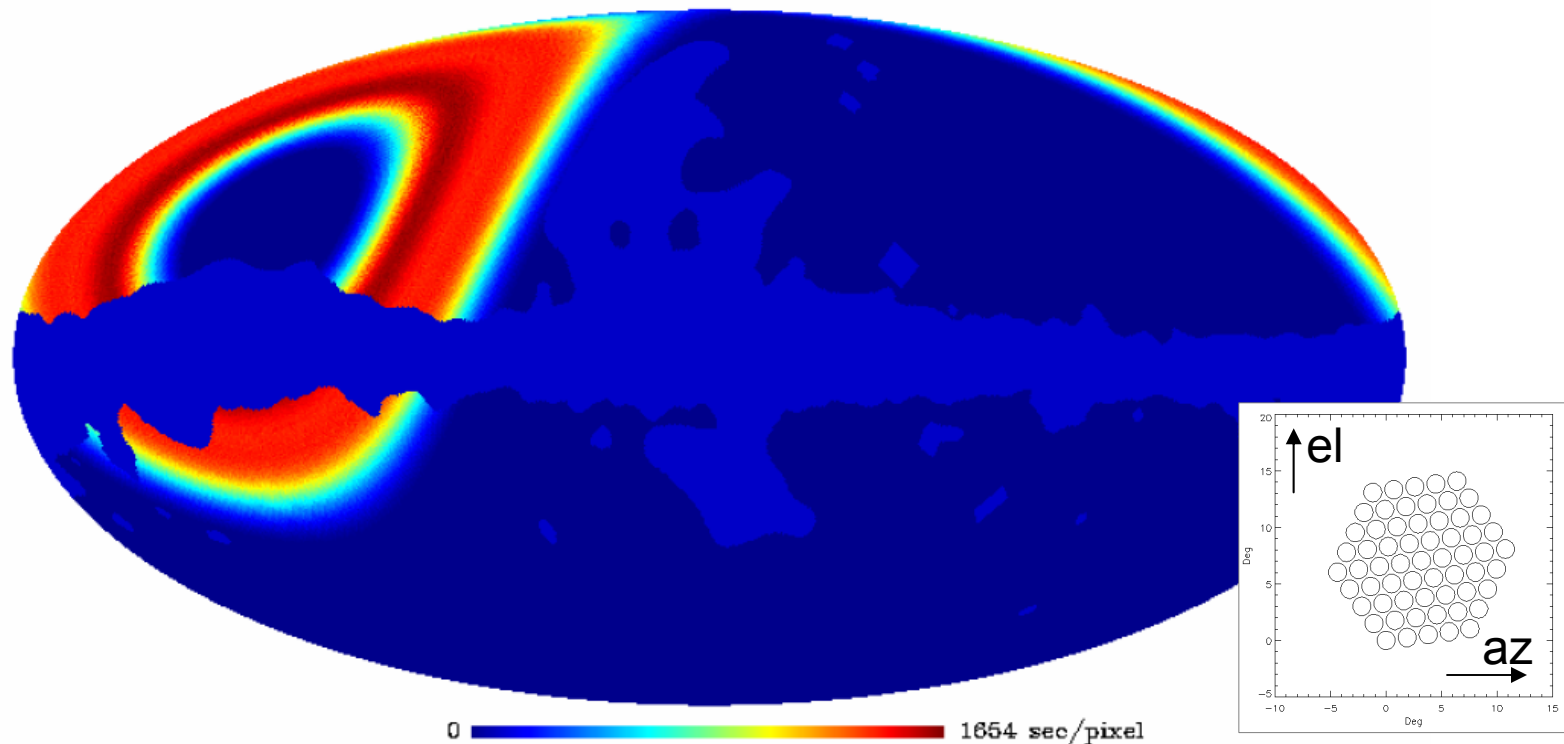
- The payload spins at 2-3 rpm
- We use an azimuth pivot with torque motors similar to the ones used in BOOMERanG and Archeops (Pascale + Boscaleri AIP Conf. Proc. **616**, 56, 2001)
- The rotation speed is sensed by a set of 3 laser-gyros, driving the ACS control loop.
- The power required to spin the payload (about 100W) is due to the friction in the thrust bearings of the azimuth pivot and is provided by Lithium batteries.
- Absolute attitude is reconstructed by means of a fast star sensor similar to the one used in Archeops (Nati et al., Review of Scientific Instruments, **74**, 4169, 2003)
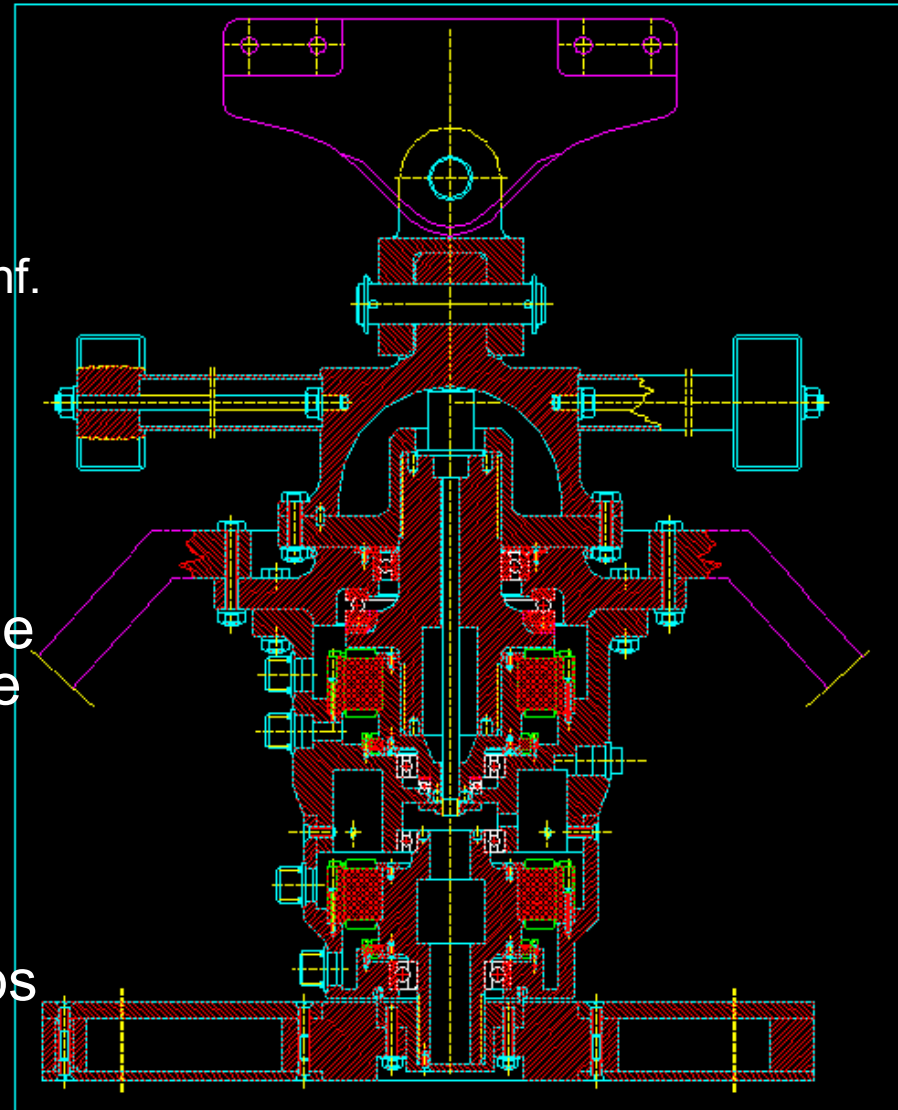
SWIPE

- The **S**hort **W**avelength **I**nstrument for the **P**olarization **E**xplorer
- Uses overmoded bolometers, trading angular resolution for sensitivity
- Sensitivity of photon-noise limited bolometers vs # of modes:

Number of modes actually coupling to the bolometer absorber

LSPE - SWIPE	eff =	0.25	
Bolometric	D lens =	0.4	m
Instrument	F =	0.8	m
N modes (geom) =	15	25	40
f (GHz)	90	145	220
λ (mm)	3.3	2.1	1.4
N det =	37	58	83
FWHM (deg) =	2.4	1.9	1.6
NET (μK/sqrt(Hz)) =	15	25	30
NET Focal Plane (μK/sqrt(Hz))=	**2.5**	**3.3**	**3.2**

SWIPE

- Overmoded detectors are obtained coupling large area bolomete absorbers to Winston horns.

- Example of large-throughput spider-web bolometer (being developed in Italy, F. Gatti)
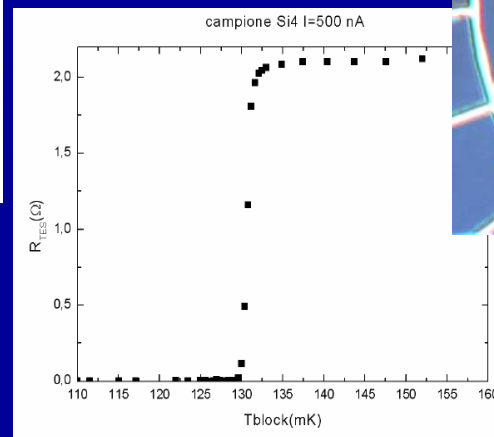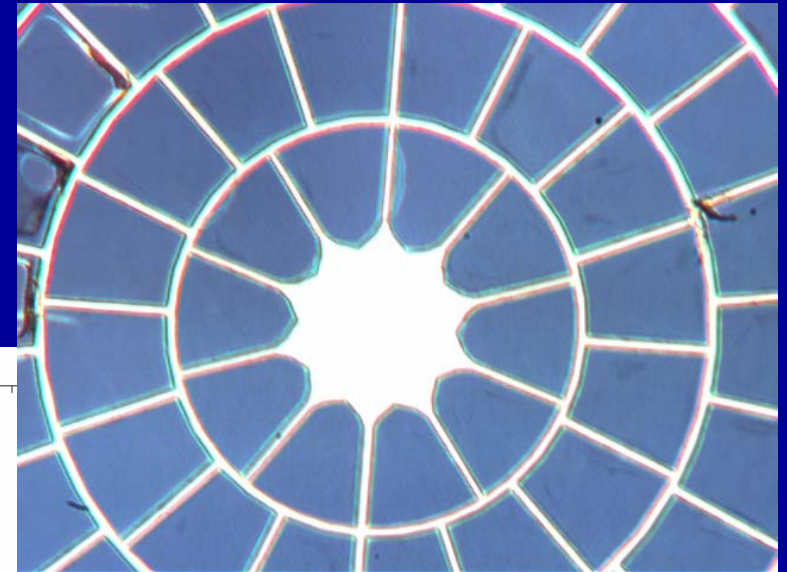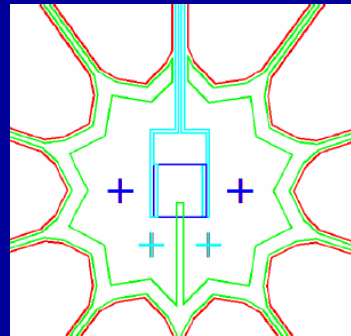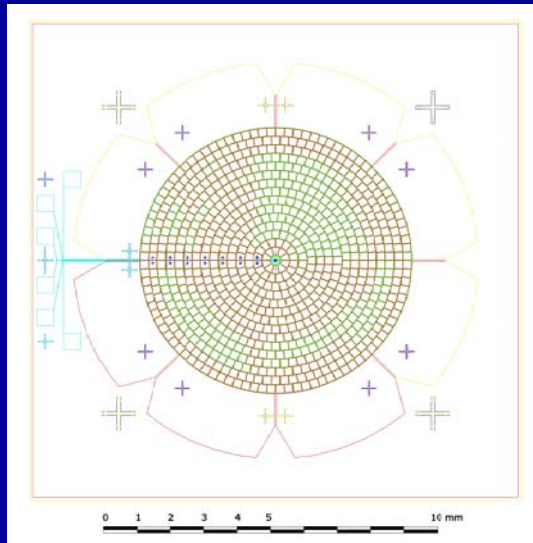
- SWIPE bolometers will be made also in Cambridge (Withington)

SWIPE

- Overmoded detectors are obtained coupling large area bolometer absorbers to Winston horns.
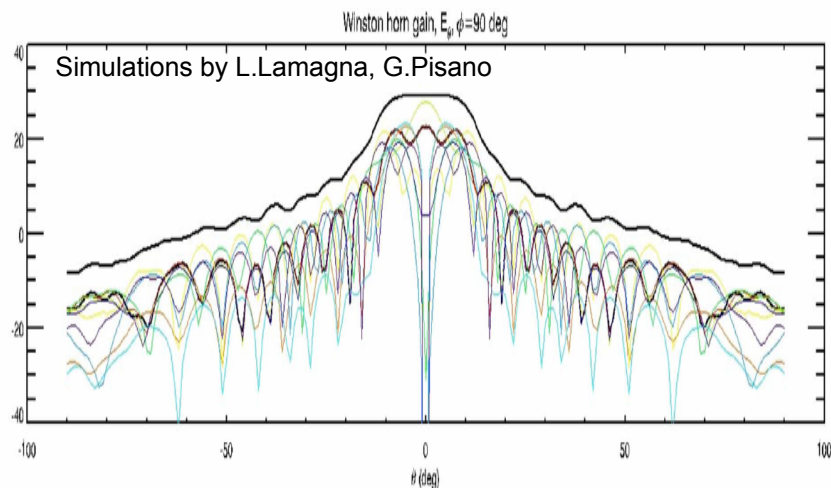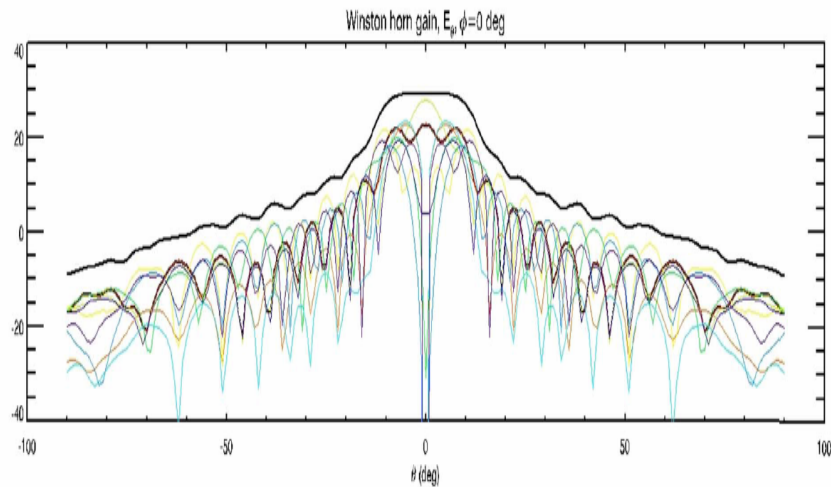
Simulations confirm that about half of the modes collected by the Winston horn actually couple to the bolometer absorber (in single-polarization detectors).

SWIPE

- Polarimetry is implemented with a classical Stokes configuration.

Dewar window

Thermal filters

Rotating HWP

40 cm diam. f/2 UHDPE Lens

2nd Focal plane (refl.)

Wire grid

20 cm diam.
1st Focal plane (transm.)
Winstons horns array
15° corrected FOV

M. De Petris

LAYOUT

LSPE - SINGLE LENS
MON MAY 16 2011
TOTAL LENGTH: 936.98124 MM

CONFIGURATION 1 DF 1
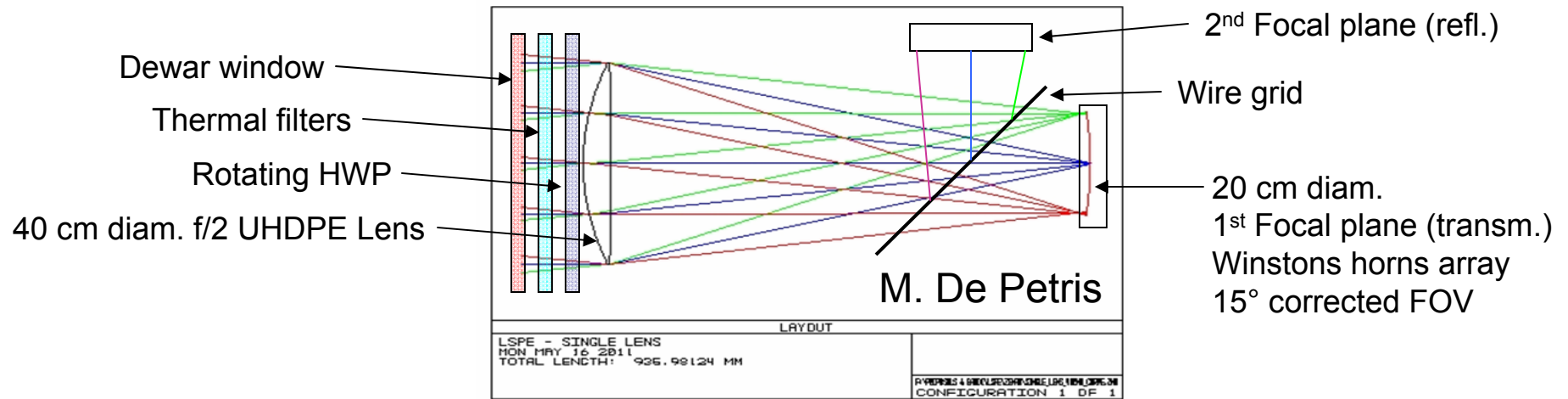
- The first optical element is a large diameter (50 cm TBC) HWP, obtained by means of diectric-embedded metal meshes (G. Pisano et al. Applied Optics, **47**, 6251, 2008, and follow-ups)

Capacitive Stack

Inductive Stack

Pol 1

Pol 2

SWIPE
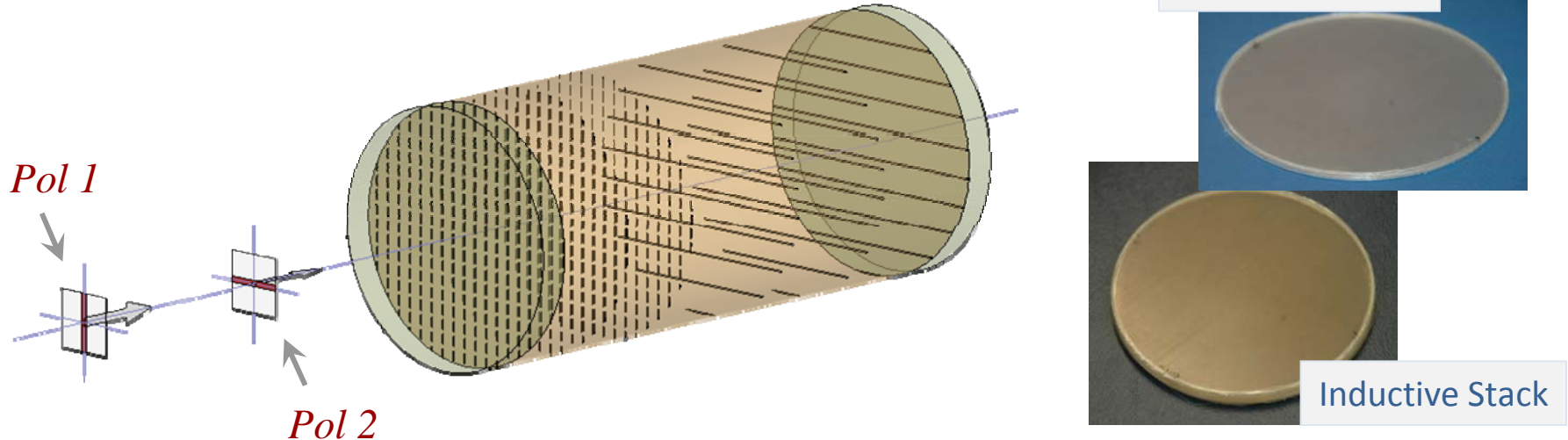
LSPE-SAF: OPTICS REQUIREMENTS

Entrance Pupil Diameter	(mm)	400		
Effective Focal Length	(mm)	800		
f-number		2		
Focal Plane Diameter	(mm)	200		
Image Object Space	(deg)	14,3		
Focal plane scale	('/mm)	4,3		
Focal Plane Surface		curved		
Optics Symmetry		cilindrical		
Spectral Range	(GHz)	90	140	220
waves	(mm)	3,33	2,14	1,36
Angular Resolution	(arcmin)	28,6	18,4	11,7
number of modes		20	20	20
throughput (N lambda^2)	(cm^2 sr)	2,22	0,92	0,37
FWHM	(deg)	1,68	1,08	0,69
Strehl Ratio		>95%		
Strehl Ratio variation along fov		<1%		
Beam ellipticity		1%		
Cross Polarization		1%		
Instrumental Polarization		<1%		
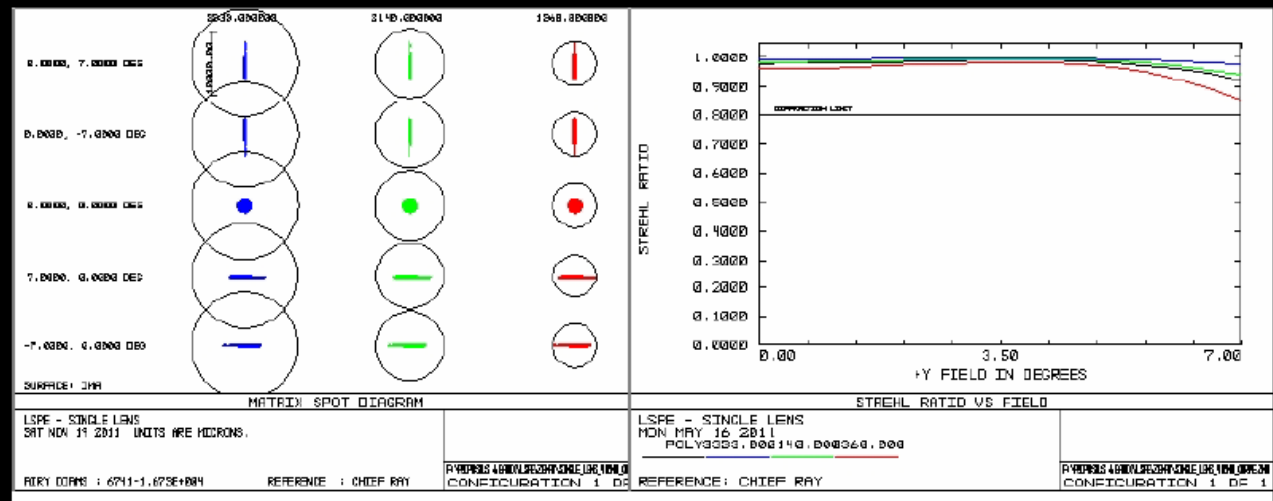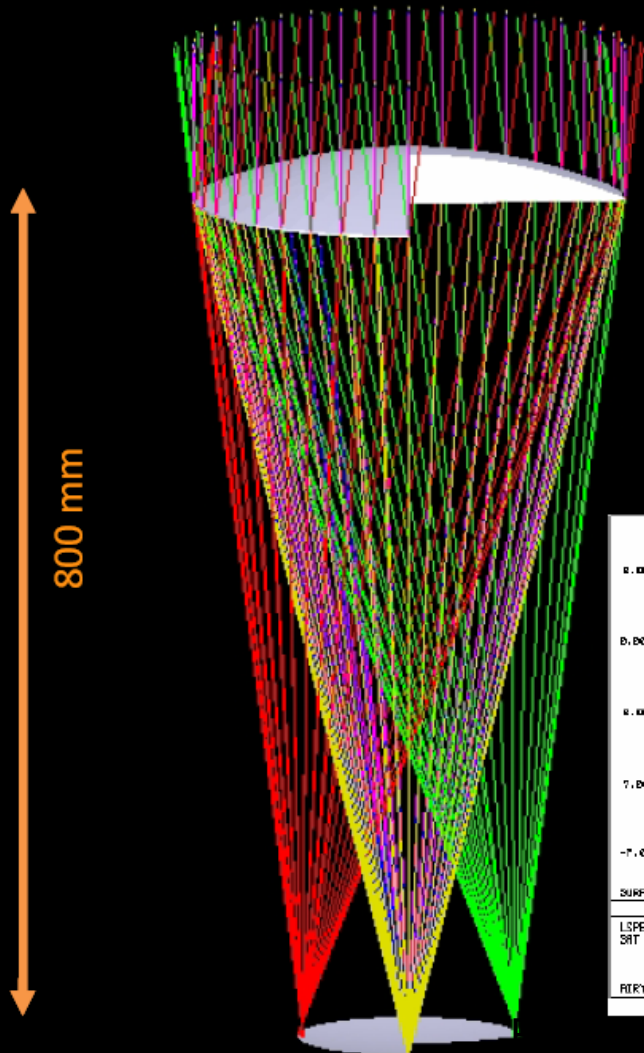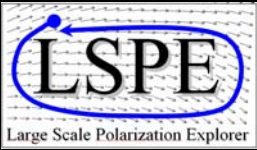
SWIPE

Custom cryostat (S. Masi)
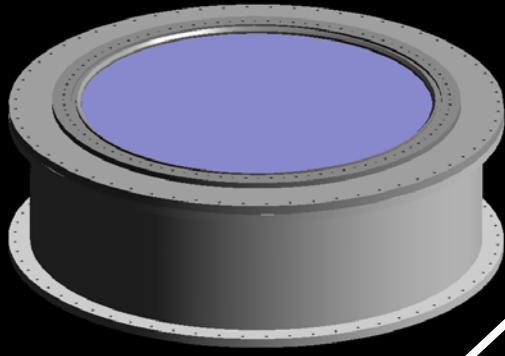
Plastazote window
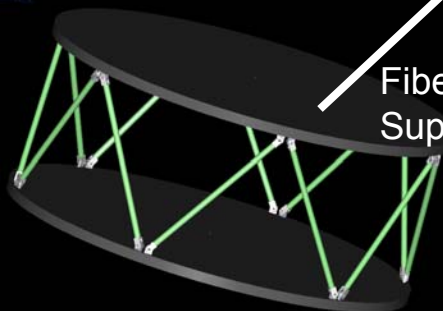
Fiberglass struts
Support system

250L LHe

Arrays 90
& 220

Array 140

1650

1140

SWIPE
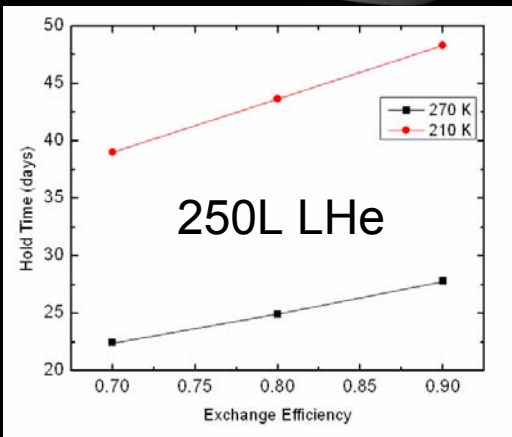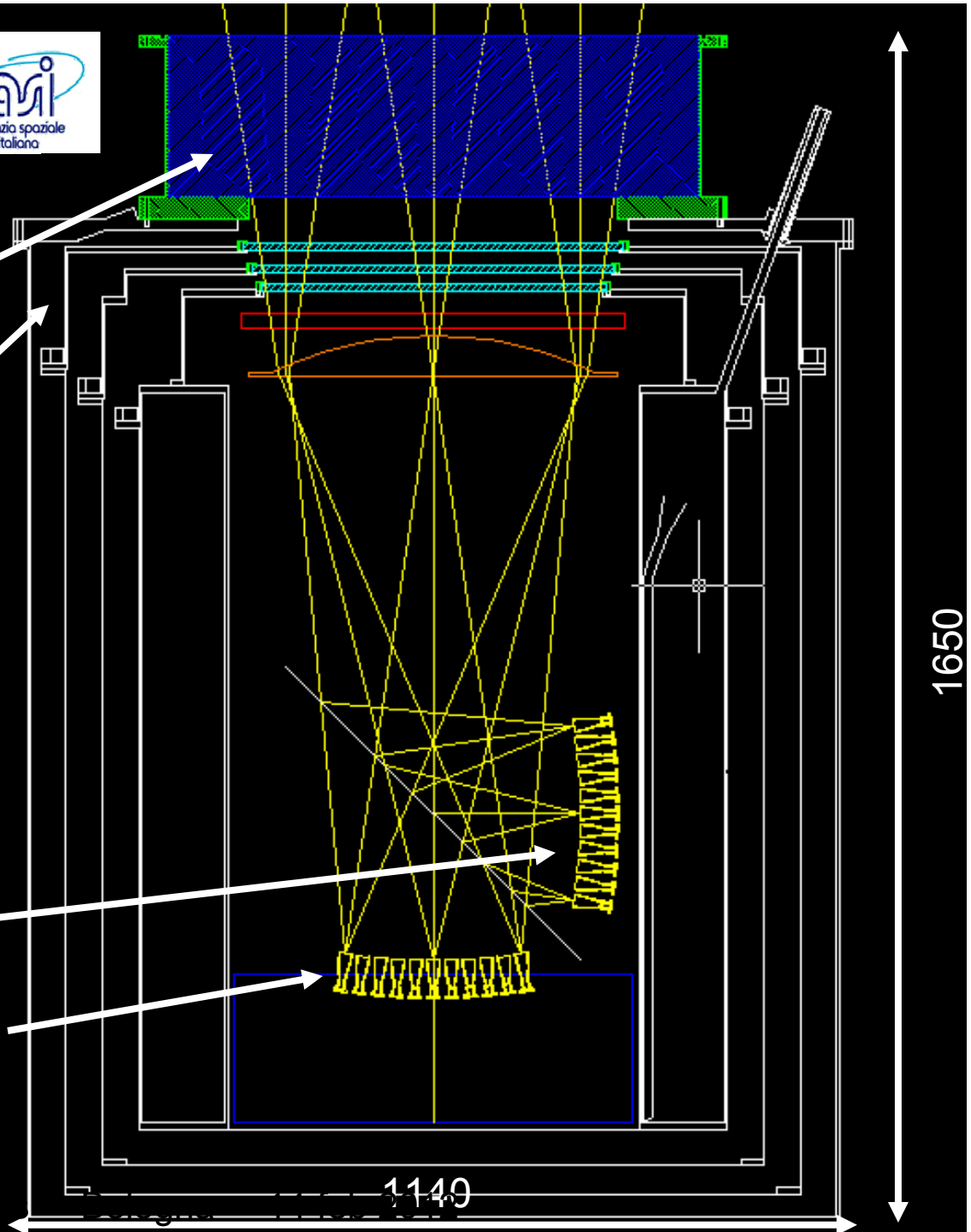
- The HWP will be rotated in steps using a low-friction cryogenic mechanism based on thrust bearings, similar to the one we have developed for PILOT (Salatino et al. A&A 528, A138, 2011).

- 11.25° step, 1 step/min, < 10mW

- Precision position readout with optical fibers & pinholes
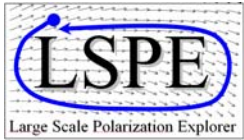
SWIPE

- Simulations show that a step/integrate approach with 11.25° per step, 1 step/min and a gondola spinning at 3 rpm is already very effective in removing 1/f and drifts.

- Assuming drifts are negligible, the white-noise sensitivity of SWIPE is compared to the HFI in the table below:

	PLANCK – HFI (full sky)						LSPE – SWIPE (20%)		
Frequency (GHz)	100	143	217	353	545	857	90	145	220
FWHM Resolution (arcmin)	9	7	6	5	5	5	144	114	96
Sky coverage (%)	100	100	100	100	100	100	20	20	20
Obs Time (months)	30	30	30	30	30	30	0.467	0.467	0.467
Bandwidth (%)	33	33	33	33	33	33	25	25	25
N_det (polarized)	8	8	8	8	0	0	37	58	83
Channel NET (uK s^1/2)	25	31	45	140	//	//	2.47	3.25	3.21
Integration/beam (s)	33	20	15	10	-	-	660	415	225
Delta Q(U) (uK) on LSPE beams	0.27	0.42	0.84	2.6	-	-	0.10	0.16	0.21
Improvement factor with respect to Planck-HFI (2° pixels)							2.8	2.7	3.9

STRIP

- The **STR**atospheric **I**talian **P**olarimeter uses coherent polarimeters working at 40 and 90 GHz, with a target sensitivity twice better than Planck LFI

- The main target is the polarized foreground (synchrotron), studied by means of 49 polarimeters in Q band. This is mandatory for an effective component separation, to remove foreground contamination from the cosmological channels (90 & 140 GHz from SWIPE).

- The 9 polarimeters in W band performs the same measurements as the bolometric W-band channel, using a completely independent technique. This provides the opportunity for a direct comparison, very efficient in detecting systematic effects.

- The required angular resolution (1.5°) is obtained by means of a 1.5m diameter telescope, focusing on an array of corrugated feedhorns, followed by high efficiency pseudo-correlation polarimeters (similar to the QUIET ones, see K. A. Cleary, Proc. SPIE 7741, 77412H, 2010).
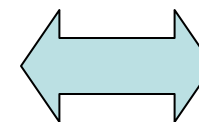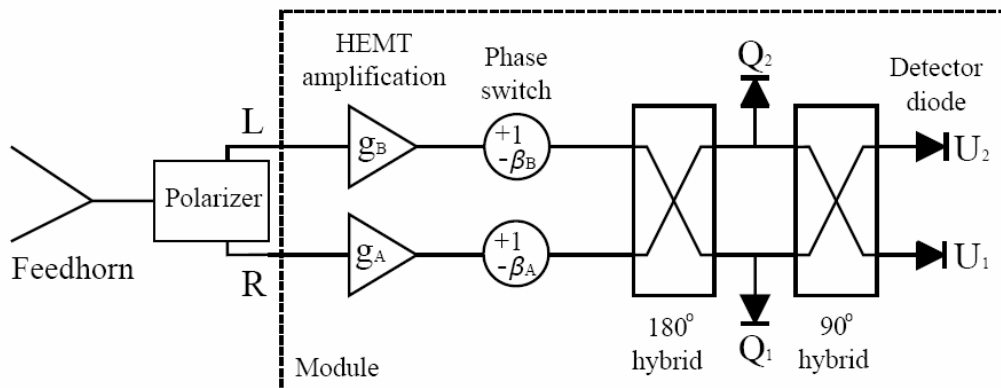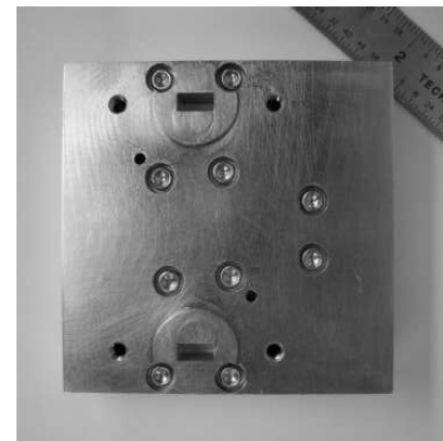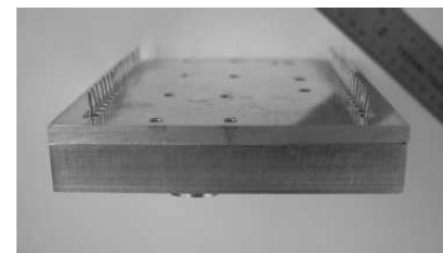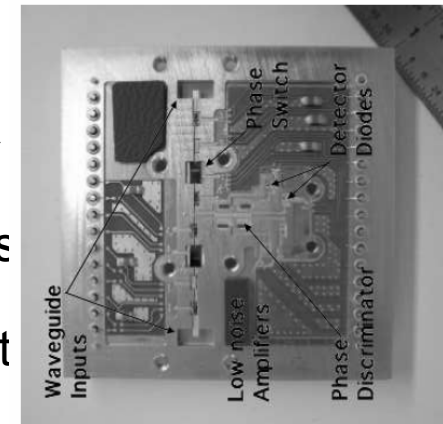
STRIP
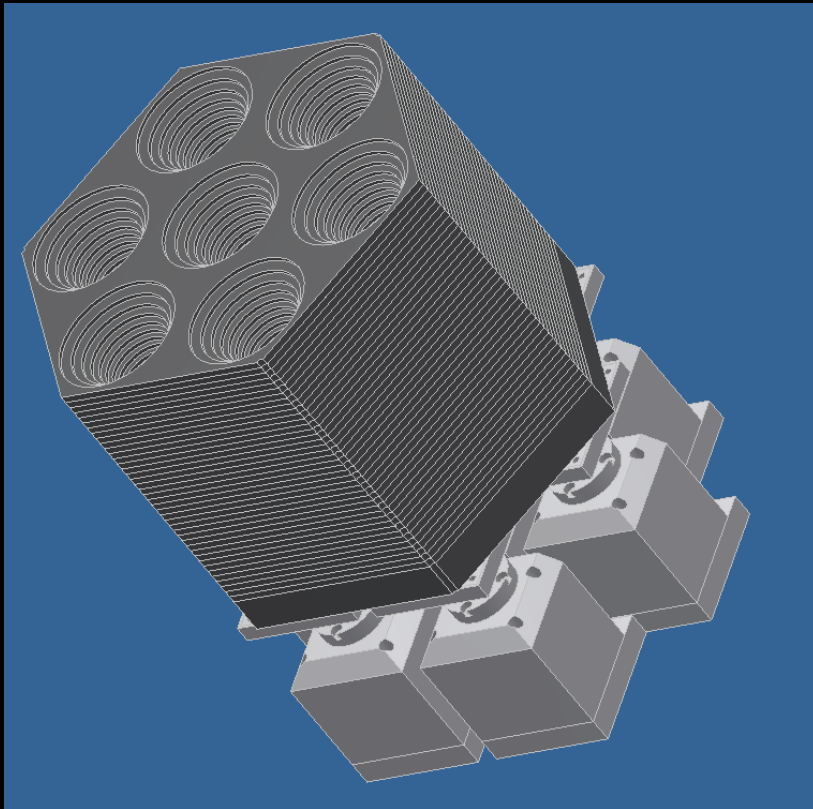
The corrugated feedhorns arrays are produced using the platelets technology (see e.g. Del Torto et al. JNST 6, 6009, 2011).

STRIP

(a)   (b)
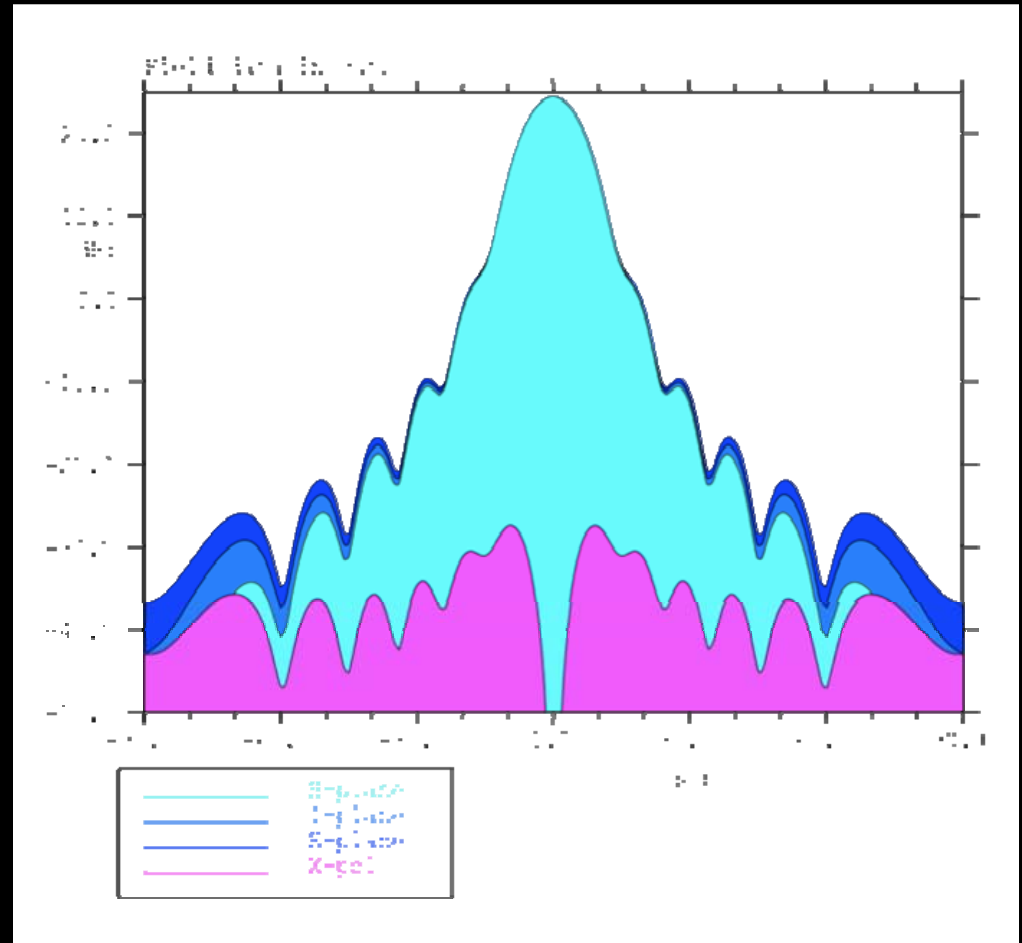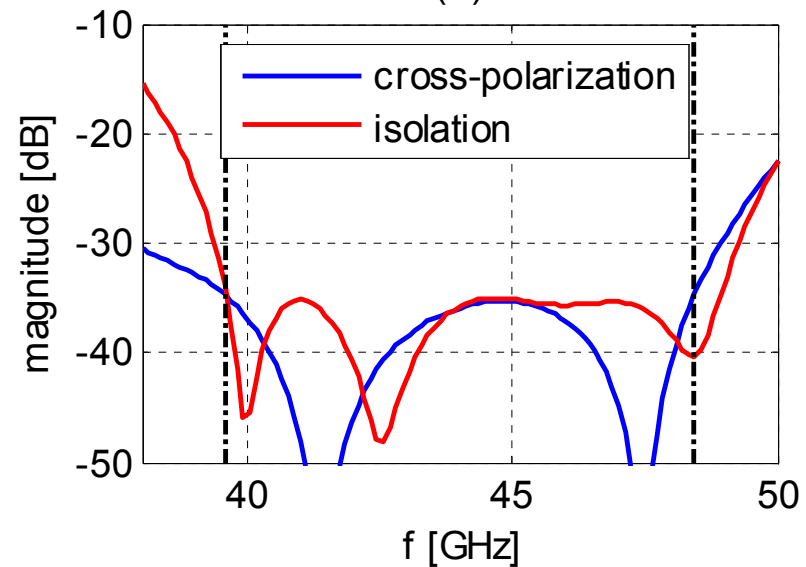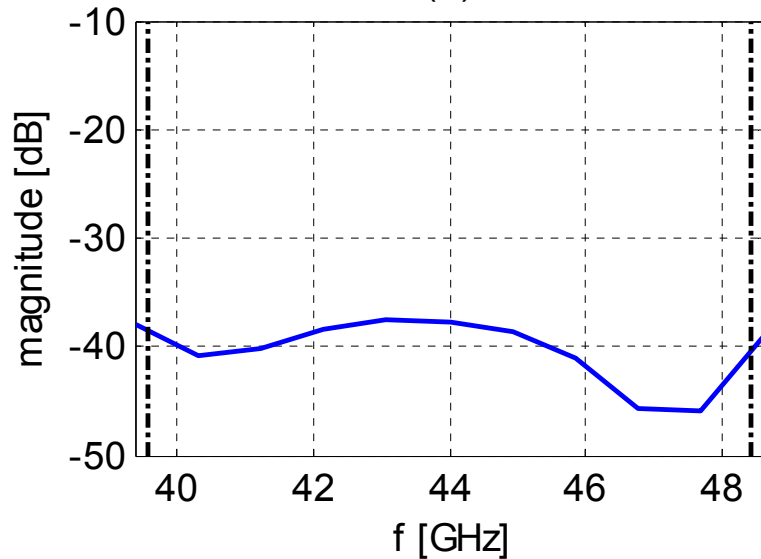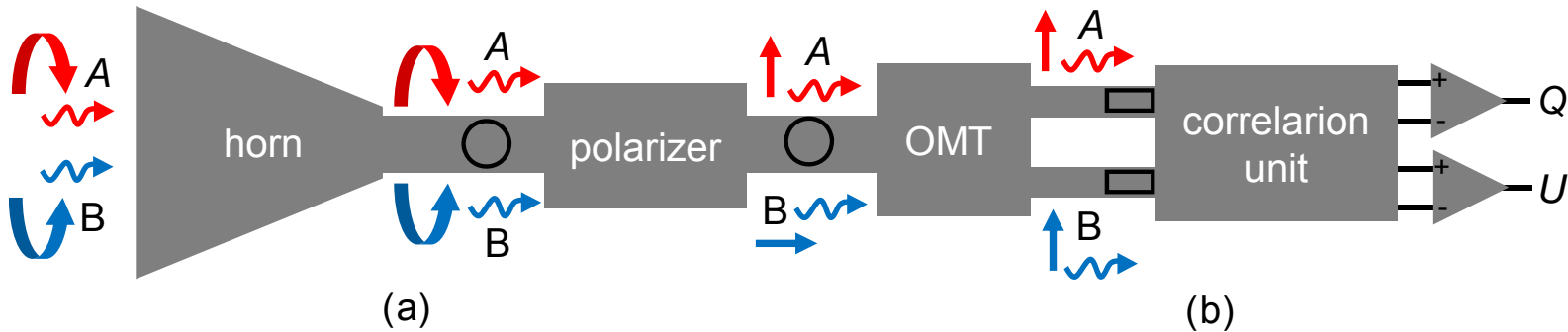
- High efficiency, wide band, polarizers and OMTs have been custom designed for this application at IEIIT

STRIP

- The polarimeters are cooled at the optimal operation temperature by cold He gas, evaporating from a large (500L) He cryostat (G. Morgante)

Stage	4K	20K	100K	Comments
Radiative (mW)	6,38	259,06	6156,87	*MLI 30 layers, 15 layers/cm*
Conductive (mW)	2,05	493,89	3052,94	*Piping in SS, Struts in G10, Wires in PhBronze (all harness in Flexi Cu with 20-30 cm thermal breaks)*
Active (mW)	832,00	1845,00	0,00	*On 4K stage heater dissipation is added on top of the parasitics load to maintain massflow, on the 20K stage the polarimeters dissipation plus active temperature control (0,2W average)*
Total (mW)	840,42	2597,95	9209,80	*no margin*
with margin	1092,55	3377,34	11972,74	*30% margin has been considered here*
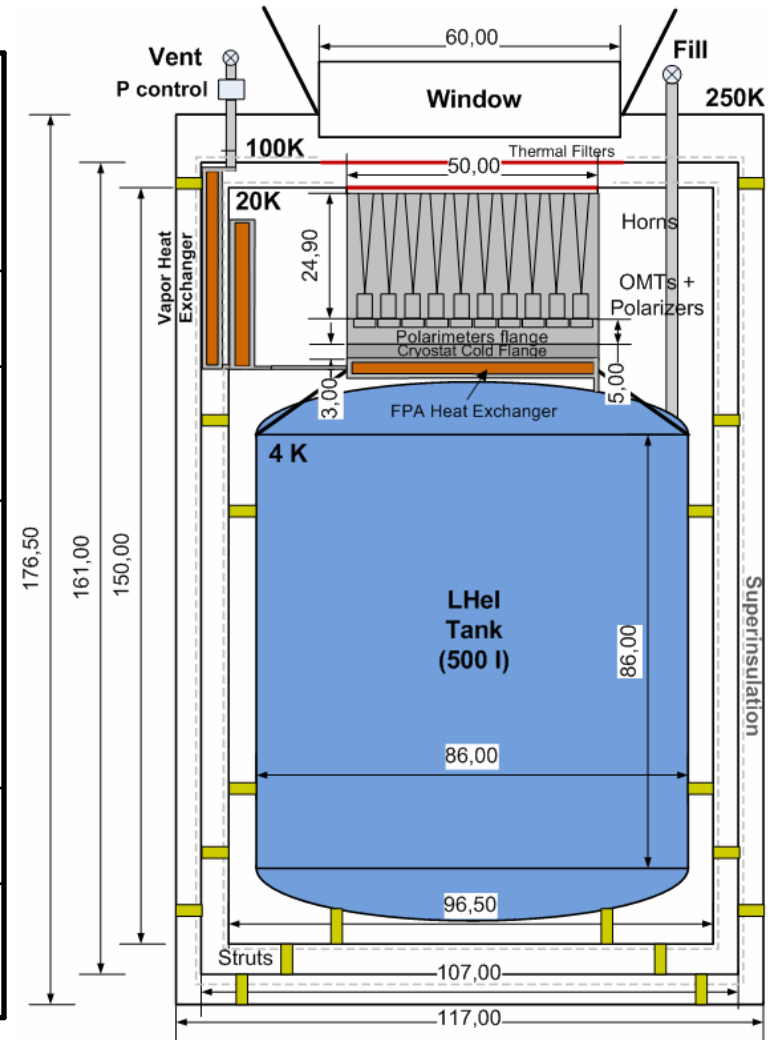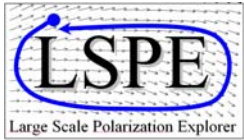
LSPE

Our target is $r = 0.03$, 3σ.

Expected performance of LSPE in constraining cosmological parameters, compared to Planck and SPIDER
(simulation by L. Pagano)

Planck 143GHz
Spider
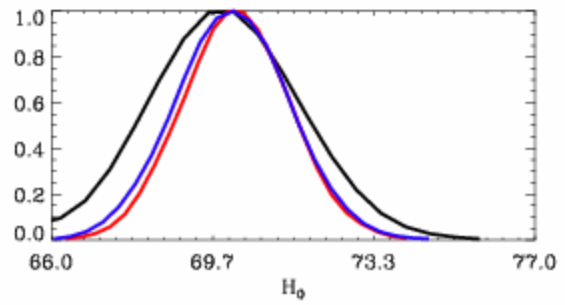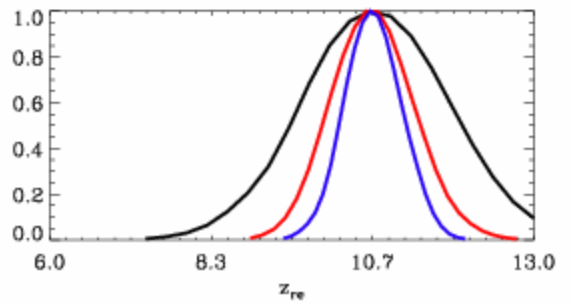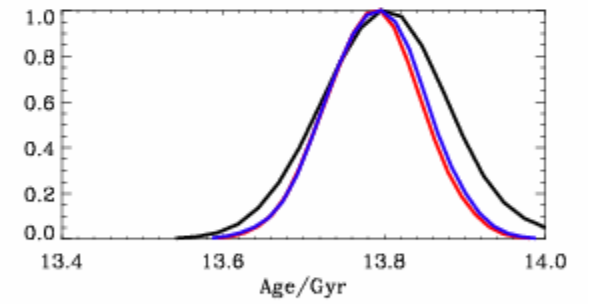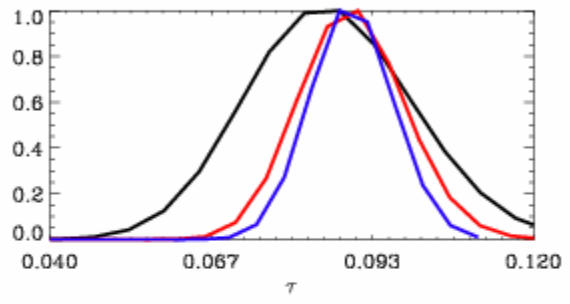LSPE
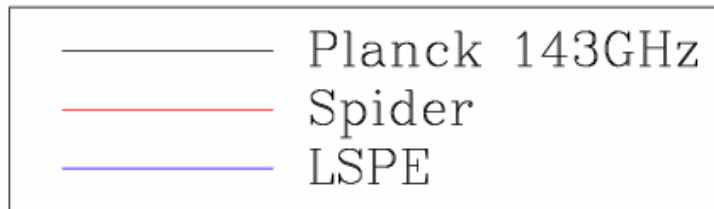
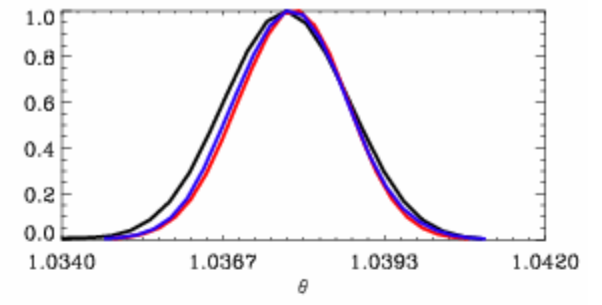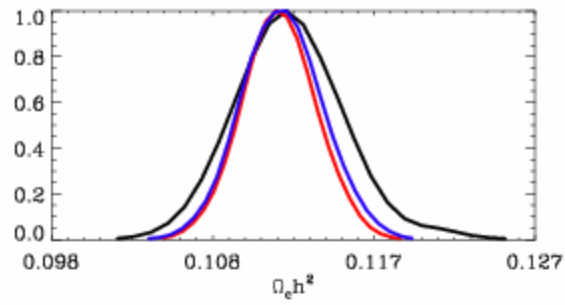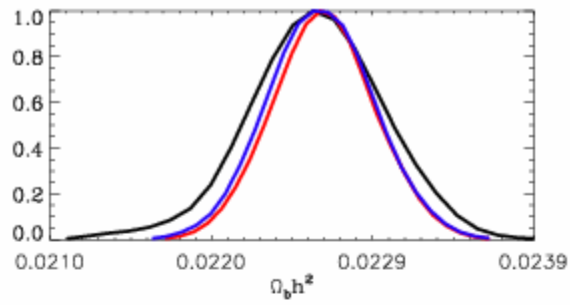On the paper, a very competitive instrument

Certainly independent and using different methodology

r = 0.03

Planck 143GHz
Spider
LSPE
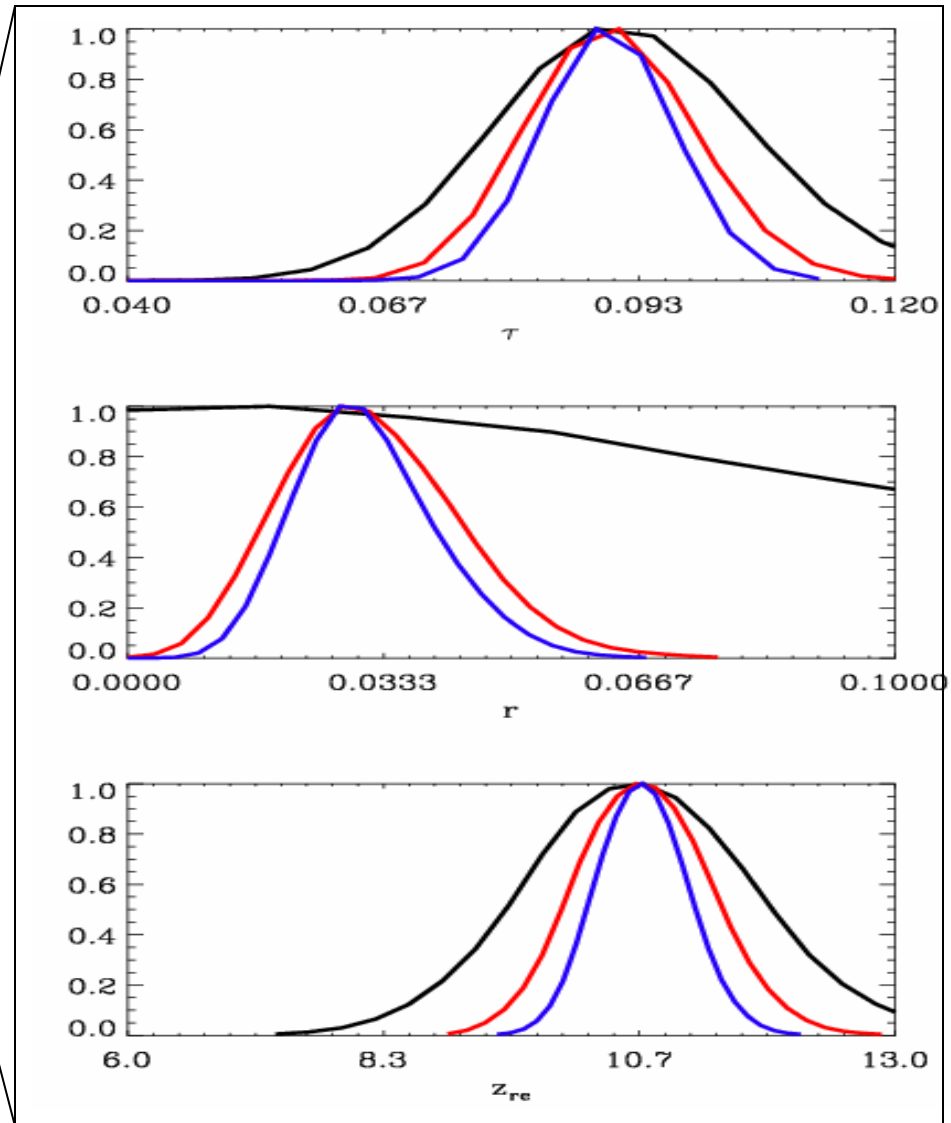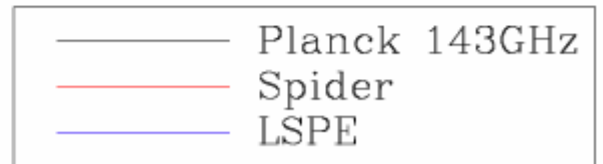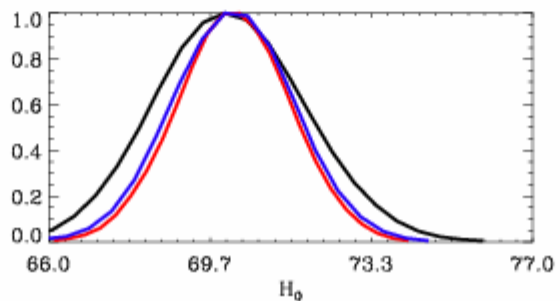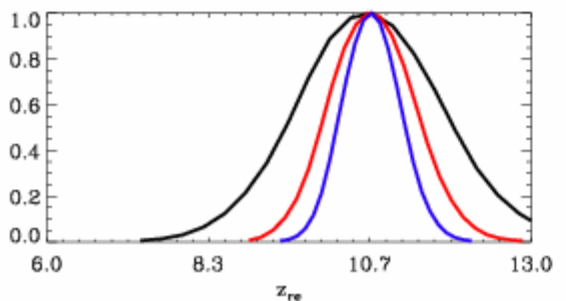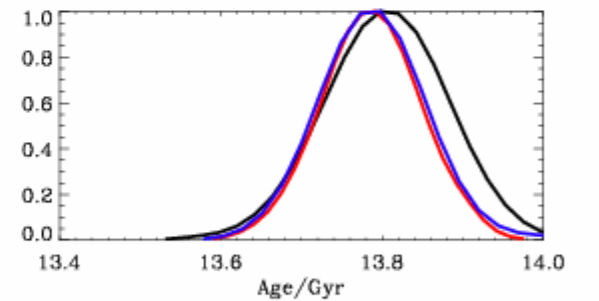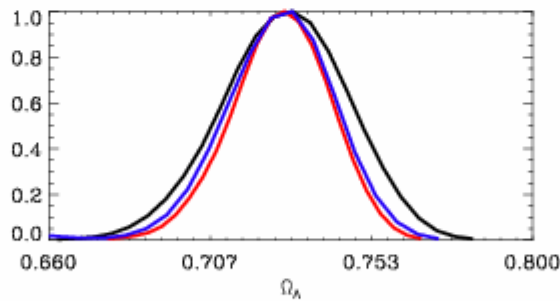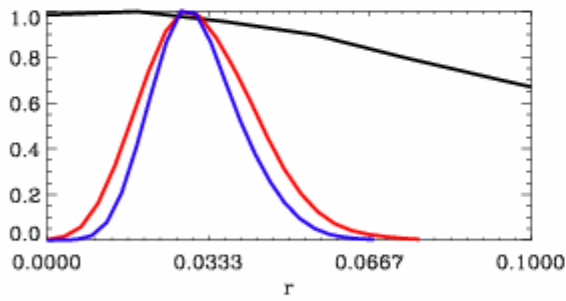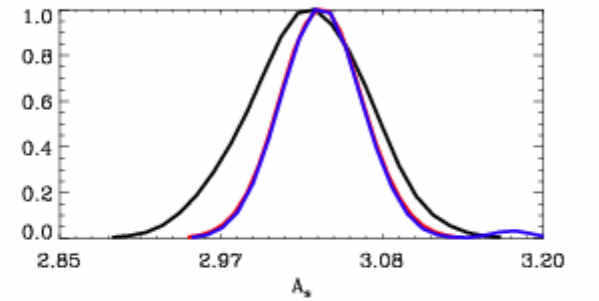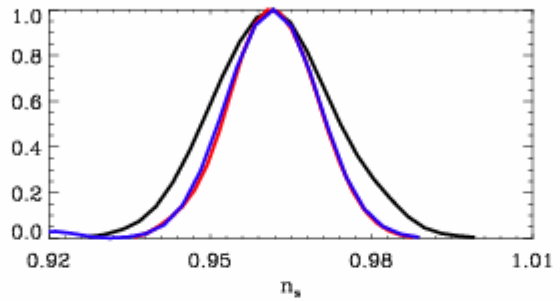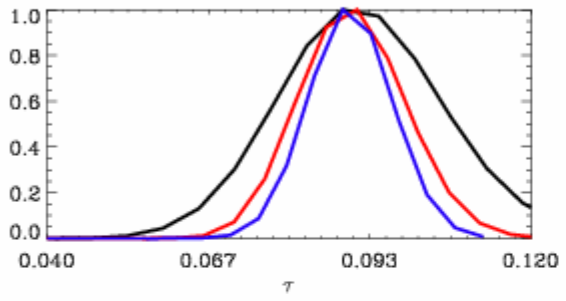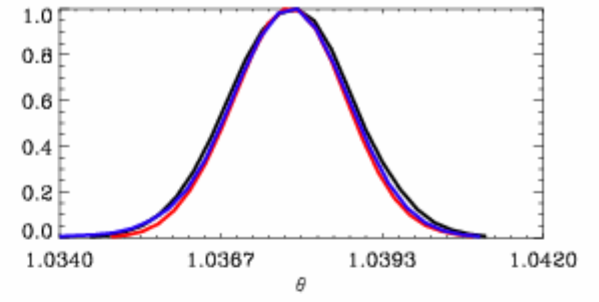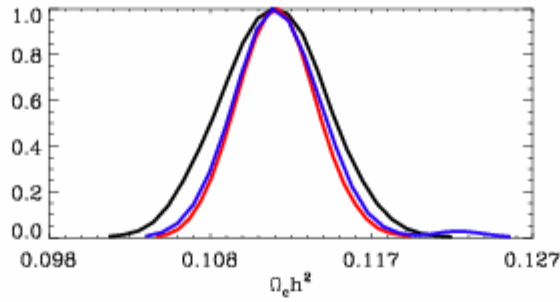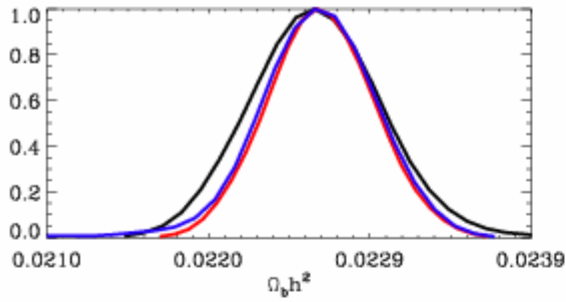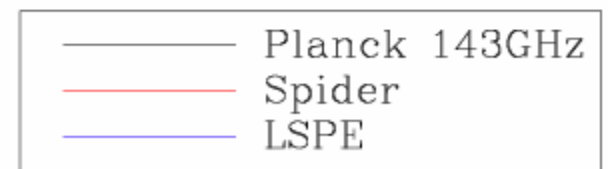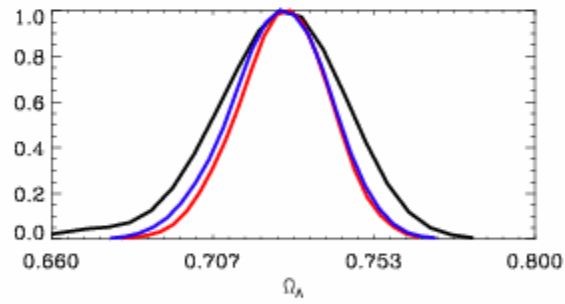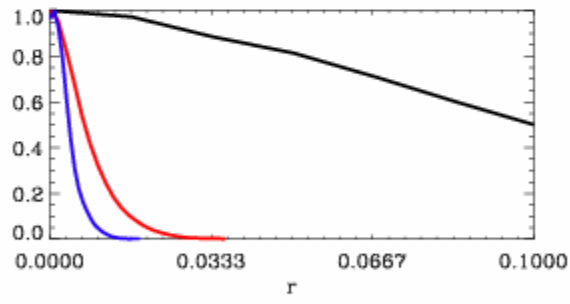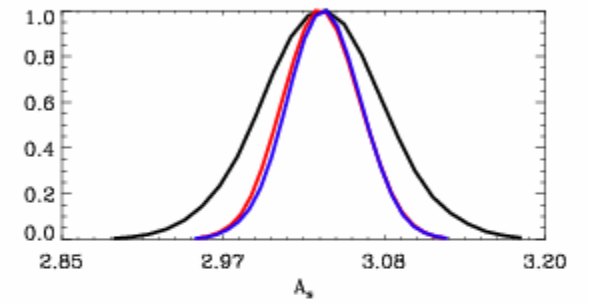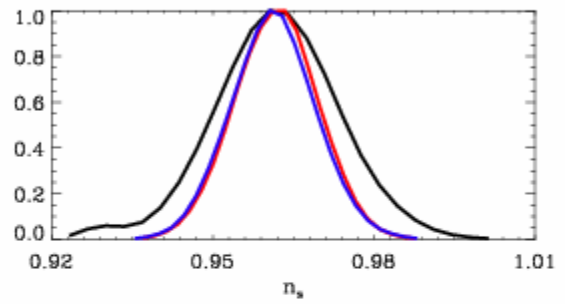
r = 0.001
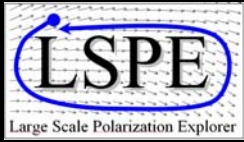
LSPE schedule

Still a long way to go …

event	date
KO	Apr. 29, 2011
PDR	Dec 20, 2011
CDR	Apr. 30, 2012
IHDR	Oct. 29, 2012
TRR	Aug. 29, 2013
FAR	Jan. 29, 2014
Flight	End of 2014

A Pathfinder for LSPE
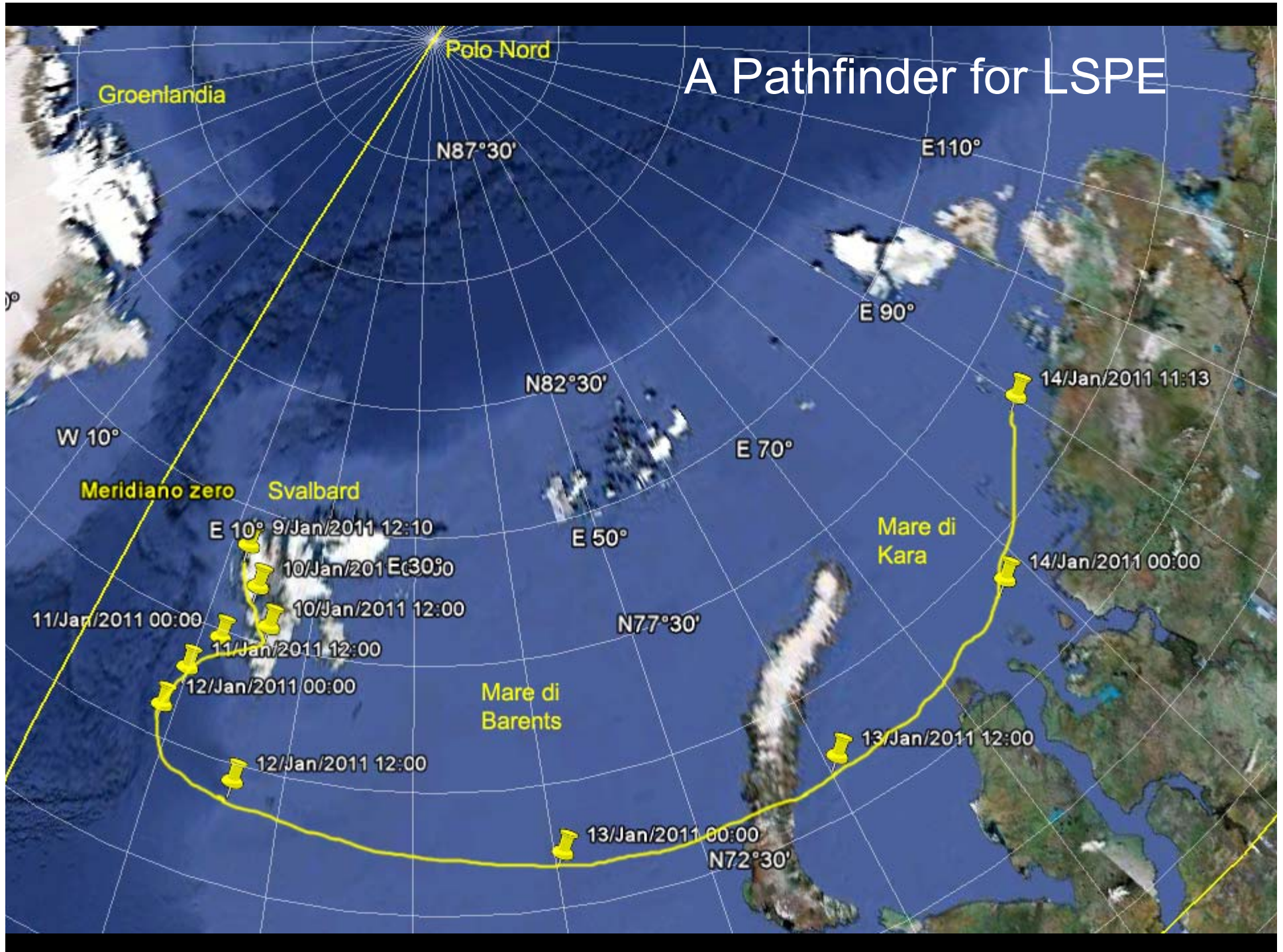
And now let's dream …
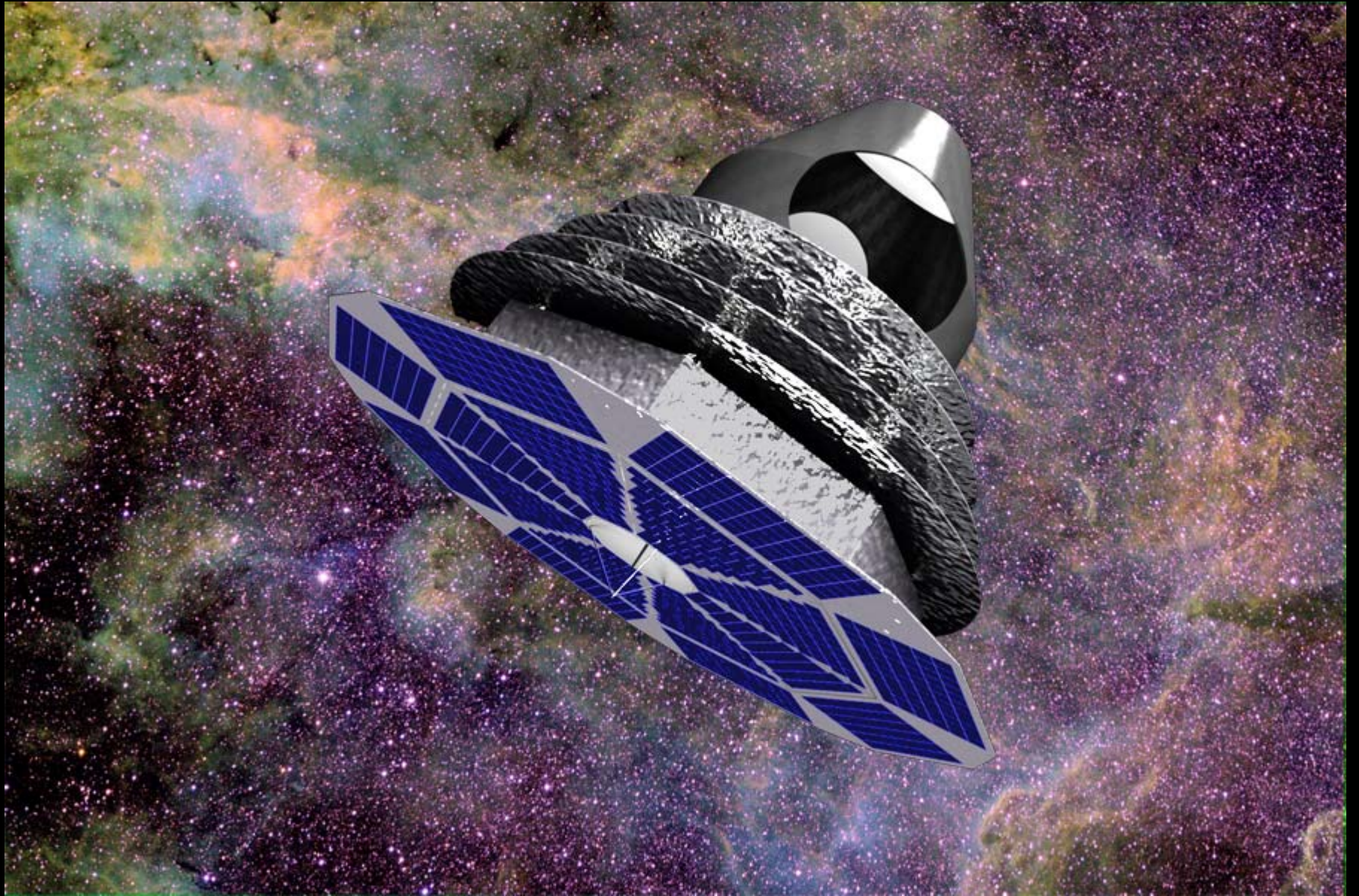
COrE: www.core-mission.org   ESA-M3 (2020)

COrE (15 channels) B-mode
Tensor to scalar ratio=1.0e-3

Lensed cmb theory
Unlensed cmb theory
Galaxy (105 GHz)
Point sources (105 GHz)
Noise (105-225 GHz)

Figure 10: Fairing accommodation of *COrE*.

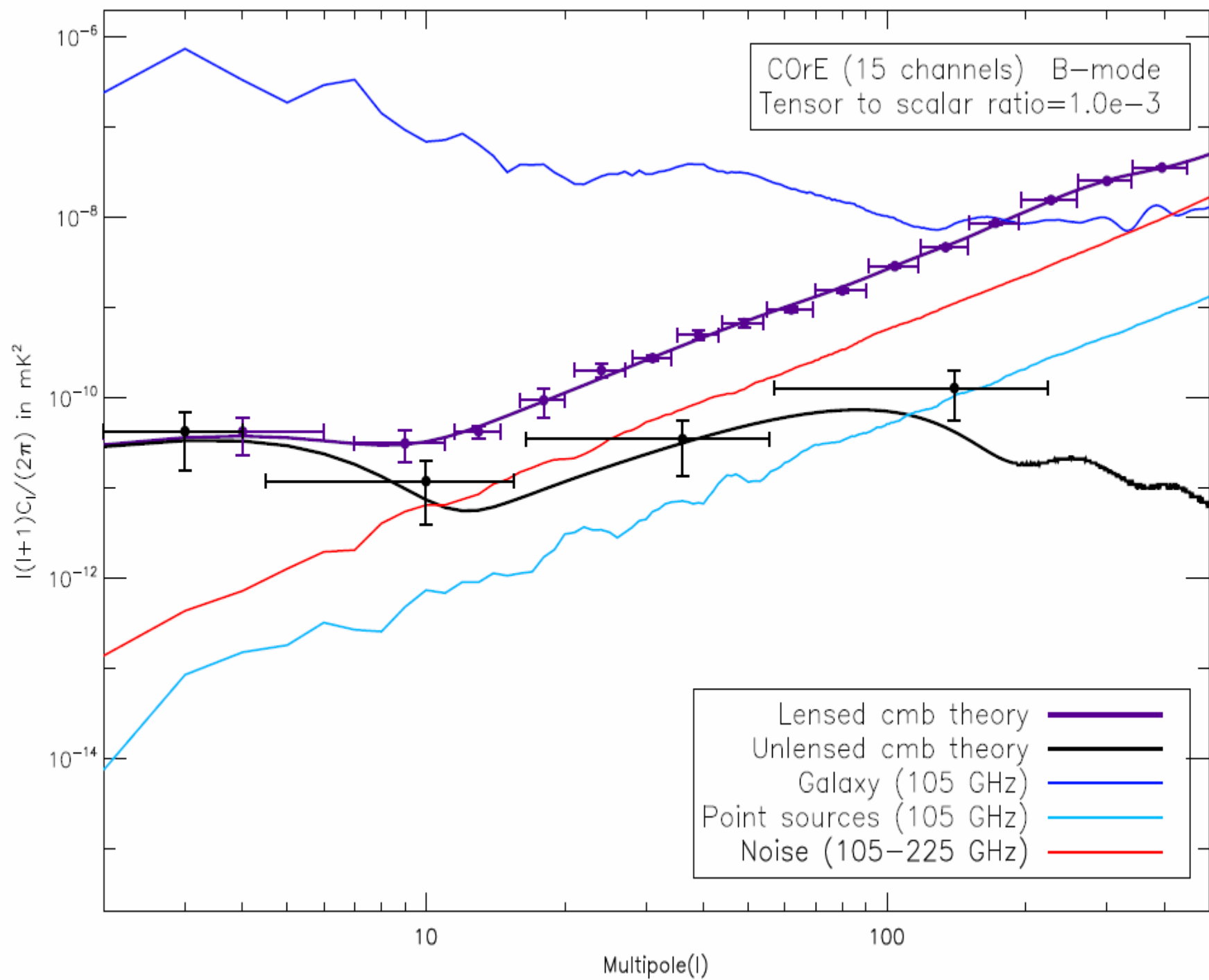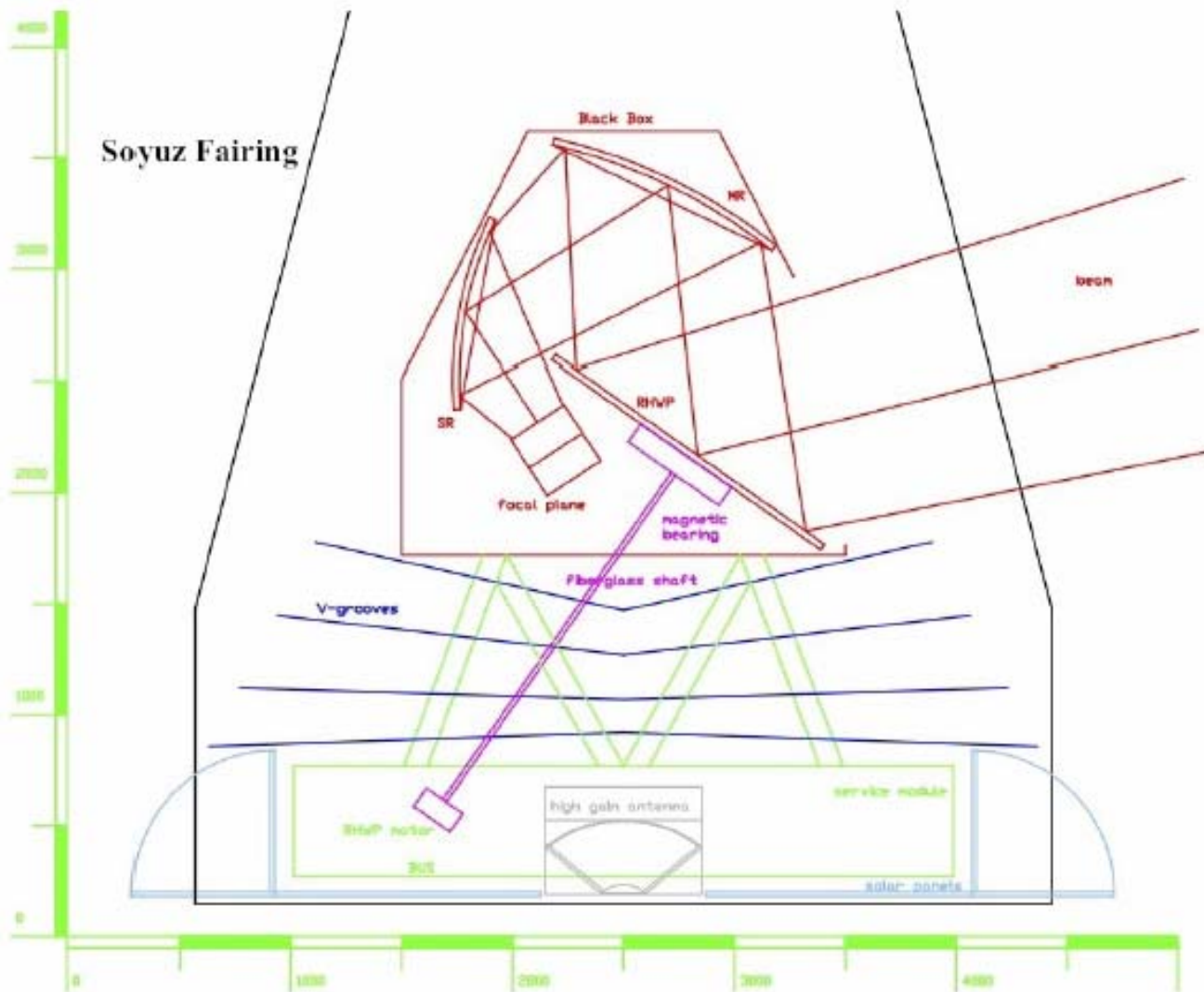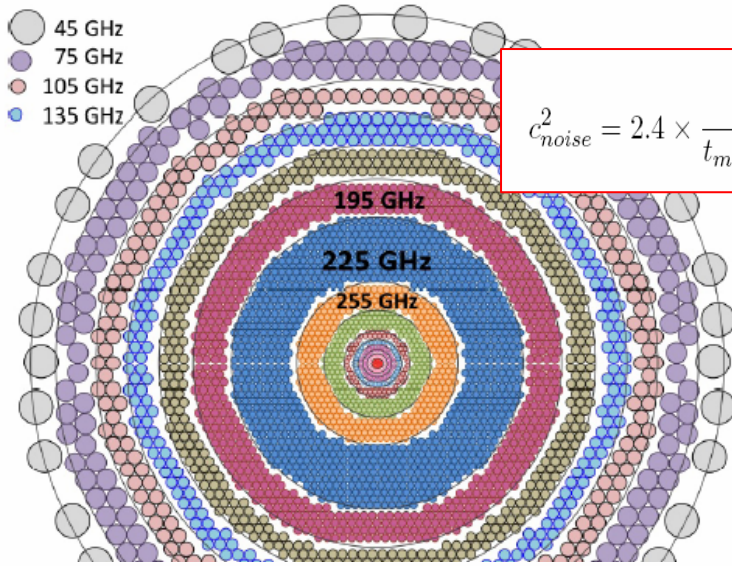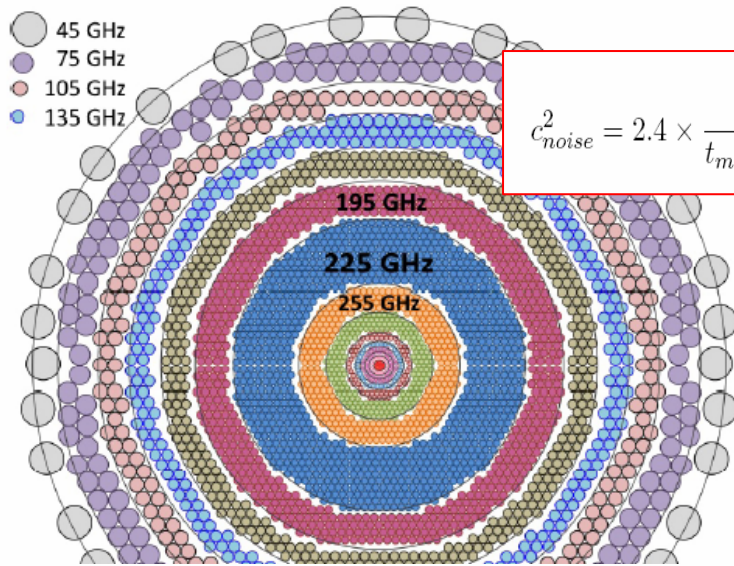$$c_{noise}^2 = 2.4 \times \frac{4\pi}{t_{miss} N_{det}} \times s_{det}^2 = (4.7\mu K.arcmin)^2 \times \left(\frac{4\ years}{t_{miss}}\right) \times \left(\frac{400}{N_{det}}\right) \times \left(\frac{s_{det}}{50\mu K.s^{\frac{1}{2}}}\right)^2 \quad (4)$$

Table 2: $COrE$ performances - assuming a 50% value for detection chain efficiency.

Central Freq. (GHz)	$\Delta\nu$ (GHz)	Nb. of detectors	FWHM (arcmin)	Unpol. sensitivity (μK.arcmin)	Q & U sensitivity (μK.arcmin)
45	15	64	23.3	5.2	9.0
75	15	300	14	2.7	4.7
105	15	400	10	2.7	4.6
135	15	550	7.8	2.6	4.5
165	15	750	6.4	2.6	4.6
195	15	1150	5.4	2.6	4.5
225	15	1800	4.7	2.6	4.5
255	15	575	4.1	6.0	10.4
285	15	375	3.7	10.0	17
315	15	100	3.3	26.6	46
375	15	64	2.8	67.8	117
435	15	64	2.4	147.6	255
555	195	64	1.9	218	589
675	195	64	1.6	1268	3420
795	195	64	1.3	7744	20881

$$c_{noise}^2 = 2.4 \times \frac{4\pi}{t_{miss} N_{det}} \times s_{det}^2 = (4.7 \mu K.arcmin)^2 \times \left(\frac{4\ years}{t_{miss}}\right) \times \left(\frac{400}{N_{det}}\right) \times \left(\frac{s_{det}}{50 \mu K.s^{\frac{1}{2}}}\right)^2 \quad (4)$$

??? …TES, KID, MMC, CEB … ???

Table 2: *COrE* performances - assuming a 50% value for detection chain efficiency.

Central Freq. (GHz)	$\Delta\nu$ (GHz)	Nb. of detectors	FWHM (arcmin)	Unpol. sensitivity (μK.arcmin)	Q & U sensitivity (μK.arcmin)
45	15	64	23.3	5.2	9.0
75	15	300	14	2.7	4.7
105	15	400	10	2.7	4.6
135	15	550	7.8	2.6	4.5
165	15	750	6.4	2.6	4.6
195	15	1150	5.4	2.6	4.5
225	15	1800	4.7	2.6	4.5
255	15	575	4.1	6.0	10.4
285	15	375	3.7	10.0	17
315	15	100	3.3	26.6	46
375	15	64	2.8	67.8	117
435	15	64	2.4	147.6	255
555	195	64	1.9	218	589
675	195	64	1.6	1268	3420
795	195	64	1.3	7744	20881

There is still so much to discover about our universe …
… but we need large arrays of cryogenic mm-wave detectors !